### RR LYRAE STARS IN LARGE MAGELLANIC CLOUD GLOBULAR CLUSTERS

By

Charles A. Kuehn III

### A DISSERTATION

Submitted to
Michigan State University
in partial fulfillment of the requirements
for the degree of

DOCTOR OF PHILOSOPHY

Astrophysics and Astronomy

2011

#### ABSTRACT

#### RR LYRAE STARS IN LARGE MAGELLANIC CLOUD GLOBULAR CLUSTERS

By

#### Charles A. Kuehn III

The Oosterhoff phenomenon presents a challenge to the accretion model for the buildup of at least part of the Milky Way halo. The existence of the Oosterhoff gap among the globular clusters in the halo of the Milky Way, while globular clusters in satellite galaxies tend to fall in this gap, seems to contradict the idea that the halo was formed through the accretion of objects similar to these current satellite galaxies. This dissertation seeks to better understand the Oosterhoff phenomenon through a systematic study of RR Lyrae stars in globular clusters in the Large Magellanic Cloud (LMC). Similar studies have been carried out on a set of Milky Way globular clusters which fall in the Oosterhoff-I (Oo-I) and Oosterhoff-II (Oo-II) classes but few studies with the requisite level of detail have been carried out on extragalactic objects.

This dissertation set out to study the differences between RR Lyrae stars in Oo-I/II clusters and those in Oo-int clusters. Answers for three specific questions were sought. 1.) How do the properties of double-mode RR Lyrae stars in Oo-int clusters compare to those in Oo-I/II clusters? 2.) How do the positions of RR Lyrae stars on the Bailey diagram differ between stars in Oo-int clusters and those in Oo-I/II clusters. 3.) How do the physical properties of RR Lyrae stars, obtained through the Fourier decomposition of their light curves, change when going from Oo-I/II clusters to Oo-int clusters? The implications that this study has on the nature of the Oosterhoff dichotomy are also discussed.

Copyright by CHARLES A. KUEHN III 2011

To Mom, Dad, Nana, Grandpa, and the rest of my family.
To my grandmother and Papa who wished that they had been able to see me received
my PhD.

#### ACKNOWLEDGMENTS

There are many people who I wish to thank for their role in making this dissertation possible. First off I want to thank my adviser Horace Smith, whose guidance over the years not only made this dissertation possible, but allowed me to even get to this point in my career. Márcio Catelan for his guidance over the years and his valuable comments on not only this thesis but other projects that we have collaborated on. Karen Kinemuchi for her proofreading of this dissertation and her advice on how to survive the dissertation writing and defense process. Nathan De Lee for his assistance on computer related matters when I was first starting out. The undergraduate students; Lisa Taylor, Randall McClellan, Kristina Looper, and Kyra Dame for their assistance with parts of this project. I wish to thank Catherine Kennedy for her support and friendship which were important in helping me get to this point. Thanks to Christopher Waters for the LATEX class used to format this thesis.

# TABLE OF CONTENTS

Li	st of Tabl	es	viii
Li	st of Figu	res	x
Li	st of Sym	bols	xiii
1	Introduc	tion	1
2	Milky W	ay Formation	4
	2.1	Structure of the Milky Way	4
	2.2	Formation of the Milky Way Halo	6
3	RR Lyra	e Variables	10
	3.1	Magnitudes	10
	3.2	RR Lyrae Properties and Pulsation Mechanism	12
	3.3	RR Lyrae Classes	16
	3.4	Oosterhoff Groups	18
	3.5	Other Types of Variable Stars	20
4	Observat	cions, Data Reduction, and Physical Property Determina-	
		• • • • • • • • • • • • • • • • • • • •	23
	4.1	Observations and Image Processing	23
	4.2	Photometry and Variable Identification	24
	4.3	Determination of RR Lyrae Physical Properties	26
	4.3.1	Fourier Decomposition	26
	4.3.2	RRab Variables	27
	4.3.3	RRc Variables	29
5	NGC 140	66	31
	5.1	Data Reduction for NGC 1466	32
	5.2	Variable Stars	34
	5.2.1	RR Lyrae Stars	43
	5.2.2	Comments on Individual RR Lyrae Stars	44
	5.2.3	RRd Stars	45
	5.2.4	Other Variables	46
	5.3	Physical Properties of the RR Lyrae Stars	50
	5.4	Distance Modulus	53
	5.5	Oosterhoff Classification	5/1

6	Reticulun	n	59
	6.1	Variable Stars	61
	6.2	Physical Properties of the RR Lyrae Stars	69
	6.3	Distance Modulus	72
	6.4	Oosterhoff Classification	73
7	NGC 178	6	75
	7.1	Variable Stars	76
	7.1.1	RR Lyrae Stars	83
	7.2	Physical Properties of the RR Lyrae Stars	87
	7.3	Distance Modulus	91
	7.4	Oosterhoff Classification	92
8	NGC 221	0	96
	8.1	RR Lyrae Stars	97
	8.2	Physical Properties of the RR Lyrae Stars	99
	8.3	Distance Modulus	101
	8.4	Oosterhoff Classification	101
9	Exploring	g Oosterhoff Intermediate Systems	104
	9.1	Structure of the Instability Strip	104
	9.2	Indicators of Oosterhoff Status	106
	9.3	Bailey Diagrams for Oosterhoff Intermediate Objects	110
	9.3.1	NGC 1466 vs Draco	113
	9.3.2	NGC 1466 vs NGC 2210	115
	9.3.3	NGC 2210 vs NGC 2257	116
	9.3.4	NGC 1466 and NGC 2210 vs Oosterhoff I/II Systems	118
	9.3.5	Oosterhoff Intermediate Locus?	120
10	Trends in	Physical Properties	122
11	Conclusio	ons	136
Δ	NGC 146	6 Light Curves	141
В	Reticulun	n Light Curves	178
$\mathbf{C}$	NGC 178	6 Light Curves	198
	Reference		235

# LIST OF TABLES

3.1	Filters and Their Wavelengths	12
3.2	Properties of RR Lyrae stars	12
3.3	Oosterhoff Group Properties	18
4.1	Instrument Properties	23
5.1	NGC 1466 Variables: Identification and Coordinates	38
5.2	NGC 1466 Variables: Photometric Properties	40
5.3	NGC 1466 Variables: Photometry	43
5.4	NGC 1466 RRd's: Photometric Parameters	45
5.5	NGC 1466 RRab Fourier Coefficients	50
5.6	NGC 1466 RRc Fourier Coefficients	51
5.7	NGC 1466 RRab Physical Properties	51
5.8	NGC 1466 RRc Physical Properties	52
6.1	Reticulum Variables: Identification and Coordinates	65
6.2	Reticulum Variables: Photometric Properties	66
6.3	Reticulum RRd's: Photometric Parameters	67
6.4	Reticulum RRab Fourier Coefficients	70
6.5	Reticulum RRc Fourier Coefficients	70
6.6	Reticulum RRab Physical Properties	71
6.7	Reticulum RRc Physical Properties	72
7.1	NGC 1786 Variables: Identification and Coordinates	77

7.2	NGC 1786 Variables: Photometric Properties	80
7.3	NGC 1786 RRd's: Photometric Parameters	83
7.4	NGC 1786 RRab Fourier Coefficients	89
7.5	NGC 1786 RRc Fourier Coefficients	89
7.6	NGC 1786 RRab Physical Properties	90
7.7	NGC 1786 RRc Physical Properties	90
8.1	NGC 2210 Variables: Photometric Properties	97
8.2	NGC 2210 RRab Fourier Coefficients	96
8.3	NGC 2210 RRc Fourier Coefficients	96
8.4	NGC 2210 RRab Physical Properties	100
8.5	NGC 2210 RRc Physical Properties	100
9.1	Properties for Stellar Systems	112
10.1	RRab Physical Properties for Previously Studied Clusters	122
10.2	RRc Physical Properties for Previously Studied Clusters	123
10.3	RRab Physical Properties for LMC Clusters	130
10.4	RRc Physical Properties for LMC Clusters	130

# LIST OF FIGURES

3.1	HR Diagram for RR Lyrae Stars	14
3.2	RR Lyrae Bailey Classes	17
3.3	Average period vs metallicity for Globular Clusters	19
3.4	Milky Way Halo Period-Amplitude Diagram	21
4.1	Example of a Fourier Series Fit	27
5.1	NGC 1466 CMD	32
5.2	NGC 1466 CMD: Horizontal Branch	33
5.3	NGC 1466: RRab Light Curves	35
5.4	NGC 1466: RRc Light Curves	36
5.5	NGC 1466: RRd Light Curves	37
5.6	NGC 1466 Petersen Diagram	47
5.7	NGC 1466: AC Light Curve	48
5.8	NGC 1466: $B$ vs $V$ Amplitudes	49
5.9	NGC 1466: $V$ -band Bailey Diagram	55
5.10	NGC 1466: <i>B</i> -band Bailey Diagram	56
5.11	NGC 1466: RR Lyrae Raw Period Distribution	57
5.12	NGC 1466: RR Lyrae Fundamentalized Period Distribution	58
6.1	Reticulum CMD	60
6.2	Reticulum CMD: Horizontal Branch	61
6.3	Reticulum: RRab Light Curves	62

6.4	Reticulum: RRc Light Curves	63
6.5	Reticulum: RRd Light Curves	64
6.6	Reticulum Petersen Diagram	69
6.7	Reticulum: $V$ -band Bailey Diagram	73
6.8	Reticulum: B-band Bailey Diagram	74
7.1	NGC 1786 CMD	84
7.2	NGC 1786 CMD: Horizontal Branch	85
7.3	NGC 1786: RRab Light Curves	86
7.4	NGC 1786: RRc Light Curves	87
7.5	NGC 1786: RRd Light Curves	88
7.6	NGC 1786: $V$ -band Bailey Diagram	93
7.7	NGC 1786: $B$ -band Bailey Diagram	94
7.8	NGC 1786 Petersen Diagram	95
8.1	NGC 2210: $V$ -band Bailey Diagram	102
8.2	NGC 2210: $B$ -band Bailey Diagram	103
9.1	Instability Strip Structure	105
9.2	$\langle P_{ab} \rangle$ vs $P_{ab,min}$	107
9.3	$\langle P_{ab} \rangle$ vs $\langle P_c \rangle$	108
9.4	$\langle P_{ab} \rangle$ vs Number Fraction of RRc's	109
9.5	$\langle P_{ab} \rangle$ vs $P_{c,max}$	110
9.6	Bailey Diagram for CVn I	111
9.7	NGC 1466 Bailey Diagram	112
9.8	NGC 1466 vs Draco: Bailey Diagram	113
9.9	NGC 1466 vs Draco: Petersen Diagram	114

9.10	NGC 1466 vs NGC 2210: Bailey Diagram	116
9.11	NGC 2210 vs NGC 2257: Bailey Diagram	117
9.12	NGC 1466 vs M3: Bailey Diagram	118
9.13	NGC 2210 vs M15: Bailey Diagram	120
10.1	$\langle T_{\rm eff} \rangle$ vs Cluster Metallicity for RRc Stars in Previously Studied Globular Clusters	125
10.2	$\langle L/L_{\odot}\rangle$ vs Cluster Metallicity for RRc Stars in Previously Studied Globular Clusters	126
10.3	$\langle M/M_{\odot}\rangle$ vs Cluster Metallicity for RRc Stars in Previously Studied Globular Clusters	127
10.4	$\langle T_{\rm eff} \rangle$ vs Cluster Metallicity for R Rab Stars in Previously Studied Globular Clusters	128
10.5	$\langle M_V \rangle$ vs Cluster Metallicity for R Rab Stars in Previously Studied Globular Clusters	129
10.6	$\langle T_{\rm eff} \rangle$ vs Cluster Metallicity for RRc Stars	131
10.7	$\langle L/L_{\odot}\rangle$ vs Cluster Metallicity for RRc Stars	132
10.8	$\langle M/M_{\odot} \rangle$ vs Cluster Metallicity for RRc Stars	133
10.9	$\langle T_{\rm eff} \rangle$ vs Cluster Metallicity for RRab Stars	134
10.10	$0\langle M_V \rangle$ vs Cluster Metallicity for RRab Stars	135
A.1	Light curves for the variable stars in NGC 1466	141
B.1	Light curves for the variable stars in Reticulum	178
C.1	Light curves for the variable stars in NGC 1786	198

# LIST OF SYMBOLS

pc	A parsec is $3.086 \times 10^{16}$ meters	5
$M_{\odot}$	Mass of the Sun	12
$R_{\odot}$	Radius of the Sun	12
$M_V$	Absolute magnitude in the Johnson V filter	12
$T_{ m eff}$	Effective temperature	13

# Chapter 1: Introduction

One of the biggest unanswered questions in astronomy is: how did our galaxy, the Milky Way, form? Answering this question is important not only for understanding our place in the universe but the Milky Way also represents what is possibly our best laboratory for understanding how other large spiral galaxies form. While being located in the middle of the disk of the Galaxy presents us with some difficulties in terms of being able to get a full picture of the Galaxy, there is no other galaxy that we can observe in as much detail as the Milky Way.

Current models of galaxy formation propose that large galaxies, like the Milky Way, form through the merging of smaller fragments. While this hierarchical formation model has become commonly accepted, the nature of the smaller fragments that merged to form the Milky Way remains a mystery. In recent years the dwarf galaxies in the vicinity of the Milky Way have been looked at as being similar to the building blocks of the halo, the spherical distribution of stars that makes up the outer regions of the Milky Way.

A large number of studies have been conducted attempting to determine if these dwarf galaxies resemble the objects that were accreted by the Milky Way to form the halo. Most of these studies have attempted to answer this question by comparing the content of elements heavier than helium in the dwarf galaxies to what is seen in the stars and globular clusters in the Galactic halo. These studies based on metallicity have yielded mixed results.

RR Lyrae stars represent another tool that can be used to study the formation of the Galactic halo. RR Lyrae are pulsating variable stars with periods on the order of a day or less. They are luminous stars which make them easy to observe. Studies of RR Lyrae stars in Milky Way globular clusters have shown that these clusters can be divided into two groups, called Oosterhoff groups, based on the properties of their RR Lyrae stars (Oosterhoff groups and other terms will be properly defined in subsequent chapters). These Oosterhoff groups are separated by a zone of avoidance called the Oosterhoff gap. When one looks at the RR Lyrae stars in the nearby dwarf galaxies and their globular clusters, the Oosterhoff gap is not present as these extragalactic objects fall in the gap, as well as in the two Oosterhoff groups. In fact these extragalactic systems seem to preferentially fall in the gap. The existence of these Oosterhoff intermediate (Oo-int) objects in the nearby dwarf galaxies and their absence in the Milky Way present a challenge to the hierarchical accretion model for Milky Way halo formation. If the halo formed through the accretion of objects similar to the present day dwarf galaxies, we would expect to see globular clusters in the halo with the same properties as in the dwarf galaxies. In order to fully understand how the Milky Way halo formed, we need to better understand the nature of Oo-int objects.

This dissertation seeks to better understand this Oosterhoff phenomenon through a systematic study of globular clusters in the Large Magellanic Cloud (LMC). Similar studies have been carried out on Oosterhoff I (Oo-I) and Oosterhoff II (Oo-II) clusters in the Milky Way but very few extragalactic systems have been looked at with this level of detail. The observations carried out as part of this dissertation allow for a detailed comparison between these LMC clusters and those in the Milky Way.

The primary goal of this dissertation is to better understand the nature of Oo-int objects. Answers to three specific questions are sought. 1.) How do the properties of double-mode RR Lyrae stars in Oo-int clusters compare to those in Oo-I/II clusters?

2.) How do the positions of RR Lyrae stars on the Bailey diagram differ between stars

in Oo-int clusters and those in Oo-I/II clusters. 3.) How do the physical properties of RR Lyrae stars, obtained through the Fourier decomposition of their light curves, change when going from Oo-I/II clusters to Oo-int clusters? The following chapters will discuss the previous work on this subject, the observations that were made and their results, and finally compare the observed clusters to previously studied globular clusters and dwarf galaxies.

# Chapter 2: Milky Way Formation

This chapter presents a quick overview of the current understanding of the physical processes involved in the formation of the Milky Way and other large galaxies. This is meant to familiarize the reader with the topics that will be talked about later in this dissertation and thus particular attention is paid to the formation of the halo. This chapter is not meant as a thorough treatment of the subject; such a treatment is beyond the scope of this dissertation, but is discussed in Lee et al. (2011), Babusiaux et al. (2010) and the references contained within this chapter.

# 2.1 Structure of the Milky Way

The Milky Way is a barred-spiral galaxy that consists of three main parts: the central bulge, the flattened disk, and a dual halo. These components differ in terms of their gas and stellar content, dynamical motion, and formation history.

The bulge is a tri-axial bar-shaped structure located at the center of the Milky Way. Most of the stars in the bulge are old, 10-12 Gyr, and display a wide range in metallicities,  $-1.5 \leq [\text{Fe/H}] \leq 0.75$  (Zoccali, 2010). Metallicity is the astronomical term used to refer to the amount of elements heavier than helium in a star or other astronomical object. Typically iron is used as a proxy for the total content of the heavier elements, and the metallicity is expressed using the shorthand [Fe/H] which

relates the iron to hydrogen ratio in a star to the ratio in the Sun via the equation:

$$[Fe/H] = \log(N_{Fe}/N_H)_{star} - \log(N_{Fe}/N_H)_{Sun}$$
(2.1)

where  $N_{Fe}$  and  $N_H$  are the number density of iron and hydrogen atoms, respectively.

When most people think of the Milky Way, they think of the spiral arms that are prominent in the commonly seen images of the Galaxy. These spiral arms are part of the disk of the Milky Way, a relatively thin component of the Galaxy that consists of stars, gas, and dust orbiting around the Galactic center in roughly circular orbits. The disk can be thought of as being made of two components, the thin and thick disks, named so due to their relative heights. The thin disk has a scale height of approximately 300pc and features a large amount of young stars due to ongoing star formation. Stars in the thin disk are relatively metal-rich,  $[Fe/H] \ge -0.5$ , with younger stars being more metal-rich than older stars. The thick disk has a scale height of approximately 1 kpc and contains stars that are older and more metal-poor than the stars in the thin disk (Ostlie & Carroll, 1996; Lee et al., 2011).

The final component of the Milky Way galaxy is the dual halo, a roughly spherical distribution of stars that surrounds the rest of the Galaxy. The stars in the halo tend to be some of the oldest and most metal-poor stars in the Galaxy. Like the disk, the halo is thought to consist of two components, the inner and outer halo. The inner halo is thought to be non-rotating, more flattened, and has a peak metallicity of  $[Fe/H] \approx -1.6$ . In contrast, the outer halo is thought have a retrograde rotation, is roughly spherical, and contains stars that are generally more metal-poor than the inner halo, with a peak metallicity of  $[Fe/H] \approx -2.2$  (Carollo et al. 2011 and references therein). The halo also contains approximately 100 globular clusters, objects with  $10^6$  or more stars that all form at the same time from a giant collapsing gas cloud and that are gravitationally bound together. How the halo formed is one of the great open questions in astronomy and answering that question is crucial to constraining overall

formation models for the Milky Way as well as other barred spiral galaxies.

# 2.2 Formation of the Milky Way Halo

Early theories of Milky Way formation suggested that the Galaxy formed from a large cloud of gas that collapsed as it cooled, forming stars and globular clusters in the process (Eggen et al., 1962). This model predicted the existence of a metallicity gradient, where stars and clusters with higher metallicity occur at smaller galactic This occurs because higher metallicity stars can only form at later times, after a previous generation of more metal-poor stars have had time to form and cast off heavier elements. In addition to being located at smaller galactic radii, higher metallicity stars are expected to have less eccentric orbits, as they form after the gas cloud has spun up in order to conserve angular momentum. Later observations did not find the expected trends between metallicity and galactic radii or orbital eccentricity, instead suggesting that the sample of stars used by Eggen et al. (1962) may have suffered from a selection bias (Chiba & Beers, 2000). While this model explains the formation of some parts of the Milky Way, such as the disk, it has been abandoned as an explanation for the origin of the halo; this is not say that the cloud collapse model has been abadoned entirely as there is evidence that it may be the method by which massive early-type galaxies form (Eliche-Moral et al., 2010).

An alternate explanation for the formation of the Milky Way was devised by Searle & Zinn (1978), hereafter referred to as SZ. Instead of having the Galaxy form from the collapse of a single gas cloud, the SZ model had the inner region of the Galaxy form from the collapse of a large gas cloud while the halo of the Galaxy was formed by the accretion of smaller gas clouds. Stars and globular clusters would form in these smaller clouds and then mix with the contents of the Galaxy, forming the outer halo.

The 1990s saw the development of the lambda-cold-dark-matter ( $\Lambda$ CDM) cosmological model which predicted that large galaxies formed through the hierarchical

assembly of smaller subgalactic fragments. In this model, stars first form from gas in dark matter halos that are smaller than galaxies and over time these halos slowly merge together and grow in size (Bekki & Chiba, 2001), eventually reaching the size of the large spiral galaxies that we see today.

When applied to the Milky Way halo, the  $\Lambda$ CDM model predicts that the halo was formed through the accretion of smaller galaxies (Bullock & Johnston, 2005; Abadi et al., 2006; Font et al., 2006). The contents of these smaller galaxies (their stars, gas, dust, globular clusters, and dark matter) merge with the Milky Way. The accretion process dissipates the smaller galaxies, spreading their contents around the halo of the Milky Way and over time making them indistinguishable from the remnants of previous mergers, as well as any pieces that may have formed within the Milky Way itself (Peñarrubia et al., 2005). Globular clusters in the smaller galaxies are dense enough that they are likely to survive the accretion process intact.

If the Milky Way halo formed through this ΛCDM merger scenario, the next question to consider is: what did the building blocks of the halo look like? The Milky Way is not an isolated galaxy, instead it belongs to a group of galaxies known as the Local Group. The Local Group consists of two large spiral galaxies, the Milky Way and the Andromeda galaxy (M31), and dozens of dwarf galaxies. The building blocks of the halo may have resembled these present day dwarf satellite galaxies (Searle & Zinn, 1978; Zinn, 1993; Mackey & van den Bergh, 2005).

Recent observations have yielded a great deal of data supporting not only the hierarchical merger model for halo formation but also suggesting that the smaller galaxies that were accreted during this process resemble the present day dwarf satellite galaxies of the Milky Way. One of the most crucial pieces of evidence in support of the merger model is the discovery of stellar streams in the halo. The first of these, the Sagittarius stream, was discovered by Ibata et al. (1994) and many others have been found since (Newberg et al., 2002; Belokurov et al., 2006, 2007). These stellar

streams originate from dwarf galaxies that are being tidally disrupted by the Milky Way.

Forbes & Bridges (2010) recently carried out a study looking at the age-metallicity relationship of 93 Milky Way halo globular clusters for which deep color-magnitude diagrams could be obtained in the literature. They found that 27-47 of the globular clusters in their sample displayed an age-metallicity relationship that is similar to what is seen in the present day dwarf galaxies, suggesting that these clusters likely originated in dwarf galaxies and were later accreted into the Milky Way.

In addition to looking at the overall trend of metallicity in stars in the Milky Way and nearby dwarf galaxies, the chemical abundance patterns in the stars of the Milky Way and nearby dwarf galaxies have been compared with mixed results. Pritzl et al. (2005b) compared previously published abundances of stars in the Galactic halo and dwarf galaxies and concluded that, based on the differences seen in the elemental abundance patterns, stars and globular clusters in the Milky Way halo could not have originated in the nearby dwarf galaxies. More recently, Frebel, Kirby, & Simon (2010) found that the Sculptor dwarf galaxy contains a star that displays the same elemental abundance pattern that is seen in metal-poor stars in the Milky Way halo. This star is extremally metal-poor, [Fe/H]= -3.8, and its discovery suggests that at least one dwarf galaxy can form the type of stars that make up the extremally metal-poor component of the Milky Way halo. Mucciarelli et al. (2010) recently carried out highresolution spectrographic studies of red giant stars in three globular clusters in the LMC, finding that these clusters had elemental abundance patterns consistent with Milky Way globular clusters. Additional observations of stars in the nearby dwarf galaxies will be needed to ultimately resolve the issue of whether or not any of the dwarf spheroidals produce stars like the ones that make up the normal metal-poor population of the haloes.

RR Lyrae stars represent an additional tool that can be used to investigate the

Galactic halo and its formation. RR Lyrae are relatively bright and can be found in all Galactic components as well as in globular clusters and nearby dwarf galaxies. These stars are some of the oldest stars in the Galaxy and existed at the time that the Galaxy was forming. RR Lyrae are relatively easy to identify in photometric time-series data sets and can also be used to establish distances. In Chapter 3 I discuss in more detail the stellar characteristics of RR Lyrae stars and how they can be utilized in the understanding of Milky Way halo formation.

# Chapter 3: RR Lyrae Variables

RR Lyrae (RRL) stars are pulsating variable stars with periods that range from several hours to just over a day. RR Lyrae have been known since the late nineteenth century thanks to the work of E.C. Pickering and Solon Bailey (Pickering & Bailey, 1895). RR Lyrae stars are very useful in several different areas of astronomy. RRL have a very narrow range of luminosities and thus are excellent standard candles that can be used to determine distances within the Milky Way and to nearby galaxies. Studies of their pulsational characteristics are useful when attempting to understand stellar evolution as they provide information about the internal structure of the star. Additionally, pulsation theory can be used to determine the masses of RR Lyrae stars that pulsate in multiple modes; these masses can then be compared against those predicted by stellar evolution theory. As will be discussed in this dissertation, comparing the properties of RR Lyraes in the Milky Way and nearby dwarf galaxies places constraints on the merger model for Milky Way halo formation.

## 3.1 Magnitudes

Before the RR Lyrae stars are discussed in more detail, it is necessary to make a brief detour to discuss the magnitude system used by astronomers. Astronomers typically express the brightness of stars using a system of magnitudes that dates back to the ancient Greeks. The system was originally created by Greek astronomer Hipparchus as a means to rank how bright stars appeared; the brightest stars were first magnitude,

slightly dimmer stars were second magnitude and so forth. These magnitudes were originally defined by the sensitivity of the human eye. Later, the magnitude system was quantified such that the difference in magnitudes between two objects is given by the equation,

$$m_1 - m_2 = -2.5 \log \left(\frac{f_1}{f_2}\right),$$
 (3.1)

where  $m_1$  and  $m_2$  are the magnitudes of the two objects and  $f_1$  and  $f_2$  are the fluxes received from those objects, respectively. As this equation clearly demonstrates, brighter objects have smaller magnitudes. For example, looking at two stars, Vega (magnitude  $\approx 0$ ) and Spica (magnitude  $\approx 1$ ), the flux received from Vega is 2.5 times the flux received from Spica.

There are two types of magnitudes, apparent and absolute, which can be used to describe an object. Absolute magnitudes are based on the flux that would be received from an object if it were at a distance of 10 parsecs. As such, absolute magnitudes reflect the actual amount of light emitted by an object. Apparent magnitudes are based on the flux from an object that is received by an observer and thus are based not only on the luminosity of the object but also the distance to that object. If one knows both the absolute and apparent magnitude of an object, the distance to it can be calculated using the following equation:

$$M = m - 5\log(d) + 5, (3.2)$$

where M is the absolute magnitude of a source, m is the apparent magnitude, and d is the distance to the source measured in parsecs.

The brightness of an object is typically measured in specific wavelength ranges which are created by using filters when taking observations. The three filters used in the observations for this dissertation are the Johnson-V, Johnson-B and the Cousins-I filters; the wavelength coverage of these filters, central wavelength and the width

at half maximum transmission, is summarized in Table 3.1. These filters were chosen as they have historically been the ones most used in studies of RR Lyrae stars.

Table 3.1: Filters and Their Wavelength Ranges

Filter	Central Wavelength (Angstroms)	FWHM (Angstroms)
В	4326	1269
V	5332	1073
Ι	8050	1500

# 3.2 RR Lyrae Properties and Pulsation Mechanism

RR Lyrae are old, Population II stars that were originally discovered in globular clusters with ages 10 billion years or more. RR Lyrae stars lie on the horizontal branch, meaning that they are fusing helium in their cores, where the horizontal branch crosses through the instability strip, Figure 3.1. RR Lyrae tend to be relatively metal poor,  $0.0 \leq [\text{Fe/H}] \leq -2.5$ . Additional properties of RR Lyrae stars are summarized in Table 3.2.

Table 3.2: Properties of RR Lyrae Stars (Smith, 1995)

Property	Value
[Fe/H]	-2.5 to 0.0
$T_{eff}$	$6100~\mathrm{K}$ to $7400~\mathrm{K}$
Mass	$pprox 0.7~M_{\odot}$
Radius	4 to 6 $R_{\odot}$
$M_V$	$+0.6 \pm 0.2 \text{ mag}$

Table 3.2: Properties of RR Lyrae stars. (continued)

Property	Value
Period	0.2  to  1.2  days
Amplitude	0.2 to $2.0$ mag in V
Spectral Type	A through F

Table 3.2 lists the absolute magnitude in the V-band for RR Lyrae stars as  $M_V = +0.6\pm0.2$ , however this is an average as there is a trend between absolute magnitude and the metallicity of the star, with metal-poor RR Lyraes being more luminous than metal-rich ones. Catelan & Cortés (2008) used theoretical models fit to the star RR Lyrae itself to find that the absolute magnitude of an RR Lyrae star is

$$\langle M_V \rangle = (0.23 \pm 0.04) [\text{Fe/H}]_{ZW84} + (0.984 \pm 0.127)$$
 (3.3)

where the metallicity of the star is given using the scale of Zinn & West (1984), hereafter referred to as ZW84.

RR Lyrae stars vary due to the fact that they are intrinsically radially pulsating stars, the change in brightness in the V-passband occurring mainly due to the change in effective temperature ( $T_{\rm eff}$ ) that occurs during the expansion and contraction of the star. The pulsations of an RR Lyrae can be described using the pulsation equation derived by Ritter (1879) which shows the relationship between the pulsational period and the density of the star,

$$Q = P\sqrt{\rho/\rho_{\odot}},\tag{3.4}$$

where P is the pulsation period measured in days,  $\rho$  is the density of the star,  $\rho_{\odot}$  is the density of the Sun, and Q is the pulsation constant which is approximately 0.04 days for RR Lyrae stars that pulsate in the fundamental mode (Smith, 1995).

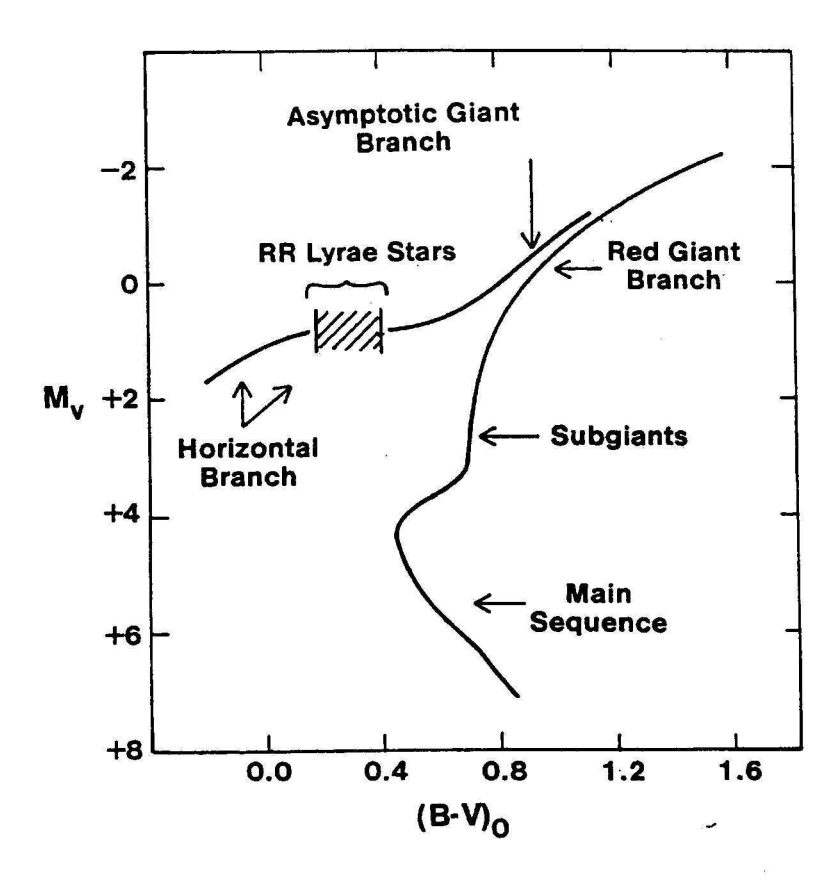


Figure 3.1: HR diagram for a typical globular cluster showing the brightness,  $M_V$ , versus color,  $(B-V)_0$ , for the stars in the cluster. Color is an indication of temperature with bluer stars being hotter and located toward the left on the diagram. The position of RRL stars on the horizontal branch, in the instability strip, is indicated. Figure from Smith (1995).

The radial pulsations of RR Lyrae stars are driven by the opacity of the outer layers of the stars which serves as a heat valve. The opacity of a region in a star is given by a Kramer's law-like opacity,

$$\kappa = \kappa_0 \rho^n T^{-s},\tag{3.5}$$

where  $\kappa$  is the opacity,  $\kappa_0$  is a constant dependent on the composition of the stellar material,  $\rho$  is the density of the region, and T is the temperature of the region. For envelopes of stars where no abundant element is being ionized,  $n \approx 1$  and  $s \approx 3.5$ .

This means that when the temperature increases, the opacity drops, allowing additional radiation to escape and thus not driving a pulsation. However, if the envelope of the star contains an abundant element that is being ionized, s can become very small or negative. Thus an increase in temperature increases the opacity, trapping more radiation. This causes the outer layers of the star to expand until the drop in the density of the gas due to expansion is enough to lower the opacity to the point where radiation can once again escape. At this point the outer layers contract, increasing the density and temperature, resulting in an increase in opacity and causing the cycle to restart. Christy (1966) showed that the zone where helium is being doubly ionized is the most important in driving pulsations in RR Lyrae stars.

The location of the zone where gas is being ionized in the star determines whether or not the star will pulsate with the  $\kappa$ -mechanism. The location of these partial ionization zones is largely dependent on the temperature of the star. If a star is too hot, its ionization zone is located near its surface where there is not enough material left to drive pulsations. Stars that are too cool suffer from an effect where the energy transport mechanism in their outer envelope is convective rather than radiative, damping the  $\kappa$ -mechanism. These temperatures set the location of the two edges of the instability strip seen in Figure 3.1.

A second mechanism also involving the ionization zones in a star, may play a role in the pulsations of RR Lyrae stars. This mechanism, referred to as the  $\gamma$ -mechanism, is based on the fact that in ionization zones, energy that would normally go into raising the temperature of the gas can instead go into ionizing more of the gas. This means that the gas can absorb heat during compression, leading to a pressure maximum that occurs just after the star has fully contracted, which can drive pulsations (King & Cox, 1968).

# 3.3 RR Lyrae Classes

RR Lyrae stars can be divided into classes based on their pulsation mode and the shape of their light curves. Bailey & Pickering (1902) used light curve shape to classify RR Lyrae stars as "a", "b", or "c" type. Later the "a" and "b" classes were combined into one class, "ab".

RR Lyrae stars of type "ab" (RRab) are fundamental mode pulsators which feature light curves that show a rapid increase in brightness followed by a slower decrease (Fig. 3.2). RRab stars tend to have periods between 0.4 and 1.2 days and amplitudes of 0.5 to 2.0 magnitudes in the V-band.

RR Lyrae stars of type "c" (RRc) pulsate in the first overtone and feature more sinusoidal light curves (Fig. 3.2). RRc stars have shorter periods,  $P \leq 0.4$  days, and smaller amplitudes,  $\leq 0.8$  magnitudes in V, than their fundamental mode counterparts.

A class of RR Lyrae which pulsate in both the fundamental mode and the first overtone (RRd) were discovered by Jerzykiewicz & Wenzel (1977). The first overtone is the dominant mode in most RRd stars and thus their light curves are similar to RRc stars but with more scatter due the presence of the fundamental mode (Fig. 3.2). The ratio of the two pulsation periods in RRd stars can be used to determine masses for these stars (Petersen, 1973).

Some RR Lyrae stars have been found to experience a periodic modulation of the light curve shape that occurs on time scales longer than that of the primary period. Despite being known for over a century (Blazhko , 1907), the cause of this Blazhko effect has yet to be determined.

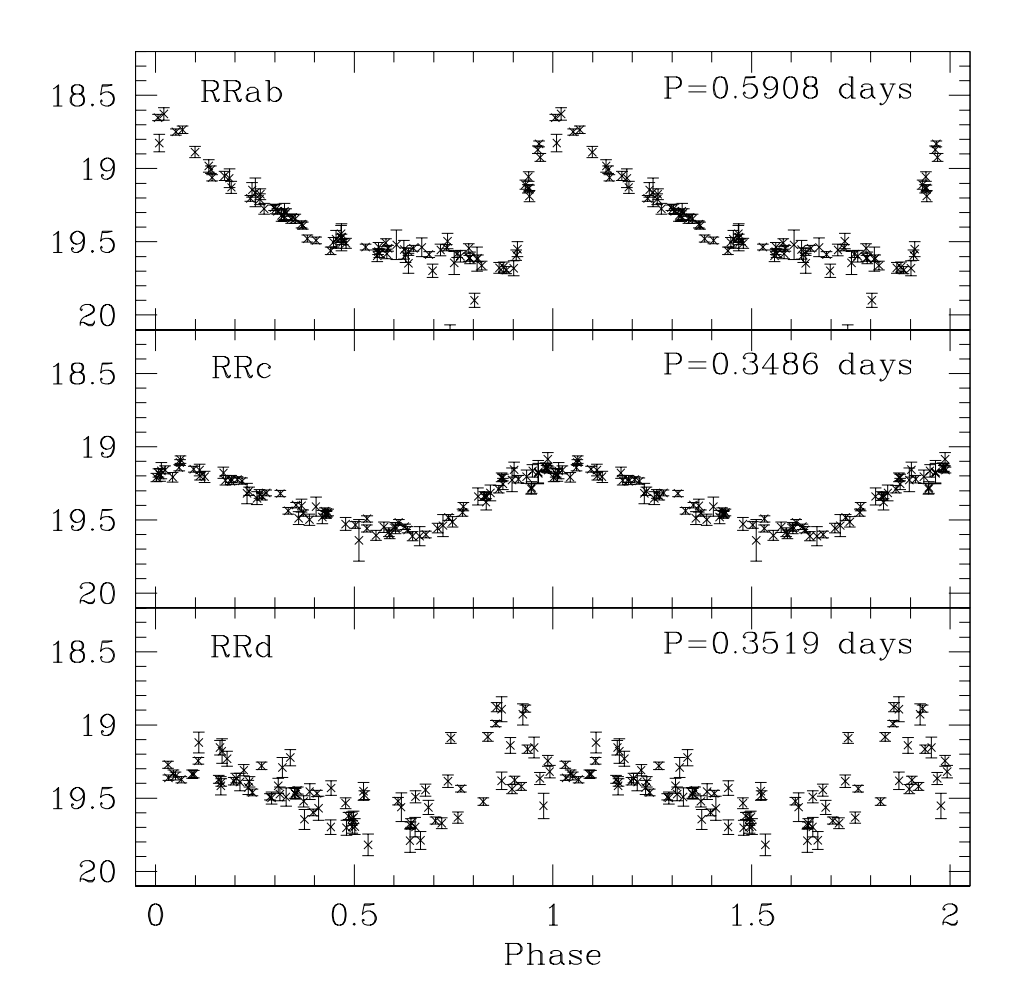


Figure 3.2: Sample light curves for RRab, RRc, and RRd stars from Kuehn et al. (2011). The RRd light curve is plotted with the first overtone mode period. The magnitudes shown in the figure are included for the purpose of demonstrating the difference in amplitudes between the different classes.

# 3.4 Oosterhoff Groups

Oosterhoff (1939) noticed that globular clusters in the Milky Way could be divided into two groups based on the average periods and number fraction of their RR Lyrae stars. Though his original sample size was only five clusters, additional analysis (Oosterhoff, 1944; Sawyer, 1944) confirmed that this division existed and these groups were subsequently named after Oosterhoff. Oosterhoff I (Oo-I) clusters tend to have shorter average periods for their RR Lyraes, and are more metal-rich than Oosterhoff II (Oo-II) clusters (Smith, 1995). Oo-I clusters also tend to have fewer RRc stars when compared to the total number of RR Lyrae stars in the cluster,  $n_{RRc}/n_{RRL}$ . Table 3.3 summarizes the properties of the Oo-I and Oo-II objects.

Table 3.3: Properties of the Oosterhoff Groups (Smith, 1995)

Property	Oo-I	Oo-II
$\langle P_{ab} \rangle$	$0.55 \mathrm{\ days}$	0.64 days
$\langle P_c \rangle$	$0.32~\mathrm{days}$	$0.37  \mathrm{days}$
$n_{RRc}/n_{RRL}$	0.17	0.44
[Fe/H]	> -1.7	< -1.7

A plot of the average RRab period ( $\langle P_{ab} \rangle$ ) vs cluster metallicity for Galactic globular clusters (Figure 3.3, left panel) clearly shows the two Oosterhoff groups as well as a zone of avoidance between them, the Oosterhoff gap. The right panel of Figure 3.3 shows  $\langle P_{ab} \rangle$  vs [Fe/H] for stellar systems in nearby dwarf galaxies. When one looks at the nearby dwarfs there is no Oosterhoff gap as the stellar systems in these dwarfs fall in the gap, as well as in the Oo-I and Oo-II groups. In fact, these extragalactic objects seem to preferentially lie in the gap (Catelan, 2009b).

These Oosterhoff intermediate (Oo-int) objects, as the objects that fall into the gap are referred to, present a challenge to the accretion model for the formation of

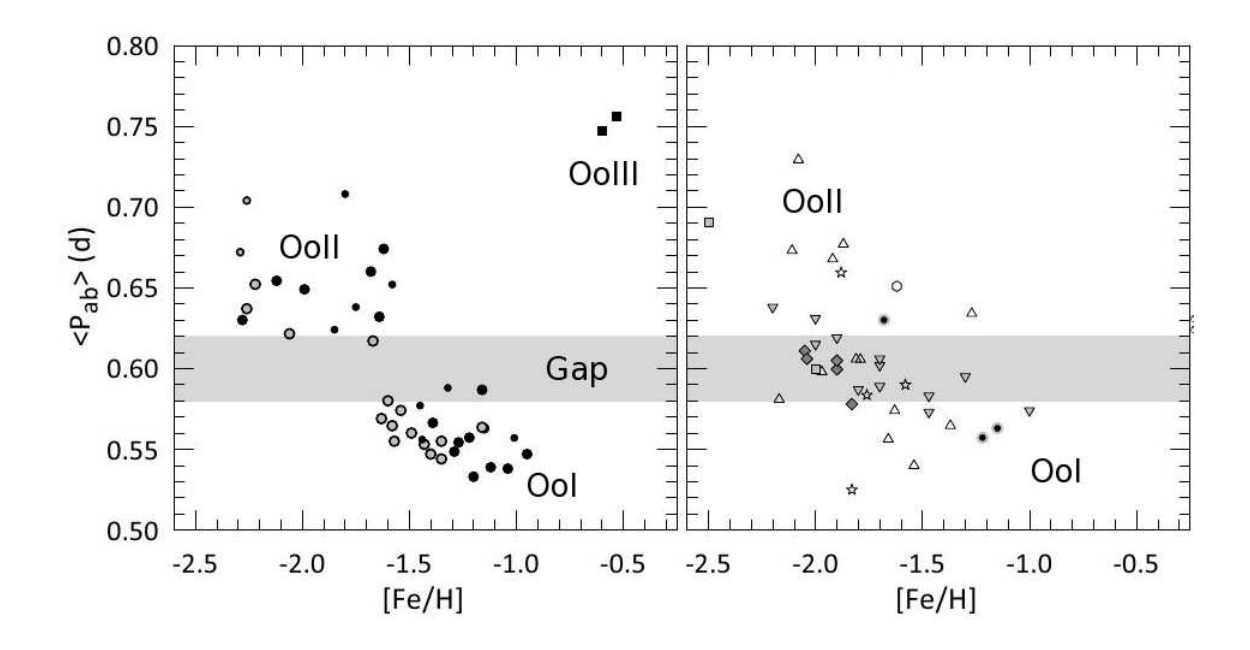


Figure 3.3: Average period for RRab stars  $\langle P_{ab} \rangle$  vs [Fe/H] for globular clusters in the Milky Way (*left*) and nearby dwarf galaxies and their globular clusters (*right*). Figure reprinted from Catelan (2009b) with permission.

the Milky Way halo. Of the 43 Milky Way globular clusters that contain at least five identified RR Lyrae stars, only four of these clusters can be classified as Ooint, and they are on the edge of the Oosterhoff gap. Looking at the nearby dwarf galaxies and their globular clusters, of the 36 objects with at least five identified RR Lyrae stars, 17 of them are classified as Oo-int. Performing a Kolmogorov-Smirnov test reveals that there is only a 1.8% chance that these two sets of objects are from the same parent population. If the Milky Way halo formed by accreting objects like the current dwarf galaxies, then we would expect to see RR Lyrae stars in the halo with the same Oosterhoff classification as we see in the dwarfs. The presence of the Oosterhoff gap when looking at the globular clusters in the Milky Way halo indicates that if the halo formed from accreting dwarf galaxies, these accreted galaxies did not look like our current dwarfs (Catelan, 2009a).

One possible explanation for this Oosterhoff phenomenon could be that Oo-int dwarf galaxies have been accreted in the past but were completely disrupted during the accretion process, leaving behind no globular clusters but instead disbursing all of their RR Lyrae stars into the field population of the halo. This possibility can be explored by looking at the Oosterhoff classification of the individual RR Lyrae stars in the field population of the halo. The Oosterhoff classification of an individual star can be determined by studying its location on a plot of period-vs-amplitude, called a Bailey diagram; this is most effective when looking at RRab stars. Figure 3.4 shows the period-amplitude diagram for RR Lyrae stars in the Milky Way halo obtained from data in the Sloan Digital Sky Survey (De Lee, 2008). Also plotted are the loci for RRab stars of Oo-I and Oo-II types. The majority of RRab stars are Oosterhoff I stars and, while there are some Oo-intermediate stars in the halo, there are not enough Oo-int stars to be consistent with the distribution of Oosterhoff types among the nearby dwarf galaxies and their globular clusters. Similar work done by Miceli et al. (2008) and Szczygiel et al. (2009) confirm the existence of the Oosterhoff dichotomy in the field stars of the Milky Way, both in the halo and in the region near the Sun. As was seen in the work by De Lee, Miceli et al., and Szcyzugiel et al., there are some Oo-int stars in the field but not enough of these stars to be consistent with the number of Oo-int objects in the nearby dwarf galaxies.

If the hierarchical merger model for the formation of the Milky Way halo is true, the absence of Oo-int objects in the Milky Way needs to be explained. In this dissertation I undertake a systematic survey of a group of globular clusters in the LMC with the goal of better understanding Oo-int objects and the differences between them and Oo-I/II objects.

# 3.5 Other Types of Variable Stars

While the primary goal of this dissertation was to study the RR Lyrae stars in the target globular clusters, variable stars of several other types were found in the process. This section is meant as a brief guide to these other types of variable stars.

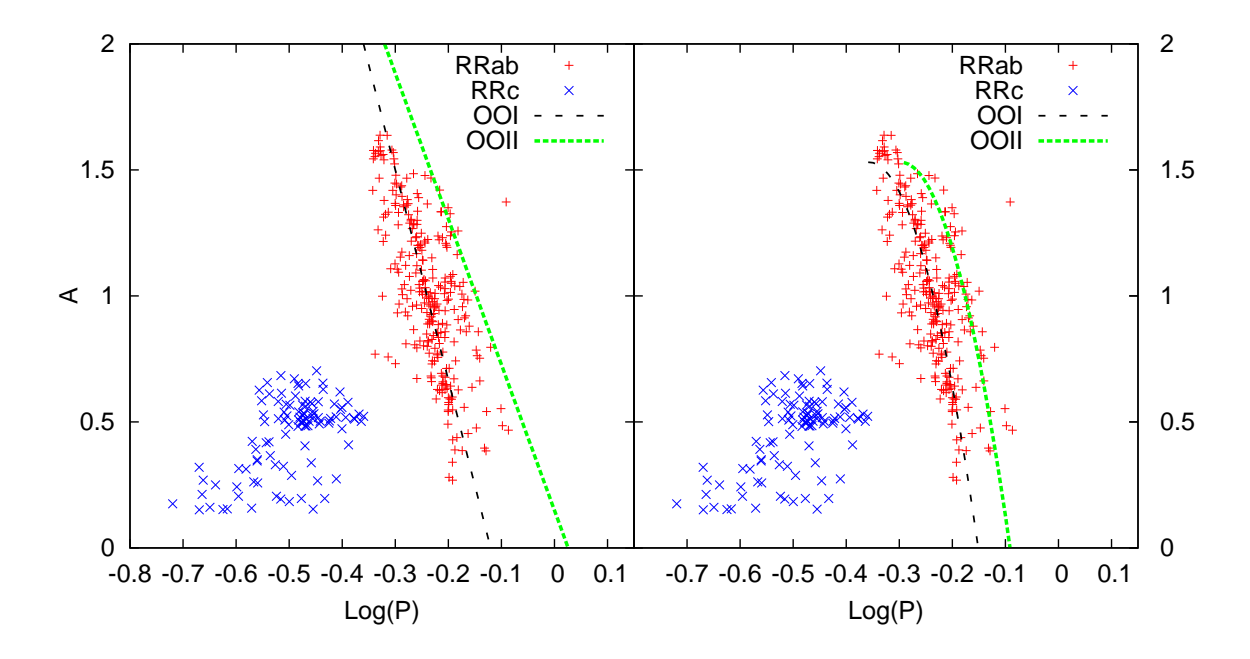


Figure 3.4: Period-amplitude diagrams for RR Lyrae in the Milky Way halo from the Sloan Digital Sky Survey. The left panel shows the Oo-I and Oo-II lines from Clement & Rowe (2000). The right panel shows the Oo-I and Oo-II lines from Cacciari et al. (2005). Each of these lines were transformed into the g band by using  $A_g/A_V=1.17$ . Figure from De Lee (2008). For interpretation of the references to color in this and all other figures, the reader is referred to the electronic version of this dissertation.

-Cepheids are pulsating supergiant stars that are located in the instability strip and which have periods in the range of 1-100 days. Cepheids can be divided into two classes: classical Cepheids and Type II Cepheids.

-Classical Cepheids are younger stars, more massive than the Sun, which are crossing the instability strip in the later stages of their evolutionary lives. Classical Cepheids typically have pulsational amplitudes between 0.5 and 1.0 magnitude in V. They are span a wide range of luminosities, having absolute V magnitudes in the range of  $-6.0 \le M_V \le -0.5$ .

-Type II Cepheids are older stars that are less massive than the Sun, 0.5-0.6 solar masses. Type II Cepheids have similar amplitudes to their classical Cepheid counterparts but are typically less luminous, having absolute magnitudes of  $-3 \le M_V \le 0$ .

-Anomalous Cepheids (AC) are another class of pulsating giant star that is located within the instability strip. ACs typically have masses between 1 and 1.5 solar masses and are either young stars,  $\approx 5$  Gyr old, or older stars that have gained mass from being in a binary (Pritzl et al., 2002). AC stars have periods between 0.4 and 1.6 days and absolute V magnitudes of  $-1.4 \le M_V \le 0.4$ .

-Delta Scuti (DS) stars are pulsating main sequence stars, meaning that they are still fusing hydrogen in their cores, that are located in the instability strip. DS stars have short periods, 0.02 to 0.3 days, and absolute V magnitudes between  $0 \le M_V \le 4.4$ .

-Long period variables (LPV) are stars that show variations with time scales on the order of months. These stars are normally red giant stars that are near the tip of the red giant, or asymptotic giant branch, and are experiencing thermal pulses. LPV light curves often show multiple variations going on at one time, not all of which are necessarily periodic.

-Eclipsing binaries occur when two stars are in a binary, orbiting around their center of mass, and the plane of their orbit is such that the stars pass between each other from the point of view of an observer.

# Chapter 4: Observations, Data Reduction, and Physical Property Determination

# 4.1 Observations and Image Processing

For this study I obtained observations of four globular clusters in the Large Magellanic Cloud (LMC): NGC 1466, NGC 1786, NGC 2210, and Reticulum. Observations were obtained with the SOAR Optical Imager (SOI) on the SOAR 4-m telescope and with ANDICAM on the SMARTS 1.3-m telescope. Table 4.1 gives the basic properties of the two instruments that were used. A quick summary of the number of observations, observation dates, and exposure times for each cluster is presented below.

Table 4.1: Properties of Instruments Used

Instrument	Field of View (arcminutes)	Pixel Scale (arcseconds/pixel)
SOI	$5.2 \times 5.2$	0.153
ANDICAM	6×6	0.369

NGC 1466 - 40~V and 37~B images were obtained using SOAR in February and December of 2008. An additional 45~V and 43~B images were obtained using SMARTS from September 2006 to January 2007. Exposure times for the SOAR observations

were between 30s and 300s for V and between 60s and 300s for B, but were usually 120s and 180s for the V and B observations, respectively. SMARTS exposures were 450s for each filter.

Reticulum - 38 V, 33 B, and 35 I images were obtained using SOAR in February of 2008 while an additional 45 V, 43 B, and 45 I images were obtained using SMARTS from September 2006 through the end of December 2006. SOAR exposure times were between 30s and 600s for V and I, and between 45s and 900s for B. SMARTS exposures were 450s for the V and B filters and 300s for the I filter.

NGC 1786 - 48 V and 48 B images were obtained using SOAR in November of 2007 and February of 2008 while 43 V and 42 B images were obtained using SMARTS from September 2006 to January 2007. SOAR exposure times were between 30s and 600s for V and between 60s and 900s for B. SMARTS exposure times were 450s in each filter.

NGC 2210 - 64 V, 61 B, and 61 I images were obtained using SOAR in February of 2008 while 45 images in V, B, and I were obtained using SMARTS from September 2006 to January 2007. SOAR exposure times were between 30 and 600s for V and I, and 45s and 900s for B. SMARTS exposure times were 450s for V and B, and 300s for I.

The images from both telescopes were bias subtracted and flat-field corrected using IRAF<sup>1</sup>.

## 4.2 Photometry and Variable Identification

Stetson's Daophot II/Allstar packages (Stetson, 1987, 1992, 1994) were run on the images in order to obtain instrumental magnitudes for each star. Observations of the Landolt standard fields PG0231, PG0942, PG1047, RU149, SA95, and SA98 (Landolt,

<sup>&</sup>lt;sup>1</sup>IRAF is distributed by the National Optical Astronomical Observatory, which is operated by the Association of Universities for Research in Astronomy, Inc., under cooperative agreement with the National Science Foundation.

1992) were used to determine a transformation from instrumental magnitudes to the standard system. This transformation was checked for each cluster by using standard stars within the cluster field or by comparing to previous photometry of that cluster. These checks are detailed in the chapters on the individual clusters.

Daophot II/Allstar determines the brightness of stars by fitting a pseudo-Gaussian point spread function profile to each star. This works even when there is some blending of stars as long as the program is able to fit a profile to each star. However, when the stars become so crowded and blended that it is not possible to fit a profile to each star, such as in the crowded centers of many clusters, the profile fitting technique fails. In order to locate variable stars in these extremely crowded regions, the SOAR data on the cluster centers were also searched using the ISISv2.2 image subtraction program (Alard, 2000). The light curves produced by ISIS are in relative fluxes.

The V-band time series, which typically had more phase points than the B-band, was used to identify candidate variable stars using Peter Stetson's Allframe/Trial package (Stetson, 1994). Period searches on the candidate variables were carried out using Supersmoother (Reimann, 1994), Period04 (Lenz & Breger, 2005), and a discrete Fourier transform (Ferraz-Mello, 1981) as implemented in the Peranso software suite<sup>2</sup>. The period phased light curves were visually inspected to confirm the validity of the variable stars. Light curves of candidate variable stars were then fit to template light curves (Layden, 1998) and checked by eye in order to confirm variable classification and period. The resulting primary periods are typically good to at least 0.0002 days (periods for the best observed stars are good to 0.00001 days); errors for the secondary periods of RRd stars are slightly worse, have an accuracy of approximately 0.0004 days. A similar search of the light curves produced with ISIS was done to find additional variables.

<sup>&</sup>lt;sup>2</sup>http://www.peranso.com/

## 4.3 Determination of RR Lyrae Physical Properties

One of the major goals of this study is to compare the physical properties of RR Lyrae stars in clusters of different Oosterhoff types in an effort to determine whether the processes that formed these stars differ with Oosterhoff type. Physical properties of RR Lyrae stars, such as mass, luminosity, and temperature; can be obtained through Fourier analysis of their light curves.

#### 4.3.1 Fourier Decomposition

The RRab light curves were fit with a Fourier series of the form

$$mag(t) = A_0 + \sum_{j=1}^{n} A_j \sin(j\omega t + \phi_j),$$
 (4.1)

where mag(t) is the magnitude as a function of time,  $A_j$  is the amplitude of each order,  $\phi_j$  is a frequency offset, and  $\omega = 2\pi/P$ , where P is the pulsation period. The RRc light curves were fit in a similar fashion but a cosine series was used instead of the sine series. The Fourier fitting was done using a Fourier fitting code originally written by Geza Kovács (Kovács & Walker, 2001) with an analysis wrapper written by Nathan De Lee (De Lee 2011, in prep.). Error analysis for the Fourier decomposition parameters was done based on Petersen (1986). A number of fits were performed for each light curve, with a varying number of terms. The resulting Fourier series was then plotted on top of the original light curve and this was checked by eye to determine if the fit successfully reproduced the shape of the original light curve. Not all light curves were fit successfully, and the optimum number of terms to fit each individual light curve varied. Figure 4.1 shows an example of a failed and a successful Fourier series fit to a light curve.

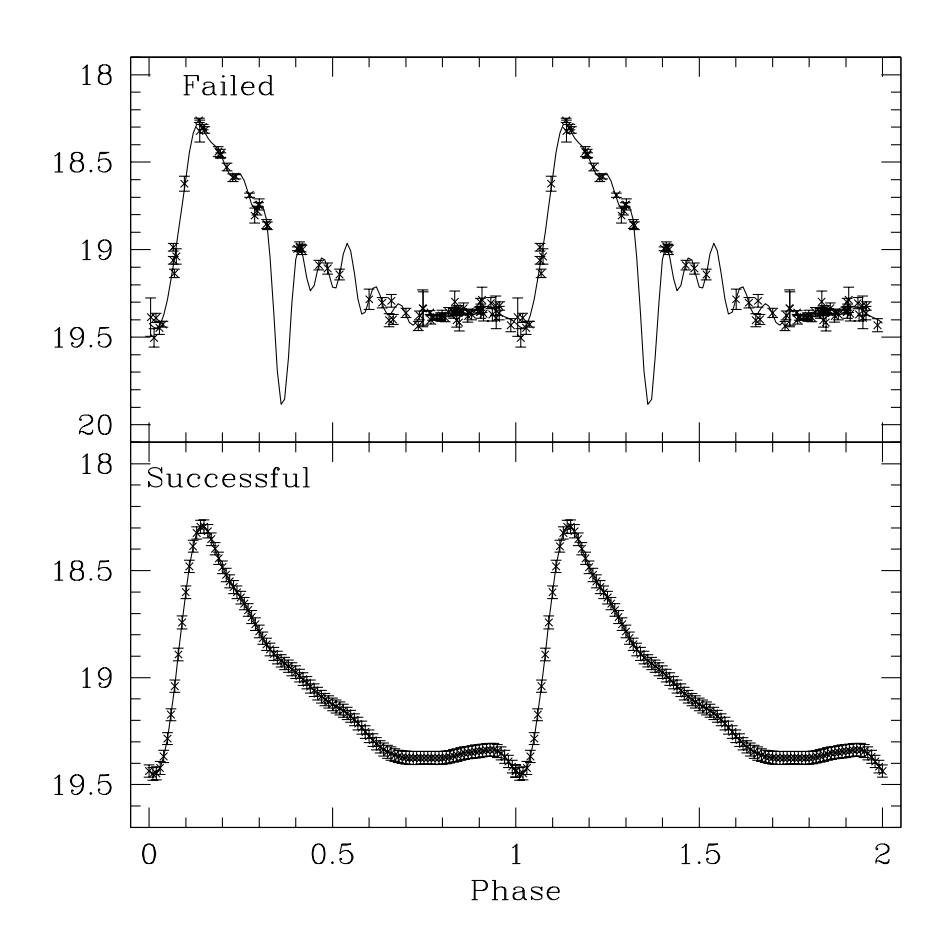


Figure 4.1: Sample results of fitting a Fourier series to a light curve. The top panel shows an unsuccessful fit where too many terms were used, producing a ringing effect. The bottom panel shows a successful fit where the Fourier series does a good job of reproducing the shape of the original light curve.

### 4.3.2 RRAB VARIABLES

Jurcsik & Kovács (1996), Jurcsik (1998), and Kovács & Walker (1999,2001) provide formulae, determined empirically from observations of field RR Lyrae stars, for calculating the metallicity, [Fe/H], absolute magnitude,  $M_V$ , and effective temperature,  $\log T_{\rm eff}^{\langle V-K\rangle}$ , of RRab stars using the Fourier coefficients from their V light curves. The stellar characteristics are determined using the following equations, which come

from equations (1), (2), (5), and (11) in Jurcsik (1998), respectively:

$$[Fe/H] = -5.038 - 5.394 P + 1.345 \phi_{31}, \tag{4.2}$$

$$M_V = 1.221 - 1.396 P - 0.477 A_1 + 0.103 \phi_{31},$$
 (4.3)

$$(V - K)_0 = 1.585 + 1.257 P - 0.273 A_1 - 0.234 \phi_{31} + 0.062 \phi_{41}, \tag{4.4}$$

and

$$\log T_{\text{eff}}^{\langle V-K \rangle} = 3.9291 - 0.1112 (V - K)_0 - 0.0032 [\text{Fe/H}]. \tag{4.5}$$

The values for [Fe/H] derived through this method are in the scale of Jurcsik (1995), which can be transformed to the more common Zinn & West (1984) scale by the relation [Fe/H]<sub>J95</sub> = 1.431[Fe/H]<sub>ZW84</sub> + 0.880 (Jurcsik, 1995). The dereddened B-V and V-I color indices were calculated using equations (6) and (9) from Kovács & Walker (2001), which are reproduced here:

$$(B - V)_0 = 0.189 \log P - 0.313 A_1 + 0.293 A_3 + 0.460$$
(4.6)

and

$$(V - I)_0 = 0.253 \log P - 0.388 A_1 + 0.364 A_3 + 0.648.$$
 (4.7)

The B-V and V-I color indices are also used to calculate effective temperatures via equations (11) and (12) in Kovács & Walker (2001),

$$\log T_{\text{eff}}^{\langle B-V\rangle} = 3.8840 - 0.3219 (B-V)_0 + 0.0167 \log(g) + 0.0070 [M/H]$$
 (4.8)

and

$$\log T_{\text{eff}}^{\langle V-I \rangle} = 3.9020 - 0.2451 (V - I)_0 + 0.0099 \log(g) - 0.0012 [M/H], \quad (4.9)$$

where g, the surface gravity of the star, is obtained from equation (12) in Kovács & Walker (1999),

$$\log(g) = 2.9383 + 0.2297 \log(M/M_{\odot}) - 0.1098 \log T_{\text{eff}} - 1.2185 \log P, \tag{4.10}$$

assuming a mass of  $M = 0.7 M_{\odot}$ .

#### 4.3.3 RRC VARIABLES

Simon & Clement (1993) demonstrated that the Fourier parameters of the V-band light curves of RRc stars could be used to calculate the mass, luminosity, temperature, and helium parameter for these stars. Unlike the empirically determined relationships between physical properties and Fourier parameters for RRab stars, the relationships for RRc stars were determined using light curves that were created with hydrodynamic pulsation models. These physical properties of RRc stars can be calculated using the equations:

$$\log T_{\text{eff}} = 3.265 - 0.3026 \log P - 0.1777 \log M + 0.2402 \log L, \tag{4.11}$$

$$\log y = -20.26 + 4.935 \log T_{eff} - 0.2638 \log M + 0.3318 \log L, \tag{4.12}$$

$$\log M = 0.52 \log P - 0.11 \phi_{31} + 0.39, \tag{4.13}$$

and

$$\log L = 1.04 \log P - 0.058 \phi_{31} + 2.41, \tag{4.14}$$

which are equations (2), (3), (6), and (7) in Simon & Clement (1993), respectively. It should be noted that the helium abundance parameter, y, is not equal to the helium abundance, Y. It should also be noted that while these equations are commonly used in the literature, the equations for mass, luminosity, and temperature violate the

pulsation equation (Catelan, 2004b; Deb & Singh, 2010). While the values calculated for these properties cannot all be physically correct, they can be used for the purpose of making comparisons with the physical properties calculated the same way for RRc stars in other clusters. Empirically-motivated equations also exist for certain physical properties of RRc stars. Equation (10) in Kovács (1998),

$$M_V = 1.261 - 0.961 P - 0.044 \phi_{21} - 4.447 A_4, \tag{4.15}$$

allows the absolute magnitude for the RRc stars to be calculated. The metallicity in the Zinn & West (1984) scale can be calculated using equation (3) from Morgan, Wahl, & Wieckhorst (2007):

$$[\text{Fe/H}]_{\text{ZW84}} = 52.466 P^2 - 30.075 P + 0.131 \phi_{31}^2 + 0.982 \phi_{31} - 4.198 \phi_{31} P + 2.424. \quad (4.16)$$

It has been noted in the literature that RRc masses calculated using the Simon & Clement (1993) equations can at times be too small,  $\simeq 0.5 M_{\odot}$ , which approaches the mass of a degenerate helium core at the helium flash (Corwin et al., 2003). This is likely due to a problem with the equations used but still produces values that are suitable for comparison purposes in this dissertation.

# CHAPTER 5: NGC 1466

NGC 1466 is an old globular cluster that is located relatively far from the center of the LMC. The cluster has a metal abundance of  $[Fe/H] \approx -1.60$  and is not very reddened,  $E(B-V) = 0.09 \pm 0.02$  (Walker, 1992b). Johnson et al. (1999) used color-magnitude diagrams obtained with the Hubble Space Telescope to determine that the age of NGC 1466 is within 1 Gyr of the ages of the Milky Way globular clusters M3 (NGC 5272) and M92 (NGC 6341), showing that NGC 1466 is as old as the oldest Galactic halo clusters.

NGC 1466 features a well-populated horizontal branch that extends through the instability strip (see Figure 5 in Walker (1992b)); thus it is expected to contain a significant number of RR Lyrae stars. RR Lyrae stars were first found in NGC 1466 by Thackeray & Wesselink (1953), and more RR Lyrae were discovered by Wesselink (1971). The most recent study of variable stars in NGC 1466 was conducted by Walker (1992b), who found 42 RR Lyrae stars; 25 RRab stars and 17 RRc's. Due to the density of unresolved stars in the cluster core, Walker did not perform photometry of stars within a radius of 13 arcsec from the cluster center, suggesting that there are probably additional RR Lyrae stars that could not be detected. The core radius of NGC 1466 is 10.7±0.4 arcsec, as measured by Mackey & Gilmore (2003) using images from the Hubble Space Telescope, which is entirely within the region of the cluster where Walker was unable to perform photometry. Advances in instrument resolution and image-subtraction techniques now make it easier for us to search for variable

stars in more crowded regions. From my observations, I obtained a total of 85 V and 80 B images of NGC 1466 which represents a larger data set than the 35 BV pairs obtained by Walker. This increase in time series photometry will improve the chances of identifying new variable stars and obtaining better sampled light curves.

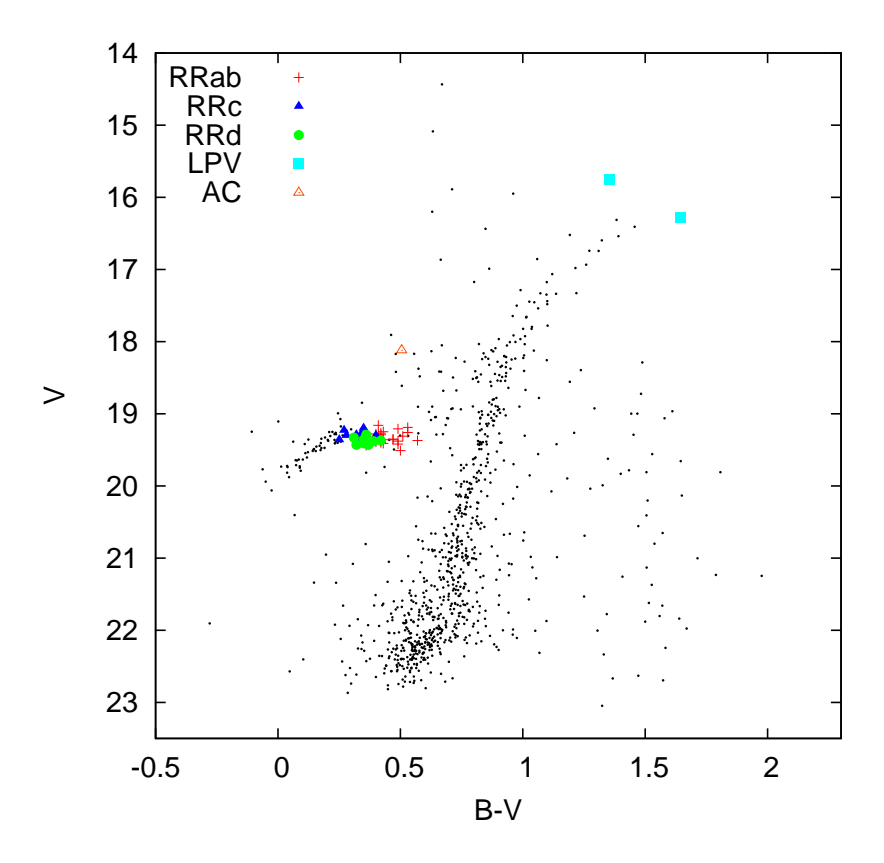


Figure 5.1: V,B-V CMD for NGC 1466. Different variable stars of interest are indicated as follows: RRab: plus sign, RRc: filled triangle, RRd: filled circle, and long period variable stars: filled squares. The potential Anomalous Cepheid is indicated by an open triangle.

## 5.1 Data Reduction for NGC 1466

Data reduction was primarily carried out following the method described in Chapter 4. However, as noted in Walker (1992b), NGC 1466 is located near two very bright stars which create problems with scattered light across some of the images, especially in many of the images obtained with the SMARTS telescope. The procedure described

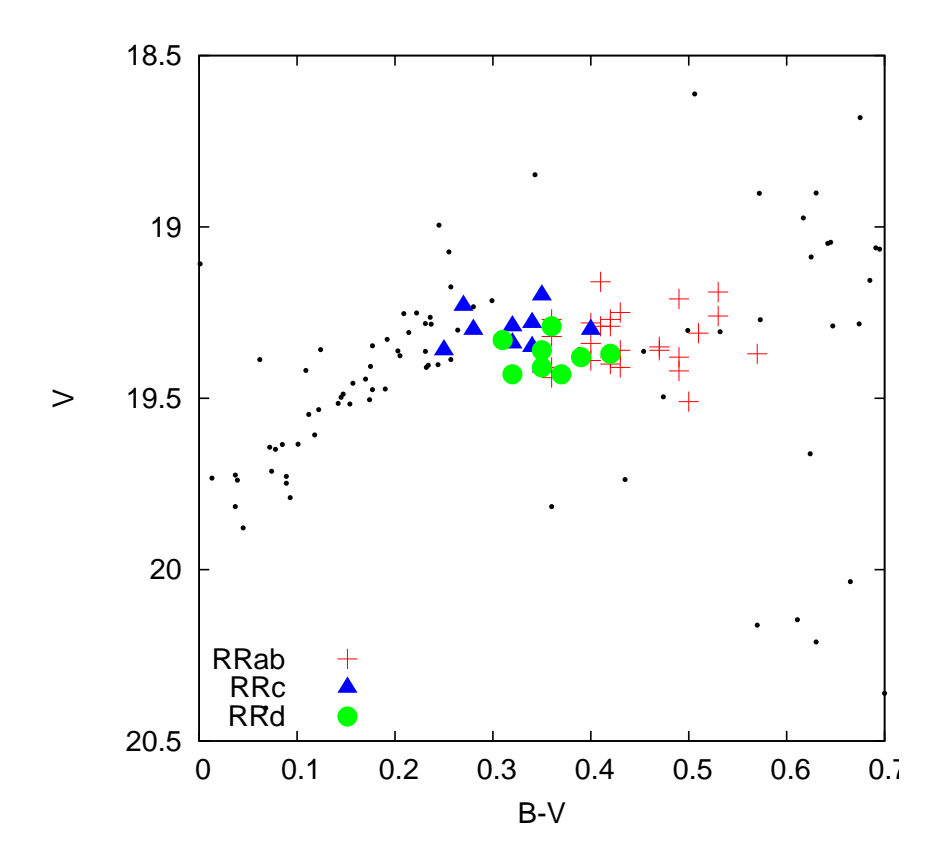


Figure 5.2: V,B-V CMD for NGC 1466 that is zoomed in on the horizontal branch. The symbols used are the same as in Figure 5.1

by Stetson & Harris (1988) was used to remove this scattered light; this was the same method employed by Walker (1992b). The Daophot II/Allstar packages (Stetson, 1987, 1992, 1994) were used to locate, measure, and subtract stars from all images. The subtracted images were then smoothed using a 40x40 pixel median filter. The average sky level in the smoothed images was determined and then the smoothed images were subtracted from the original images. The average sky values were then added back into the new images, creating a final set of images with a constant sky background.

Johnson et al. (1999) showed the photometry in Walker (1992b) to be in good agreement with HST/WFPC2 observations of NGC 1466,  $\Delta V = 0.008 \pm 0.02$ , after these observations were transformed from the on-board HST system to the standard

Johnson-Cousins system. I compared the results of the initial transformation to the standard system, calibrated using observations of Landolt standard fields, to Walker's photometry of isolated non-variable stars across a range of brightnesses within the cluster. Small corrections were made to the zero points and color terms from the initial transformation equations in order to achieve better agreement with Walker's photometry. This produced an average difference between my data and Walker's of  $\Delta V = 0.012 \pm 0.012$  and  $\Delta B = 0.026 \pm 0.020$ . This is a similar level of deviation to that obtained by Johnson et al. (1999) in their comparison with Walker.

The center of NGC 1466 is too crowded for profile fitting photometry to be accurately performed and thus the results from ISIS were relied on in order to identify variables in the most crowded portion of the cluster. Four of the variable stars were found only by ISIS (V31,V51, V54, V60). These stars are located deep in the cluster center and are too crowded to obtain accurate profile fitting photometry. These four light curves are shown in relative fluxes; for the other variables their light curves obtained from Daophot II/Allstar are presented.

## 5.2 Variable Stars

A total of 62 variables were found, including 49 RR Lyraes, 1 additional candidate RR Lyrae, 2 long-period variables, a candidate Anomalous Cepheid, and 9 variables of unknown classification. As described below, double-mode (RRd) variables in the RR Lyrae population of NGC 1466 were able to be identified for the first time. Of the confirmed RR Lyrae stars, 30 were RRab stars, 11 were RRc stars, and 8 were RRd type. The RRd variable stars are discussed separately in section 5.2.3. Figures 5.3, 5.4, and 5.5 show sample light curves for the RRab, RRc, and RRd stars; the full set of light curves for all of the variable stars in NGC 1466 can be found in Appendix A. Table 5.1 lists the variable stars and their coordinates, classification, and period, while Table 5.2 gives the photometric properties (V and B amplitudes, intensity-

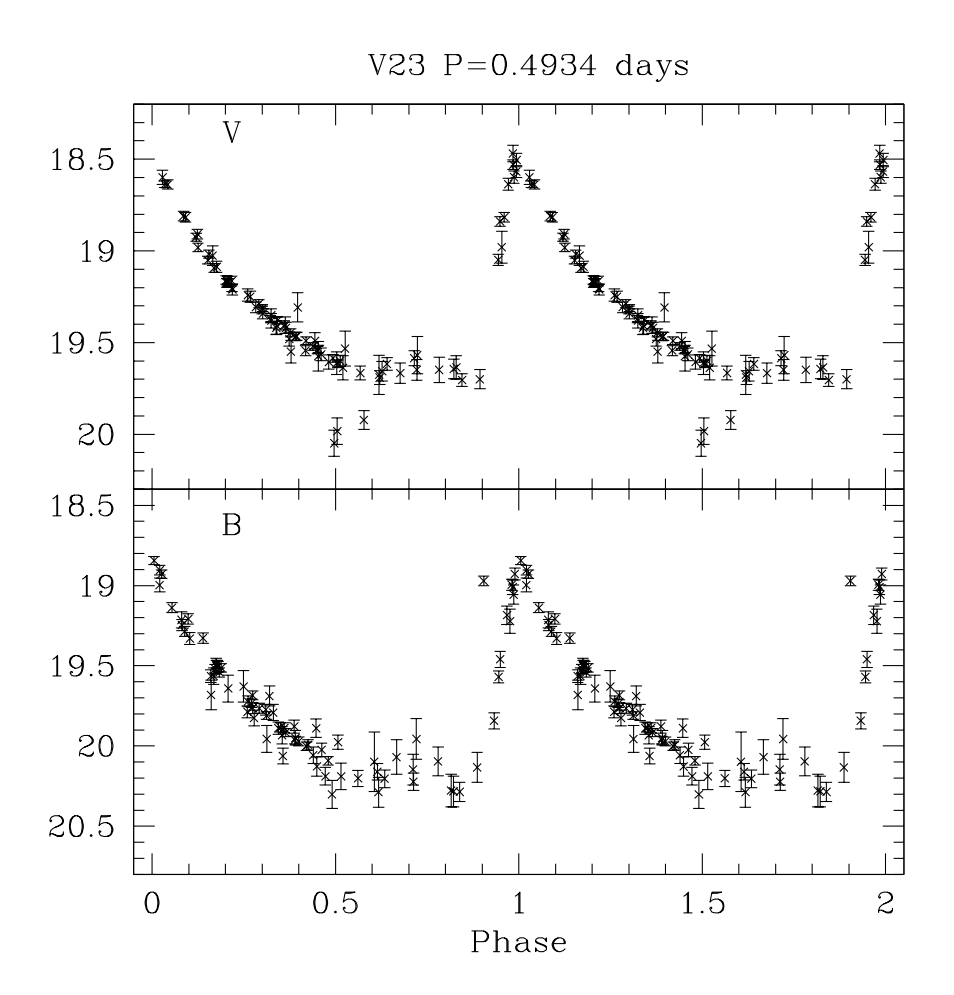


Figure 5.3: Sample light curve for the RRab stars in NGC 1466. The top panel shows the V-band light curve while the B-band light curve is shown in the bottom panel. The full set of light curves can be found in Appendix A.

weighted V and B mean magnitudes, and magnitude-weighted mean B-V color) for the variable stars, except for the RRd stars. Notes on some of the individual stars are in the following subsections. Table 5.3 contains a sample of the photometric data for the variable stars, the full version can be found in Kuehn et al. (2011).

I use a naming system that is an extension of the one used in Wesselink (1971). All variables are named in the form of Vxx, with stars up through V42 being ones that were originally found by Wesselink. A cross identification of the naming system used by Walker and my variable star numbers is included in Table 5.2.

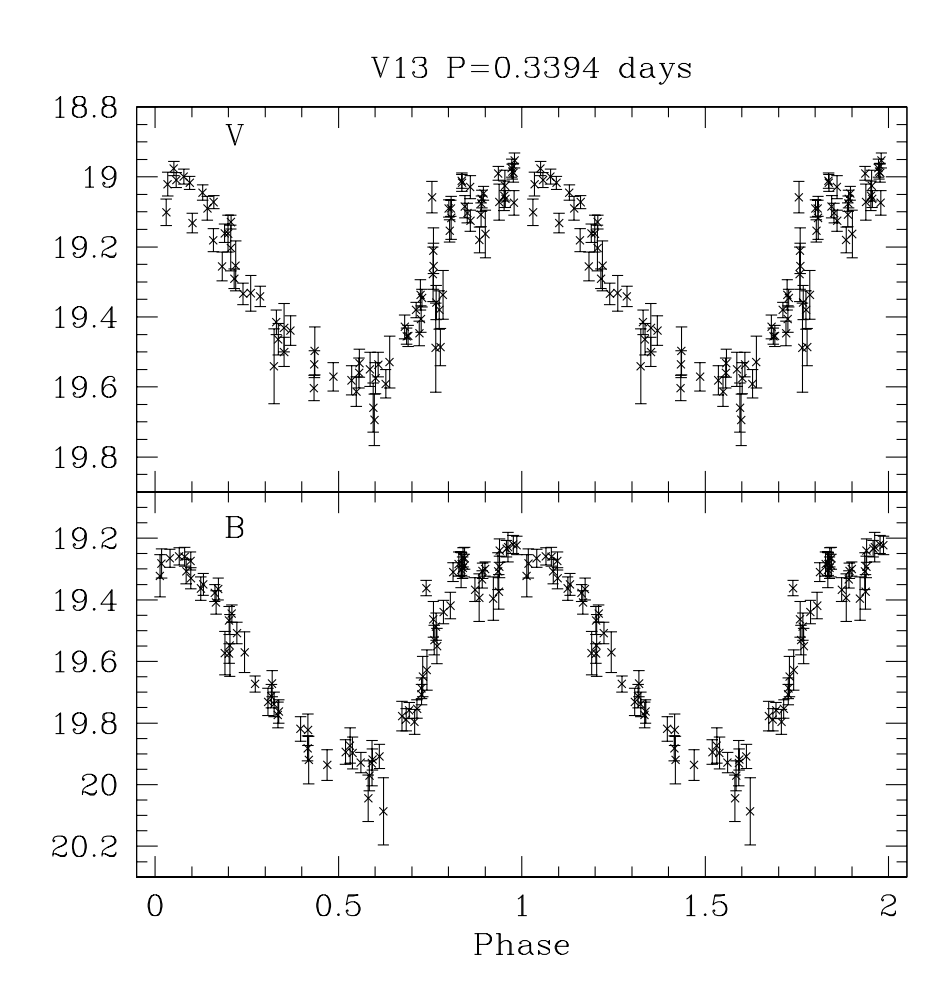


Figure 5.4: Sample light curve for the RRc stars in NGC 1466. The full set of light curves can be found in Appendix A.

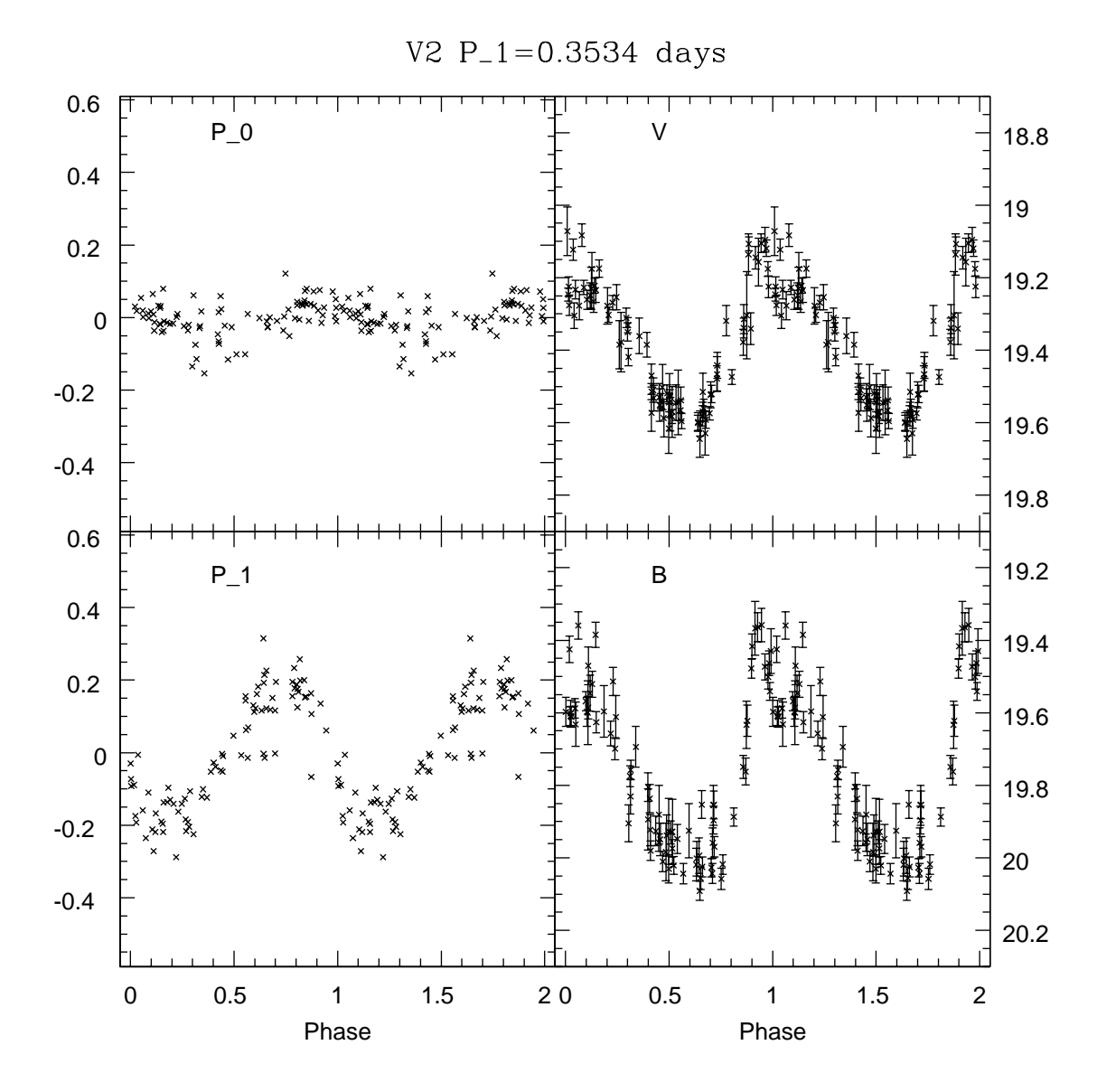


Figure 5.5: Sample light curve for the RRd stars in NGC 1466. The right-hand panels show the raw light curves, as plotted with the first overtone mode period (the first overtone amplitude is larger than the fundamental mode amplitude for all RRd stars in NGC 1466), while the left-hand panels show the deconvolved V light curves. The full set of light curves can be found in Appendix A.

Table 5.1: Variable Stars in NGC 1466

ID	RA (J2000)	DEC (J2000)	Type	P (days)	Other IDs
V1	03:44:44.7	-71:40:44.9	RRab-BL	0.55035	Wa415
V2	03:44:27.4	-71:40:59.7	RRd	0.4751	Wa124
V3	03:44:20.2	-71:40:00.2	RRd	0.4717	Wa66
V4	03:44:20.3	-71:39:57.1	RRab-BL	0.57239	Wa67
V5	03:44:26.6	-71:39:48.9	RRab	0.57863	Wa108
V6	03:44:30.8	-71:39:54.8	RRab-BL	0.52805	Wa182
V7	03:44:28.4	-71:39:13.3	RRd	0.4859	Wa135
V8	03:44:26.3	-71:40:06.5	RRab-BL	0.51970	Wa106
V9	03:44:26.7	-71:40:17.2	RRab	0.52260	Wa109
V10	03:44:27.4	-71:40:19.0	RRd	0.4730	
V12	03:44:28.9	-71:40:15.0	RRab	Wa146	
V13	03:44:33.8	-71:40:48.1	RRc	0.33936	Wa262
V14	03:44:36.2	-71:40:48.7	RRab-BL	0.56414	Wa320
V15	03:44:35.4	-71:40:44.2	RRab	0.56708	Wa303
V16	03:44:34.9	-71:40:45.1	RRab	0.69427	Wa290
V18	03:44:26.7	-71:40:14.5	?	0.48	Wa110
V19	03:44:47.1	-71:40:39.8	RRab	0.61620	Wa426
V20	03:44:30.7	-71:41:22.5	RRab	0.59084	Wa183
V21	03:44:51.9	-71:39:53.4	RRab	0.52150	Wa448
V22	03:44:35.5	-71:41:05.7	RRc	0.33081	Wa301
V23	03:44:38.6	-71:41:24.7	RRab	0.49342	Wa361
V24	03:44:19.9	-71:41:25.5	RRd	0.4938	Wa65
V25	03:44:36.4	-71:39:53.9	RRd	0.4715	Wa323
V26	03:44:34.2	-71:40:51.4	RRab	0.51364	Wa274

Table 5.1 (continued)

ID	RA (J2000)	DEC (J2000)	Туре	P (days)	Other IDs
V28	03:44:21.3	-71:40:38.1	RRc	0.32039	Wa71
V29	03:44:15.5	-71:40:11.9	RRd	0.4824	Wa53
V30	03:44:31.3	-71:39:52.0	RRab	0.69445	Wa194
V31	03:44:32.1	-71:39:50.5	?	0.34272	
V32	03:44:29.4	-71:40:13.7	AC?	0.49661	
V33	03:44:29.0	-71:40:43.9	RRc	0.27841	Wa148
V34	03:44:28.0	-71:39:60.0	?	0.61549	Wa129
V35	03:44:29.7	-71:40:42.5	RRab-BL	0.58172	Wa164
V38	03:44:49.0	-71:40:48.7	RRc	0.34858	Wa437
V39	03:44:30.6	-71:40:07.2	RRab	0.56248	Wa179
V40	03:44:31.0	-71:40:01.1	RRab	0.53606	Wa185
V41	03:44:39.4	-71:40:21.3	RR?		
V42	03:44:30.4	-71:41:00.6	RRab	0.63482	Wa177
V44	03:44:22.0	-71:38:13.1	RRab		Wa75,S27
V45	03:44:23.1	-71:41:16.0	RRc	0.31043	Wa82,S27
V46	03:44:27.4	-71:39:14.0	RRab	0.68909	Wa121
V47	03:44:28.9	-71:40:27.8	RRd	0.4733	
V48	03:44:29.4	-71:40:00.0	RRc	0.37697	Wa153,S3
V49	03:44:30.2	-71:40:09.5	RRab	0.68635	
V50	03:44:31.1	-71:40:28.7	RRab-BL	0.58194	
V51	03:44:31.6	-71:40:12.7	?	0.35892	
V52	03:44:31.6	-71:40:34.6	RRc		
V53	03:44:31.9	-71:40:15.8	LP		
V54	03:44:32.1	-71:40:12.9	?	0.55608	
V55	03:44:32.5	-71:40:13.3	RRab-BL	0.60951	

Table 5.1 (continued)

ID	RA (J2000)	DEC (J2000)	Type	P (days)	Other IDs
V56	03:44:33.4	-71:40:01.8	RRab	0.62238	
V57	03:44:33.5	-71:39:51.7	RRc	0.35692	Wa249,S29
V58	03:44:33.5	-71:39:59.0	RRab	0.56752	
V59	03:44:33.7	-71:40:20.2	?		
V60	03:44:33.9	-71:40:11.4	AC?,RRab?	0.52210	
V61	03:44:33.9	-71:40:01.7	RRab-BL	0.66927	
V62	03:44:35.5	-71:40:35.8	?	0.50414	
V63	03:44:35.6	-71:39:54.0	RRab	0.58760	Wa306,S31
V64	03:44:38.4	-71:40:39.5	RRab	0.68767	Wa356,S30
V65	03:44:39.0	-71:40:03.7	LP		
V66	03:44:40.0	-71:41:10.3	RRc	0.33633	Wa382,S17
V67	03:44:45.1	-71:42:13.1	?		
V68	03:44:56.5	-71:38:54.3	RRc	0.34914	Wa458

Table 5.2: Photometric Parameters for Variables in NGC 1466, Excluding RRd Stars

ID	Type	P (days)	$\overline{A}_V$	$\overline{A}_B$	$\langle V \rangle$	$\langle B \rangle$	$\langle B-V \rangle$	Other IDs
V1	RRab-BL	0.55035	0.64	0.77	19.380	19.793	0.421	Wa415
V4	RRab-BL	0.57239	0.87	1.16	19.406	19.804	0.425	Wa67
V5	RRab	0.57863	0.67	0.82	19.391	19.781	0.403	Wa108
V6	RRab-BL	0.52805	1.19	1.49	19.290	19.672	0.410	Wa182
V8	RRab-BL	0.51970	0.89	1.2	19.273	19.599	0.358	Wa106
V9	RRab	0.52260	1.24	1.52	19.414	19.743	0.362	Wa109
V12	RRab							Wa146

Table 5.2 (continued)

ID	Туре	P (days)	$A_V$	$A_B$	$\langle V \rangle$	$\langle B \rangle$	$\langle B - V \rangle$	Other IDs
V13	RRc	0.33936	0.55	0.69	19.298	19.564	0.276	Wa262
V14	RRab-BL	0.56414	0.93	1.29	19.402	19.803	0.421	Wa320
V15	RRab	0.56708	0.81	1.05	19.209	19.675	0.487	Wa303
V16	RRab	0.69427	0.53	0.69	19.360	19.817	0.466	Wa290
V18	?	0.48	0.15	0.29	18.903	20.168	1.268	Wa110
V19	RRab	0.61620	0.61	0.79	19.360	19.785	0.435	Wa426
V20	RRab	0.59084	1.05	1.33	19.280	19.648	0.396	Wa183
V21	RRab	0.52150	1.22	1.54	19.315	19.632	0.359	Wa448
V22	RRc	0.33081	0.51	0.65	19.200	19.543	0.353	Wa301
V23	RRab	0.49342	1.25	1.51	19.291	19.681	0.421	Wa361
V26	RRab	0.51364	1.03	1.38	19.339	19.702	0.400	Wa274
V28	RRc	0.32039	0.57	0.7	19.338	19.652	0.324	Wa71
V30	RRab	0.69445	0.66	0.91	19.273	19.677	0.421	Wa194
V31	?	0.34272						
V32	AC?	0.49661	0.42	0.70	18.118	18.614	0.505	
V33	RRc	0.27841	0.51	0.57	19.355	19.600	0.247	Wa148
V34	?	0.61549	0.31	0.45	18.194	18.896	0.709	Wa129
V35	RRab-BL	0.58172	0.6	0.78	19.248	19.668	0.432	Wa164
V38	RRc	0.34858	0.44	0.54	19.354	19.682	0.335	Wa437
V39	RRab	0.56248	1.12	1.37	19.156	19.538	0.407	Wa179
V40	RRab	0.53606						Wa185
V41	RR?			0.59		19.598		
V42	RRab	0.63482	0.51	0.66	19.384	19.865	0.489	Wa177
V44	RRab							Wa75,S27
V45	RRc	0.31043	0.38	0.49	19.233	19.503	0.275	Wa82,S27

Table 5.2 (continued)

ID	Type	P (days)	$A_V$	$A_B$	$\langle V \rangle$	$\langle B \rangle$	$\langle B - V \rangle$	Other IDs
V46	RRab	0.68909	0.38	0.49	19.352	19.813	0.466	Wa121
V48	RRc	0.37697	0.44	0.54	19.288	19.580	0.316	Wa153,S3
V49	RRab	0.68635	0.53	0.7	19.255	19.773	0.528	
V50	RRab-BL	0.58194	1.05	1.24	19.444	19.778	0.356	
V51	?	0.35892						
V52	RRc							
V53	LP							
V54	?	0.55608						
V55	RRab-BL	0.60951						
V56	RRab	0.62238	0.73	0.96	19.189	19.701	0.527	
V57	RRc	0.35692	0.42	0.5	19.295	19.685	0.395	Wa249,S29
V58	RRab	0.56752	1.05	1.28	19.368	19.905	0.570	
V59	?		0.46	0.54	18.194	18.651	0.460	
V60	AC?,RRab?	0.52210						
V61	RRab-BL	0.66927	0.86	1.13	19.510	19.985	0.497	
V62	?	0.50414	0.71	1.08	18.758	19.266	0.531	
V63	RRab	0.58760	0.82	0.99	19.415	19.890	0.490	Wa306,S31
V64	RRab	0.68767	0.49	0.59	19.307	19.809	0.508	Wa356,S30
V65	LP							
V66	RRc	0.33633	0.52	0.67	19.277	19.608	0.342	Wa382,S17
V67	?							
V68	RRc	0.34914	0.47	0.65	19.410	19.749	0.348	Wa458

Table 5.3: Sample Photometry of the Variable Stars

ID	Filter	JD	Phase	Mag	Mag Error
V01	V	2453980.8494	0.13881	19.252	0.034
V01	V	2453987.7614	0.69800	19.841	0.105
V01	V	2453991.7381	0.92371	19.199	0.052
V01	V	2453994.7980	0.48359	19.552	0.035
V01	V	2453996.7729	0.07200	19.350	0.042

#### 5.2.1 RR Lyrae Stars

I found 41 of Walker's (1992) 42 RR Lyrae stars along with 6 new RRab stars, 1 new RRc, and 2 new RRd stars. Six of the previously identified RR Lyrae stars in NGC 1466 were reclassified as RRd stars. I was unable to find Walker's variable 145, which appears to be a blend of two stars in my images, neither of which displays variability. The additional RR Lyrae stars are all located in the central region of the cluster. The RRab stars have intensity-weighted mean magnitudes of  $\langle V \rangle = 19.331 \pm 0.016$  and  $\langle B \rangle = 19.751 \pm 0.020$ , while the mean magnitudes for the RRc stars are  $\langle V \rangle = 19.305 \pm 0.019$  and  $\langle B \rangle = 19.617 \pm 0.023$ . Walker found  $\langle V \rangle = 19.33 \pm 0.02$  and  $\langle B \rangle = 19.71 \pm 0.02$  for the RRab stars while the RRcs had  $\langle V \rangle = 19.32 \pm 0.02$  and  $\langle B \rangle = 19.62 \pm 0.02$ , which are in good agreement with my results. The stars with a large discrepancy from Walker's photometry are discussed in detail in subsection 5.2.2.

There were no significant differences between my periods and those calculated by Walker (1992b). V33 was the only star, that did not turn out to be a misclassified RRd, to display a difference in period greater than 0.01 days. Walker found a period

of 0.38250 days while I found a period of 0.27841 days. A period search was run on Walker's light curve for this star and a secondary signal for a period around 0.27 days was found, suggesting that this disagreement in periods is due to aliasing in Walker's light curve. The accuracy of the periods determined by both Walker and myself is not high enough to allow for the identification of any change in period for the RR Lyrae stars.

#### 5.2.2 Comments on Individual RR Lyrae Stars

V18, Walker 110, is listed as an unclassified variable. V18 is slightly brighter than the horizontal branch but is very red, B - V = 1.27. It has a period of 0.48 days and an amplitude of 0.15 mag in V. Walker (1992b) noted that in his images this star had an elongated shape that suggested an unresolved companion. My images also show this star to be elongated.

Periods were unable to be determined for V44 (Walker 75) and V12 (Walker 146) due to not having enough data points for accurate period determination. These two RRab stars were not detected in all images, but the shape of the partial light curves is entirely consistent with their classification as RRab stars.

V41 was classified only as a candidate RR Lyrae star due to aliasing issues which prevented us from determining a period or classification as RRab or RRc. Walker (1992b) was unable to measure this star due to its proximity to a brighter star.

Not enough observations were obtained to definitively determine if any of the RR Lyrae stars have the Blazhko effect. However, based on the scatter in their light curves, V1, V4, V6, V8, V14, V35, and V50 are potential Blazhko stars. V55 and V61 also show scatter in their light curves that could be due to the Blazhko effect, but these two stars are located in the crowded region near the cluster center so the scatter could also be due to contamination.

V40 features a light curve that has a fair amount of scatter as well as a shape that

is unusually symmetric for an RRab star. Despite its unusual shape, the light curve was best fit with a period of 0.536 days and thus is tentatively classified as an RRab.

#### 5.2.3 RRD STARS

The increased number of observations (over Wesselink (1971) Walker (1992b)) allowed for the identification of eight RRd stars in NGC 1466. Table 5.4 lists the identified RRd stars, their fundamental mode and first overtone periods (in days) and amplitudes, and their period ratios. Periods were calculated using the period04 program (Lenz & Breger, 2005). The periods are typically good to  $\pm 0.0001$  or 0.0002 days.

Six of the RR Lyrae identified by Walker (1992b) turned out to be RRd stars. Five were originally identified as RRc stars and one as an RRab. V2, V3, V24, and V25 all have first overtone periods that agree with the RRc period that was found by Walker. V7 was previously classified as an RRc with a period of 0.34925 days; however, a first overtone period of 0.3615 days was obtained. Walker classified V29 as an RRab star with a period of 0.56030 days, which does not correspond with either the fundamental or first overtone period that I found.

Table 5.4: Photometric Parameters for the RRd Variables in NGC 1466

ID	Type	$P_0$ (d)	$P_1$ (d)	$P_1/P_0$	$A_{V,0}$	$A_{V,1}$	$A_{B,0}$	$A_{B,1}$	$\langle V \rangle$	$\langle B \rangle$	$\langle B - V \rangle$
V2	RRd	0.4751	0.3534	0.7451	0.12	0.42	0.15	0.53	19.375	19.758	0.389
V3	RRd	0.4717	0.3505	0.7431	0.13	0.41	0.15	0.53	19.368	19.779	0.416
V7	RRd	0.4859	0.3615	0.7440	0.35	0.43	0.42	0.52	19.326	19.642	0.310
V10	RRd	0.4730	0.3518	0.7437	0.26	0.48	0.30	0.52	19.425	19.797	0.370
V24	RRd	0.4938	0.3675	0.7442	0.12	0.43	0.15	0.60	19.292	19.642	0.357
V25	RRd	0.4715	0.3508	0.7440	0.20	0.44	0.40	0.65	19.360	19.705	0.350
V29	RRd	0.4824	0.3589	0.7440	0.45	0.58	0.36	0.38	19.428	19.750	0.320
V47	RRd	0.4733	0.3519	0.7435	0.42	0.58	0.48	0.60	19.410	19.760	0.350

Of the two new RRd stars, V10 was thought to be a potential variable by Wesselink (1971). Walker (1992b) did not classify this star as a variable due to its proximity to a blue HB star, which made observations difficult.

Figure 5.6 shows the ratio of the first overtone period to the fundamental mode period vs fundamental period, Petersen diagram (Petersen, 1973), for the RRd stars in NGC 1466; the RRd stars in the LMC field (Soszyński et al., 2003) are also plotted. The NGC 1466 RRd stars fall in the same area of the Petersen diagram as the majority of the LMC field stars. This is the same region where RRd stars in Milky Way Oosterhoff-I clusters tend to fall (see, e.g., Fig. 1 in Popielski et al. (2000), and Fig. 13 in Clementini et al. (2004)).

#### 5.2.4 Other Variables

Two long-period variables, V53 and V65, were found in NGC 1466. Periods were unable to be determined for either of these stars; in fact, I do not have observations of them over a long enough period of time to say for sure that their variability is periodic. Both stars are located near the tip of the giant branch on the CMD, as can be seen in Figure 5.1, and have several possible period solutions in the range of 60 to 90 days.

V32 (Fig. 5.7) appears to be a potential Anomalous Cepheid (AC), having an average V luminosity that is approximately 1.2 magnitudes brighter in V than the RR Lyrae stars. The star has a possible period of either 0.331 days or 0.497 days. The 0.497 day period would be consistent with the period-luminosity diagram for ACs from Pritzl et al. (2005a). Based on Equations 2 through 5 in Pritzl et al. (2002) and the distance modulus that I derive for NGC 1466 from the RR Lyrae stars, V32 would most likely be a first overtone pulsator. If the 0.331 day period is correct, the star would be too bright to be an AC, based on the period-luminosity diagram,

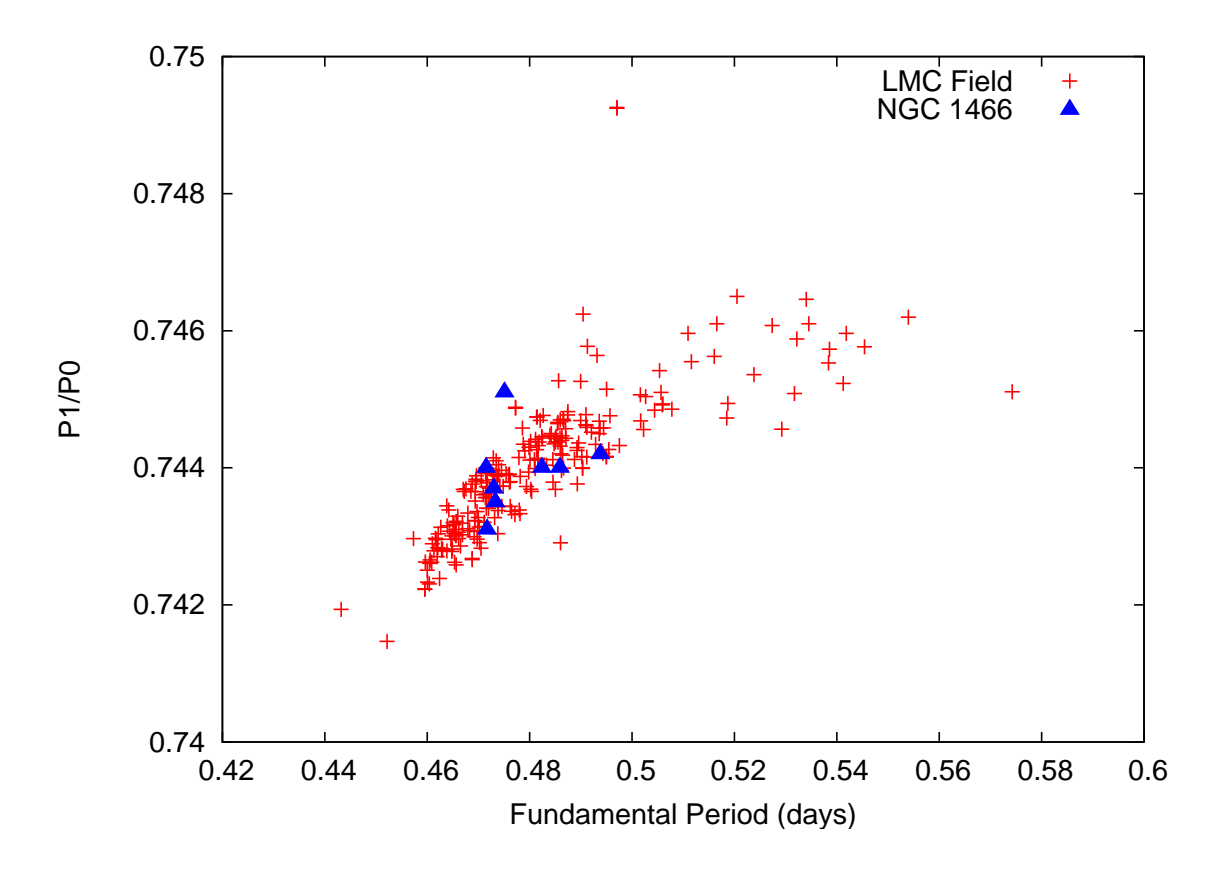


Figure 5.6: Petersen diagram showing the ratio of the first overtone period to the fundamental mode period vs. fundamental mode period for the RRd stars in the cluster (blue triangles). Also plotted are the RRd stars in the LMC field (red plus symbols) from Soszyński et al. (2003).

and would most likely be a foreground RR Lyrae. The shape of V32's light curve is similar to an RRab star, which would be inconsistent with a 0.331 day period. Based on this I feel that the 0.497 day period is correct and that this star is either an AC or, less likely, a foreground RRab.

Nine variables of unknown classification were found. Of these stars, 4 were only found by ISIS as they were either located in the crowded cluster center (V31, V51, and V54) or near the bright star in the southeast corner of the images (V67). Thus their light curves are in differential fluxes, which does not allow positive classifications to be obtained. While periods and light curve shape can be used to determine potential classifications, without having a magnitude it is not possible to distinguish between

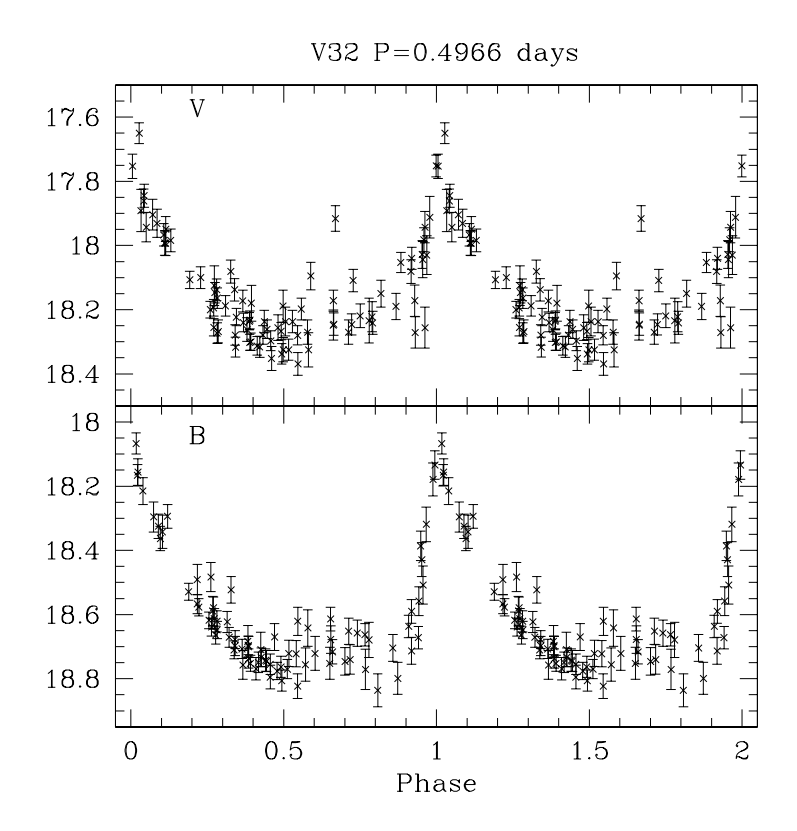


Figure 5.7: Light curve for the potential Anomalous Cepheid in NGC 1466.

a cluster RR Lyrae, a foreground RR Lyrae, or an AC. Notes on the other stars with unknown classification follow.

- V34 (Walker 129) is about one magnitude brighter than the horizontal branch and has a B-V=0.70. Wesselink (1971) had labeled this star as a variable but Walker (1992b) considered it a constant RHB star. The period, 0.61594 days, and light curve shape of this star suggest that it could be an RRab star whose color and brightness are affected by contamination.
- Star V59 is located in the cluster center and has an ISIS light curve that suggests several possible periods. The light curves from Daophot photometry suggest that it has a similar color to the RR Lyrae stars but is about one magnitude brighter; this is possibly due to contamination, but V59 displays a B to V amplitude ratio that is similar to the other RR Lyraes in the cluster (Fig. 5.8). V59 could also potentially

be an AC or a Type II Cepheid.

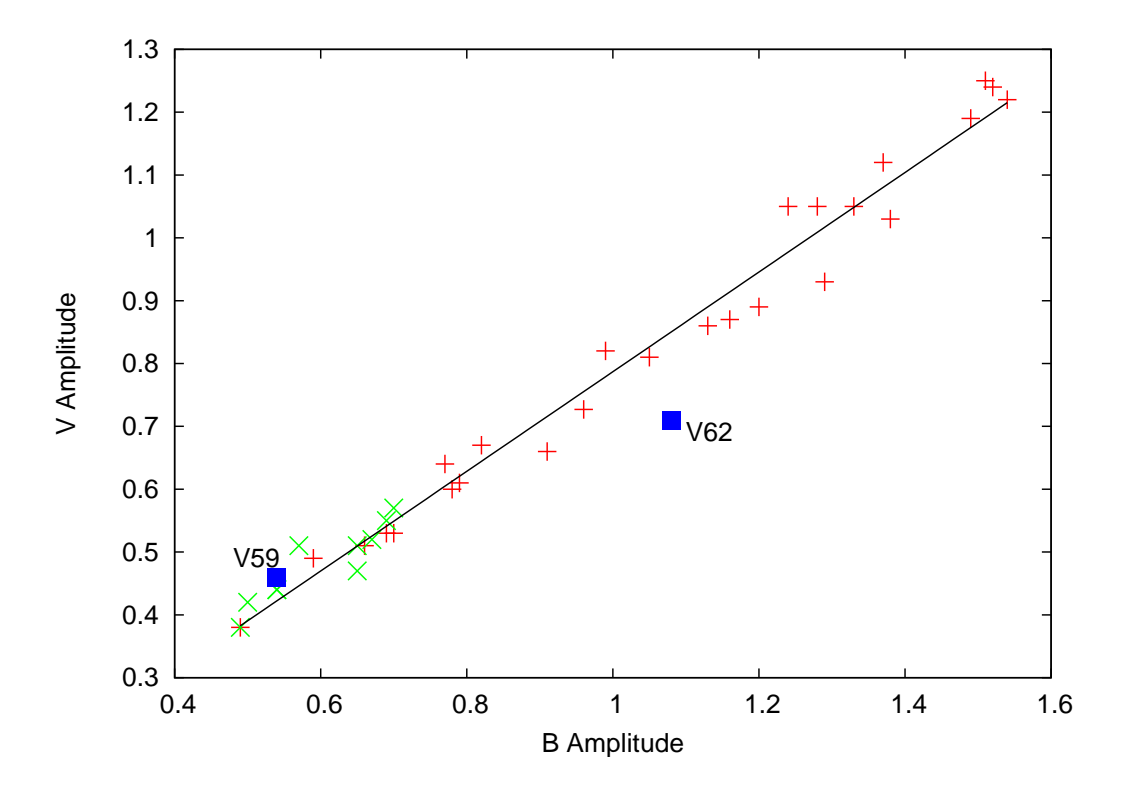


Figure 5.8: V vs B amplitudes for the RRab stars (plus symbols) and RRc stars (crosses). Also plotted are two of the variables of unknown classification (labeled squares) for purposes of determining if they are RR Lyrae stars that are affected by blending. V59 follows the trend of the RR Lyrae stars, suggesting that it is not blended, while V62 departs from this trend, supporting the explanation that it is blended (see discussion in section 3.3). The plotted line shows the relationship between V and B amplitudes for NGC 2257 (Nemec et al., 2009), an Oo-int globular cluster in the LMC. The agreement between this line and the RR Lyrae stars in NGC 1466 suggests a similarity between Oo-int globular clusters, though we cannot rule out that this relationship exists regardless of Oosterhoff type.

- V60 is located in the crowded cluster center and has a clean ISIS light curve that suggests a period of 0.522 days. The light curve from Daophot suggests a luminosity approximately two magnitudes brighter than the RR Lyrae stars but the light curve is messy, possibly due to blending.
- Star V62 is located in the cluster center and has a light curve that suggests that it is a variable with a period near 0.5 days. The period and the light curve shape suggest that V62 is possibly an RR Lyrae but the light curve is messy and it is

brighter than the other RR Lyrae stars, likely due to contamination by nearby stars. The contamination explanation is supported by the fact that V62 has a B amplitude that is slightly too large for its V amplitude, compared to the RR Lyrae stars in NGC 1466 (Fig. 5.8.

## 5.3 Physical Properties of the RR Lyrae Stars

Physical properties for the RR Lyrae stars were determined using the Fourier decomposition parameters with the empirical relations described in Chapter 4. For this Fourier decomposition analysis, 13 RRab and 7 RRc light curves were used. Tables 5.5 and 5.6 give the amplitude ratios,  $A_{j1} = A_j/A_1$ , and phase differences,  $\phi_{j1} = \phi_j - j\phi_1$ , for the low-order terms (j = 2, 3, 4), and the number of terms used in the Fourier fit, for the RRab and RRc stars, respectively. For the RRab stars, the Jurcsik-Kovács  $D_m$  value (Jurcsik & Kovács, 1996) is also listed. The  $D_m$  value helps to separate RRab stars with "regular" light curves from those with "anomalous" light curves, with lower  $D_m$  values representing more "regular" light curves. Tables 5.7 and 5.8 give the physical properties of the RRab and RRc stars, respectively.

Table 5.5: Fourier Coefficients for RRab Variables

ID	$A_1$	$A_{21}$	$A_{31}$	$A_{41}$	$\phi_{21}$	$\phi_{31}$	$\phi_{41}$	$D_{max}$	Order
V4	0.346	0.498	0.301	0.155	2.16	4.77±0.18	1.12	30.46	8
V5	0.243	0.380	0.361	0.206	2.31	$5.12 \pm 0.21$	1.69	49.89	8
V6	0.422	0.322	0.303	0.174	2.68	$5.30 \pm 0.27$	1.83	9.62	6
V8	0.349	0.402	0.324	0.194	2.47	$5.02 \pm 0.37$	1.39	40.96	7
V9	0.463	0.416	0.244	0.099	2.30	$4.52 \pm 0.17$	1.10	7.63	7
V14	0.355	0.440	0.351	0.205	2.25	$4.84 \pm 0.14$	1.34	14.33	9
V19	0.252	0.432	0.177	0.117	1.94	$4.93 \pm 0.37$	1.17	6.53	7
V20	0.363	0.502	0.356	0.271	2.26	$4.99 \pm 0.09$	1.26	45.97	6

Table 5.5 (continued)

ID	$A_1$	$A_{21}$	$A_{31}$	$A_{41}$	$\phi_{21}$	$\phi_{31}$	$\phi_{41}$	$D_{max}$	Order
V23	0.424	0.456	0.361	0.237	2.25	$4.66 \pm 0.08$	1.04	47.39	10
V26	0.367	0.369	0.249	0.139	2.26	$4.80 \pm 0.19$	0.78	34.99	7
V30	0.232	0.457	0.305	0.153	2.36	$5.22 \pm 0.34$	1.93	23.20	10
V42	0.204	0.411	0.251	0.098	2.46	$5.51 \pm 0.16$	2.20	10.83	10
V56	0.276	0.400	0.282	0.135	2.50	$5.38 \pm 0.12$	1.67	5.31	8

Table 5.6: Fourier Coefficients for RRc Variables

ID	$A_1$	$A_{21}$	$A_{31}$	$A_{41}$	$\phi_{21}$	$\phi_{31}$	$\phi_{41}$	Order
V22	0.272	0.179	0.085	0.067	4.67	$2.55 \pm 0.30$	0.89	6
V28	0.276	0.252	0.103	0.126	4.73	$3.15 \pm 0.37$	1.55	6
V33	0.246	0.255	0.039	0.011	4.38	$2.72 \pm 0.75$	4.95	8
V38	0.228	0.114	0.064	0.028	4.58	$4.16 \pm 0.57$	1.74	6
V45	0.199	0.090	0.042	0.055	4.41	$2.71 \pm 0.79$	1.53	6
V57	0.222	0.139	0.080	0.045	4.71	$3.97 \pm 0.60$	2.01	7
V66	0.259	0.181	0.090	0.033	4.30	$3.93 \pm 0.54$	3.24	9

Table 5.7: Derived Physical Properties for RRab Variables

ID	$[\mathrm{Fe/H}]_{\mathrm{J95}}$	$\langle M_V \rangle$	$\langle V - K \rangle$	$\log T_{\rm eff}^{\langle V-K\rangle}$	$\langle B-V \rangle$	$\log T_{\rm eff}^{\langle B-V\rangle}$	$\log T_{\rm eff}^{\langle V-I\rangle}$
V4	-1.717	0.748	1.164	3.805	0.336	3.810	3.811
V5	-1.278	0.824	1.153	3.805	0.365	3.804	3.802
V6	-0.764	0.828	1.008	3.819	0.313	3.825	3.818

Table 5.7 (continued)

ID	$[\mathrm{Fe/H}]_{\mathrm{J95}}$	$\langle M_V \rangle$	$\langle V - K \rangle$	$\log T_{\rm eff}^{\langle V-K\rangle}$	$\langle B-V \rangle$	$\log T_{\rm eff}^{\langle B-V\rangle}$	$\log T_{\rm eff}^{\langle V-I\rangle}$
V8	-1.085	0.846	1.054	3.815	0.330	3.817	3.813
V9	-1.774	0.736	1.125	3.810	0.295	3.824	3.825
V14	-1.577	0.762	1.149	3.806	0.338	3.811	3.811
V19	-1.725	0.749	1.209	3.800	0.354	3.804	3.805
V20	-1.511	0.737	1.139	3.807	0.341	3.810	3.810
V23	-1.434	0.810	1.064	3.815	0.314	3.821	3.819
V26	-1.359	0.823	1.057	3.816	0.317	3.820	3.818
V30	-1.759	0.679	1.292	3.791	0.378	3.795	3.797
V42	-1.056	0.805	1.175	3.802	0.374	3.802	3.799
V56	-1.155	0.775	1.136	3.806	0.357	3.807	3.804
Mean	-1.400	0.779	1.133	3.808	0.339	3.812	3.810
$\sigma$	0.088	0.013	0.021	0.002	0.007	0.003	0.002

Table 5.8: Derived Physical Properties for RRc Variables

ID	$[\mathrm{Fe}/\mathrm{H}]_{\mathrm{ZW84}}$	$\langle M_V \rangle$	$M/M_{\odot}$	$\log(L/L_{\odot})$	$\log T_{\mathrm{eff}}$	Y
V22	-1.970	0.657	0.724	1.762	3.859	0.254
V28	-1.669	0.591	0.611	1.713	3.864	0.272
V33	-1.420	0.788	0.633	1.675	3.871	0.281
V38	-1.419	0.696	0.495	1.693	3.864	0.284
V45	-1.764	0.720	0.672	1.724	3.864	0.266
V57	-1.614	0.666	0.526	1.715	3.862	0.276
V66	-1.425	0.711	0.515	1.690	3.865	0.283
Mean	-1.612	0.690	0.597	1.710	3.86	0.274

table 5.8 (continued)

ID	$[{ m Fe/H}]_{ m ZW84}$	$\langle M_V \rangle$	$M/M_{\odot}$	$\log(L/L_{\odot})$	$\log T_{ m eff}$	Y
$\sigma$	0.079	0.023	0.033	0.011	0.001	0.004

The mean metallicity of the NGC 1466 RRab stars is  $[Fe/H]_{J95} = -1.40 \pm 0.09$ which in the Zinn & West scale is  $[Fe/H]_{ZW84} = -1.59 \pm 0.06$ . The mean metallicity of the RRc stars is  $[Fe/H]_{ZW84} = -1.61 \pm 0.08$ , which is in good agreement with the value obtained for the RRab stars. Previously published metallicities for NGC 1466 showed a wide range of values. Olszewski et al. (1991) reported a metallicity of Fe/H= -2.17 based on spectroscopic observations of the calcium triplet in two giant stars in the cluster whose individual metallicities were [Fe/H] = -1.85 and -2.48. Walker (1992b) argued that the more metal-poor of these two stars was not a cluster member, and instead reported the cluster metallicity was [Fe/H] = -1.85, which is based on the remaining star from Olszewski et al. Walked reported that this metallicity was supported by comparisons of the RR Lyrae stars and the cluster CMD to that of other clusters. Wolf et al. (2007) used stellar popular synthesis models to find metallicities of [Fe/H] = -1.30 and -2.00, depending on whether they used the full spectrum or just the CN spectrum. A more metal poor result of [Fe/H] = -2.25 was adopted by Mackey & Gilmore (2003) for their work with cluster surface brightness profiles. A far more metal rich value of [Fe/H] = -1.64 was found by Santos & Piatti (2004) using the equivalent widths of metal lines in integrated spectra. My value of [Fe/H] = -1.59is most consistent with the Santos & Piatti result.

## 5.4 Distance Modulus

The absolute magnitude for the RR Lyrae stars is obtained by using the absolute magnitude-metallicity relation for RR Lyrae stars by Catelan & Cortés (2008).

The average of the Fourier derived metallicities for the RRab and RRc stars is  $[Fe/H]_{ZW84} = -1.60 \pm 0.05$ , which gives an absolute magnitude of  $M_V = 0.62 \pm 0.14$ . The average apparent magnitude of the RRab and RRc stars are  $\langle V \rangle = 19.331 \pm 0.02$  and  $\langle V \rangle = 19.305 \pm 0.02$ , respectively. Since the average magnitude for the RRab and RRc stars are essentially the same, I combine them for the purpose of calculating the distance, resulting in an average magnitude of  $\langle V \rangle = 19.324 \pm 0.013$ . Using the reddening value of  $E(B-V) = 0.09 \pm 0.02$  from Walker (1992b) and a standard extinction law with  $A_V/E(B-V) = 3.1$ , a reddening-corrected distance modulus of  $(m-M)_0 = 18.43 \pm 0.15$  is obtained. This distance modulus is approximately equal to the distance modulus of  $(m-M)_{LMC} = 18.44 \pm 0.11$  that Catelan & Cortés (2008) derived for the LMC.

## 5.5 Oosterhoff Classification

The average periods for the RR Lyrae stars in NGC 1466 are  $\langle P_{ab} \rangle = 0.591$  days and  $\langle P_c \rangle = 0.335$  days. I found 30 RRab, 11 RRc, and 8 RRd stars, giving the cluster a  $N_{c+d}/N_{c+d+ab} = 0.39$ . All three of these values are consistent with an Oosterhoff-intermediate (Oo-int) classification for NGC 1466. The minimum period for RRab stars has also been shown to be a good indicator of Oosterhoff class. NGC 1466 has a minimum period for RRab stars of  $P_{ab,min} = 0.4934$  days, which is consistent with it being an Oo-int object (Section 9.2).

Another indicator of Oosterhoff status is the position of the RR Lyrae stars in the Bailey diagram. Figures 5.9 and 5.10 show the Bailey (period-amplitude) diagrams for NGC 1466 for both the V-band amplitudes and B-band amplitudes. The typical location of the RRab and RRc stars in Oosterhoff I (Oo-I) and II (Oo-II) clusters are indicated by red and green lines, respectively (Cacciari et al., 2005; Zorotovic et al., 2010). In both diagrams the RRab stars display a wide scatter. Many are located between the Oo-I and O-II loci, which is consistent with an Oo-int object. However,

there is a significant number of RRab stars that are clustered around the Oo-I line, which is more typical for an Oo-I object. The RRc stars fall almost exclusively between the reference lines, as is expected for an Oo-int object.

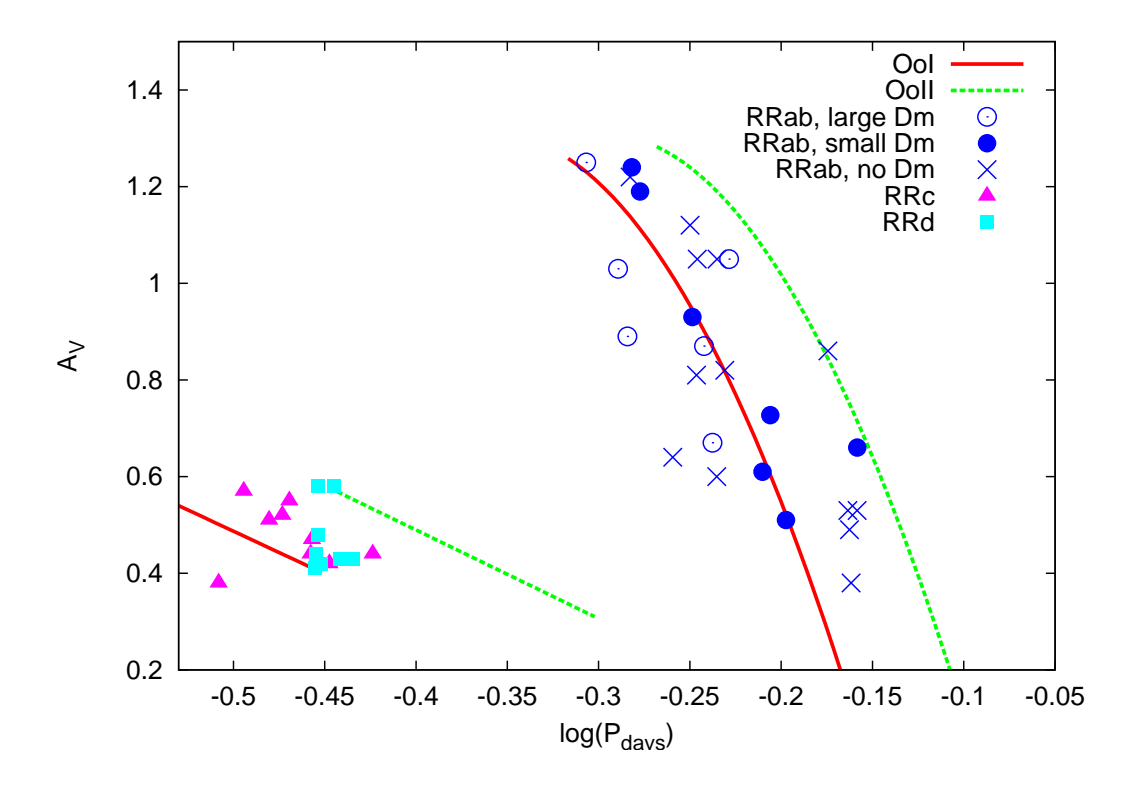


Figure 5.9: Bailey diagram, log period vs V-band amplitude, for the RR Lyrae stars in NGC 1466. Red and green lines indicate the typical position for RR Lyrae stars in Oosterhoff I and Oosterhoff II clusters, respectively (Cacciari et al., 2005; Zorotovic et al., 2010). RRab stars with a value of  $D_m < 25$  are indicated with filled circles, those with a  $D_m > 25$  are indicated with open circles, and the RRab stars for which a good Fourier fit was not obtained are indicated by crosses.

The horizontal branch type of a cluster is another tool that is useful for determining its Oosterhoff classification. The HB type is a measure of the distribution of the stars on the horizontal branch and is defined as HB type= (B-R)/(B+V+R) where B is the number of stars on the horizontal branch that are located blueward of the instability strip, R is the number of stars located redward of the instability strip, and V is the number of variable stars on the horizontal branch. Large values indicate a horizontal branch whose stars trend more toward the blue. I found an HB type of

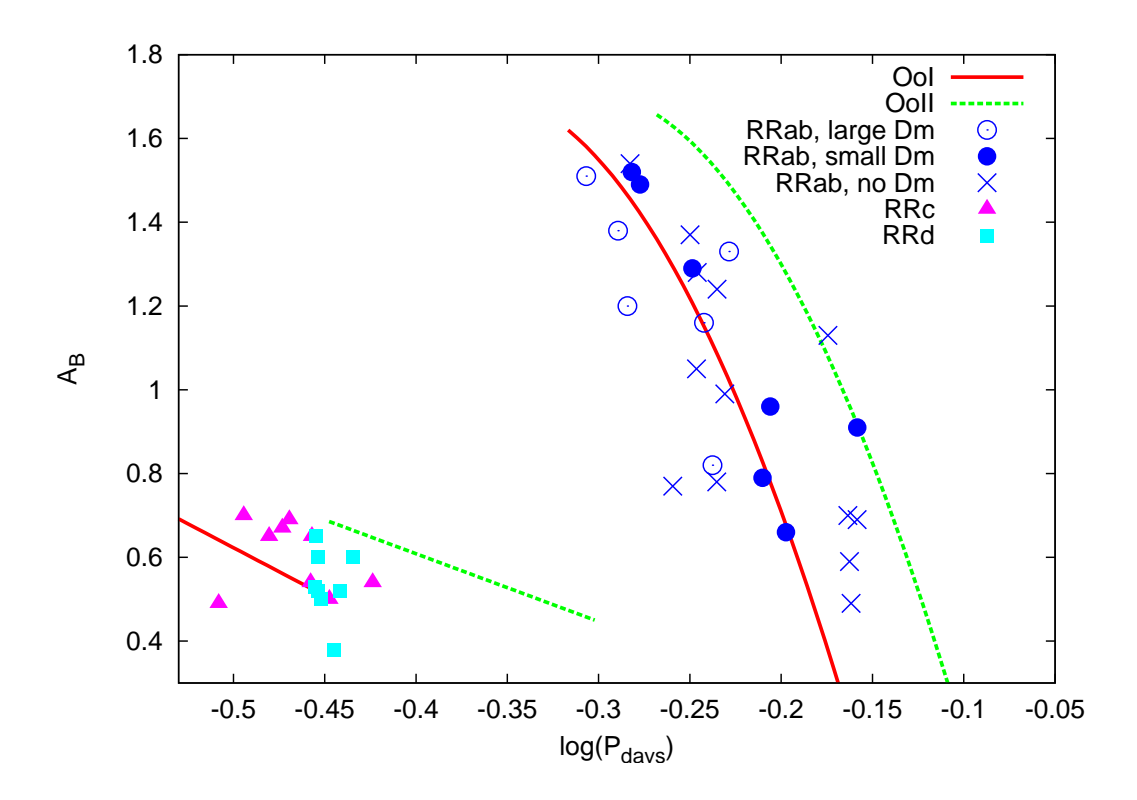


Figure 5.10: Bailey diagram, log period vs *B*-band amplitude, for the RR Lyrae stars in NGC 1466. Symbols are the same as in Figure 5.9

 $(B-R)/(B+V+R)=0.38\pm0.05$  for NGC 1466. This was determined using the stars in an annulus with an inner radius of 10 arcsec and an outer radius of 75 arcsec; this represented a region for which I felt the sample of the HB stars was complete. This HB type, combined with the metallicity of  $[Fe/H]\approx-1.60$  that was obtained from the RR Lyrae stars, places the cluster outside of the "forbidden region", where Oo-int objects tend to fall, in the HB type-metallicity diagram (Fig. 7 in Catelan 2009). If one used a lower metallicity similar to what was favored by Walker (1992b) or Olszewski et al. (1991), NGC 1466 would be located much closer to the forbidden region. A lower metallicity would also be consistent with the theoretical predictions by Bono et al. (1994) for Oo-int behavior, whereas the higher metallicity would indicate an HB morphology that is too red with respect to the predictions of the models (see Fig. 8 in Catelan 2009).

Figures 5.11 and 5.12 show the histograms of both the raw and the fundamental-

ized periods, respectively, for the RRab and RRc stars in NGC 1466. RRc periods are fundamentalized by adding 0.128 to the logarithm of their period (van Albada & Baker, 1973); this artificially transforms the RRc stars into RRab stars and allows for a study of the period distribution in a cluster without the effects of the transition from RRab to RRc stars. Catelan (2004a) found that a number of OoI and OoII clusters in the Milky Way have sharply peaked fundamentalized period distributions. In contrast, NGC 1466 shows a broad peak in its fundamentalized period distribution, consistent with it being an Oo-int cluster. The distribution of the raw periods for the RRab stars displays two peaks, a broad one around 0.55 days and a sharper peak at 0.70 days. This is similar to the distribution seen in NGC 1835, an Oo-int cluster, (Soszyński et al., 2003) although the shorter period peak for NGC 1466 is broader and its longer period peak occurs at a slightly longer period. Soszyński suggested that this two-peaked distribution may be an indicator of a sum of Oo-I and Oo-II characteristics, but the Bailey diagram shows no evidence of an Oo-II population.

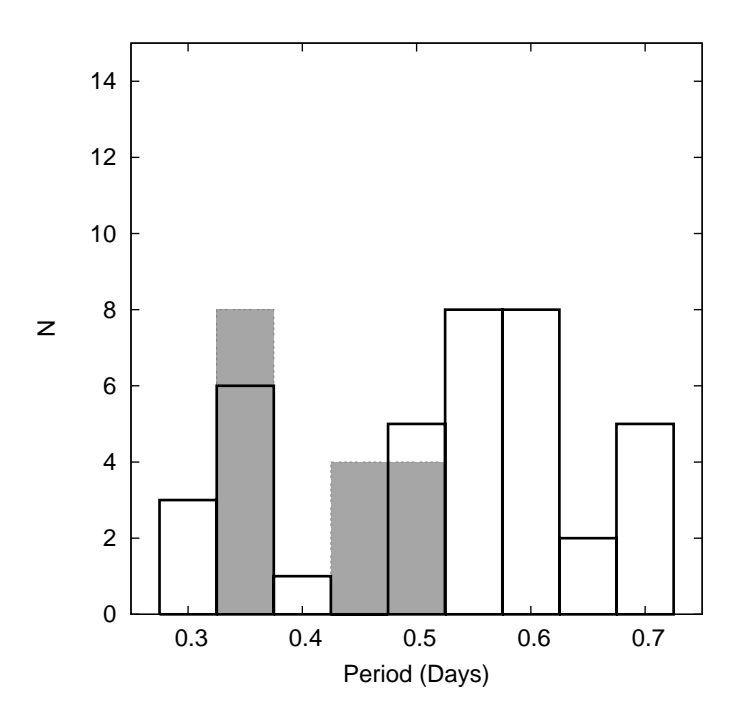


Figure 5.11: Distribution of raw periods of the RRab and RRc stars found in NGC 1466.

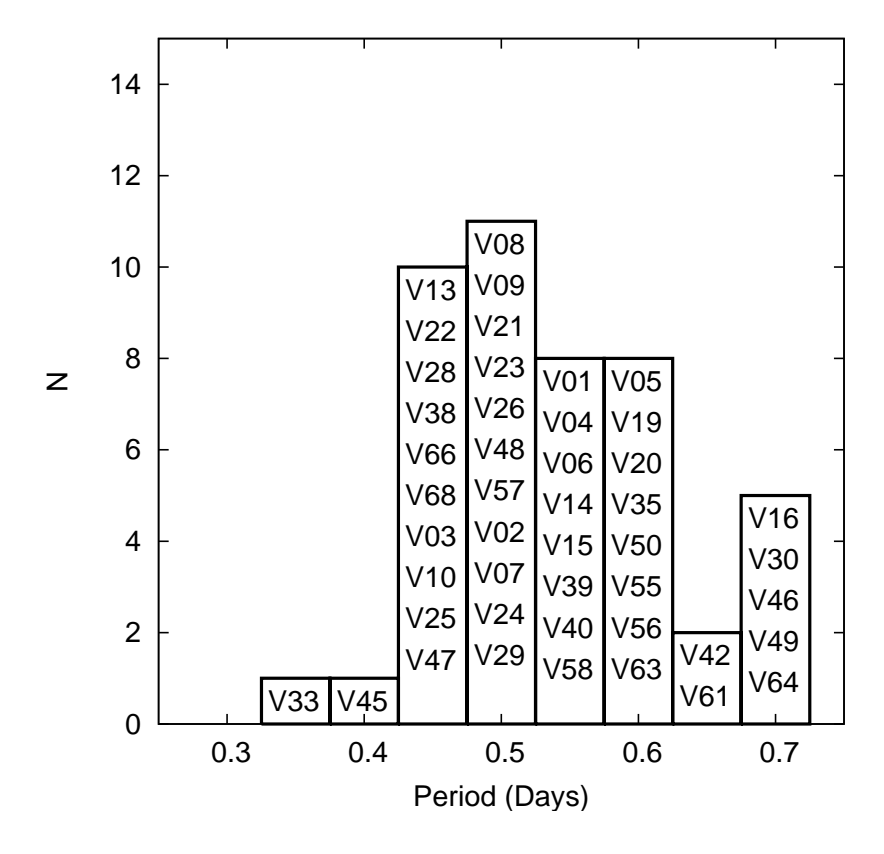


Figure 5.12: Distribution of fundamentalized periods of the RRab and RRc stars found in NGC 1466.

Tables 10.1 and 10.2 give the mean physical parameters for RRab and RRc stars, respectively, in a selection of previously studied globular clusters. The parameters that were calculated for NGC 1466 fall between those for Oo-I and Oo-II clusters, consistent with NGC 1466 having an Oo-int classification. A more thorough comparison of the physical parameters for the RR Lyrae stars in NGC 1466 and the other globular clusters in this study is carried out in Chapter 10.

# CHAPTER 6: RETICULUM

Like NGC 1466, Reticulum is an old globular cluster that is located  $\approx 11^{\circ}$  from the center of the LMC (Demers & Kunkel, 1976). It has a metal abundance of [Fe/H]  $\approx -1.66$  (Mackey & Gilmore, 2004a) and is not very reddened, E(B-V) = 0.016 (Schlegel, 1998). Mackey & Gilmore found that the age of Reticulum is similar to the ages of the oldest globular clusters in the Milky Way and the LMC, having an age that is approximately 1.4 Gyr younger than Milky Way globular cluster M3. Johnson et al. (2002) used Hubble Space Telescope observations to determine that Reticulum formed within 2 Gyr of the other old LMC clusters.

Reticulum is a sparsely populated cluster, but it does have a distinct horizontal branch that stretches across the instability strip (Figures 6.1 and 6.2). Twenty-two RR Lyrae stars were first found in the cluster by Demers & Kunkel (1976). Walker (1992a) later found an additional ten RR Lyrae stars, bringing the total in the cluster to 32; 22 RRab stars, 9 RRc's, and 1 candidate RRd. Ripepi et al. (2004) found RRd behavior in four of the RR Lyrae that had previously been discovered. No new RR Lyrae stars are expected to be found in the central regions of Reticulum since this area is uncrowded and blending is not an issue. I obtained 82 V, 72 B, and 78 I images which comprise a larger data set than the 33 BV pairs obtained by Walker, allowing me to better sample the light curves of the variable stars.

Data reduction and variable identification were carried out as described in Chapter 4. The uncrowded nature of Reticulum was ideal for Daophot's point spread function

photometry and while ISIS was run on the images for completeness, it did not find any additional variable stars. Photometry from Daophot was transformed to the standard system using the Landolt standard fields PG0231, SA95, and SA98. I compared my resulting photometry to four of the local standard stars used by Walker (1992a), finding that for these four stars my photometry was  $0.034\pm0.010$  magnitudes brighter in V and  $0.040\pm0.008$  in B. I decided not to adjust the photometry due to the relatively small number of local standards from Walker with which to compare.

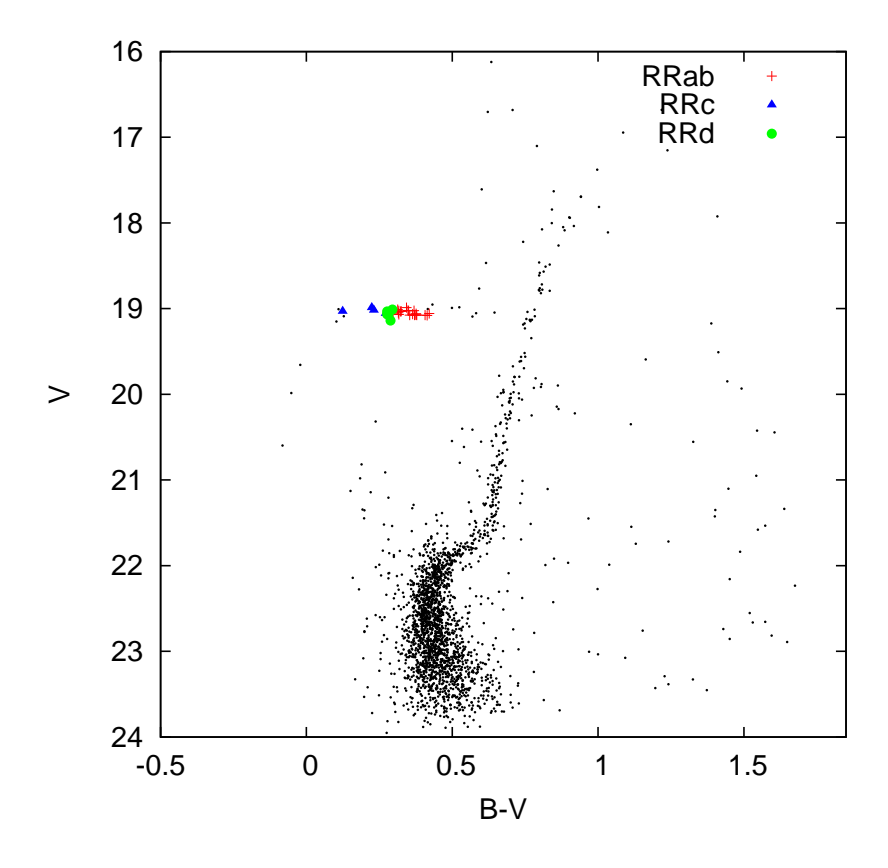


Figure 6.1: V,B-V CMD for Reticulum with the position of the RR Lyrae variables also indicated. Plus symbols indicate RRab stars, filled triangles indicated RRc's, and circles indicate RRd's.

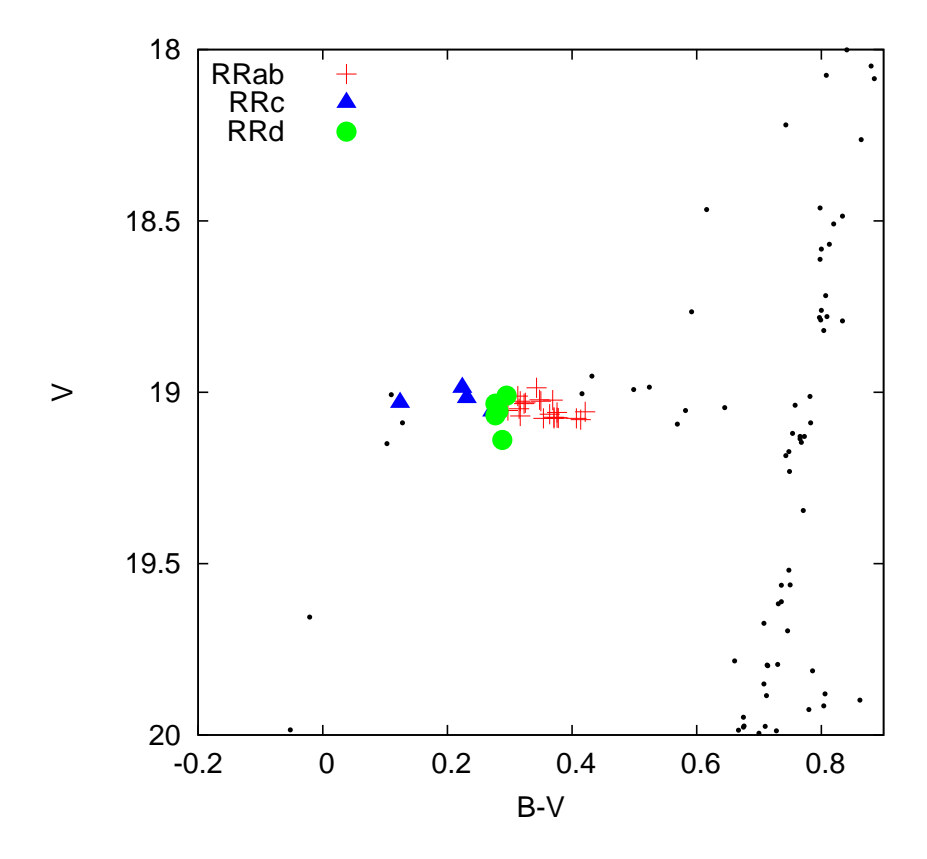


Figure 6.2: V, B-V CMD for Reticulum that is zoomed in on the horizontal branch. The symbols used are the same as in Figure 6.1

## 6.1 Variable Stars

A total of 32 RR Lyrae stars were found: 22 RRab stars, 4 RRc's, 5 RRd's, and 1 candidate RR Lyrae. The study by Walker (1992a) recovered all of these stars. The 5 RRd stars were originally classified as RRc stars by Walker but the larger number of observations in my data set allowed for the identification of them as double mode RR Lyrae. The variable stars in Reticulum, their classification, and their coordinates are listed in Table 6.1. The RRab and RRc stars and their observed characteristics (periods, V and B amplitudes, intensity-weighted V and B mean magnitudes, and magnitude-weighted mean B-V color) are listed in Table 6.2. The RRd stars, their fundamental and first overtone periods and amplitudes, their period ratios, and their mean magnitudes and color are listed in Table 6.3. Walker identified the variables

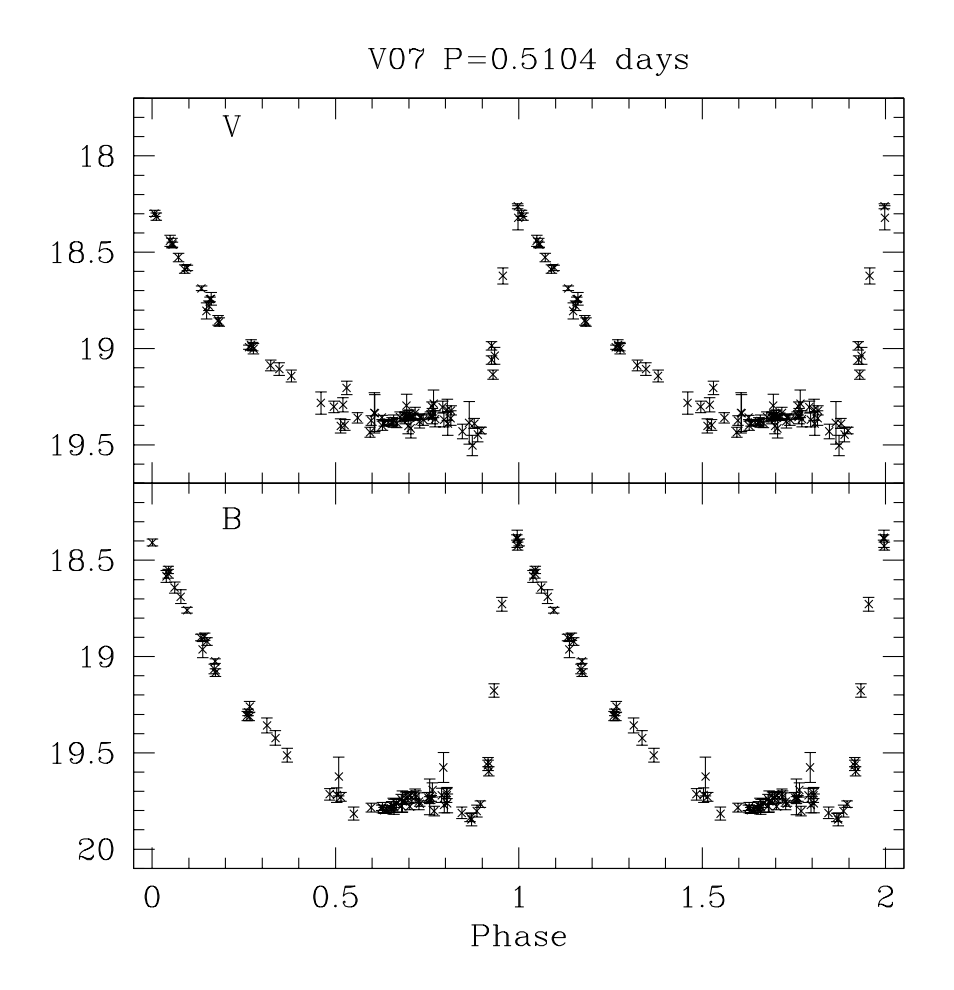


Figure 6.3: Sample light curve for RRab stars in Reticulum.

in his paper using their star number in the catalog compiled in Demers & Kunkel (1976). I introduce a new naming system that features only the variable stars and is ordered based on increasing RA. The names used by Walker are listed in the last column in Tables 6.2 and 6.3. Figures 6.3, 6.4, and 6.5 show example light curves for the RRab, RRc, and RRd stars, respectively; the full set of light curves can be found in Appendix B.

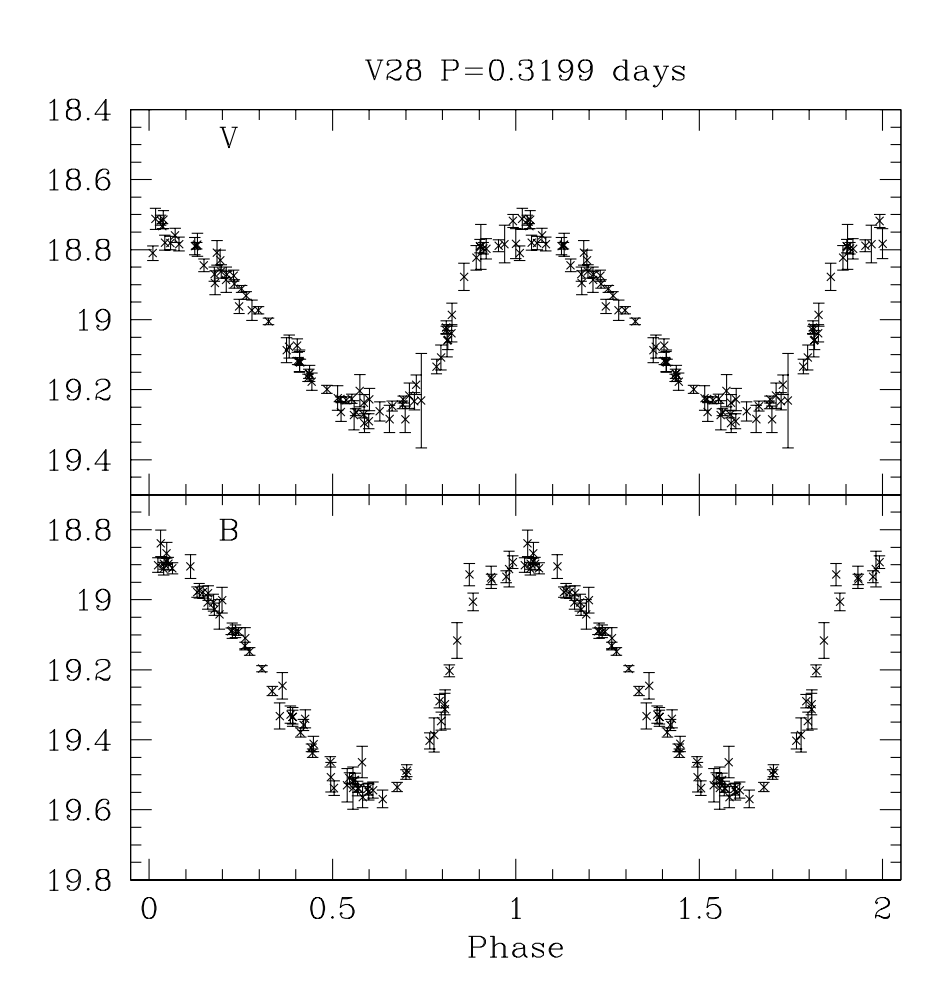


Figure 6.4: Sample light curve for RRc stars in Reticulum.

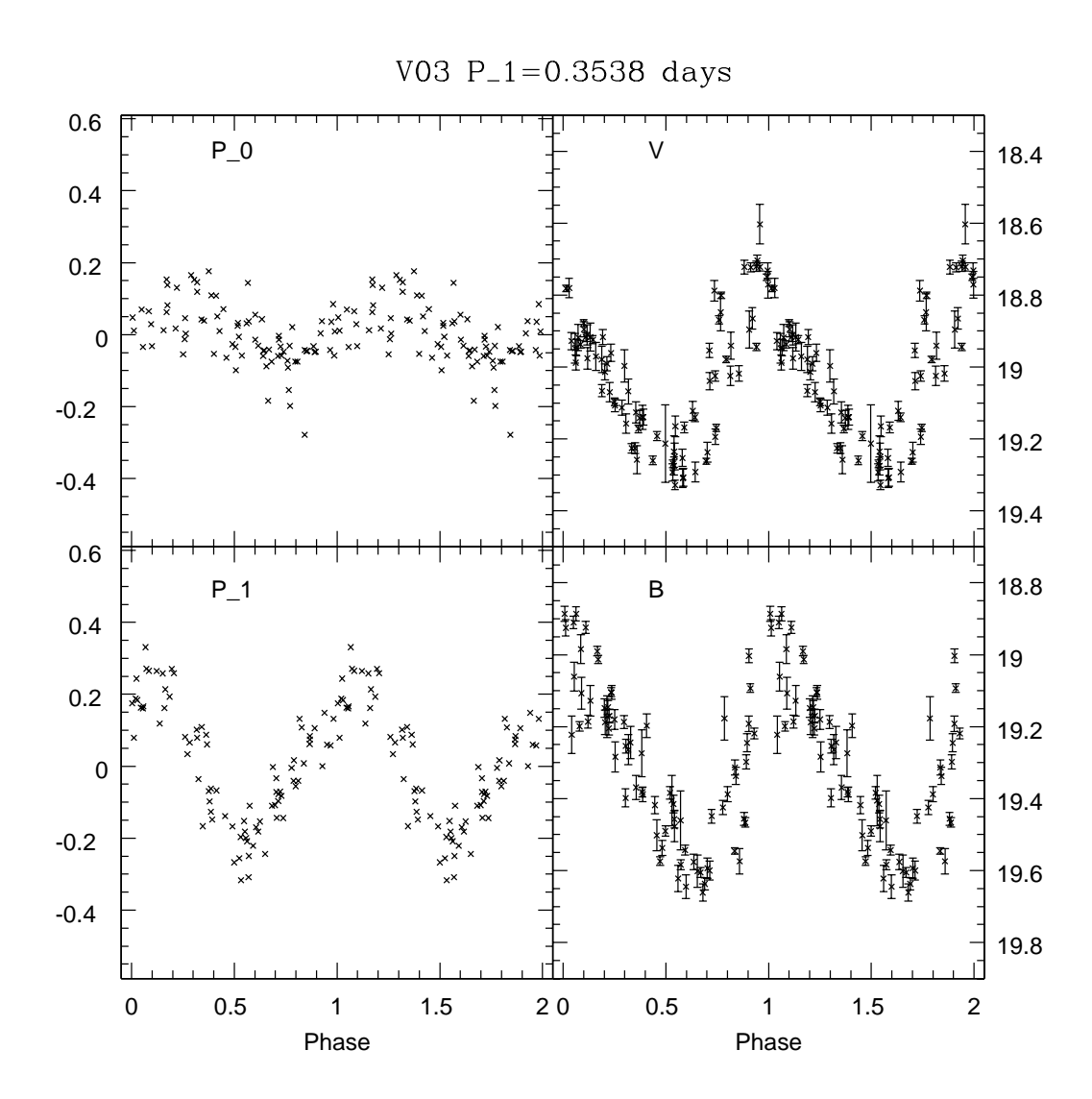


Figure 6.5: Sample light curve for RRd stars in Reticulum.

Table 6.1: Variable Stars in Reticulum

•	ID	RA (J2000)	DEC (J2000)	Type	P (days)	Other IDs
•	V01	04:35:51.4	-58:51:03.4	RRab	0.50988	DK92
	V02	04:35:56.5	-58:52:32.0	RRab	0.61868	DK7
	V03	04:35:58.6	-58:53:06.7	RRd	0.4746	DK41
	V04	04:36:00.3	-58:52:50.0	RRd	0.4748	DK4
	V05	04:36:04.1	-58:52:29.4	RRab	0.57185	DK80
	V06	04:36:05.4	-58:51:48.0	RRab	0.59529	DK97
	V07	04:36:05.5	-58:50:51.9	RRab	0.51044	DK117
	V08	04:36:05.8	-58:49:35.1	RRab	0.64495	DK135
	V09	04:36:05.9	-58:50:24.6	RRab	0.54493	DK137
	V10	04:36:06.4	-58:52:12.8	RRc	0.35257	DK77
	V11	04:36:06.4	-58:51:48.7	-	-	DK98
	V12	04:36:07.1	-58:50:55.0	RRc	0.29627	DK181
	V13	04:36:07.7	-58:51:47.0	RRab	0.60958	DK99
	V14	04:36:07.8	-58:51:44.6	RRab	0.58659	DK100
	V15	04:36:09.1	-58:52:25.9	RRd	0.4762	DK72
	V16	04:36:09.8	-58:52:50.8	RRab	0.52289	DK49
	V17	04:36:10.2	-58:53:13.7	RRab	0.51288	DK38
	V18	04:36:10.6	-58:49:50.4	RRab	0.56005	DK142
	V19	04:36:11.9	-58:49:18.2	RRab	0.48486	DK146
	V20	04:36:12.2	-58:51:23.3	RRab	0.56073	DK112
	V21	04:36:12.3	-58:49:24.5	RRab	0.60704	DK145
	V22	04:36:13.4	-58:52:32.1	RRab	0.51358	DK57
	V23	04:36:13.8	-58:51:19.3	RRab	0.46862	DK108
	V24	04:36:17.3	-58:51:26.3	RRd	0.4670	DK110

Table 6.1 (continued)

ID	RA (J2000)	DEC (J2000)	Type	P (days)	Other IDs
V25	04:36:17.4	-58:53:02.7	RRc	0.32990	DK36
V26	04:36:18.5	-58:51:52.0	RRab	0.65616	DK67
V27	04:36:18.7	-58:51:44.6	RRab	0.51383	DK64
V28	04:36:19.2	-58:50:15.7	RRc	0.31993	DK151
V29	04:36:20.1	-58:52:33.6	RRab	0.50815	DK37
V30	04:36:20.2	-58:52:47.7	RRab	0.53500	DK35
V31	04:36:24.4	-58:50:40.1	RRab	0.50517	DK25
V32	04:36:31.9	-58:49:53.2	RRd	0.4739	DK157

Table 6.2: Photometric Parameters for Variables in Reticulum, Excluding RRd Stars

ID	Type	P (days)	$A_V$	$A_B$	$\langle V \rangle$	$\langle B \rangle$	$\langle B - V \rangle$	Other IDs
V01	RRab	0.50988	1.24	-	19.051	-	-	DK92
V02	RRab	0.61868	0.67	0.87	19.076	19.432	0.371	DK7
V05	RRab	0.57185	0.95	1.13	19.059	19.413	0.376	DK80
V06	RRab	0.59529	0.92	1.10	19.064	19.412	0.364	DK97
V07	RRab	0.51044	1.21	1.53	19.026	19.304	0.317	DK117
V08	RRab	0.64495	0.48	0.64	19.080	19.486	0.414	DK135
V09	RRab	0.54493	0.76	0.91	19.011	19.310	0.313	DK137
V10	RRc	0.35257	0.43	0.56	19.056	19.321	0.272	DK77
V11	-	-	-	-	-	-	-	DK98
V12	RRc	0.29627	0.27	0.30	19.031	19.154	0.124	DK181
V13	RRab	0.60958	0.77	0.91	19.075	19.439	0.378	DK99
V14	RRab	0.58659	0.82	1.01	19.057	19.456	0.421	DK100

Table 6.2 (continued)

ID	Type	P (days)	$A_V$	$A_B$	$\langle V \rangle$	$\langle B \rangle$	$\langle B - V \rangle$	Other IDs
V16	RRab	0.52289	1.27	1.50	19.031	19.308	0.325	DK49
V17	RRab	0.51288	0.98	1.12	19.022	19.334	0.348	DK38
V18	RRab	0.56005	1.00	1.30	19.076	19.401	0.354	DK142
V19	RRab	0.48486	1.27	1.62	19.048	19.312	0.315	DK146
V20	RRab	0.56073	1.03	1.36	19.073	19.425	0.371	DK112
V21	RRab	0.60704	0.81	0.97	19.074	19.433	0.376	DK145
V22	RRab	0.51358	0.98	1.24	19.033	19.329	0.323	DK57
V23	RRab	0.46862	1.27	1.54	19.053	19.312	0.297	DK108
V25	RRc	0.32990	0.55	0.69	19.017	19.238	0.231	DK36
V26	RRab	0.65616	0.35	0.53	19.076	19.474	0.407	DK67
V27	RRab	0.51383	1.28	1.53	19.023	19.347	0.369	DK64
V28	RRc	0.31993	0.53	0.65	18.987	19.201	0.224	DK151
V29	RRab	0.50815	1.22	1.44	19.026	19.350	0.350	DK37
V30	RRab	0.53500	1.27	1.53	18.987	19.300	0.343	DK35
V31	RRab	0.50517	1.17	1.59	19.069	19.328	0.317	DK25

Table 6.3: Photometric Parameters for the RRd Variables in Reticulum

ID	Type	$P_0$ (d)	$P_1$ (d)	$P_1/P_0$	$A_{V,0}$	$A_{V,1}$	$A_{B,0}$	$A_{B,1}$	$\langle V \rangle$	$\langle B \rangle$	$\langle B - V \rangle$
V03	RRd	0.4746	0.3538	0.7455	0.18	0.42	0.21	0.51	19.010	19.306	0.295
V04	RRd	0.4748	0.3532	0.7439	0.07	0.45	0.11	0.53	19.067	19.337	0.277
V15	RRd	0.4762	0.3541	0.7435	0.30	0.35	0.42	0.42	19.139	19.425	0.288
V24	RRd	0.4670	0.3476	0.7443	0.27	0.40	0.31	0.49	19.054	19.327	0.282
V32	RRd	0.4739	0.3523	0.7434	0.08	0.41	0.12	0.53	19.033	19.302	0.277

The RRab stars have intensity-weighted mean magnitudes of  $\langle V \rangle = 19.05 \pm 0.01$  and  $\langle B \rangle = 19.38 \pm 0.01$  while the RRc stars have mean magnitudes of  $\langle V \rangle = 19.02 \pm 0.01$  and  $\langle B \rangle = 19.23 \pm 0.04$ . The results for RRab stars are brighter than the mean magnitudes of  $\langle V \rangle = 19.08 \pm 0.01$  and  $\langle B \rangle = 19.41 \pm 0.02$  found by Walker. My values for the RRc stars are also slightly brighter than Walker's mean magnitudes of  $\langle V \rangle = 19.05 \pm 0.02$  and  $\langle B \rangle = 19.28 \pm 0.04$ . These differences in brightness for the RR Lyrae stars are on the same order as, and are likely due to, the previously mentioned slight photometric disagreement between my results and those of Walker.

In general my periods agreed with those of Walker to within 0.0002 days. V08 and V19 were the only stars for which a difference in period greater than 0.01 days was found. V08 showed an increase in period of 0.012 days in my data while V19 showed a decrease of 0.016 days. These differences in period could be due to either an error in period determination in the previous studies or due to actual period changes. Period changes in RR Lyrae stars can be used to study the evolution of these stars as they move through the instability strip (Catelan, 2009a). A decrease in period indicates a blueward movement on the HR diagram while an increase in period indicates a redward move. In addition to period changes due to evolution, RR Lyrae stars are also known to undergo irregular period changes, of which the exact cause is not known. The size of these period changes is larger than expected for evolutionary period change and larger than seen in other RR Lyrae, and are thus most likely due to an error in period determination by Walker.

The first overtone periods for the RRd stars show good agreement with the periods that Walker had reported. Three of the five RRd stars (V03, V15, V24) were also found by Ripepi et al. (2004). The candidate RR Lyrae, V11, was classified as an RRd star by Ripepi et al. (2004) and in my data it displays RRd like behavior but I was unable to determine a reliable period. Figure 6.6 shows the Petersen diagram

for the RRd stars in Reticulum along with those in the field of the LMC, similar to Figure 5.6. The RRd stars for Reticulum fall in the same region of the diagram as Milky Way Oo-I clusters tend to fall (Clementini et al., 2004).

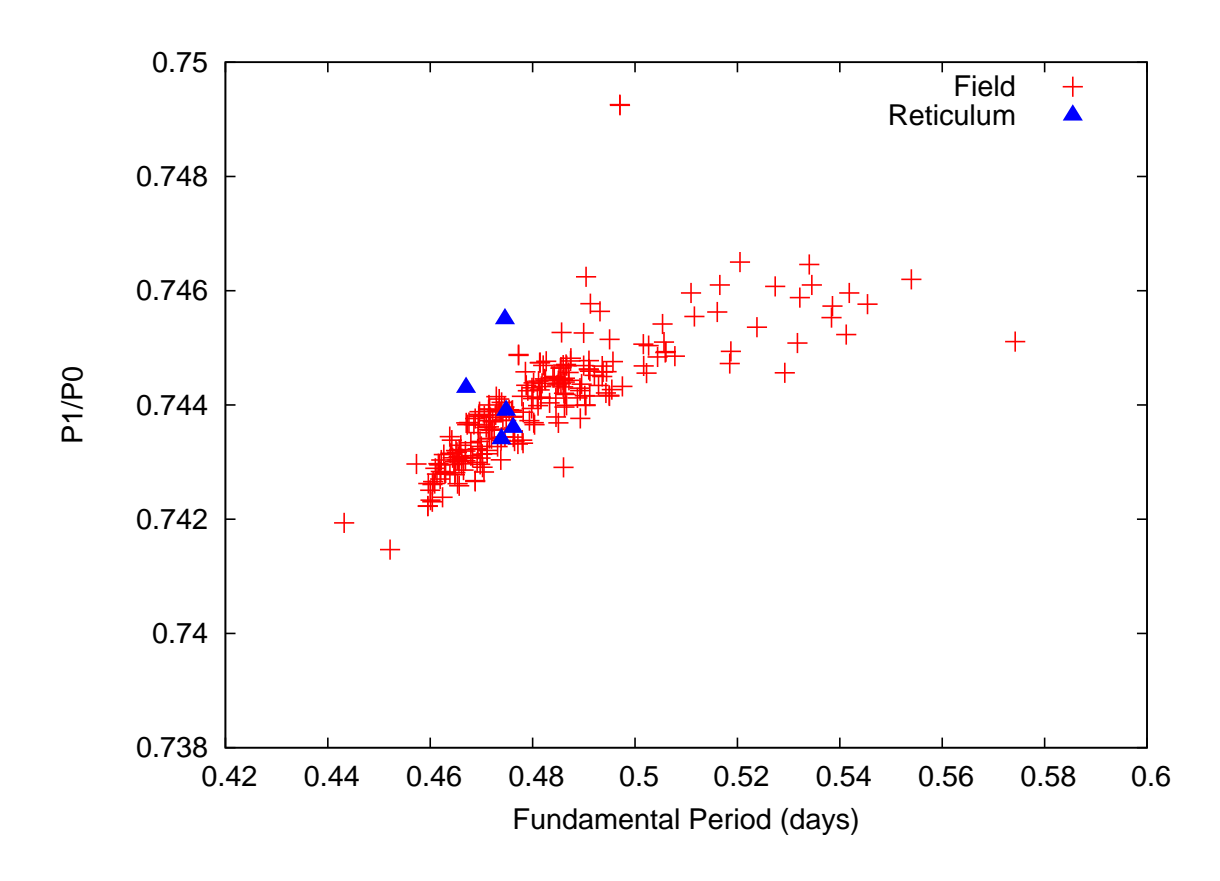


Figure 6.6: Petersen diagram showing the ratio of the first overtone period to the fundamental mode period vs. fundamental mode period for the RRd stars in Reticulum (blue triangles). Also plotted are the RRd stars in the LMC field (red plus symbols) from Soszyński et al. (2003).

# 6.2 Physical Properties of the RR Lyrae Stars

RR Lyrae physical properties were determined using the equations in Sections 4.3.2 and 4.3.3. A Fourier decomposition was performed for 12 RRab and 3 RRc light curves. Tables 6.4 and 6.5 give the Fourier coefficients for the RRab and RRc stars, respectively. The physical properties determined from these coefficients are given in Tables 6.6 and 6.7.

Table 6.4: Fourier Coefficients for RRab Variables

ID	$A_1$	$A_{21}$	$A_{31}$	$A_{41}$	$\phi_{21}$	$\phi_{31}$	$\phi_{41}$	$D_{max}$	Order
V02	0.246	0.435	0.2746	0.1546	2.5163	$5.1796 \pm 0.0881$	1.8363	10.34	7
V06	0.328	0.459	0.362	0.232	2.356	$4.941 \pm 0.092$	1.525	1.93	10
V07	0.404	0.437	0.359	0.219	2.277	$4.692 \pm 0.097$	1.023	46.09	9
V13	0.278	0.437	0.331	0.171	2.364	$5.121 \pm 0.078$	1.640	3.89	9
V14	0.301	0.388	0.300	0.185	2.473	$5.068 \pm 0.103$	1.490	48.47	9
V16	0.443	0.416	0.329	0.231	2.386	$4.918 \pm 0.074$	1.288	41.67	11
V18	0.351	0.462	0.349	0.221	2.221	$4.852 \pm 0.088$	1.320	45.79	10
V20	0.363	0.457	0.353	0.226	2.311	$4.756 \pm 0.086$	1.085	44.65	8
V21	0.281	0.499	0.326	0.195	2.311	$5.126 \pm 0.088$	1.623	2.97	7
V27	0.432	0.447	0.347	0.207	2.164	$4.599 \pm 0.062$	0.980	38.92	9
V30	0.439	0.372	0.293	0.212	2.368	$4.817 \pm 0.110$	1.309	50.98	8
V31	0.389	0.454	0.370	0.212	2.109	$4.668 \pm 0.086$	1.004	47.03	10

Table 6.5: Fourier Coefficients for RRc Variables

ID	$A_1$	$A_{21}$	$A_{31}$	$A_{41}$	$\phi_{21}$	$\phi_{31}$	$\phi_{41}$	Order
V10	0.221	0.165	0.0602	0.066	4.789	$3.712 \pm 0.491$	2.227	8
V25	0.277	0.171	0.0967	0.043	4.551	$2.873 \pm 0.174$	1.118	6
V28	0.274	0.176	0.071	0.041	4.578	$2.762 \pm 0.216$	1.640	8

The mean metallicity of the RRab stars is  $[Fe/H]_{J95} = -1.48 \pm 0.03$  which on the Zinn & West scale is  $[Fe/H]_{ZW84} = -1.65 \pm 0.02$ . This value is in good agreement with the metallicity of  $[Fe/H] \simeq -1.66$  found by Mackey & Gilmore (2004a). On the other

hand, the relation from Morgan, Wahl, & Wieckhorst (2007) gives a metallicity for the RRc stars of  $[Fe/H]_{ZW84} = -1.80 \pm 0.05$ , which is significantly more metal-poor than the values obtained from the RRab stars and the literature. While this difference in metallicity could be caused by errors in the Fourier analysis, the fact that the other physical properties obtained for the RRc stars are consistent with expectations lends support to the validity of the obtained Fourier coefficients.

Table 6.6: Derived Physical Properties for RRab Variables

ID	$[\mathrm{Fe/H}]_{\mathrm{J95}}$	$\langle M_V \rangle$	$\langle V - K \rangle$	$\log T_{\rm eff}^{\langle V-K\rangle}$	$\langle B-V \rangle$	$\log T_{\rm eff}^{\langle B-V\rangle}$	$\log T_{\rm eff}^{\langle V-I\rangle}$
V02	-1.409	0.773	1.197	3.800	0.363	3.803	3.802
V06	-1.603	0.742	1.182	3.803	0.350	3.806	3.807
V07	-1.481	0.799	1.082	3.814	0.321	3.818	3.812
V13	-1.439	0.765	1.179	3.803	0.359	3.804	3.804
V14	-1.386	0.781	1.147	3.806	0.348	3.808	3.807
V16	-1.244	0.786	1.050	3.816	0.311	3.822	3.819
V18	-1.534	0.771	1.140	3.807	0.338	3.811	3.810
V20	-1.666	0.755	1.145	3.807	0.336	3.811	3.811
V21	-1.418	0.768	1.172	3.803	0.358	3.805	3.804
V27	-1.625	0.771	1.098	3.812	0.314	3.819	3.819
V30	-1.446	0.761	1.092	3.812	0.309	3.821	3.820
V31	-1.484	0.811	1.084	3.813	0.324	3.817	3.816
Mean	-1.478	0.774	1.131	3.808	0.336	3.812	3.811
σ	0.034	0.005	0.014	0.002	0.006	0.002	0.002

Table 6.7: Derived Physical Properties for RRc Variables

ID	$[\mathrm{Fe}/\mathrm{H}]_{\mathrm{ZW84}}$	$\langle M_V \rangle$	$M/M_{\odot}$	$\log(L/L_{\odot})$	$\log T_{\mathrm{eff}}$	Y
V10	-1.701	0.646	0.558	1.724	3.861	0.271
V25	-1.864	0.691	0.666	1.742	3.861	0.261
V28	-1.826	0.702	0.674	1.735	3.862	0.263
Mean	-1.797	0.680	0.633	1.734	3.861	0.265
$\sigma$	0.049	0.017	0.038	0.005	0.001	0.006

#### 6.3 Distance Modulus

As with NGC 1466, the absolute magnitude-metallicity relationship from Catelan & Cortés (2008) is used to provide the absolute magnitude of the RR Lyrae stars in Reticulum. The disagreement between the metallicities for RRab and RRc stars raises an issue as to which metallicity to use for calculating the absolute magnitude. Since the metallicity obtained from the RRab stars is consistent with what has been reported in the literature and is drawn from a larger number of stars, that value is used,  $[Fe/H]_{ZW84} = -1.65 \pm 0.02$ . This value gives an absolute magnitude of  $M_V = 0.61 \pm 0.16$ . The average magnitude of the RRab stars,  $\langle V \rangle = 19.050 \pm 0.055$ , and the reddening value of E(B-V) = 0.016 from Schlegel (1998) are used, along with a standard extinction law of  $A_V/E(B-V) = 3.1$ , to obtain a reddening-corrected distance modulus of  $(m-M)_0 = 18.39 \pm 0.17$ . This distance modulus is the same as the value of  $18.39 \pm 0.12$  found by Ripepi et al. (2004). This is shorter than the distance modulus of  $(m-M)_{LMC} = 18.44 \pm 0.11$  that Catelan & Cortés (2008) derived for the LMC, though the two distance moduli agree within the errors. This is not necessarily a surprise as Reticulum is widely separated from the disk of the

LMC, having a location that is about 11 degrees from the center of the LMC (Walker, 1992a).

#### 6.4 Oosterhoff Classification

The average periods for the RR Lyrae stars in Reticulum are  $\langle P_{ab} \rangle = 0.552$  days and  $\langle P_c \rangle = 0.324$  days. I found 22 RRab stars, 4 RRc's, 5 RRd's, and 1 potential RRd which gives the cluster a number fraction of  $N_{c+d}/N_{c+d+ab} = 0.31$ . The average periods for the RRab and RRc stars strongly indicate an Oosterhoff I classification and, while the number fraction is high, it is still consistent with the cluster being an Oo-I object. The minimum period for an RRab star in Reticulum is  $P_{ab,min} = 0.46862$  days, which is also consistent with an Oo-I classification for Reticulum (Section 9.2).

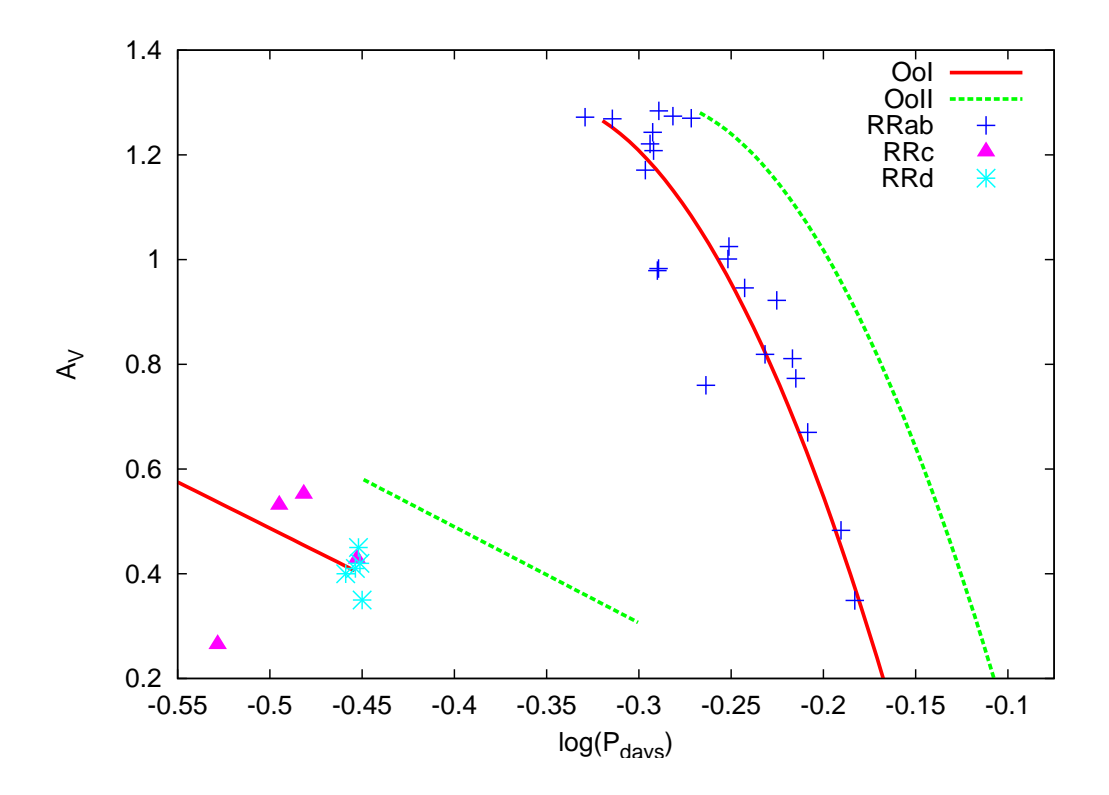


Figure 6.7: Bailey diagram, log period vs V-band amplitude for the RR Lyrae stars in Reticulum. Red and green lines indicate the typical position for RR Lyrae stars in Oosterhoff I and Oosterhoff II clusters, respectively (Cacciari et al., 2005; Zorotovic et al., 2010).

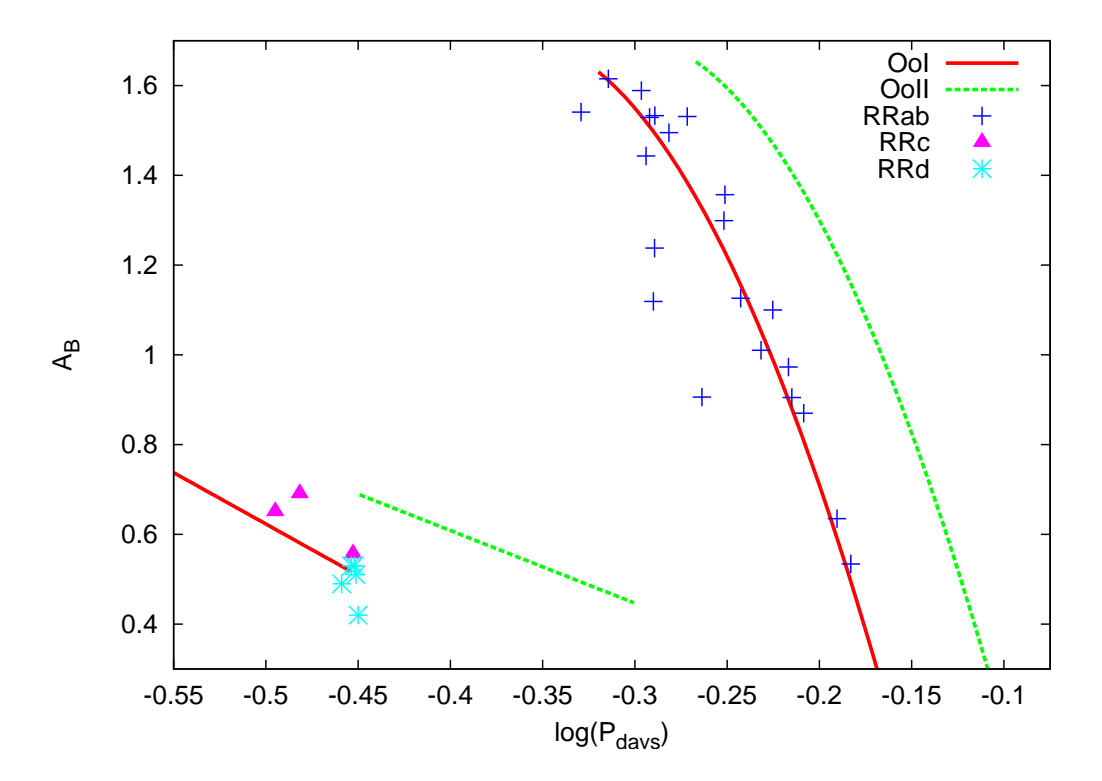


Figure 6.8: Same as Figure 6.7 except with B-band amplitudes in place of the V-band amplitudes.

Figures 6.7 and 6.8 show the V and B band period-amplitude diagrams for Reticulum. Both diagrams show that the RRab stars cluster along the line that indicates the typical location for RRab stars in Oo-I clusters. There is more scatter in the positions of the RRc stars but most of them still are located near the Oo-I locus, confirming the classification of Reticulum as an Oo-I object.

# CHAPTER 7: NGC 1786

Unlike the previous clusters discussed in Chapters 5 and 6, NGC 1786 is located near the center of the LMC. Mucciarelli et al. (2009) found a metallicity of  $[Fe/H] = -1.75 \pm 0.01$  from high-resolution spectroscopy of seven red giant stars. However, Olszewski et al. (1991) found a slightly lower value of  $-1.87 \pm 0.20$  from the low-resolution spectra of two giant stars; these values are consistent within the error bars. Sharma et al. (2010) reported that NGC 1786 is not very reddened, having an E(B-V) = 0.06, and has an age of 12.3 Gyr. This age is consistent with Johnson et al. (2002) finding that NGC 1786 formed within 2 Gyr of the other old LMC clusters through the comparison of the cluster CMD with theoretical isochrones.

NGC 1786 is a fairly centrally concentrated cluster which, combined with its location near the center of the LMC, makes it difficult to get accurate photometry of the stars in the center due to blending. Graham (1985) was the first to find variable stars in NGC 1786. Graham found 12 variables, for which he determined periods of 10. Walker & Nemec (1988) later observed NGC 1786 and confirmed the variable nature of 11 of Graham's stars, though Walker was also only able to determine periods for ten of the stars. Of the variables with known periods, 4 were classified as RRab stars, 5 as RRc stars, and one as a likely Anomalous Cepheid.

More recently the Optical Gravitational Lensing Experiment-III (OGLE-III) observed the central portion of the LMC and many of its associated globular clusters, including NGC 1786 (Udalski et al., 2008). The OGLE-III survey is designed to find

instances of gravitational lensing by looking for small changes in the brightness of stars in its field of view; a natural consequence of this project is the discovery and monitoring of variable stars. OGLE-III greatly increased the number of identified variable stars in NGC 1786. A total of 55 RR Lyrae stars within the tidal radius were reported by Soszyński et al. (2009): 28 RRab, 18 RRc, and 9 RRd stars. The location of NGC 1786 near the center of the LMC means that some of these RR Lyrae stars likely belong to the field population of the LMC and not to the cluster.

Data reduction and variable identification was carried out in the same way as the other clusters in my study. Photometry was converted to the standard system using standard stars from Stetson (2000) which were located within the field of NGC 1786. Of the 25 Stetson standard stars that appeared in my observations, the average difference between my photometry and that of Stetson is  $0.002 \pm 0.008$  mags in V and  $0.002 \pm 0.011$  mags in B. The extremely crowded nature of NGC 1786 meant that ISIS had to be used extensively to locate variable stars in the center of the cluster.

# 7.1 Variable Stars

I found 65 variable stars within the my 5.2×5.2 arcminute field of view in the direction of NGC 1786. This includes the cluster as well as the surrounding area. The variables include 36 RR Lyraes (15 RRab, 17 RRc, and 4 RRd), 15 candidate RR Lyraes, 3 classical Cepheids, 1 Type II Cepheid, 1 Anomalous Cepheid, 2 eclipsing binaries, 2 Delta Scuti variables, and 5 variables of undetermined type. The extreme crowding in the central region of NGC 1786 posed some difficulties for the identification and classification of the variable stars due to many of the stars being blended with near neighbors. Table 7.1 lists the variable stars in NGC 1786, their coordinates, and their classification while Table 7.2 lists the photometric properties for all of the variables with the exception of the RRd stars which are listed in Table 7.3. Variable stars V01 through V11 were originally found by Graham (1985) and have periods confirmed by

Walker & Nemec (1988). The names for these stars are the same as the ones used by Graham and Walker.

NGC 1786's location toward the center of the LMC means that a significant amount of contamination from LMC field stars is expected in the images. This makes it difficult to determine with absolute certainty whether an individual variable star is a member of the cluster. NGC 1786 has a tidal radius of 2 arcminutes (Bica et al., 2008) and 60 of the 65 variable stars are located within that tidal radius. The 5 stars (2 RRab stars, 1 RRc, 1 classical Cepheid, and 1 eclipsing binary) outside the tidal radius are not cluster members and they are noted in Table 7.1 with the word 'Field' after their name. The field of view in the images obtained with SOAR is  $5.2 \times 5.2$ arcminutes, thus approximately half of the image is contained within the tidal radius of NGC 1786. The LMC field should feature a roughly even distribution of variable stars, thus the majority of the 60 variables found within the tidal radius should be members of the cluster. Classical Cepheids are younger stars, thus the two classical Cepheids that are within the tidal radius of NGC 1786 should be members of the LMC field. The amount of LMC field star contamination is still significant within the tidal radius of the cluster, as can be seen in Figures 7.1 and 7.2, where the presence of the field stars makes it difficult to distinguish a horizontal branch in the CMD for NGC 1786. The scatter in the position of the RR Lyrae stars in the CMD is likely due to the crowded nature of the central region of the cluster which results in many of the RR Lyrae being partially blended with nearby stars, affecting their brightness and color.

Table 7.1: Variable Stars in NGC 1786

ID	RA (J2000)	DEC (J2000)	Type	P (days)	Ogle-III ID
V01	04:58:51.3	-67:44:23.7	AC	0.80006	ACEP-009
V02	04:58:52.623	-67:43:53.75	RRd	0.4906	RRLYR-02626

Table 7.1 (continued)

ID	RA (J2000)	DEC (J2000)	Type	P (days)	Ogle-III ID
V03	04:59:00.4	-67:44:40.3	RRab	0.62195	RRLYR-02661
V04	04:59:01.1	-67:43:29.4	RRab	0.55583	RRLYR-02662
V05	04:59:02.8	-67:46:06.0	RRab	0.69706	RRLYR-02674
V06	04:59:07.9	-67:45:29.4	?	0.30420	RRLYR-02712
V07	04:59:08.9	-67:44:08.0	RRc	0.29536	RRLYR-02727
V08	04:59:12.0	-67:43:52.6	RRab	0.57169	RRLYR-02748
V09	04:59:12.5	-67:44:15.0	RRc	0.36347	RRLYR-02757
V10	04:59:14.1	-67:44:23.7	RRab	0.69652	RRLYR-02770
V11	04:59:14.8	-67:44:21.3	RRc	0.31536	RRLYR-02777
V13	04:59:08.9	-67:44:39.6	RR?	0.55944	
V14	04:59:03.1	-67:44:39.1	RRc	0.31786	RRLYR-02676
V15	04:59:09.4	-67:44:39.0	RR?	0.42735	RRLYR-02732
V16	04:59:06.0	-67:44:39.6	RR?	0.35429	RRLYR-02693
V17	04:59:06.3	-67:44:38.3	RR?	0.52470	RRLYR-02697
V18	04:59:11.4	-67:44:36.3	RRab	0.64515	RRLYR-02747
V19	04:59:04.2	-67:44:35.6	RRab	0.74479	RRLYR-02680
V20	04:59:09.4	-67:44:34.4	?	0.29193	
V21	04:58:59.309	-67:44:32.06	RRd	0.4920	RRLYR-02653
V22	04:59:10.1	-67:44:27.2	RRc	0.32920	RRLYR-02738
V23	04:59:04.8	-67:44:24.9	RR?	0.52851	RRLYR-02683
V24	04:59:11.2	-67:44:17.4	RR?	0.41110	RRLYR-02743/02746
V25-Field	04:59:41.3	-67:44:16.8	Ceph	3.27005	CEP-0591
V26	04:59:09.2	-67:44:14.3	RRab	0.73891	RRLYR-02729
V27	04:59:14.5	-67:43:52.2	RRab	0.66428	RRLYR-02776
V28	04:58:59.684	-67:43:52.12	RRd	0.4854	RRLYR-02658

Table 7.1 (continued)

ID	RA (J2000)	DEC (J2000)	Type	P (days)	Ogle-III ID
V29	04:59:14.1	-67:43:46.2	RRc	0.36944	RRLYR-02771
V30	04:59:07.2	-67:43:30.9	Ceph	11.71808	CEP-0561
V31	04:59:06.6	-67:43:26.2	Eclipse	0.61/1.6	
V32-Field	04:59:34.7	-67:42:46.7	RRab	0.53199	RRLYR-02855
V33-Field	04:59:28.9	-67:42:40.1	RRab	0.53278	RRLYR-02834
V34-Field	04:58:59.3	-67:42:38.3	Eclipse	1.6/3.2	
V35-Field	04:59:36.0	-67:42:31.9	RRc	0.33059	RRLYR-02864
V36	04:59:39.4	-67:42:15.1	Delta Scuti	0.07723	DSCT-400
V37	04:59:09.0	-67:46:14.9	RRc	0.35528	RRLYR-02728
V38	04:59:21.2	-67:46:06.7	RRab	0.75890	RRLYR-02802
V39	04:59:03.0	-67:45:36.2	Delta Scuti	0.08040	
V40	04:58:59.6	-67:45:24.6	RRc	0.33496	RRLYR-02657
V41	04:59:06.1	-67:45:24.4	T2Ceph	1.10416	T2CEP-020
V42	04:59:01.4	-67:45:21.5	RRc	0.37066	RRLYR-02667
V43	04:58:49.9	-67:45:10.7	?	0.06096	
V44	04:59:15.6	-67:45:02.9	RRc	0.36458	RRLYR-02781
V45	04:59:08.8	-67:45:01.9	RRc	0.29913	RRLYR-02724
V46	04:59:09.2	-67:45:01.6	Ceph	2.16504	CEP-0563
V47	04:59:06.2	-67:44:56.3	RR?	0.37080	RRLYR-02698
V48	04:59:12.197	-67:44:56.28	RRd	0.4786	RRLYR-02750
V49	04:59:05.7	-67:44:55.9	?	0.55403	
V50	04:59:10.0	-67:44:55.6	RRab	0.49336	RRLYR-02737
V51	04:59:03.0	-67:44:54.1	RR?	0.56363	RRLYR-02675
V52	04:59:09.3	-67:44:53.4	RRc	0.32653	RRLYR-02730
V53	04:59:05.6	-67:44:52.8	RR?	0.36824	RRLYR-02688

Table 7.1 (continued)

ID	RA (J2000)	DEC (J2000)	Type	P (days)	Ogle-III ID
V54	04:59:05.0	-67:44:51.8	RRc	0.30898	RRLYR-02686
V55	04:59:08.9	-67:44:51.7	RRab	0.51904	RRLYR-02725
V56	04:59:04.0	-67:44:50.7	RR?	0.52757	RRLYR-02678
V57	04:59:09.5	-67:44:50.5	RR?	0.52083	RRLYR-02733
V58	04:59:04.9	-67:44:49.1	RRab	0.55049	RRLYR-02685
V59	04:59:07.3	-67:44:48.7	RR?	0.56507	RRLYR-02706
V60	04:59:11.6	-67:44:46.8	RRc	0.29205	
V61	04:59:12.0	-67:44:43.9	RRc	0.36061	RRLYR-02749
V62	04:59:05.9	-67:44:43.3	RRc	0.36411	RRLYR-02692
V63	04:59:07.9	-67:44:48.6	RR?	0.62312	RRLYR-02714
V64	04:59:07.8	-67:44:52.6	RR?	0.70228	RRLYR-02711
V65	04:59:06.6	-67:44:42.0	RR?	0.64660	RRLYR-02702
V66	04:59:07.5	-67:44:35.7	RR?	0.50999	RRLYR-02671

Table 7.2: Photometric Parameters for Variables in NGC 1786, Excluding RRd Stars

ID	Type	P (days)	$A_V$	$A_B$	$\langle V \rangle$	$\langle B \rangle$	$\langle B-V \rangle$
V01	AC	0.80006	0.61	0.71	17.774	18.133	0.367
V03	RRab	0.62195	0.91	1.17	19.457	19.959	0.526
V04	RRab	0.55583	1.10	1.35	19.218	19.560	0.377
V05	RRab	0.69706	0.61	0.82	19.301	19.730	0.441
V06	?	0.30420	0.64	0.89	20.539	20.924	0.402
V07	RRc	0.29536	0.56	0.75	19.292	19.603	0.325
V08	RRab	0.57169	0.86	1.17	19.220	19.661	0.463

Table 7.2 (continued)

ID	Type	P (days)	$A_V$	$A_B$	$\langle V \rangle$	$\langle B \rangle$	$\langle B-V \rangle$
V09	RRc	0.36347	0.47	0.56	19.445	19.571	0.132
V10	RRab	0.69652	0.69	0.79	19.474	19.962	0.494
V11	RRc	0.31536	0.54	0.63	19.339	19.608	0.275
V13	RR?	0.55944	0.36	0.68	17.761	18.500	0.746
V14	RRc	0.31786	0.62	0.77	19.473	19.806	0.345
V15	RR?	0.42735	-	-	-	-	-
V16	RR?	0.35429	-	-	-	-	-
V17	RR?	0.52470	0.33	0.68	17.855	18.693	0.852
V18	RRab	0.64515	0.97	1.20	19.083	19.491	0.439
V19	RRab	0.74479	0.43	0.57	18.807	19.322	0.522
V20	?	0.29193	-	0.43	-	19.215	-
V22	RRc	0.32920	0.63	0.72	19.330	19.564	0.243
V23	RR?	0.52851	0.50	0.93	18.383	19.030	0.672
V24	RR?	0.41110	0.30	0.39	18.682	18.955	0.275
V25-Field	Ceph	3.27005	0.84	1.16	15.694	16.258	0.601
V26	RRab	0.73891	0.39	0.48	19.179	19.630	0.455
V27	RRab	0.66428	0.58	0.60	18.990	19.234	0.245
V29	RRc	0.36944	0.26	0.38	19.083	19.523	0.444
V30	Ceph	11.71808	1.11	1.75	14.324	14.799	0.607
V31	Eclipse	0.61/1.6	-	-	18.340	18.376	0.036
V32-Field	RRab	0.53199	1.11	1.46	19.089	19.384	0.322
V33-Field	RRab	0.53278	0.67	0.71	19.587	20.028	0.430
V34-Field	Eclipse	1.6/3.2	-	-	19.514	19.754	0.240
V35-Field	RRc	0.33059	0.49	0.60	19.186	19.551	0.371
V36	Delta Scuti	0.07723	0.56	0.62	20.319	20.485	0.172

Table 7.2 (continued)

ID	Туре	P (days)	$A_V$	$A_B$	$\langle V \rangle$	$\langle B \rangle$	$\langle B - V \rangle$
V37	RRc	0.35528	0.47	0.59	19.355	19.590	0.241
V38	RRab	0.75890	0.40	0.47	19.014	19.438	0.427
V39	Delta Scuti	0.08040	0.28	0.41	20.699	21.044	0.349
V40	RRc	0.33496	0.55	0.66	19.631	20.026	0.403
V41	T2Ceph	1.10416	1.01	1.26	18.462	18.746	0.328
V42	RRc	0.37066	0.47	0.54	19.307	19.633	0.329
V43	?	0.06096	0.70	0.84	21.365	21.636	0.283
V44	RRc	0.36458	0.48	0.58	19.297	19.648	0.356
V45	RRc	0.29913	0.68	0.71	19.389	19.560	0.180
V46	Ceph	2.16504	0.30	0.41	15.829	16.328	0.504
V47	RR?	0.37080	0.75	1.00	19.977	20.444	0.491
V49	?	0.55403	0.20	0.24	17.294	18.223	0.929
V50	RRab	0.49336	0.74	0.88	18.601	18.866	0.263
V51	RR?	0.56363	0.40	0.58	18.335	18.898	0.574
V52	RRc	0.32653	0.47	0.57	18.989	19.317	0.333
V53	RR?	0.36824	-	-	-	-	-
V54	RRc	0.30898	0.41	0.48	19.332	19.669	0.339
V55	RRab	0.51904	0.97	1.14	18.720	18.860	0.154
V56	RR?	0.52757	0.44	0.67	19.736	20.036	0.318
V57	RR?	0.52083	-	-	-	-	-
V58	RRab	0.55049	0.63	0.712 18.821	19.185	0.371	
V59	RR?	0.56507	-	-	-	-	-
V60	RRc	0.29205	0.32	0.42	19.217	19.502	0.289
V61	RRc	0.36061	0.48	0.60	19.274	19.900	0.624
V62	RRc	0.36411	0.28	0.44	18.969	19.512	0.550

Table 7.2 (continued)

ID	Type	P (days)	$A_V$	$A_B$	$\langle V \rangle$	$\langle B \rangle$	$\langle B - V \rangle$
V63	RR?	0.62312	-	-	-	-	-
V64	RR?	0.70228	-	-	-	-	-
V65	RR?	0.64660	-	-	-	-	-
V66	RR?	0.50999	-	-	-	-	-

Table 7.3: Photometric Parameters for the RRd Variables in NGC 1786

ID	Type	$P_0$ (d)	$P_1$ (d)	$P_1/P_0$	$A_{V,0}$	$A_{V,1}$	$A_{B,0}$	$A_{B,1}$	$\langle V \rangle$	$\langle B \rangle$	$\langle B - V \rangle$
V02	RRd	0.4906	0.3647	0.7434	0.12	0.19	0.10	0.25	19.144	19.442	0.306
V21	RRd	0.4920	0.3664	0.7448	0.08	0.23	0.11	0.29	19.443	19.806	0.367
V28	RRd	0.4854	0.3605	0.7427	0.14	0.22	0.16	0.31	19.200	19.493	0.308
V48	RRd	0.4786	0.3555	0.7427	0.32	0.32	0.43	0.42	19.324	19.729	0.409

#### 7.1.1 RR Lyrae Stars

A total of 13 RRab, 16 RRc, 4 RRd, and 15 candidate RR Lyrae stars were found within the tidal radius of NGC 1786; 1 RRc and 1 candidate RR Lyrae are new discoveries that have not been found in any of the previous studies of the cluster. All of the 9 RR Lyrae stars originally identified by Graham (1985) were found. V2 had been classified as an RRc star by Graham (1985) and Walker & Nemec (1988). However, the larger number of epochs in my data set allowed for the detection of a second pulsation mode in this star and it has been reclassified as an RRd star. These nine stars have intensity-weighted mean magnitudes of  $\langle V \rangle = 19.321 \pm 0.039$  and

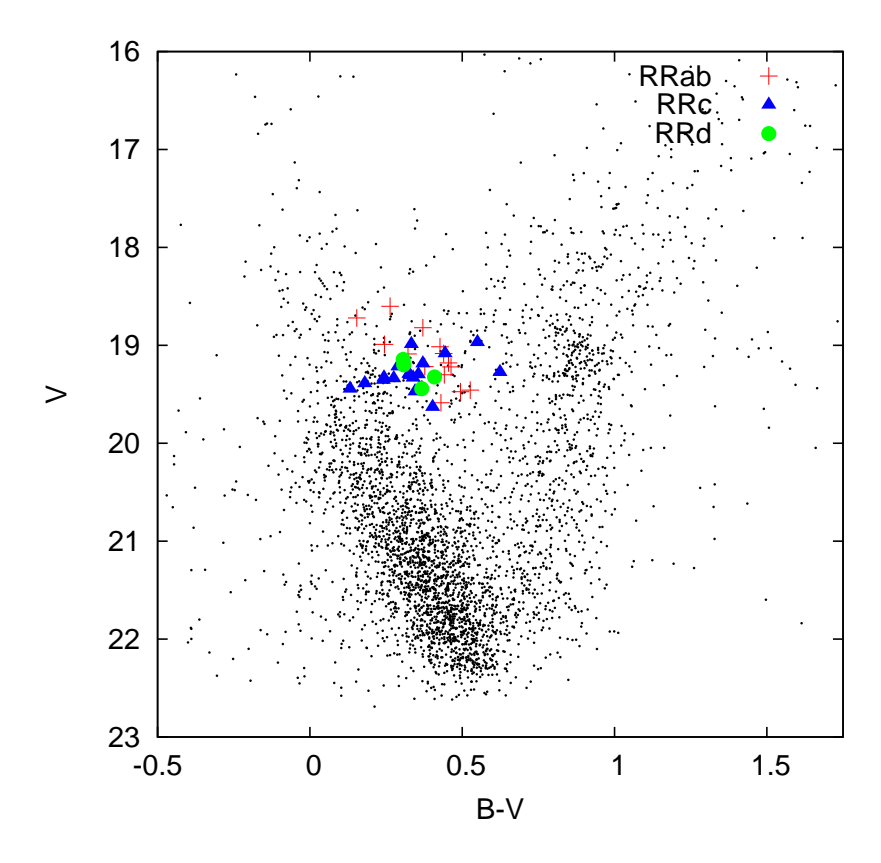


Figure 7.1: V,B-V CMD for stars within the tidal radius of NGC 1786 with the positions of the RR Lyrae variables also indicated. Plus symbols indicate RRab stars, filled triangles indicate RRc's, and circles indicate RRd's. The contamination by LMC field stars is readily apparent. The scatter in the positions of the RR Lyrae stars is a consequence of blending that arises from the crowded nature of the central region of the cluster.

 $\langle B \rangle = 19.677 \pm 0.059$ . These are fainter than Walker's values ( $\langle V \rangle = 19.203 \pm 0.073$  and  $\langle B \rangle = 19.526 \pm 0.066$ ). This disagreement in brightness is potentially due to the improved resolution of my observations decreasing the effect of blending between the RR Lyrae stars and other nearby stars. Sample light curves for the RR Lyrae stars in NGC 1786 are shown in Figures 7.3-7.5, the full set of light curves can be found in Appendix C.

Soszyński et al. (2009) found 55 RR Lyrae stars within the tidal radius of NGC 1786 using the OGLE-III data. I found 49 of these stars in my data, the remaining six are located within the extremely crowded core of the cluster. Of the OGLE-III

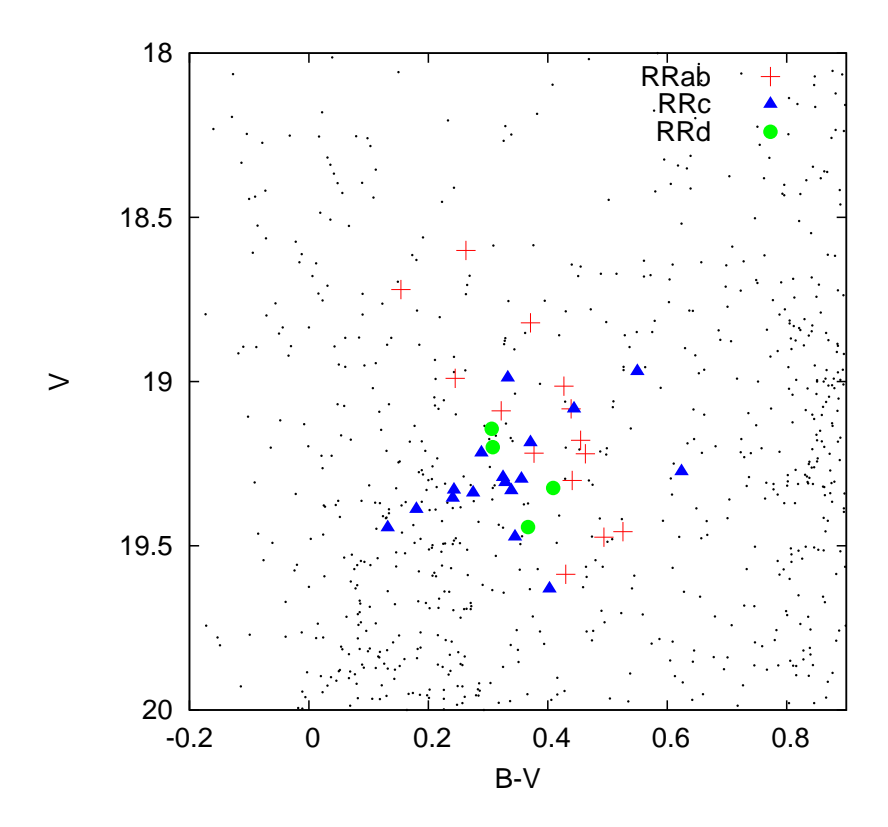


Figure 7.2: V,B-V CMD for NGC 1786 that is zoomed in on the horizontal branch. The symbols used are the same as in Figure 7.1

stars that were found in my data set, 32 were classified as RR Lyrae stars (13 RRab, 15 RRc, and 4 RRd), 16 as candidate RR Lyrae, and 1 as a variable of undetermined type.

V06 (OGLE-III RRLYR-02712) was classified as an RRab star by Soszyński et al. (2009), however I found it to have an intensity-weighted mean magnitude of  $\langle V \rangle = 20.539$ , about one magnitude fainter than the horizontal branch. Sosyński found a mean magnitude of  $\langle V \rangle = 19.410$  for this star, about one magnitude brighter than my value. Since V06 is not in a very crowded region of the cluster, the reason for this disagreement in brightness is unknown.

OGLE-III stars RRLYR-02743 and RRLYR-07246 are only slightly separated on the sky ( $\approx 0.15$  arcseconds) and can potentially be a single star. My photometry only found one variable star at this location, V24, which has an RR Lyrae-like shape and

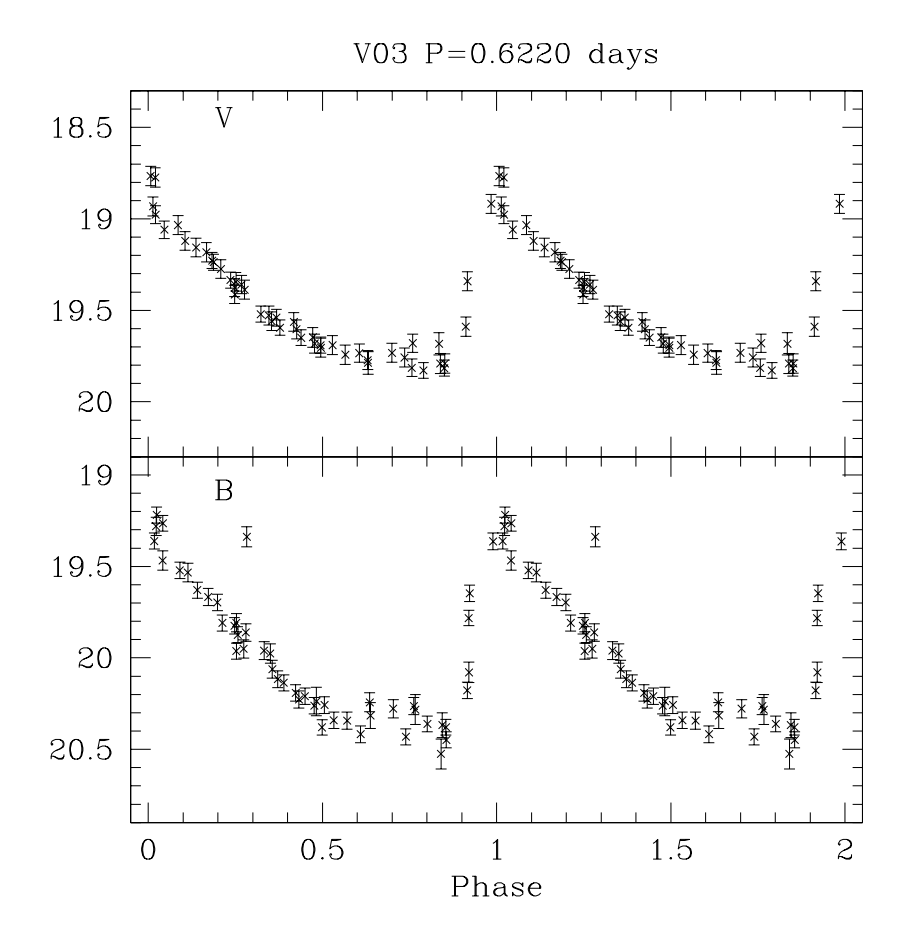


Figure 7.3: Sample light curve for RRab stars in NGC 1786.

period but is brighter than the horizontal branch, likely due to blending with nearby non-variable neighbors, and thus has been listed as a candidate RR Lyrae.

The candidate RR Lyrae stars are all located toward the center of the cluster. ISIS was used to find 9 of the candidate RR Lyrae stars (V15, V16, V53, V57, V59, V63-V66); the location of these stars in the extremely crowded center of the cluster did not allow Daophot light curves to be obtained. Of the remaining candidate RR Lyrae stars, V17, V23, and V51 are more than one magnitude brighter than the horizontal branch and have colors that are redder than the confirmed RR Lyrae stars, possibly due to blending. V47 is approximately 0.5 magnitudes fainter than the horizontal branch and shows potential RRd behavior but a second period could not be determined. V56 has a large gap in its light curve which potentially impacts

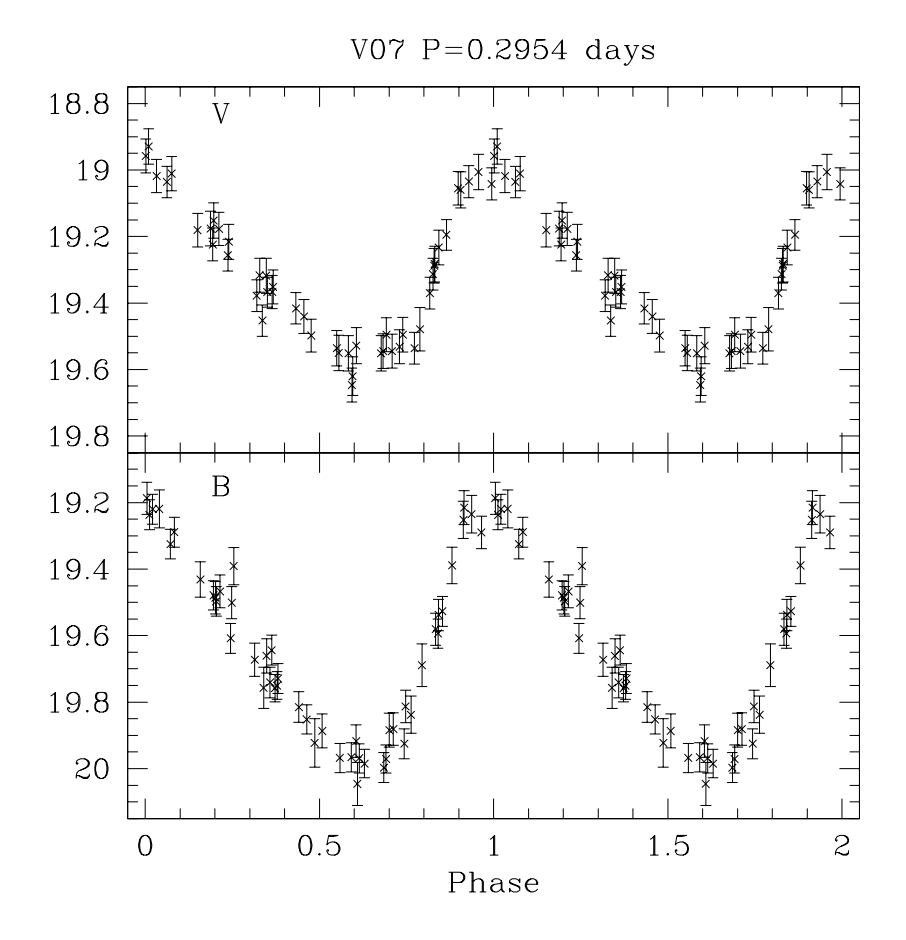


Figure 7.4: Sample light curve for RRc stars in NGC 1786.

the accuracy of the determination of its period and amplitude.

# 7.2 Physical Properties of the RR Lyrae Stars

Physical properties for 7 RRab and 7 RRc stars were calculated using the Fourier decomposition of their light curves, as described in Chapter 4. One of the RRc stars, V35, is located outside of the tidal radius of NGC 1786 and is thus a member of the LMC field. Tables 7.4 and 7.5 list the Fourier coefficients for the RRab and RRc stars, respectively, while Tables 7.6 and 7.7 list the physical properties of these stars. The averages of the physical properties for the RRc stars are calculated using only the 6 stars that are within the tidal radius of the cluster.

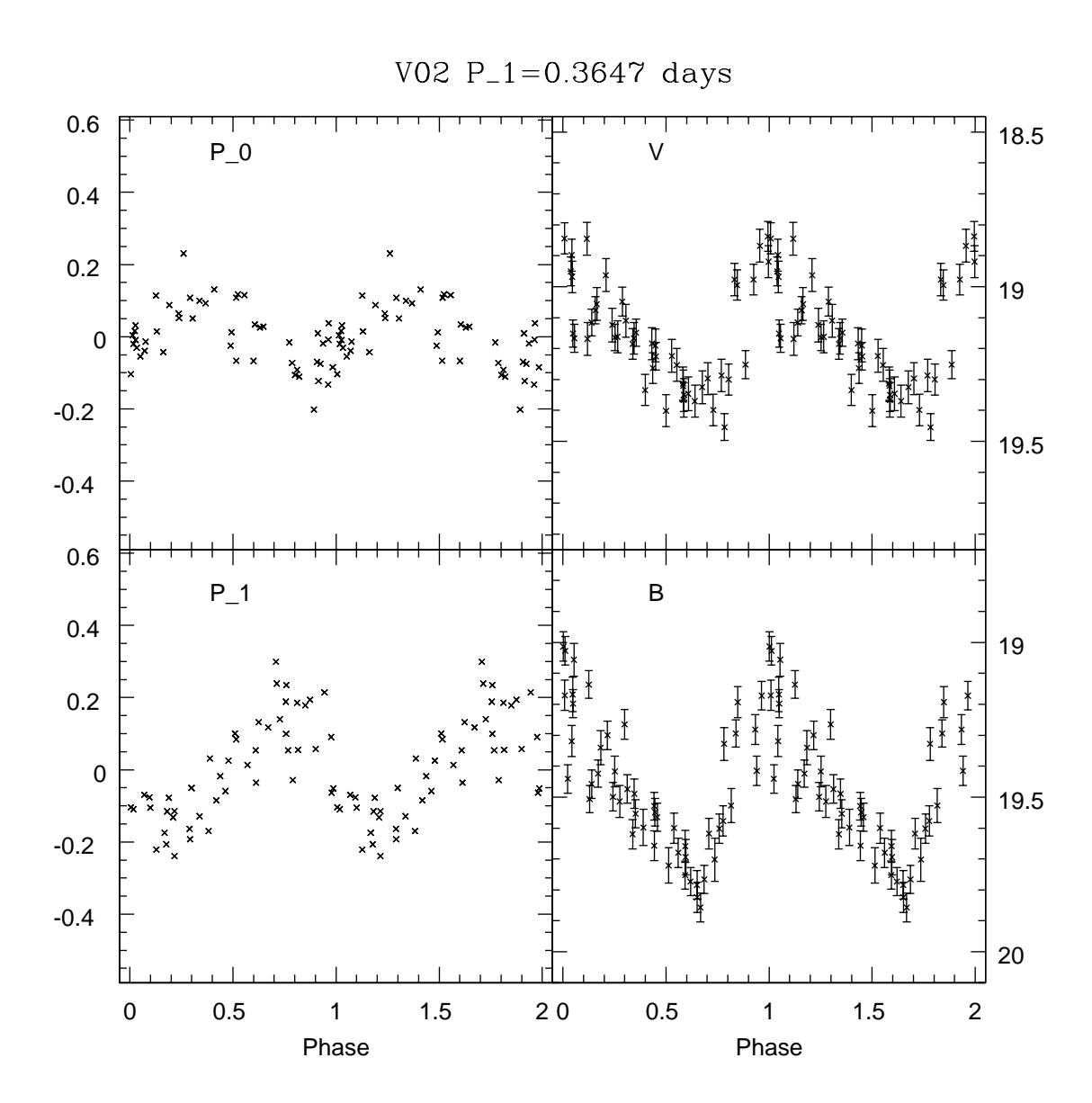


Figure 7.5: Sample light curve for RRd stars in NGC 1786.

Table 7.4: Fourier Coefficients for RRab Variables

ID	$A_1$	$A_{21}$	$A_{31}$	$A_{41}$	$\phi_{21}$	$\phi_{31}$	$\phi_{41}$	$D_{max}$	Order
V03	0.369	0.446	0.249	0.178	2.47	$5.03\pm0.18$	1.25	46.35	6
V04	0.454	0.396	0.232	0.090	2.30	$4.93 \pm 0.10$	1.09	26.97	10
V05	0.229	0.397	0.318	0.122	2.26	$5.54 \pm 0.17$	2.34	12.15	7
V08	0.308	0.492	0.320	0.107	2.13	$4.75 \pm 0.27$	1.20	5.65	7
V10	0.235	0.564	0.300	0.173	2.39	$4.97 \pm 0.30$	1.76	6.73	7
V26	0.175	0.377	0.153	0.076	2.46	$5.88 \pm 0.36$	2.27	39.77	8
V38	0.161	0.336	0.192	0.102	2.96	$6.05 \pm 0.32$	2.32	8.42	7

Table 7.5: Fourier Coefficients for RRc Variables

ID	$A_1$	$A_{21}$	$A_{31}$	$A_{41}$	$\phi_{21}$	$\phi_{31}$	$\phi_{41}$	Order
V07	0.274	0.284	0.121	0.079	4.44	$2.23 \pm 0.36$	1.22	8
V11	0.276	0.202	0.109	0.051	4.70	$2.67 \pm 0.43$	1.58	6
V37	0.231	0.109	0.073	0.026	4.40	$2.35 \pm 0.82$	5.90	6
V44	0.246	0.171	0.088	0.054	4.93	$3.66 \pm 0.43$	3.02	8
V45	0.285	0.303	0.103	0.060	3.94	2.17±1.11	1.15	8
V62	0.128	0.223	0.122	0.042	3.49	$2.19 \pm 0.50$	1.11	7
V35-Field	0.242	0.066	0.062	0.035	5.31	$4.17 \pm 0.46$	2.64	7

Table 7.6: Derived Physical Properties for RRab Variables

ID	$[\mathrm{Fe/H}]_{\mathrm{J95}}$	$\langle M_V \rangle$	$\langle V - K \rangle$	$\log T_{\rm eff}^{\langle V-K\rangle}$	$\langle B-V \rangle$	$\log T_{\rm eff}^{\langle B-V\rangle}$	$\log T_{\rm eff}^{\langle V-I\rangle}$
V03	-1.625	0.695	1.166	3.805	0.332	3.811	3.812
V04	-1.399	0.737	1.073	3.814	0.301	3.824	3.822
V05	-1.346	0.709	1.247	3.795	0.380	3.797	3.796
V08	-1.741	0.764	1.184	3.803	0.347	3.807	3.808
V10	-2.106	0.649	1.342	3.787	0.377	3.793	3.798
V26	-1.120	0.711	1.232	3.796	0.388	3.795	3.793
V38	-0.994	0.708	1.223	3.796	0.396	3.794	3.790
Mean	-1.476	0.710	1.210	3.800	0.3602	3.803	3.803
$\sigma$	0.144	0.134	0.031	0.001	0.013	0.004	0.004

Table 7.7: Derived Physical Properties for RRc Variables

ID	$[\mathrm{Fe}/\mathrm{H}]_{\mathrm{ZW84}}$	$\langle M_V \rangle$	$M/M_{\odot}$	$\log(L/L_{\odot})$	$\log T_{ m eff}$	Y
V07	-1.804	0.685	0.739	1.730	3.864	0.261
V11	-1.819	0.689	0.685	1.734	3.862	0.263
V37	-2.112	0.700	0.790	1.806	3.853	0.240
V44	-1.820	0.634	0.575	1.742	3.859	0.266
V45	-1.850	0.725	0.755	1.738	3.863	0.259
V62	-2.139	0.733	0.833	1.827	3.851	0.234
V35-Field	-1.197	0.672	0.480	1.668	3.868	0.292
Mean	-1.924	0.694	0.699	1.763	3.859	0.259
σ	0.064	0.014	0.047	0.017	0.002	0.007

The mean metallicity for the RRab stars is  $[Fe/H]_{J95} = -1.48 \pm 0.14$  which in the Zinn & West scale is  $[Fe/H]_{ZW84} = -1.65 \pm 0.10$ . This is more metal-rich than the literature values, see introduction to this chapter, though it is consistent within the error bars. The mean metallicity found for the RRc stars is  $[Fe/H]_{ZW84} = -1.92 \pm 0.06$ , which is more metal-poor than any of the literature values. The LMC field RRc star, V35, in Table 7.7 immediately stands out by being much more metal-rich than any of the other RRc stars.

### 7.3 DISTANCE MODULUS

The absolute magnitude-metallicity relationship from Catelan & Cortés (2008) is used to find the absolute magnitude of the RR Lyrae stars in NGC 1786. Since the metallicity obtained for the RRab stars,  $[Fe/H]_{ZW84} = -1.65 \pm 0.10$ , is closer to the metallicities reported in the literature, it is used for this calculation, giving a Vabsolute magnitude of  $\langle M_V \rangle = 0.605 \pm 0.216$ . Using the mean observed V magnitude for the RRab stars,  $\langle V \rangle = 19.090 \pm 0.079$ , the reddening value given by Sharma et al. (2010), E(B-V) = 0.06, and a standard extinction law with  $A_V/E(B-V) = 3.1$ gives a reddening-corrected distance modulus of  $(m-M)_0 = 18.30 \pm 0.23$ . This is shorter than the distance modulus of  $(m-M)_{LMC}=18.44\pm0.11$  that Catelan & Cortés (2008) derived for the LMC. The location of NGC 1786 is near the center of the LMC, and the cluster distance modulus is expected to be similar to that of the LMC. In order to determine if the discrepancies between these two values are a result of blending, the distance modulus is recalculated using on the six RRab stars within the cluster radius that do not have any nearby neighbors that could cause blending (V03, V04, V05, V10, V26, and V27). The average observed V magnitude for these six stars is  $\langle V \rangle = 19.270 \pm 0.075$  which changes the distance modulus to  $(m-M)_0 = 18.48 \pm 0.23$ . This new value agrees with the distance modulus found by Catelan & Cortés (2008), indicating that the distance modulus using the full set of RRab stars was effected by blending.

#### 7.4 Oosterhoff Classification

The average periods for the RR Lyrae stars in NGC 1786 are  $\langle P_{ab} \rangle = 0.626$  days and  $\langle P_{c} \rangle = 0.335$  days. The division between Oosterhoff intermediate and Oosterhoff II clusters occurs at an average RRab period of 0.62 days; the average RRab period for NGC 1786 is just on the Oo-II side of this division. In contrast, the average period for the RRc stars suggests an Oosterhoff I classification. I found 13 RRab, 16 RRc, and 4 RRd stars in NGC 1786 which gives the cluster a  $N_{c+d}/N_{c+d+ab} = 0.606$ . This ratio suggests an Oo-II classification, though it is a higher ratio than is typically seen. The minimum RRab period in the cluster is  $P_{ab,min} = 0.49336$  days which is on the shorter period end of what is seen for Oo-II objects (Section 9.2).

Figures 7.6 and 7.7 show the V and B band period-amplitude diagrams for NGC 1786. Both diagrams show a great deal of scatter in the location of both the RRab and RRc stars. The RRc stars tend to be located closer to the Oo-I locus which would be consistent with the average RRc period. Figure 7.8 shows the Petersen diagram which includes the RRd stars in NGC 1786 as well as those in the LMC field. The RRd stars in NGC 1786 fall in the same region as RRd stars in Milky Way Oo-I objects.

The Oosterhoff classification of NGC 1786 is more complicated than that of the other clusters observed for this dissertation. The first overtone dominant pulsators, the RRc and RRd stars, suggest an Oo-I classification for the cluster. However the fundamental mode pulsators, the RRab stars, suggest an Oo-II classification. The picture is further complicated by the fact that some of the RR Lyrae within the tidal radius are likely LMC field stars and should not be included when looking at the behavior of the cluster RR Lyrae stars.

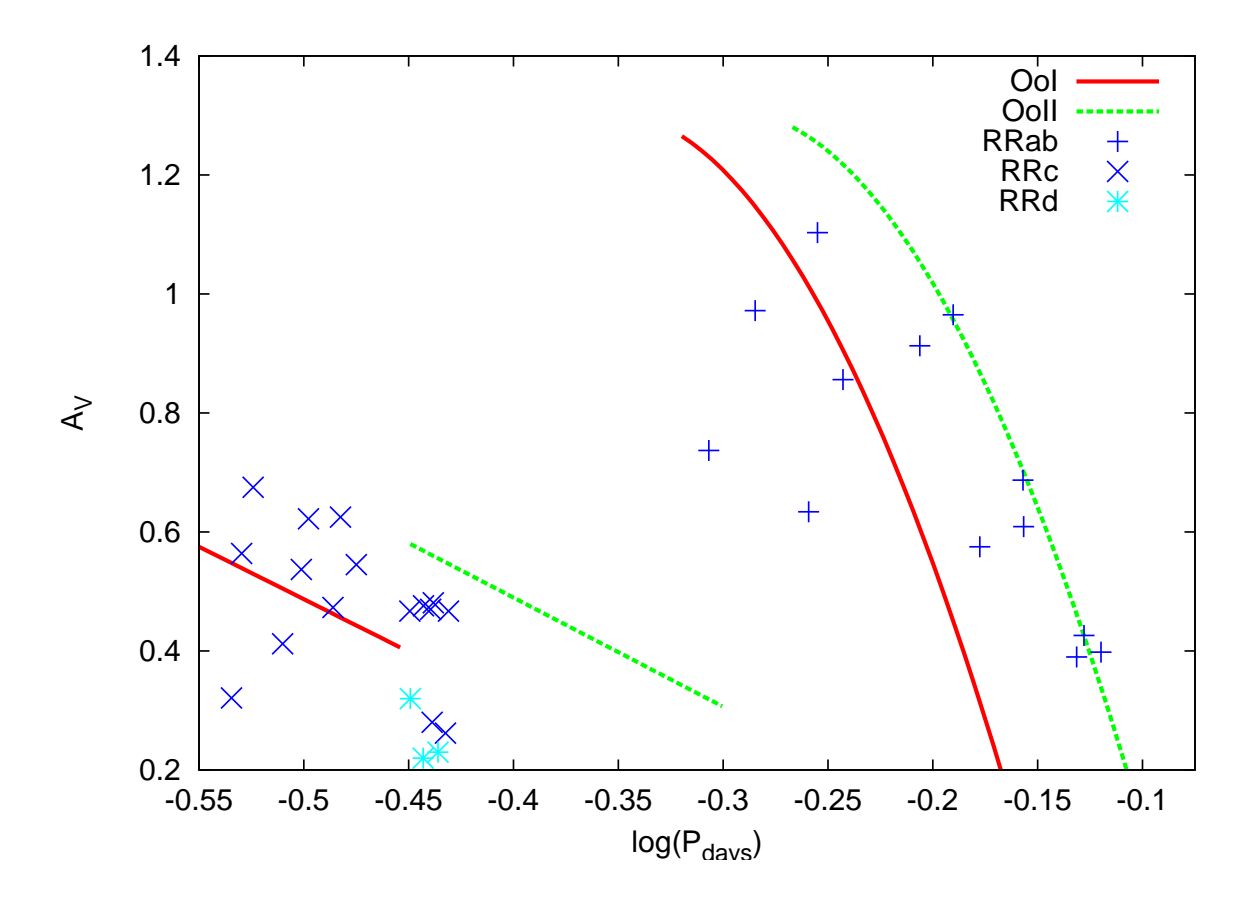


Figure 7.6: Bailey diagram, log period vs V-band amplitude (for the RR Lyrae stars in NGC 1786. Red and green lines indicate the typical position for RR Lyrae stars in Oosterhoff I and Oosterhoff II clusters, respectively (Cacciari et al., 2005; Zorotovic et al., 2010).

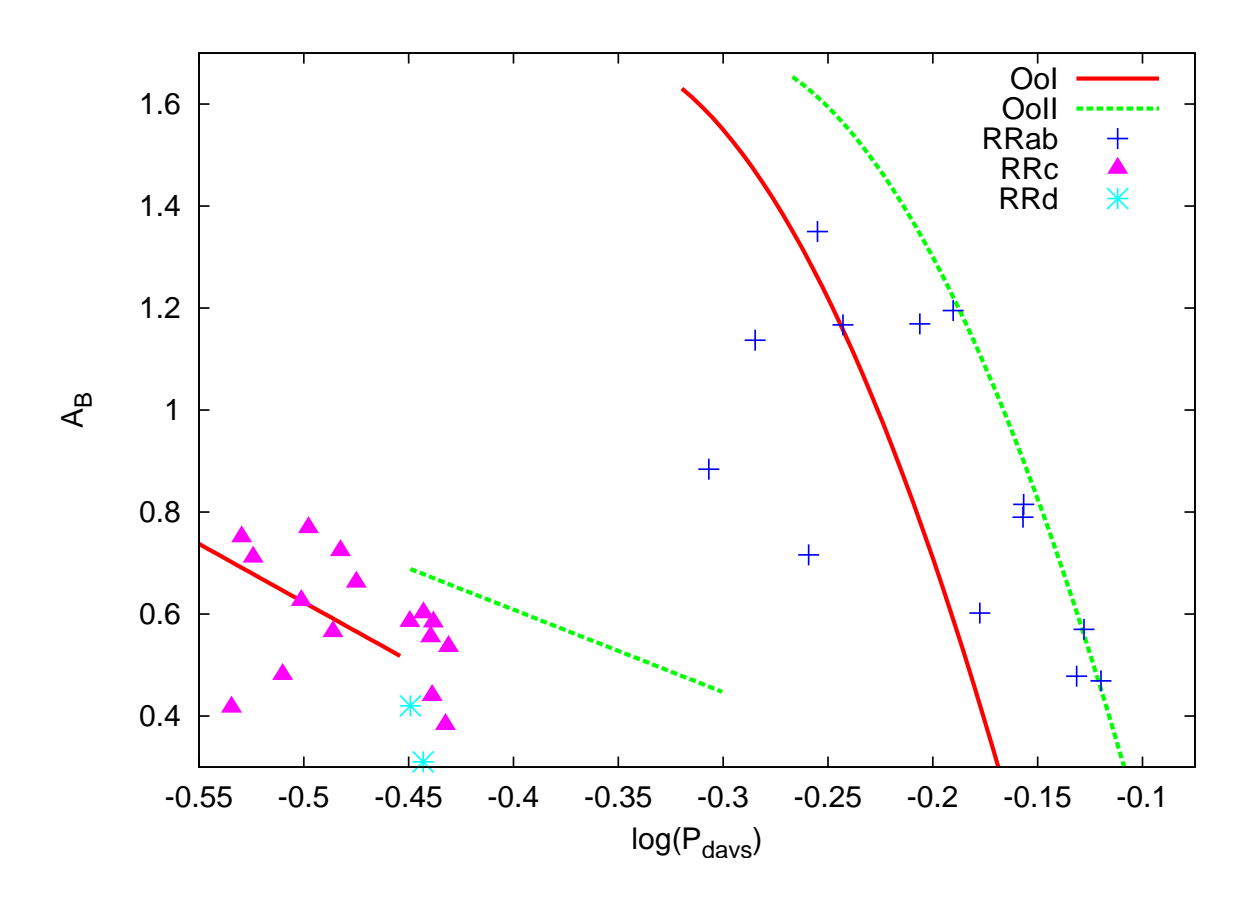


Figure 7.7: Same as Figure 7.6 except with B-band amplitudes in place of the V-band amplitudes.

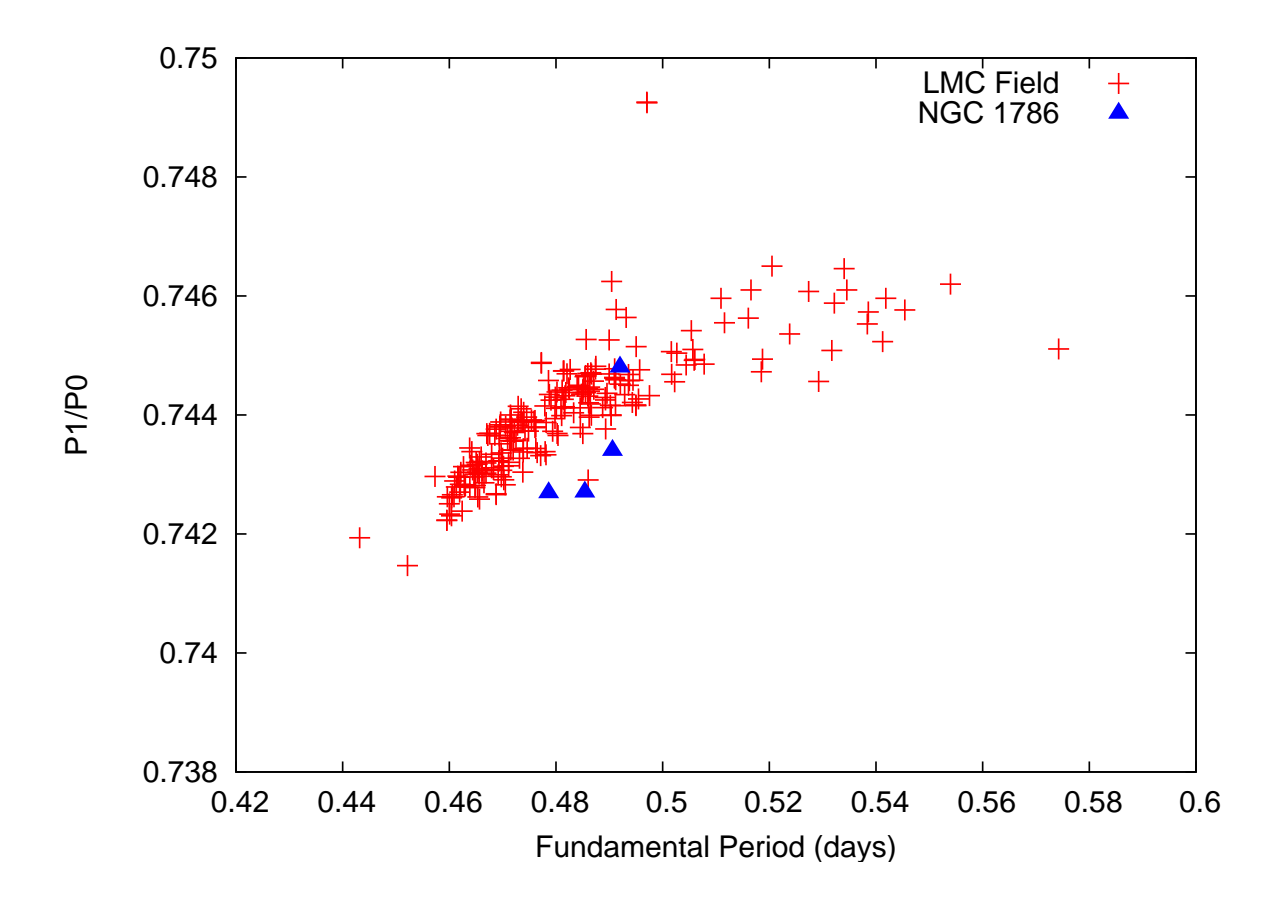


Figure 7.8: Petersen diagram showing the ratio of the first overtone period to the fundamental mode period vs. fundamental mode period for the RRd stars in NGC 1786 (blue triangles). Also plotted are the RRd stars in the LMC field (red plus symbols) from Soszyński et al. (2003).

# CHAPTER 8: NGC 2210

NGC 2210 is the fourth and final LMC cluster investigated as part of this dissertation. NGC 2210 is located closer to the center of the LMC than either NGC 1466 or Reticulum but is farther from the center than NGC 1786, and thus does not suffer from the effects of LMC field contamination to the same extent as NGC 1786 does. Mucciarelli et al. (2010) found a metallicity for the cluster of  $[Fe/H] = -1.65 \pm 0.02$  from spectral observations of 5 red giant stars. Olszewski et al. (1991) found a more metal poor value of  $[Fe/H] = -1.97 \pm 0.20$  based on the spectra of 4 stars in the cluster. The cluster is not very reddened, having an E(B-V) = 0.075 (Schlegel, 1998).

Graham (1977) and Nemec (1981) were the first to search NGC 2210 and the surrounding area for variable stars. Walker (1985) found 9 RR Lyrae stars in the cluster. The number of known RR Lyrae stars grew thanks to work done by Hazen & Nemec (1992) which found 33 variables, including 11 RR Lyrae, in the cluster as well as 52 field RR Lyrae in the nearby vicinity. Reid & Freedman (1994) observed a 15 × 15 arcminute area around NGC 2210, finding 44 variable stars (at least 27 were RR Lyraes). Like NGC 1786, NGC 2210 was observed by the OGLE survey which found 58 RR Lyrae stars in the direction of the cluster (Soszyński et al., 2009).

I obtained a total of  $109\ V$ ,  $106\ B$ , and  $106\ I$  images on the SOAR and SMARTS telescopes. I reduced the data as described in Chapter 4 and the photometry was transformed to the standard system using observation of the Landolt standard fields PG0231, PG0942, PG1047, SA95, and SA98 (Landolt, 1992). I had combined the

data sets from the two telescopes and was in the process of identifying and classifying the variable stars in NGC 2210 when I became aware that similar work on the cluster was being carried out by another group of investigators (Young-Beom Jeon, James Nemec, and Alistair Walker). This group had obtained 270 B and V images using the CTIO 0.9-m telescope. Considering the size of the two data sets, it was decided that it would be best to collaborate on this cluster, with Young-Beom Jeon handling the process of combining my photometry with theirs.

### 8.1 RR Lyrae Stars

The work of combining the data sets and identifying the variable stars is primarily being carried out by Young-Beom Jeon and is still underway. Currently 49 RR Lyrae stars (32 RRab, 16 RRc, and 1 RRd) have been identified. Table 8.1 lists the identified RR Lyrae stars, their classification, period, and V and B-band amplitudes.

Table 8.1: Photometric Parameters for Variables in NGC 2210

ID	Type	P (days)	$A_V$	$A_B$	$\langle V \rangle$	$\langle B \rangle$	$\langle B-V \rangle$
v767	RRc	0.306089	0.49	0.70	19.089	19.259	0.170
v861	RRab	0.535503	1.05	1.36	19.163	19.449	0.286
v873	RRc	0.369854	0.42	0.51	18.658	18.956	0.298
v900	RRab	0.66241	1.13	1.52	18.924	19.264	0.340
v909	RRc	0.398029	0.51	0.67	19.252	19.528	0.276
v920	RRab	0.6565	0.89	1.13	19.038	19.411	0.373
v938	RRab	0.64005	1.05	1.30	19.009	19.368	0.359
v942	RRab	0.52391	1.21	1.62	19.106	19.407	0.301
v974	RRab	0.60238	1.11	1.38	19.137	19.46	0.323
v980	RRc	0.357005	0.38	0.49	19.008	19.233	0.225
v998	RRc	0.310231	0.44	0.54	19.162	19.353	0.191

Table 8.1 (continued)

ID	Type	P (days)	Au	$A_B$	$\langle V \rangle$	$\langle B \rangle$	$\langle B - V \rangle$
v1020	RRc	0.397151	•				
v1087	RRab	0.722514					
v1109	RRab	0.733037				19.513	
v1127	RRab	0.684187	0.74	0.94	19.016	19.33	0.314
v1143	RRab	0.627733	1.09	1.41	19.068	19.395	0.327
v1204	RRab	0.562166	1.22	1.57	19.184	19.48	0.296
v1206	RRc	0.383952	0.47	0.61	19.092	19.335	0.243
v1217	RRab	0.623082	0.94	1.15	19.134	19.475	0.341
v1233	RRab	0.705148	0.55	0.73	19.106	19.485	0.379
v1252	RRc	0.270223	0.34	0.43	19.371	19.543	0.172
v1296	RRc	0.358951	0.55	0.71	19.200	19.461	0.261
v1301	RRd	0.3552	0.69	0.88	19.093	19.325	0.232
v1349	RRc	0.282076	0.56	0.70	19.259	19.46	0.201
v1372	RRc	0.285777	0.34	0.43	19.238	19.426	0.188
v1385	RRc	0.435544	0.48	0.61	19.118	19.387	0.269
v1411	RRab	0.523234	1.08	1.37	19.222	19.49	0.268
v1452	RRab	0.608591	0.42	0.56	19.505	19.931	0.426
v1465	RRab	0.610946	1.07	1.38	19.278	19.585	0.307
v1484	RRab	0.583317	0.92	1.20	19.240	19.584	0.344
v1560	RRab	0.63577	0.81	1.07	19.273	19.651	0.378
v1584	RRab	0.512013	1.23	1.59	19.170	19.45	0.280
v2110	RRab	0.617179	0.55	0.71	19.413	19.796	0.383
v2404	RRab	0.436395	0.99	1.28	19.713	20.093	0.380
v16940	RRab	0.60227	0.87	1.10	19.275	19.596	0.321
v17861	RRc	0.376606	0.45	0.56	19.144	19.46	0.316

### 8.2 Physical Properties of the RR Lyrae Stars

Prior to deciding to combine data sets with the other group, I had performed Fourier fits on 4 RRab and 4 RRc stars that I had identified from my data. The Fourier coefficients from these fits are given in Tables 8.2 and 8.3 for the RRab and RRc stars, respectively. The physical properties obtained are given in Tables 8.4 and 8.5. The RRab star v2404 has a metallicity that is nearly one dex higher than any of the other three RRab stars. This combined with the star's location away from the center of the cluster make it likely that it is an LMC field star, not a cluster member, and thus it is not included in the calculation of the mean values for the physical properties.

Table 8.2: Fourier Coefficients for RRab Variables

ID	$A_1$	$A_{21}$	$A_{31}$	$A_{41}$	$\phi_{21}$	$\phi_{31}$	$\phi_{41}$	$D_{max}$	Order
v942	0.438	0.415	0.350	0.233	2.198	$4.562 \pm 0.0484$	0.849	44.35	10
v1109	0.199	0.394	0.215	0.102	2.561	$5.641 \pm 0.092$	2.483	15.67	9
v1143	0.383	0.467	0.340	0.213	2.396	$5.154 \pm 0.053$	1.636	2.24	8
v2404	0.316	0.517	0.333	0.192	2.382	$5.109 \pm 0.071$	1.582	1.56	9

Table 8.3: Fourier Coefficients for RRc Variables

ID	$A_1$	$A_{21}$	$A_{31}$	$A_{41}$	$\phi_{21}$	$\phi_{31}$	$\phi_{41}$	Order
v980	0.179	0.122	0.088	0.025	4.79	3.11±0.20	1.83	6
v998	0.220	0.135	0.018	0.028	4.79	$3.20 \pm 0.92$	0.81	7
v1296	0.233	0.142	0.053	0.012	4.63	$3.47 \pm 0.32$	2.64	8
v1372	0.161	0.120	0.011	0.040	4.41	$0.66 \pm 1.47$	3.23	5

Table 8.4: Derived Physical Properties for RRab Variables

ID	$[\mathrm{Fe/H}]_{\mathrm{J95}}$	$\langle M_V \rangle$	$\langle V - K \rangle$	$\log T_{\rm eff}^{\langle V-K\rangle}$	$\langle B-V \rangle$	$\log T_{\rm eff}^{\langle B-V\rangle}$	$\log T_{\rm eff}^{\langle V-I\rangle}$
v942	-1.728	0.751	1.109	3.811	0.315	3.818	3.819
v1109	-1.405	0.684	1.286	3.791	0.385	3.795	3.795
v1143	-1.492	0.693	1.165	3.804	0.340	3.810	3.809
v2404	-0.521	0.987	0.950	3.825	0.324	3.825	3.816
Mean	-1.542	0.709	1.187	3.802	0.347	3.807	3.808
$\sigma$	0.097	0.021	0.052	0.006	0.020	0.007	0.007

Table 8.5: Derived Physical Properties for RRc Variables

ID	$[\mathrm{Fe}/\mathrm{H}]_{\mathrm{ZW84}}$	$\langle M_V \rangle$	$M/M_{\odot}$	$\log(L/L_{\odot})$	$\log T_{ m eff}$	Y
v980	-1.965	0.688	0.653	1.764	3.857	0.256
v998	-1.542	0.725	0.594	1.696	3.866	0.277
v1296	-1.857	0.696	0.599	1.746	3.859	0.263
v1372	-1.973	0.764	1.082	1.806	3.857	0.232
Mean	-1.834	0.718	0.732	1.753	3.860	0.257
σ	0.101	0.017	0.117	0.023	0.002	0.009

The mean metallicity of the RRab stars is  $[Fe/H]_{J95} = -1.54 \pm 0.10$ , which in the Zinn & West scale is  $[Fe/H]_{ZW84} = -1.69 \pm 0.07$ . This value is consistent with the value of  $[Fe/H] = -1.65 \pm 0.02$  found by Mucciarelli et al. (2010). As was seen in Reticulum and NGC 1786, the Morgan, Wahl, & Wieckhorst (2007) calibration gives

a lower metallicity for the RRc stars, [Fe/H]  $_{\rm ZW84} = -1.83 \pm 0.10.$ 

### 8.3 DISTANCE MODULUS

The absolute magnitude-metallicity relation from Catelan & Cortés (2008) and the metallicity from the RRab stars was used to obtain an absolute magnitude of  $M_V = 0.60 \pm 0.21$  The average magnitude for the RRab stars is  $19.189 \pm 0.038$  and the reddening is E(B-V)=0.075 (Schlegel, 1998). These values, along with a standard extinction law with  $A_V/E(B-V)=3.1$ , gives a reddening-corrected distance modulus of  $(m-M)_0=18.36 \pm 0.21$ . This is shorter than the distance modulus of  $(m-M)_{LMC}=18.44 \pm 0.11$  that Catelan & Cortés (2008) derived for the LMC, though it is consistent within the errors.

### 8.4 Oosterhoff Classification

The average periods for the RR Lyrae stars in NGC 2210 are  $\langle P_{ab} \rangle = 0.612$  days and  $\langle P_c \rangle = 0.350$  days. With a total of 32 RRab, 16 RRc, and 1 RRd, NGC 2210 has a  $N_{c+d}/N_{c+d+ab} = 0.35$ . All three of these values are indicative of an Oo-int classification for the cluster. The minimum period for the RRab stars in the cluster is  $P_{ab,min} = 0.51049$  days which supports an Oo-int classification (Section 9.2).

Figures 8.1 and 8.2 show the V and B-band Bailey diagrams for the cluster. The RRab stars in the diagrams have a large scatter with a significant portion of them being located between the Oo-I and II loci, consistent an Oo-int classification, though there is a significant number that cluster along the Oo-II locus. The RRc stars also show a significant amount of scatter with a large portion of them falling between the Oo-I and II lines.

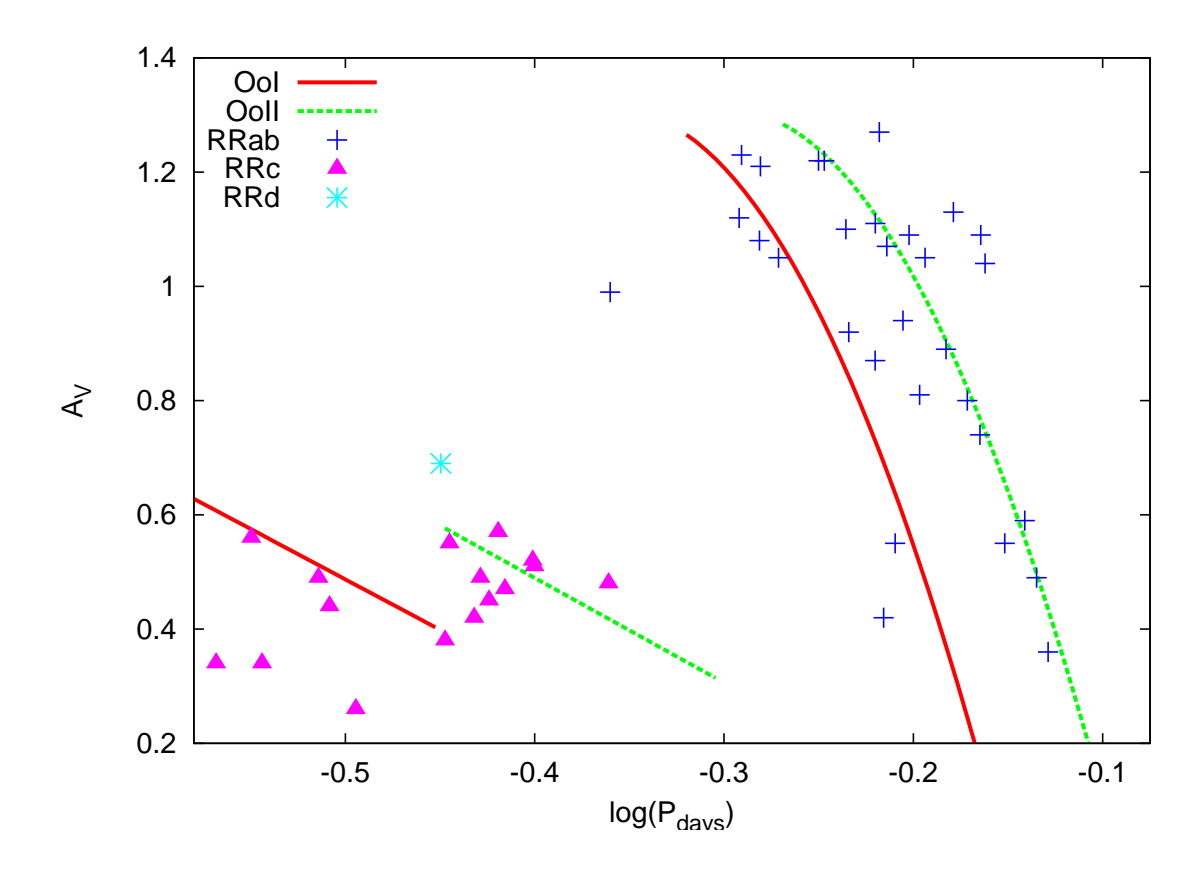


Figure 8.1: Bailey diagram, log period vs V-band amplitude for the RR Lyrae stars in NGC 2210. Red and green lines indicate the typical position for RR Lyrae stars in Oosterhoff I and Oosterhoff II clusters, respectively (Cacciari et al., 2005; Zorotovic et al., 2010).

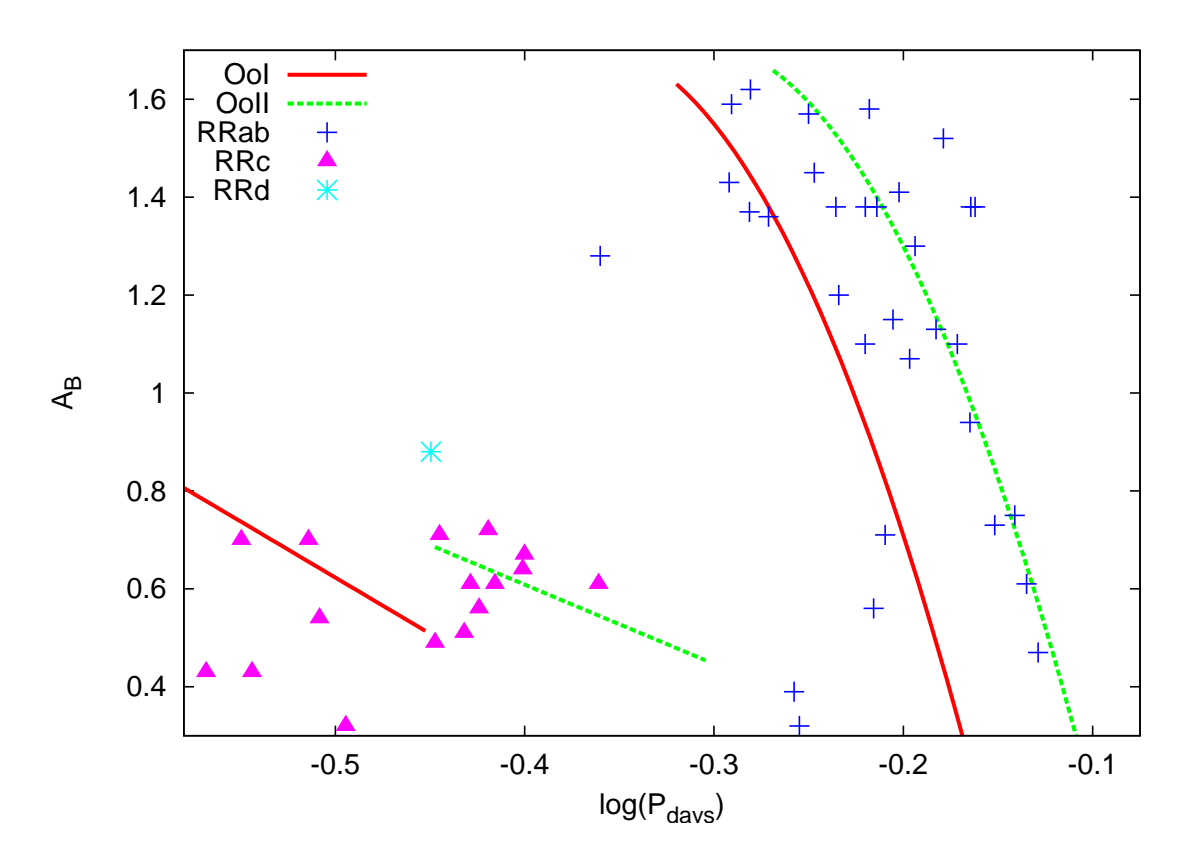


Figure 8.2: Same as Figure 8.1 except with B-band amplitudes in place of the V-band amplitudes.

## Chapter 9: Exploring Oosterhoff Intermediate Systems

As discussed in Chapter 3, the fact that Oosterhoff intermediate stellar systems are not seen in the Milky Way, but are prevalent in the nearby dwarf galaxies and their globular clusters, presents a challenge to the hierarchical model for Milky Way formation. Since Oo-int stellar systems do not occur in the Milky Way, they have not been studied to the same extent as Oo-I/II stellar systems, which occur at closer distances and thus have been easier to observe. In fact, the greater distances involved mean that extragalactic Oo-I/II stellar systems have not been studied as well as their Milky Way counterparts. I undertook this study in an attempt to compare extragalactic Oo-I/II stellar systems to their Galactic counterparts, as well as study the differences between the RR Lyrae stars in Oo-int systems and those in Oo-I/II systems.

### 9.1 Structure of the Instability Strip

RR Lyrae variable stars inhabit a region of the horizontal branch where the instability strip intersects it (see Figure 3.1). The effective temperatures of stars determine the red and blue edges of the instability strip. The blue edge of the instability strip marks where stars become too hot, pushing their ionization zones outward to the point where they are too close to the surface for pulsations to occur. The red edge marks the point where stars become too cool and convection takes over as the primary

method of energy transport in the outer layers of the star.

In addition to the instability strip having defined edges, there is an internal structure to the position of different classes of RR Lyrae stars within the instability strip. RRab stars tend to be located to the red side of the instability strip while the RRc stars are located on the blue side. This is illustrated in Figure 9.1 and can also be seen clearly in Figure 5.2 which shows the horizontal branch of NGC 1466. The RRd stars also tend to be on the blue side of the instability strip, though they do not appear as far blue as some RRc stars, which is consistent with the first overtone being the dominant pulsation mode in most RRd stars.

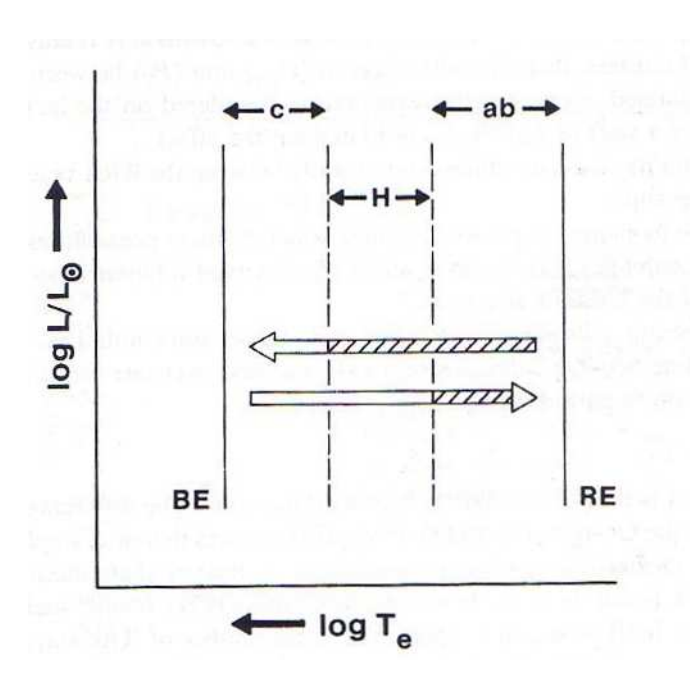


Figure 9.1: Depiction of the structure of the instability strip theorized by van Albada & Baker (1973). The blue (left) end of the instability strip is populated by RRc stars while RRab stars populate the red (right) end. The center of the instability strip is a "hysteresis zone" (labeled with an H) where the pulsation mode depends on the direction of evolution. Evolution toward the blue (left pointing arrow) produces mainly RRab stars in the hysteresis zone, as in an Oo-I cluster, while redward evolution produces primarily RRc stars in this zone, as in an Oo-II cluster. Figure from Smith (1995)

As can be seen in Figure 5.2, the transition between the RRab and RRc stars within the instability strip is not sudden, instead there is a region in the middle of

the strip which contains both fundamental mode and first overtone pulsators. Van Albada & Baker (1973) theorized that the central part of the instability strip is a "hysteresis zone", into which the RR Lyrae stars in this zone have evolved from elsewhere in the instability strip and their mode of pulsation is set by where they started out. Thus RRc stars in the hysteresis zone originally started out further to the blue and have evolved redward while RRab stars in this region are evolving toward the blue from initial positions that are on the red side of the hysteresis zone.

The period/temperature which marks the transition point between RRab and RRc stars is not constant. Instead this transition point, which can be represented through the period of the RRab star with the shortest period in a cluster,  $P_{ab,min}$ , is an indicator of Oosterhoff status. The transition between RRab and RRc stars occurs at shorter periods, and thus higher temperatures, in Oosterhoff I objects (Catelan et al. 2011, in preparation). Van Albada & Baker (1973) explain this connection between the transition period and the Oosterhoff type of the cluster as being due to the hysteresis zone and the general direction of horizontal branch evolution in the cluster. In this explanation the RR Lyrae stars in Oo-I objects are primarily evolving from red to blue, meaning that more RRab stars are moving into the hysteresis zone, pushing the transition between RRab and RRc stars more toward the blue and shorter periods. In Oo-II objects the evolution is occuring from blue to red, populating the hysteresis zone with more RRc stars and thus pushing the transition toward the red and longer periods (Fig. 9.1). Stellingwerf (1975) and Stellingwerf & Bono (1993) made similar predictions regarding the hysteresis zone.

### 9.2 Indicators of Oosterhoff Status

Catelan et al. 2011 (in prep) are currently working on examining how well  $P_{ab,min}$ , as well as other properties, serve as indicators of Oosterhoff type. As part of this effort I helped to compile and analyze an updated list of the properties of RR Lyrae

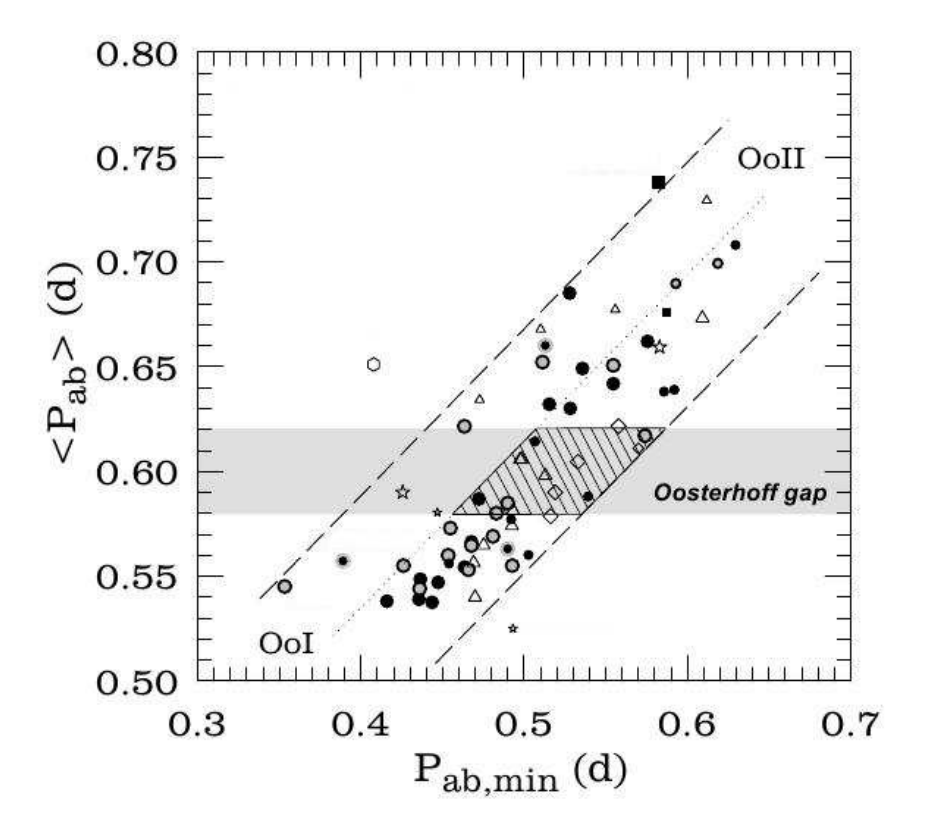


Figure 9.2: Average period of RRab stars vs  $P_{ab,min}$  for globular clusters with at least 5 known RRab stars. Large symbols indicate clusters with more than 10 RRab stars while small symbols indicate clusters with less that 10 RRab stars. The dashed lines define the region occupied by the majority of the globular clusters. The hatched area is the region occupied by the majority of the Oo-int clusters.

stars in all globular clusters known to have at least 5 RRab stars. This list includes a total of 65 Galactic and Local Group globular clusters; 27 are Oo-I, 22 Oo-II, and 14 are Oo-int. The properties that were examined include the number of RRab, RRc, and RRd stars, the number fraction of first overtone dominant pulsators, the mean periods for the RRab and RRc stars, the minimum period for an RRab star ( $P_{ab,min}$ ), and the maximum RRc period in the cluster ( $P_{c,max}$ ).

The average RRab period is the strongest indicator of Oosterhoff status, in fact the Oosterhoff gap, and thus Oo-int objects, are defined as having an average RRab period that falls in the range of  $0.58 \le \langle P_{ab} \rangle \le 0.62$  days (Catelan, 2004b). The other properties were plotted against  $\langle P_{ab} \rangle$  in an attempt to see if there were any

correlations, especially ones that pertained to Oosterhoff status.

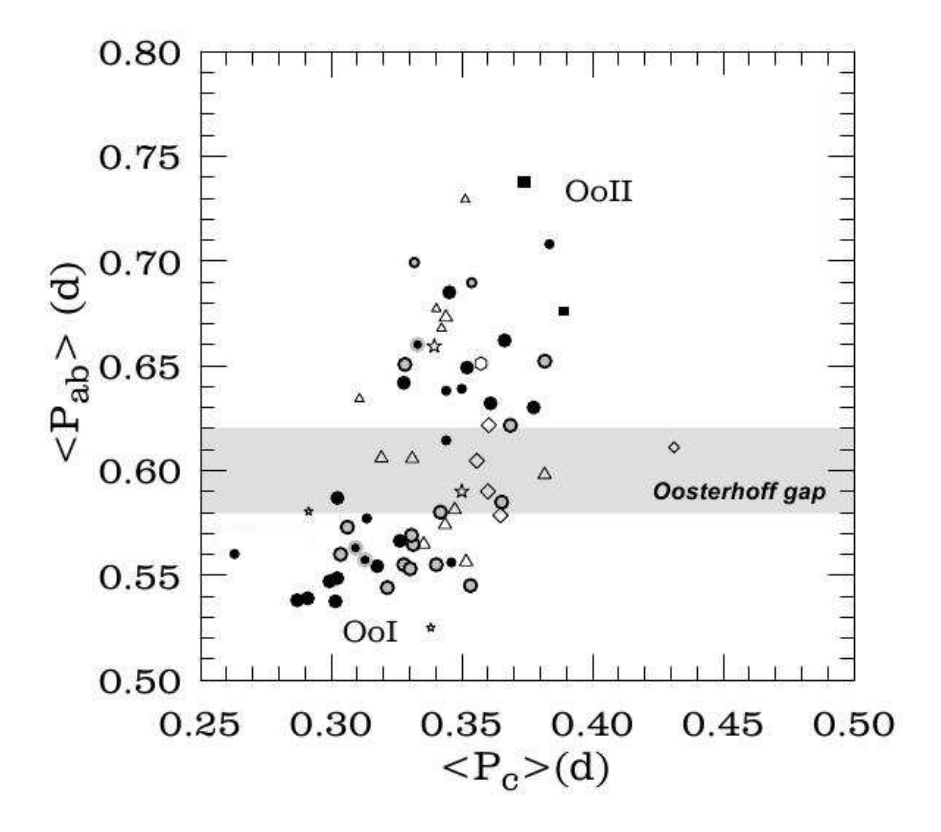


Figure 9.3: Correlation between  $\langle P_{ab} \rangle$  and  $\langle P_c \rangle$  for globular clusters with at least 5 known RRab stars.

Figure 9.2 shows the correlation between  $\langle P_{ab} \rangle$  and  $P_{ab,min}$ . There is a clear trend between the two properties that includes both Oo-I and Oo-II clusters, with clusters that have a large  $\langle P_{ab} \rangle$  also having a large value for  $P_{ab,min}$ . While there is range of  $P_{ab,min}$  values at a given  $\langle P_{ab} \rangle$ , there is very little overlap in  $P_{ab,min}$  values between Oo-I and Oo-II clusters. Oo-int objects fall on the same trend, forming a smooth transition between the Oo-I and Oo-II clusters. This suggests that Oo-int clusters form a link between the other two Oosterhoff groups.

The property that shows the next strongest correlation with  $\langle P_{ab} \rangle$ , and thus Oosterhoff type, is the average period for RRc stars,  $\langle P_c \rangle$ . As can be seen in Figure 9.3, there is a general correlation between these two properties, with clusters that have longer  $\langle P_{ab} \rangle$  also having longer  $\langle P_c \rangle$ . Despite this trend, and in contrast to traditional

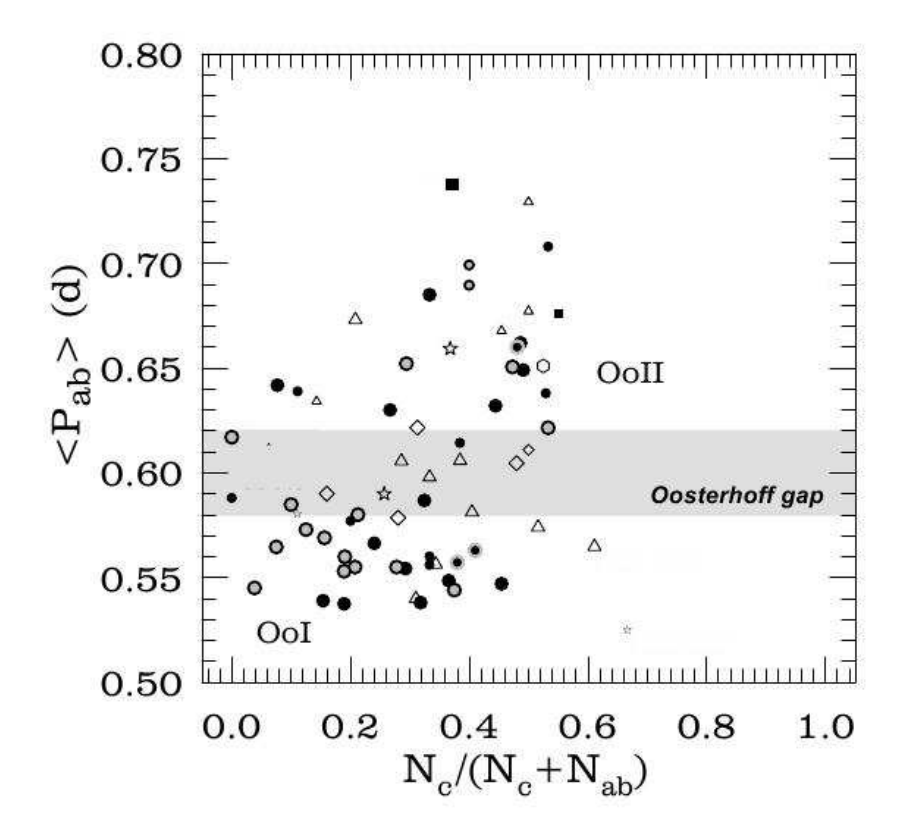


Figure 9.4: Correlation between  $\langle P_{ab} \rangle$  and the number fraction of RRc stars for globular clusters with at least 5 known RRab stars.

views (Smith, 1995),  $\langle P_c \rangle$  does not serve as a good indicator of Oosterhoff status due to the large range in  $\langle P_c \rangle$  values that overlap for the different Oosterhoff groups.

The number fraction of RRc stars,  $(N_c)/(N_{ab} + N_c)$ , and  $P_{c,max}$  also do not serve as good indicators of Oosterhoff type. Figures 9.4 and 9.5 show that there is considerable scatter in the relationship between both of these quantities and  $\langle P_{ab} \rangle$ . There is also almost complete overlap between the Oosterhoff groups with respect to  $P_{c,max}$  and the number fraction.

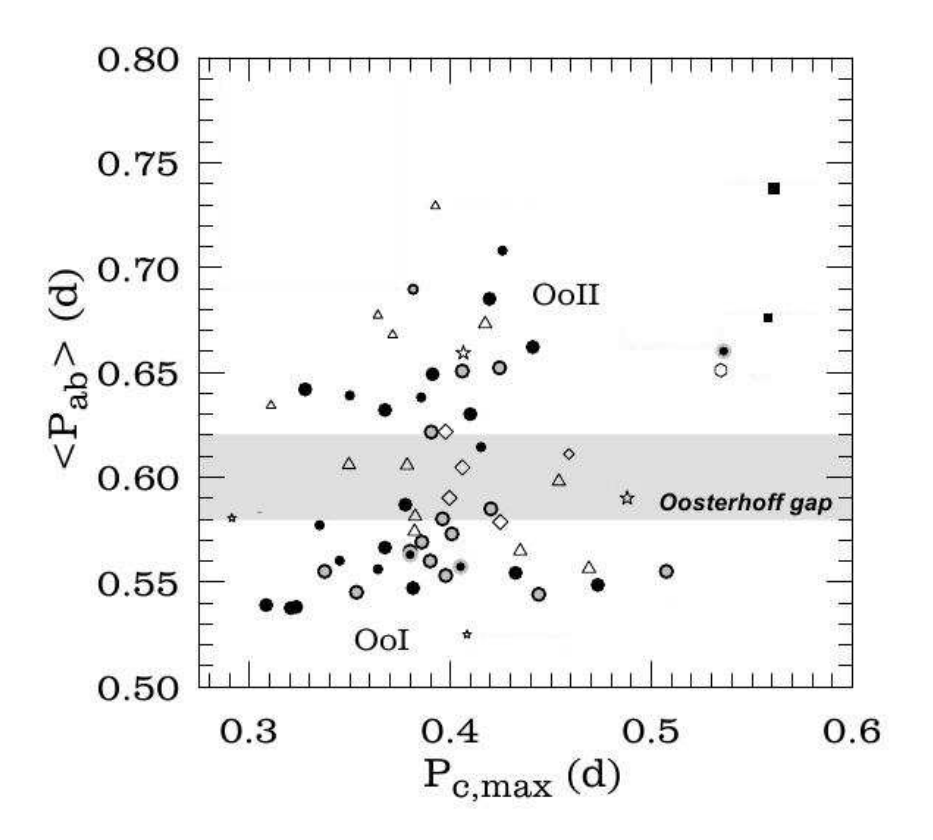


Figure 9.5: Correlation between  $\langle P_{ab} \rangle$  and  $P_{c,max}$  for globular clusters with at least 5 known RRab stars.

# 9.3 Bailey Diagrams for Oosterhoff Intermediate Objects

One question that can be asked about Oosterhoff intermediate objects is whether these objects are a mixture of Oo-I and Oo-II stars or whether they represent a population of RR Lyrae that fall in between the two Oosterhoff groups. One can answer this question by looking at the Bailey (period-amplitude) diagrams of Oo-int objects. If these objects are actually a mix of stars with Oo-I and Oo-II properties, one would expect to see significant populations of RR Lyrae stars near both the Oo-I and Oo-II loci on the diagram. Figure 9.6 shows the Bailey diagram for Canes Venatici I (CVn I), a nearby dwarf spheroidal galaxy. CVn I is an Oo-int object and instead of showing signs of a mix of Oo-I and Oo-II stars, the majority of its RRab stars fall between the

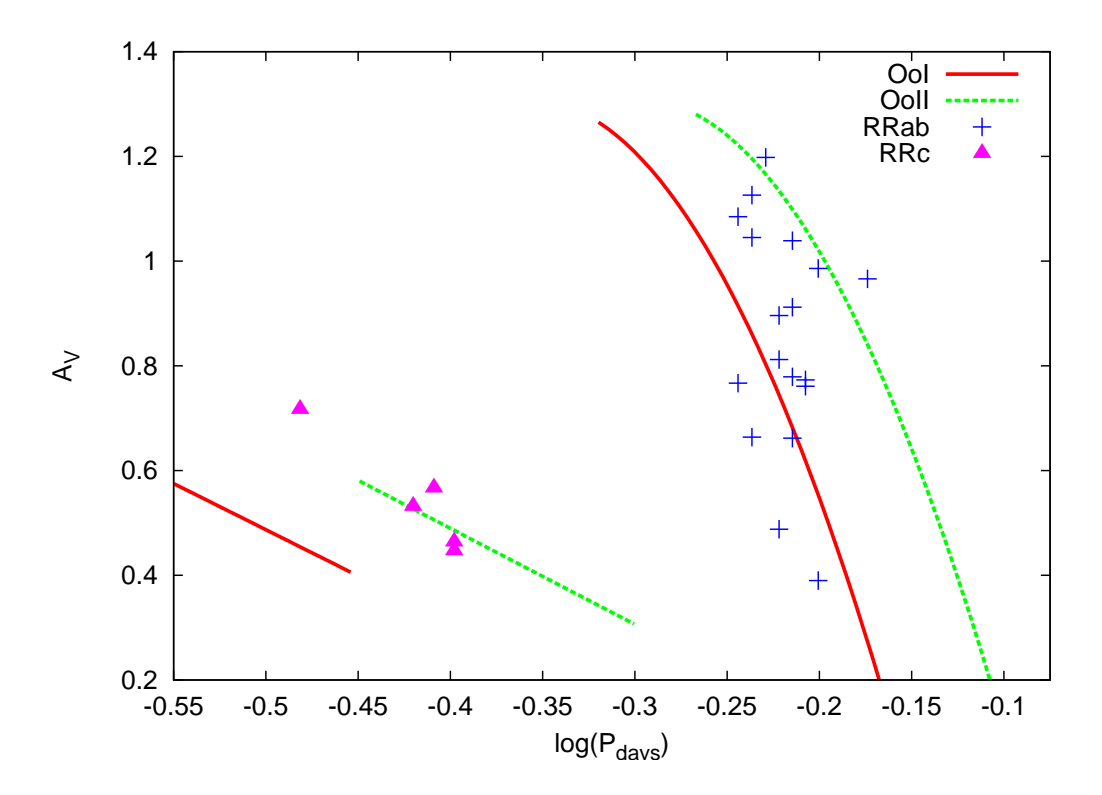


Figure 9.6: Bailey diagram, log period vs V-band amplitude for the RR Lyrae stars in the dwarf galaxy Canes Venatici I. Data from Kuehn et al. (2008).

Oo-I and Oo-II loci (Kuehn et al., 2008). The Bailey diagram for NGC 1466 (Figure 9.7) supports the case that Oo-int objects are not a mix of Oo-I and Oo-II stars as the RRab stars fall along a line that has a slightly longer period than the Oo-I locus; there is no sign of a significant population of stars with Oo-II properties.

Previous work such as van Albada & Baker (1973) and Sandage et al. (1981) have compared the Bailey diagram behavior of clusters of differing Oosterhoff types. This work led to the realization that the Oosterhoff effect exists on a star-by-star basis, with RR Lyrae stars in Oo-II stellar systems being systematically shifted to longer periods at a given amplitude. In the subsections below I carry out a similar analysis, comparing the Bailey diagrams of several Oo-int systems. Table 9.1 lists the metallicity, average periods for the RRab and RRc stars,  $P_{ab,min}$ ,  $P_{c,max}$ , and the number fraction of first overtone dominant pulsators ( $f_{cd}$ ) for the stellar systems that are examined.

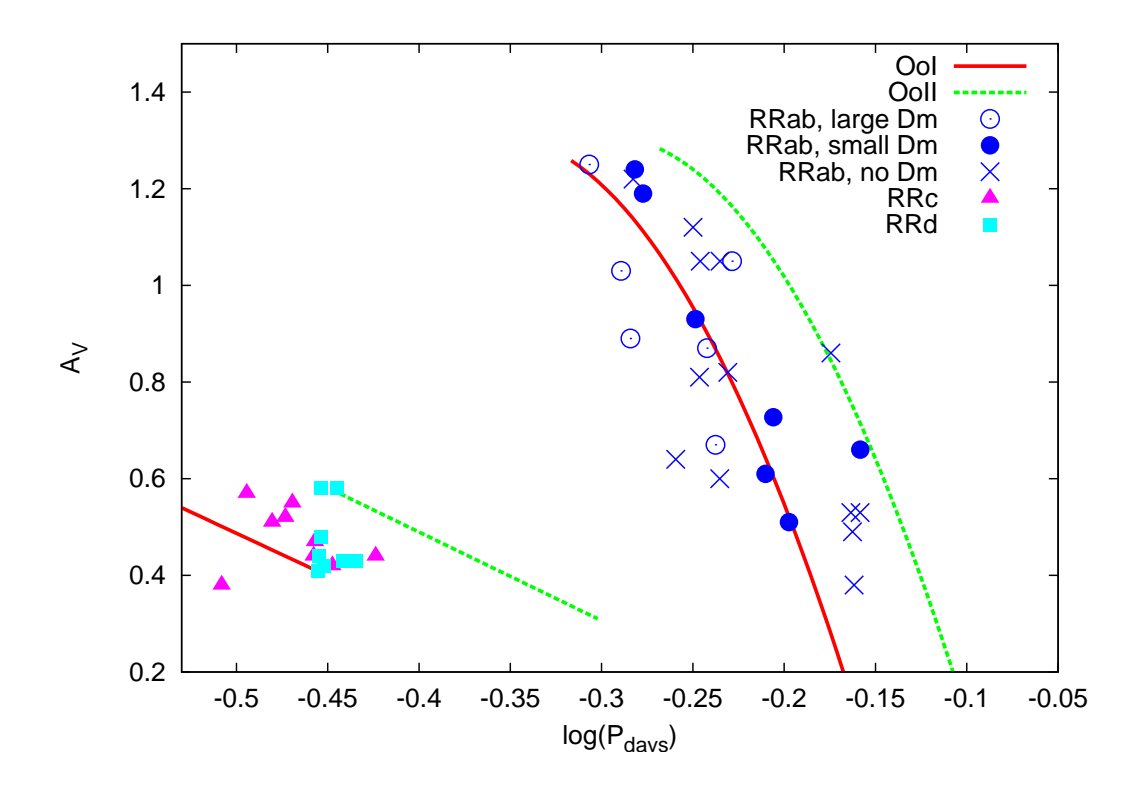


Figure 9.7: Bailey diagram, log period vs V-band amplitude for the RR Lyrae stars in NGC 1466.

Table 9.1: Properties of Stellar Systems Examined in Section 9.3

Object	[Fe/H]	НВ Туре	$\langle P_{ab} \rangle$	$\langle P_c \rangle$	$P_{ab,min}$	$P_{c,max}$	$f_{cd}$
NGC 1466	-1.64	0.38	0.591	0.335	0.4934	0.3770	0.39
NGC 2210	-1.65	0.65	0.612	0.350	0.5105	0.4355	0.35
Draco	-2.1		0.615	0.375	0.5366	0.4310	0.21
NGC 2257	-1.95	0.46	0.611	0.333	0.5042	0.3823	0.50
M3	-1.55	0.18	0.555	0.340	0.4560	0.4860	0.21
M15	-2.26	0.67	0.644	0.370	0.5527	0.4406	0.58

### 9.3.1 NGC 1466 vs Draco

The fact that not all Oo-int objects are alike is reinforced when one compares my results for the globular cluster NGC 1466 and the results for the Draco dwarf spheroidal galaxy obtained by Kinemuchi et al. (2008). Draco is more metal poor, [Fe/H]=-2.1, and has a longer average RRab period,  $\langle P_{ab}\rangle=0.615$  days, than NGC 1466. However, if we compare the Bailey diagrams of these two clusters (Figure 9.8) we see that their RRab stars occupy similar positions on the diagram and show a similar level of scatter. The shortest period RRab star in NGC 1466 has a much shorter period,  $P_{ab,min,1466}=0.4934$  days, than the shortest period RRab star in Draco,  $P_{ab,min,Draco}=0.5366$  days; since Draco contains more RR Lyrae stars than NGC 1466, this is unlikely to be due to statistical effects.

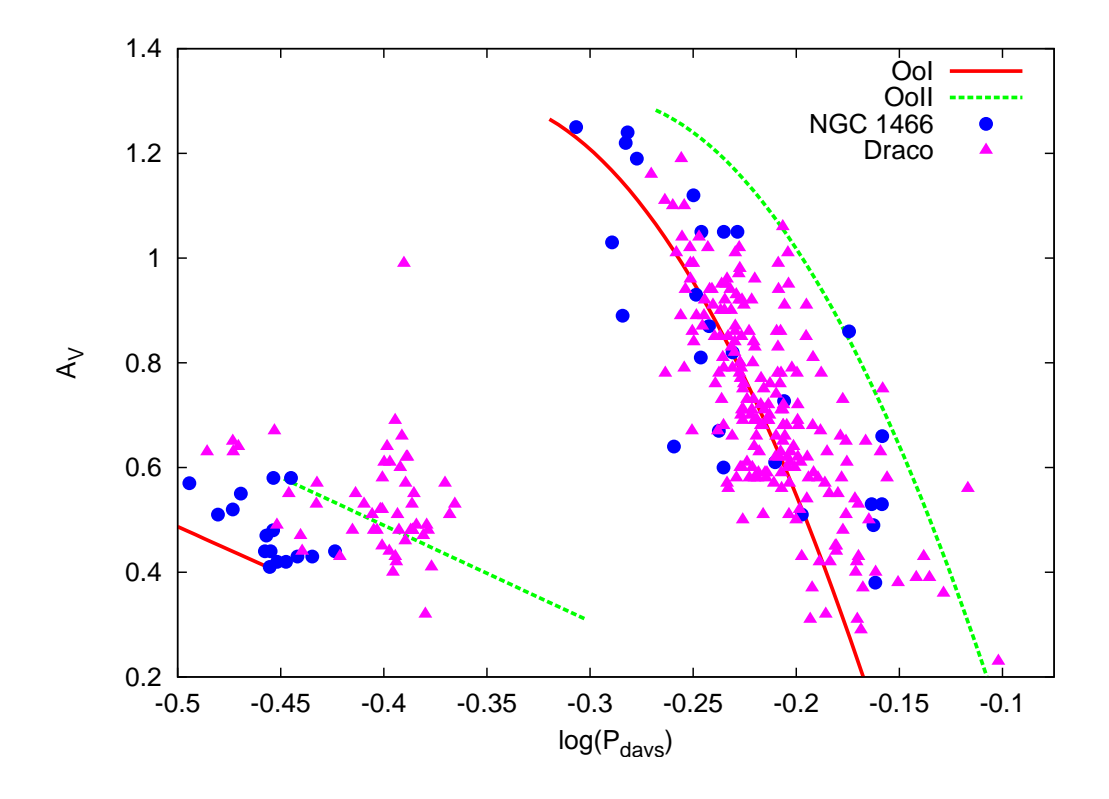


Figure 9.8: Bailey diagram, log period vs V-band amplitude, for the RR Lyrae stars in NGC 1466 (blue circles) and Draco (purple triangles).

In contrast to the RRab stars, the majority of RRc stars in NGC 1466 have shorter

periods than those in Draco. Combined with the shorter  $P_{ab,min}$ , this suggests that the transition between RRc and RRab stars occurs at a shorter fundamental mode period in NGC 1466 than in Draco.

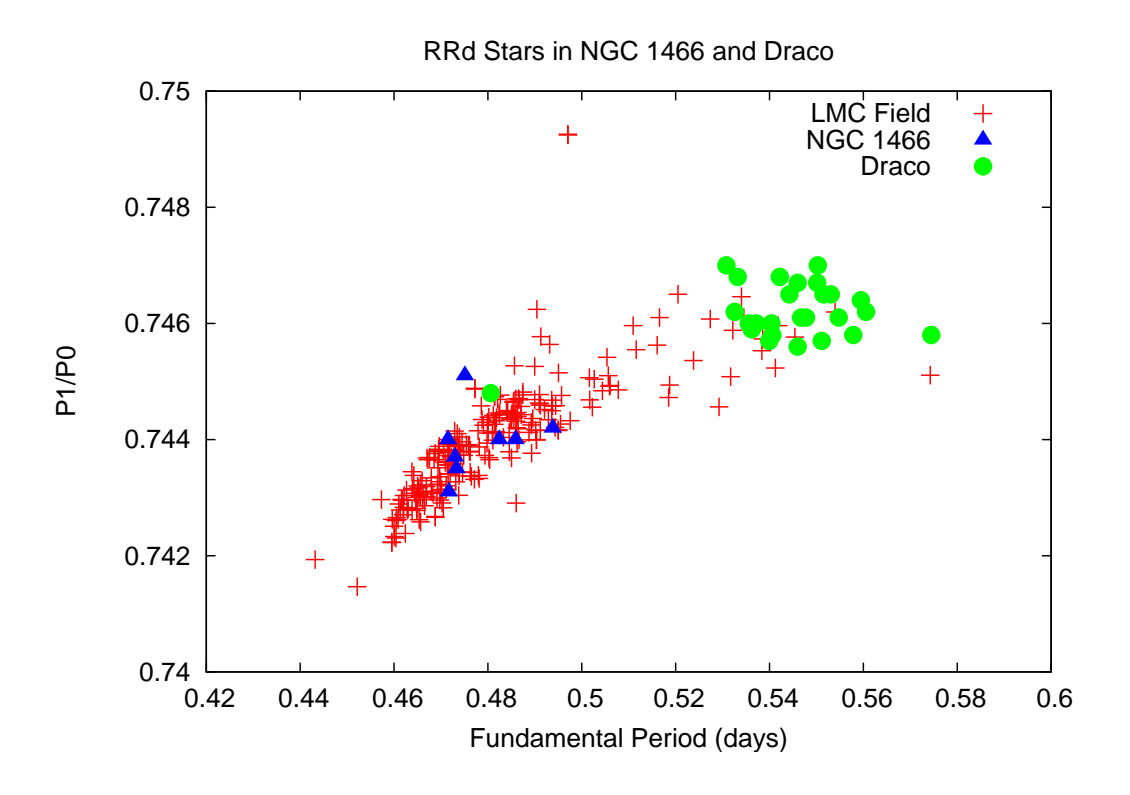


Figure 9.9: Petersen diagram showing the ratio of the first overtone period to the fundamental mode period vs. fundamental mode period for the RRd stars in NGC 1466 (blue triangles) and Draco (green circles). Also plotted are the RRd stars in the LMC field (red plus symbols) from Soszyński et al. (2003)

The RRd stars in both objects show different Oosterhoff natures. Figure 9.9 shows the RRd stars for both NGC 1466 and Draco plotted on a Petersen diagram. All but one of the RRd stars in Draco have longer fundamental mode periods and higher period ratios than their counterparts in NGC 1466. The RRd stars in Draco occupy a similar position to what is typically seen in Oo-II clusters while those in NGC 1466 enjoy a position similar to those in Oo-I objects (Popielski et al., 2000). Despite their status as Oo-int stellar systems, neither NGC 1466 or Draco have RRd stars that occupy an intermediate position between Oo-I/II clusters.

### 9.3.2 NGC 1466 vs NGC 2210

While Draco and NGC 1466 have a significant difference in metallicity, NGC 1466 and NGC 2210 present an opportunity to compare two Oosterhoff intermediate objects that have nearly equivalent metallicities,  $[Fe/H] \approx -1.65$ . The average RRab period for NGC 2210 is  $\langle P_{ab,2210} \rangle = 0.612$  days, similar to Draco and longer than the average period of NGC 1466,  $\langle P_{ab,1466} \rangle = 0.591$  days. As was the case with Draco, NGC 1466 has a shorter minimum RRab period,  $P_{ab,min,1466} = 0.4934$  days, than NGC 2210,  $P_{ab,min,2210} = 0.51049$  days. If one compares the Bailey diagrams for the two clusters (Fig. 9.10), one sees very different behaviors. Both clusters show a great deal of scatter among their RRab stars, with most of those stars falling between the Oo-I and Oo-II loci. NGC 1466 has a group of RRab stars that cluster around the Oo-II locus while NGC 2210 shows essentially the opposite behavior, having a group of RRab stars that cluster around the Oo-II line. The difference in positions of the RRab stars between these two clusters looks very similar to systematic shift in RRab position found by Sandage et al. (1981) when comparing the Galactic globular clusters M3 (Oo-I) and M15 (Oo-II).

The strong difference in RRab period-amplitude behavior between NGC 1466 and NGC 2210, despite their similarity in metallicity, indicates that metallicity is not the dominant factor in determining the position of RRab stars on the Bailey diagram, at least not within Oo-int clusters. NGC 1466 has a horizontal branch type of (B-R)/(B+V+R)=0.38 which is redder than the HB type of 0.65 of NGC 2210 (Mackey & Gilmore, 2004b). Figure 8 in Catelan (2009a) plots the relationship between metallicity and HB type; both clusters would fall within the Oo-int region on this figure, however NGC 1466 is located close to the red edge of the Oo-int region while NGC 2210 is located close to the blue edge. If NGC 1466 had a horizontal branch that was slightly redder it would fall in the Oo-I region while if the HB of NGC 2210 was slightly bluer it would fall in the Oo-II region. This suggests that the

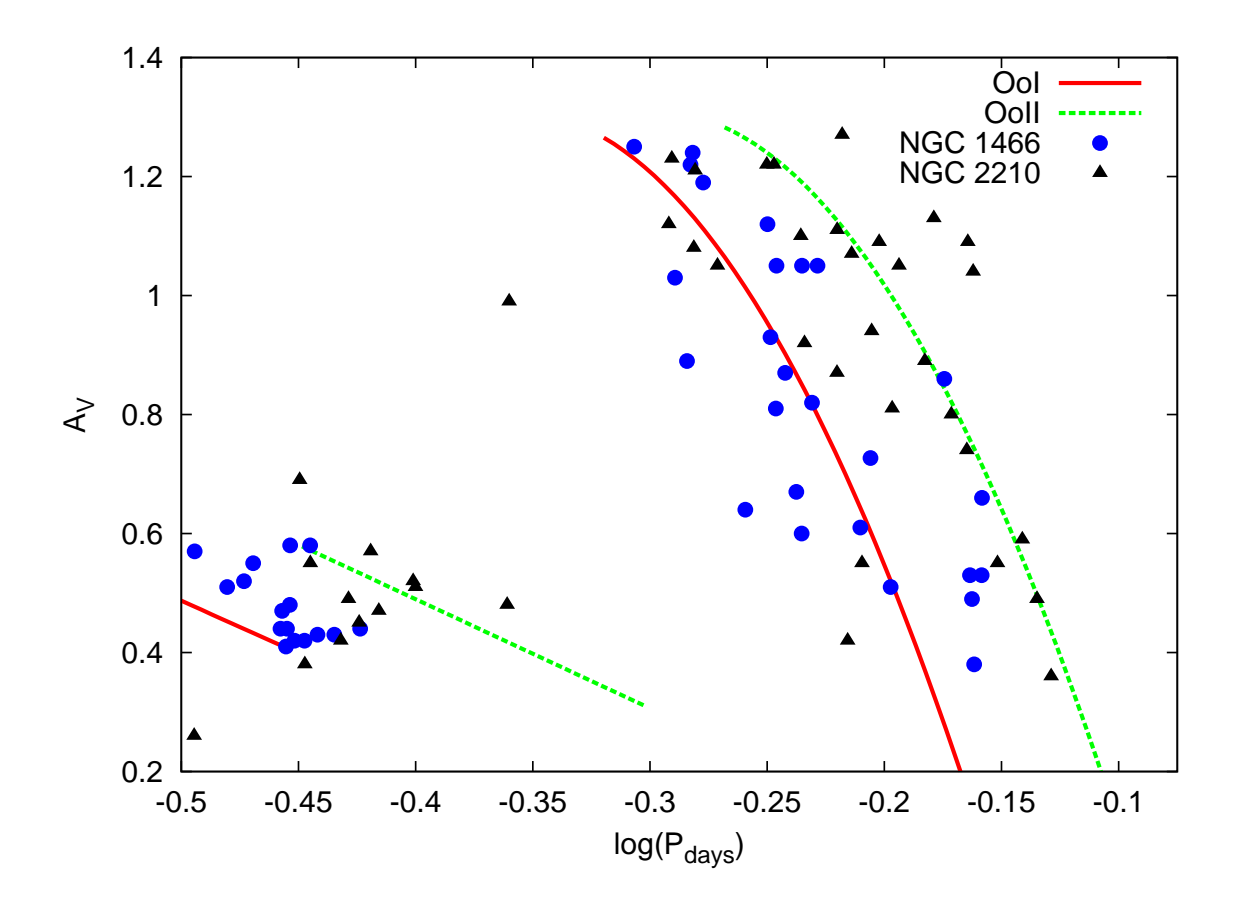


Figure 9.10: Bailey diagram, log period vs V-band amplitude, for the RR Lyrae stars in NGC 1466 (blue circles) and NGC 2210 (black triangles).

difference in RRab period-amplitude behavior between these two clusters is related to the morphology of their horizontal branches.

### 9.3.3 NGC 2210 vs NGC 2257

NGC 2257 is another Oosterhoff intermediate globular cluster located in the LMC. It is more metal-poor than NGC 1466 and NGC 2210 with a metallicity of [Fe/H] =  $-1.95\pm0.02$  dex (Mucciarelli et al., 2010). NGC 2257 has a  $\langle P_{ab} \rangle = 0.611$  days, similar to NGC 2210, and a  $P_{ab,min} = 0.5042$  days (Nemec et al., 2009), which is slightly shorter than in NGC 2210. The combined Bailey diagram for the two clusters (Fig. 9.11) shows that the RRab stars in the two clusters occupy similar positions. The RRab stars exhibit a large amount of scatter, with many being located between the

Oo-I and Oo-II loci; however, there is clustering, especially among the low-amplitude RRab stars, near the Oo-II locus. The comparison between NGC 2210 and NGC 2257 is similar to the one involving NGC 1466 and Draco in that both Oo-int stellar systems with different metallicities show similar behavior of their RRab stars on the Bailey diagram.

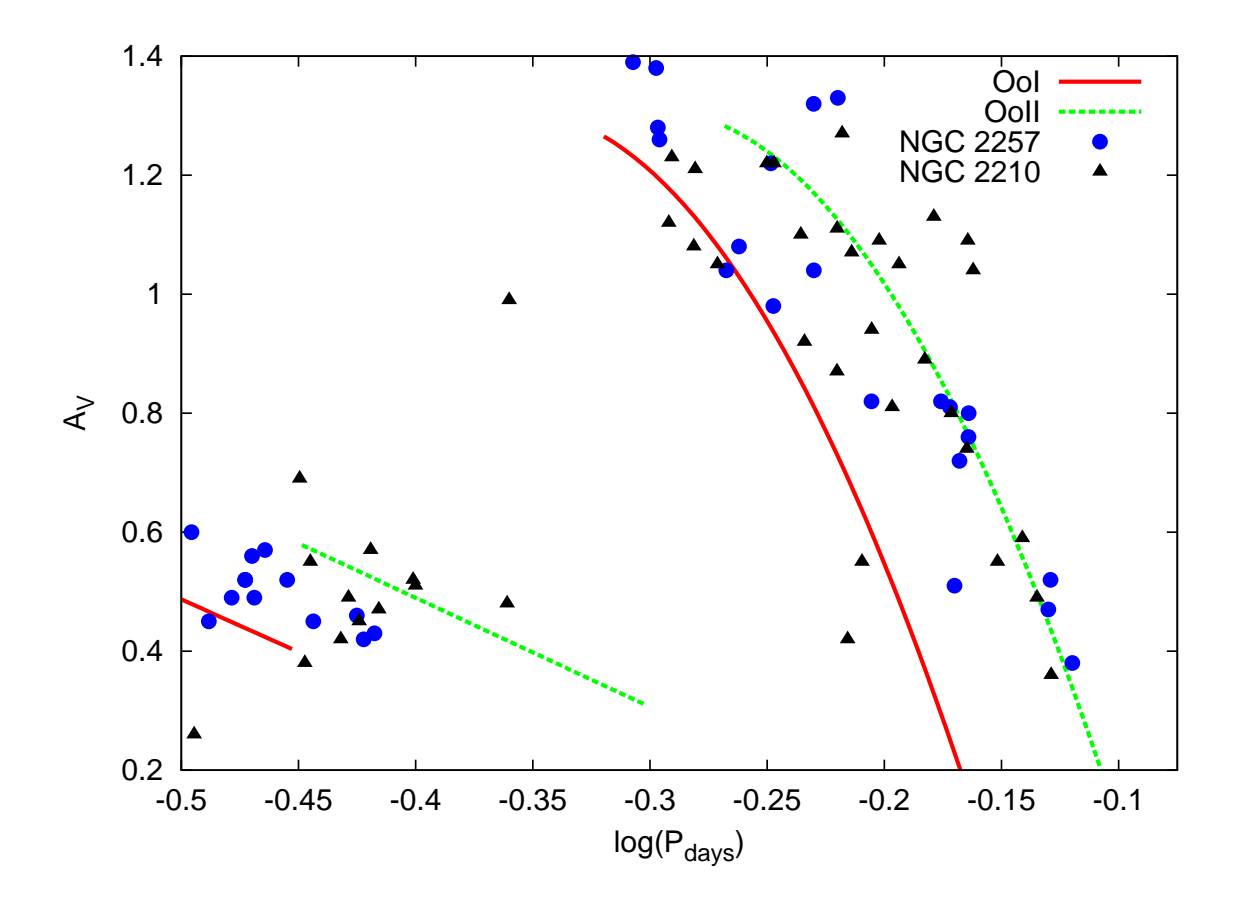


Figure 9.11: Bailey diagram, log period vs V-band amplitude, for the RR Lyrae stars in NGC 2210 (black triangles) and NGC 2257 (blue circles). Data for NGC 2257 from Nemec et al. (2009).

Even though the RRab stars in NGC 2257 fall closer to the Oo-II locus, the 3 RRd stars in the cluster all fall in the region of the Petersen diagram that is typically occuppied by RRd stars in Milky Way Oo-I globular clusters (see Figure 20 in Nemec et al. (2009)). As mentioned in Section 9.3.1, Draco features RRab stars that fall closer to the Oo-I locus but its RRd stars mostly fall in the region of

the Petersen diagram that is typically occupied by Oo-II clusters. These two stellar systems strongly indicate that in Oosterhoff intermediate objects, the behavior of the RRab and RRd stars are unrelated to each other. There is some indication that the behavior of the RRd stars may be related to the behavior of the RRc stars. The RRc stars for Draco fall near the Oo-II locus (Fig. 9.8) while the RRc stars in NGC 2257 fall more toward the Oo-I locus, consistent with the groupings of their RRd stars on the Petersen diagram.

### 9.3.4 NGC 1466 AND NGC 2210 VS OOSTERHOFF I/II SYSTEMS

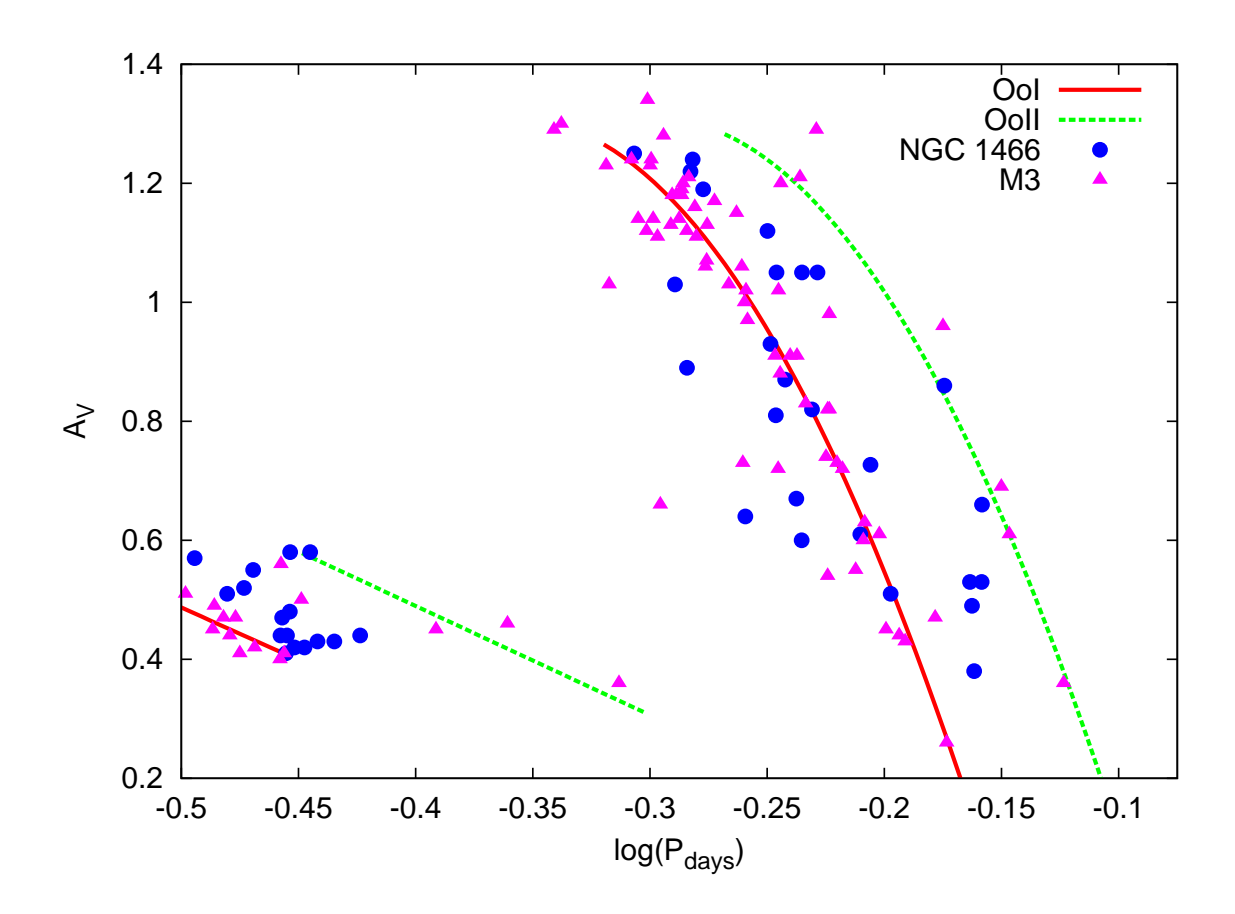


Figure 9.12: Bailey diagram, log period vs V-band amplitude, for the RR Lyrae stars in NGC 1466 (blue circles) and M3 (purple triangles). Data for M3 is from Cacciari et al. (2005).

Since NGC 1466 and NGC 2210 feature RRab stars that tend toward either the

Oo-I or Oo-II loci in the Bailey diagram, it is worth examining how these two clusters compare to bona fide Oo-I/II clusters. Figure 9.12 shows the combined Bailey diagram for the RR Lyrae stars in NGC 1466 and M3, an Oo-I cluster located in the halo of the Milky Way. M3 has a metallicity of  $[Fe/H] = -1.55 \pm 0.13$  (Smolinski et al., 2011), somewhat more metal-rich than NGC 1466. M3's  $\langle P_{ab} \rangle = 0.555$  days and  $P_{ab,min} = 0.4560$  days (Cacciari et al., 2005) are both shorter than what is seen in NGC 1466. The RRab stars in the two clusters occupy similar positions. However, the majority of the RRab stars in M3 show tighter clustering around the Oo-I locus than those in NGC 1466. A bigger difference is seen among the RRc stars; the majority of the RRc stars in M3 are tightly clustered around the Oo-I locus while the RRc stars in NGC 1466 occupy positions between the Oo-I and Oo-II loci. The majority of the RRc stars in M3 are shifted toward a shorter period than their counterparts in NGC 1466. This shift in RRc periods, along with M3 having a shorter  $P_{ab,min}$ , supports the transition between RRab and RRc stars in M3 occuring at a shorter period than in NGC 1466.

NGC 2210 can also be compared to the Milky Way Oo-II globular cluster M15. M15 is very metal-poor, [Fe/H] = -2.26 (Harris, 2010), and has an average RRab period of  $\langle P_{ab} \rangle = 0.644$  days and a minimum RRab period of  $P_{ab,min} = 0.5527$  days (Corwin et al., 2008), both of which are longer than the values for NGC 2210. Figure 9.13 shows the Bailey diagram for these two clusters. The RRab stars in both clusters show a great deal of scatter and largely occupy similar positions. The major difference in the RRab stars between the two clusters is that the RRab stars in NGC 2210 extend to a shorter period than those in M15. If you remove the five NGC 2210 RRab stars that have a  $\log(P) \leq -0.25$ , the distributions of RRab stars in the two clusters would be essentially the same. The shorter period RRab to RRc transition in NGC 2210 seems to be responsible for the Oo-int classification of the cluster.

When compared to bona fide Oo-I/II clusters, the RRab stars in NGC 1466 and

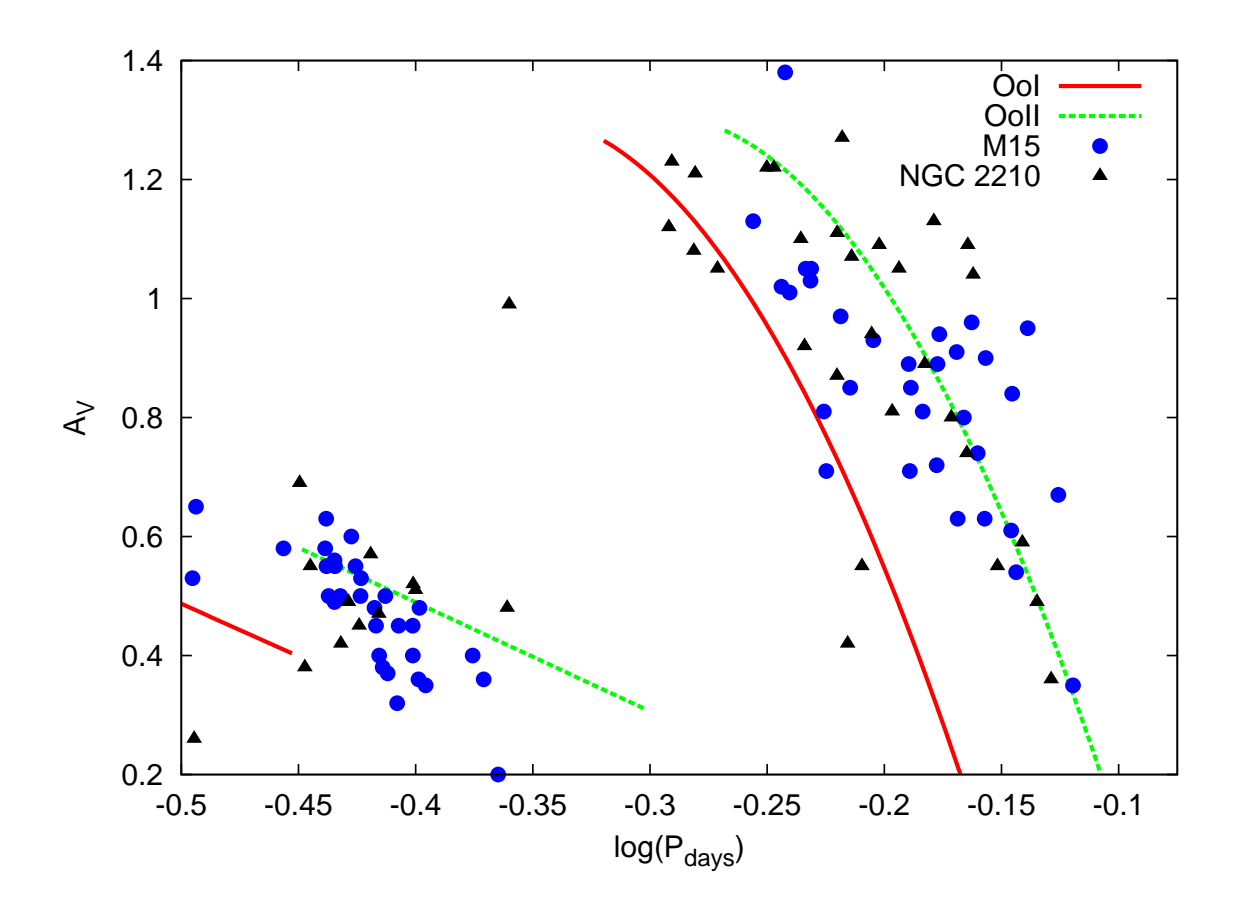


Figure 9.13: Bailey diagram, log period vs V-band amplitude, for the RR Lyrae stars in NGC 2210 (black triangles) and M15 (blue circles). Data for M15 is from Corwin et al. (2008).

NGC 2210 seem to occupy similar positions in the Bailey diagram to the RRab stars in the comparison cluster. While the Oo-int clusters show slightly more scatter in the position of their RRab stars, the factor that seems to drive the Oosterhoff classification of these clusters is the transition period between RRab and RRc stars, as indicated by  $P_{ab,min}$ .

### 9.3.5 Oosterhoff Intermediate Locus?

As can been seen in the numerous Bailey diagrams that have been presented in this dissertation, Oo-I and Oo-II objects have loci that mark the typical positions of the RRab stars in these types of clusters. One question that this dissertation hoped to

answer pertained to whether a similar locus existed for the RRab stars in Oo-int clusters. A quick look at the Bailey diagram for CVn-I (Fig. 9.6), and the combined Bailey diagrams comparing NGC 1466 to Draco (Fig. 9.8) and to NGC 2210 (Fig. 9.10), shows that such a locus does not exist for Oo-int objects.

Despite having a considerable scatter, the RRab stars in NGC 1466 and Draco tend to fall toward the Oo-I locus while the RRab stars in NGC 2210 and NGC 2257 fall more toward the Oo-II locus. CVn-I displays a middle ground between these two extremes with the majority of its RRab stars falling between the Oo-I and Oo-II loci, showing no clustering near either one. Obviously the Bailey diagram behavior of Oo-int objects is complex and further work is needed in order to understand this behavior.

The results in this chapter reveal that Oosterhoff intermediate objects do not constitute a homogeneous and entirely separate class. Instead, Oo-int objects seem to represent a transition between Oo-I and Oo-II objects. Many Oo-int objects look very similar to Oo-I/II objects while CVn-I indicates that at least some Oo-int objects represent more of a middle ground. The difference between Oo-int objects that are similar to Oo-I objects and those that are more similar to Oo-II objects may result from a difference in the luminosity of the RR Lyrae stars in these objects, similar to the explanation for the difference between Oo-I and Oo-II clusters. This difference in luminosity has been explained as possibly arising from a difference in the helium content of the stars (Sandage et al., 1981). Applying this to the case of the Oo-int objects this would mean that RR Lyrae stars in objects that are similar to Oo-II objects, such as NGC 2210, have a higher helium content and a higher luminosity than RR Lyrae stars in Oo-int clusters that are more similar to Oo-I objects, such as NGC 1466. Differences between Oo-int and Oo-I/II objects seem to arise due to differences in the transition period between RRab and RRc stars.

## Chapter 10: Trends in Physical Properties

The physical properties of RR Lyrae stars obtained through Fourier analysis, as discussed in Chapter 4, provide another way to look at the difference between RR Lyrae stars in various clusters. Tables 10.1 and 10.2 give the average physical properties for the RRab and RRc stars, respectively, in previously studied clusters. The majority of the data for the physical properties comes from Lázaro et al. (2006) and Contreras et al. (2010), with the data on M75 coming from Corwin et al. (2003). The metallicity listed in the tables is the cluster metallicity and comes from Harris (2010).

Table 10.1: Mean Physical Properties Obtained for RRab Stars in Previously Studied Globular Clusters

Cluster	Oo Type	# Stars	[Fe/H]	$\langle T_{\rm eff} \rangle$	$\langle M_V \rangle$
NGC 6362	Ι	14	-0.99	6555	0.86
NGC 6171	I	3	-1.02	6619	0.85
NGC 1851	I	7	-1.18	6494	0.80
M62	I	39	-1.18	6501	0.83
M5	Ι	26	-1.29	6465	0.81
NGC 6229	I	9	-1.47	6477	0.81
NGC 6934	I	24	-1.47	6455	0.81
M3	I	17	-1.50	6438	0.78
NGC 4147	I	5	-1.80	6633	0.80

Table 10.1 (continued)

Cluster	Oo Type	# Stars	[Fe/H]	$\langle T_{\rm eff} \rangle$	$\langle M_V \rangle$
M75	Int	5	-1.24	6529	0.81
M2	II	9	-1.65	6276	0.71
NGC 5286	II	12	-1.69	6266	0.72
M9	II	5	-1.77	6305	0.68
M55	II	5	-1.94	6333	0.67
NGC 5466	II	9	-1.98	6328	0.52
M92	II	5	-2.31	6160	0.67
M15	II	11	-2.37	6237	0.67

Table 10.2: Mean Physical Properties Obtained for RRc Stars in Previously Studied Globular Clusters

Cluster	Oo Type	# Stars	[Fe/H]	$\langle M/M_{\odot} \rangle$	$\langle log(L/L_{\odot}) \rangle$	$\langle T_{eff} \rangle$	$\langle Y \rangle$
NGC 6362	I	15	-0.99	0.53	1.66	7429	0.29
NGC 6171	I	6	-1.02	0.53	1.65	7447	0.29
M62	I	21	-1.18	0.53	1.66	7413	0.29
M5	I	14	-1.29	0.54	1.69	7353	0.28
NGC 6229	I	9	-1.47	0.56	1.69	7332	0.28
NGC 6934	I	4	-1.47	0.63	1.72	7290	0.27
M3	I	5	-1.50	0.59	1.71	7315	0.27
NGC 4147	I	9	-1.80	0.55	1.693	7335	0.28
M75	$\operatorname{Int}$	7	-1.29	0.53	1.67	7399	0.29
M2	II	2	-1.65	0.54	1.74	7215	0.27
NGC 5286	II	12	-1.69	0.60	1.72	7276	0.27

Table 10.2 (continued)

Cluster	Oo Type	# Stars	[Fe/H]	$\langle M/M_{\odot} \rangle$	$\langle log(L/L_{\odot}) \rangle$	$\langle T_{eff} \rangle$	$\langle Y \rangle$
M9	II	2	-1.77	0.60	1.74	7247	0.27
NGC 2298	II	2	-1.92	0.59	1.75	7200	0.26
M55	II	5	-1.94	0.53	1.75	7193	0.27
NGC 5466	II	7	-1.98	0.52	1.696	7191	0.25
M68	II	16	-2.23	0.70	1.79	7145	0.25
M92	II	3	-2.31	0.64	1.77	7186	0.26
M15	II	8	-2.37	0.76	1.81	7112	0.24

Figures 10.1-10.5 show the average physical properties for the RR Lyrae stars in these clusters plotted against the cluster metallicity; the error bars that are included are meant to be representative and come from the sources referenced in Contreras et al. (2010). The majority of these plots reveal a linear trend with cluster metallicity. The trend of average mass for RRc stars versus cluster metallicity (Fig. 10.3) has the greatest number of outliers from its roughly linear trend. It is also important to note that the Oo-I and Oo-II objects fall along the same linear trend when we look at most of these physical properties. This agreement suggests that the physical properties responsible for the formation of RR Lyrae stars are the same in Oo-I and Oo-II objects. The one exception occurs when looking at average RRab V-band absolute magnitude  $(M_V)$  versus cluster metallicity (Fig. 10.5). This physical property displays a trend that is more like a step function. The Oo-I clusters demonstrate a linear relationship where more metal-poor clusters feature RRab stars that have slightly brighter absolute magnitudes than more metal-rich clusters. There are not enough Oo-II clusters to determine if they display a similar variation with cluster metallicity or if they occur at a constant absolute magnitude.

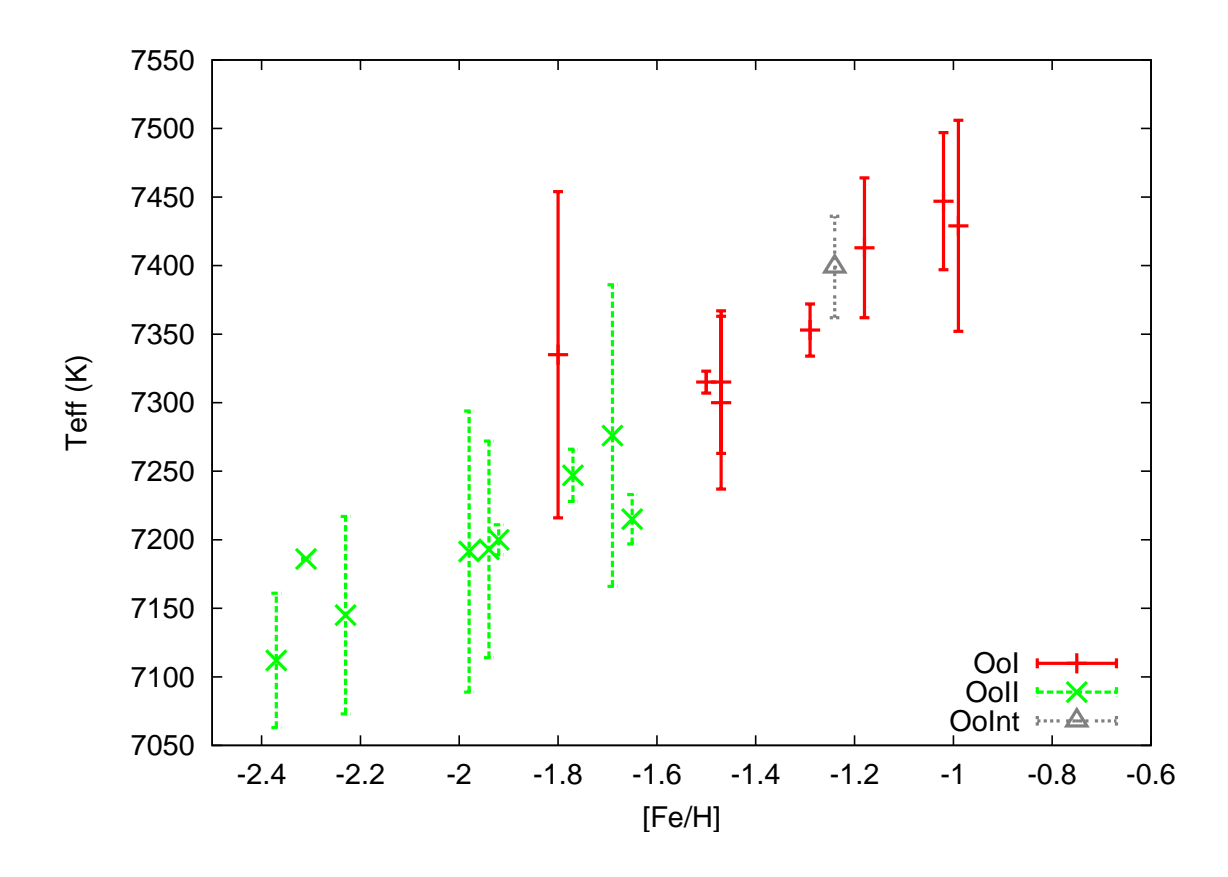


Figure 10.1: The average effective temperature,  $\langle T_{\rm eff} \rangle$ , for RRc stars in previously studied globular clusters vs cluster metallicity.

These previously studied clusters are all located in the Milky Way halo and include only one Oo-int cluster, M75; the other three Oo-int clusters in the Milky Way have not had physical properties derived for their RR Lyrae stars. M75, represented by a gray triangle in Figures 10.1-10.5, follows the same trends as the Oo-I and Oo-II clusters. In Figure 10.5, M75 has an absolute magnitude that is similar to the Oo-I clusters.

The work done in this dissertation allows us to see if extragalactic Oo-I/II globular clusters follow the same trend as their Milky Way counterparts. This sample increases the number Oo-int clusters for which physical properties have been calculated, allowing for a much better comparison between Oo-int and Oo-I/II clusters. Tables 10.3 and 10.4 summarize the average physical properties for the clusters discussed in this

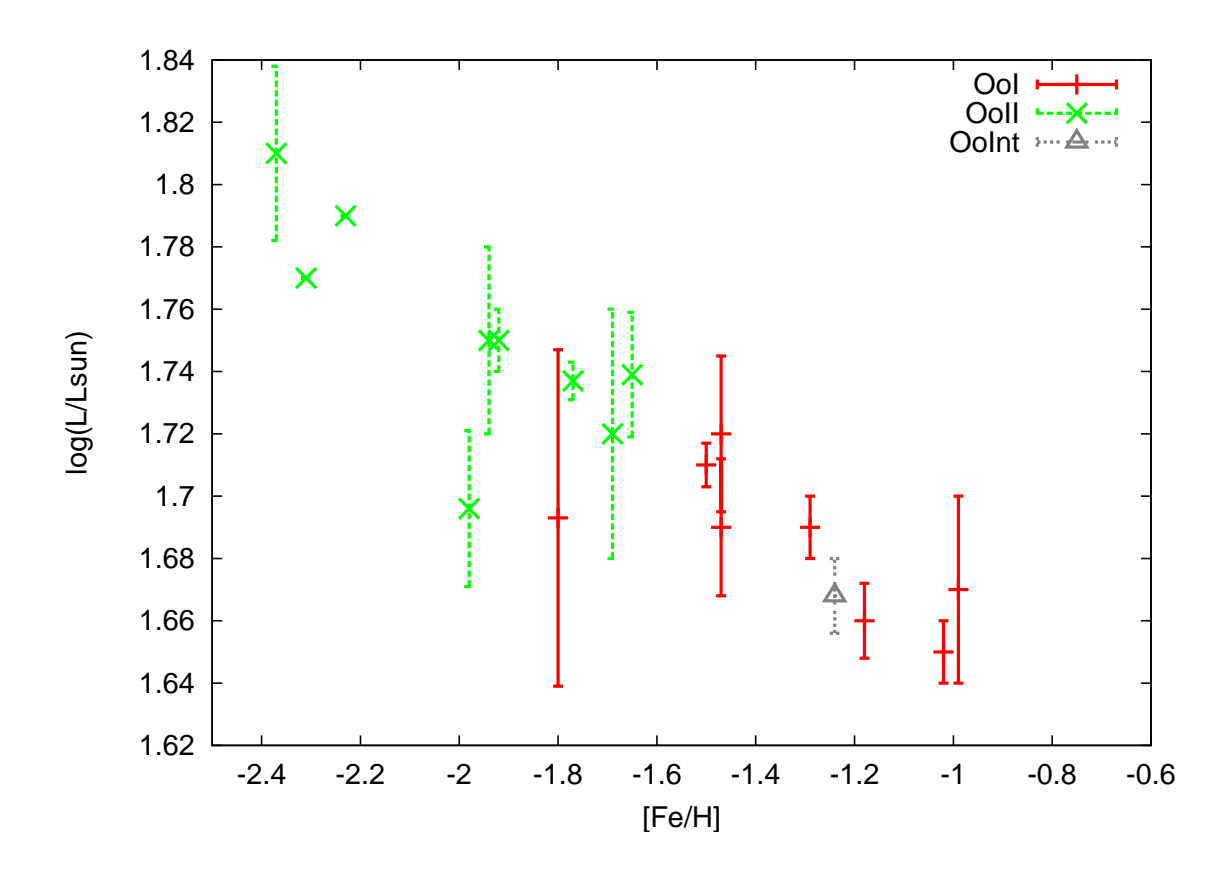


Figure 10.2: Average luminosity (in terms of the luminosity of the Sun),  $\langle L/L_{\odot}\rangle$ , for RRc stars in previously studied globular clusters vs cluster metallicity.

thesis.

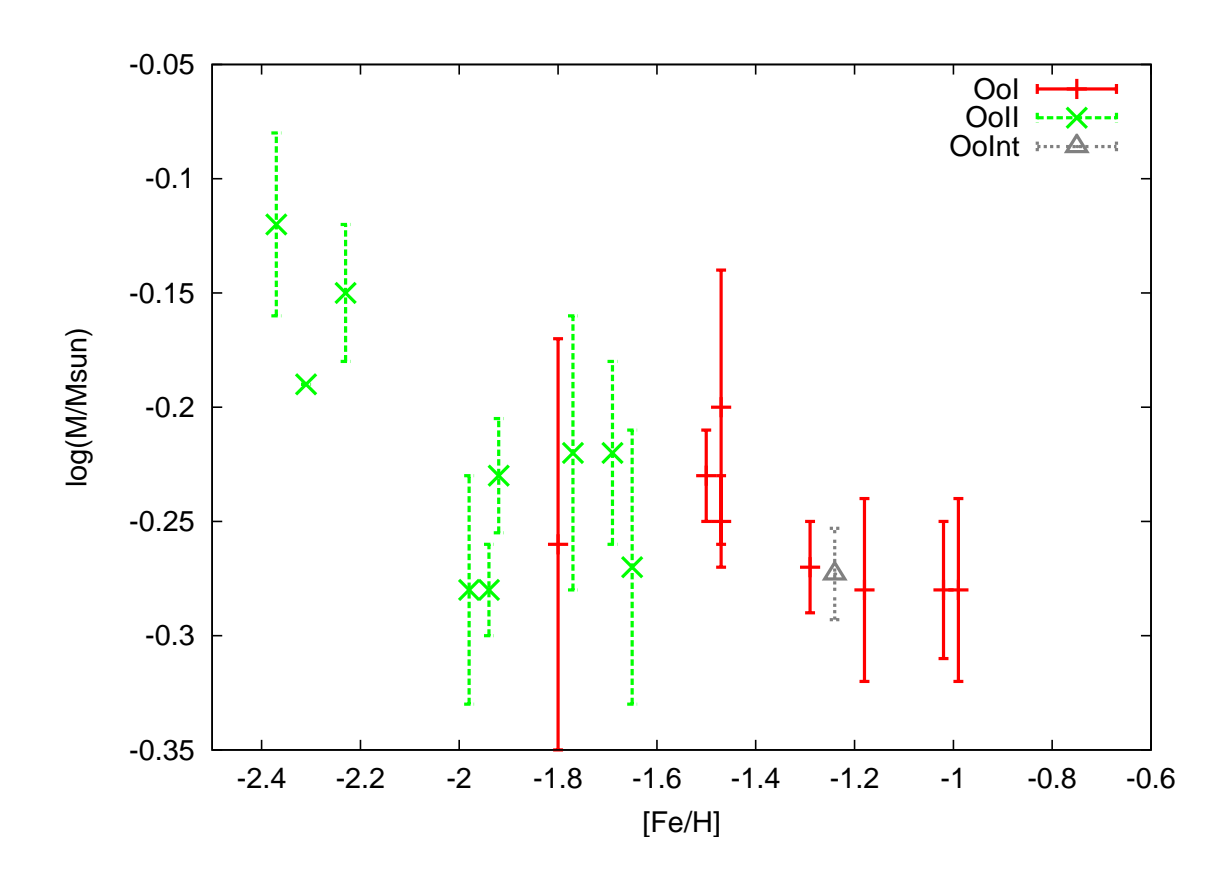


Figure 10.3: Average mass (in terms of the mass of the Sun),  $\langle M/M_{\odot}\rangle$ , for RRc stars in previously studied globular clusters vs cluster metallicity.

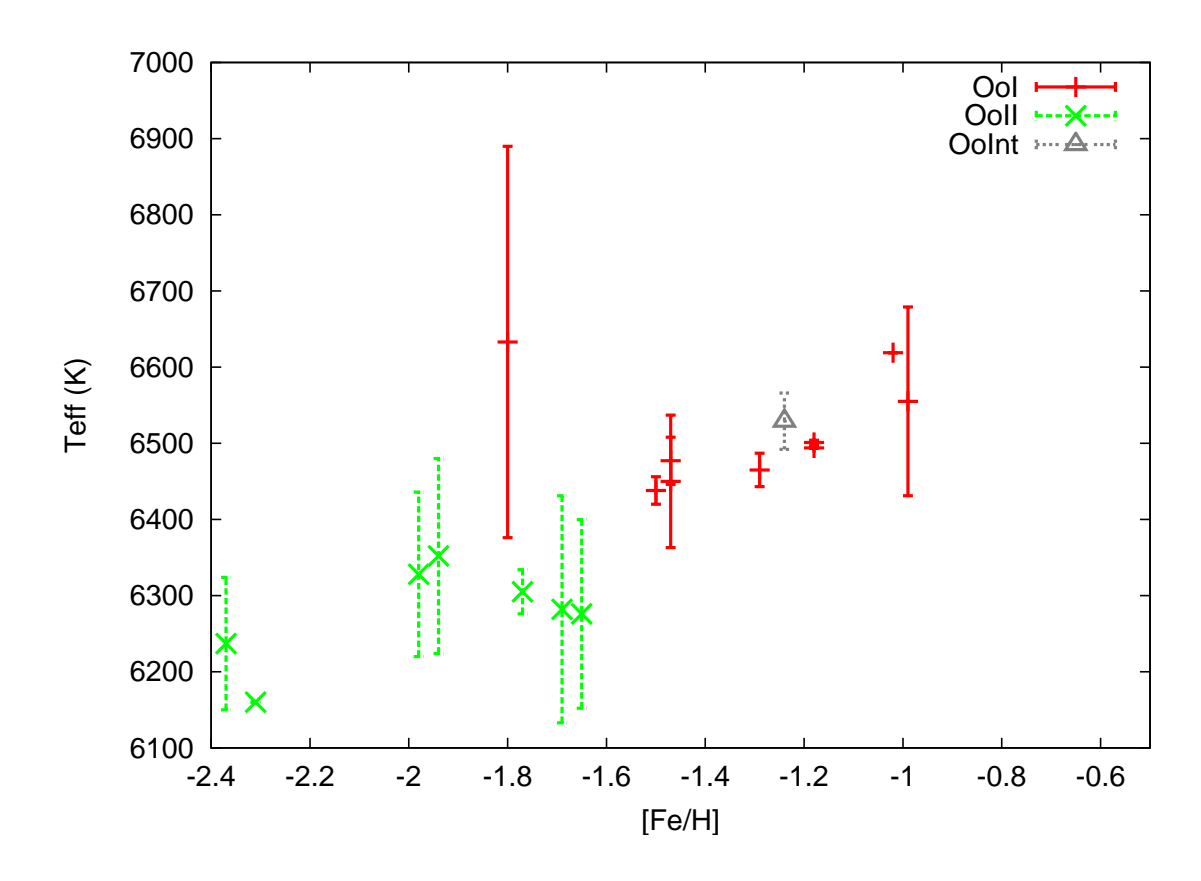


Figure 10.4: The average effective temperature,  $\langle T_{\rm eff} \rangle$ , for RRab stars in previously studied globular clusters vs cluster metallicity.

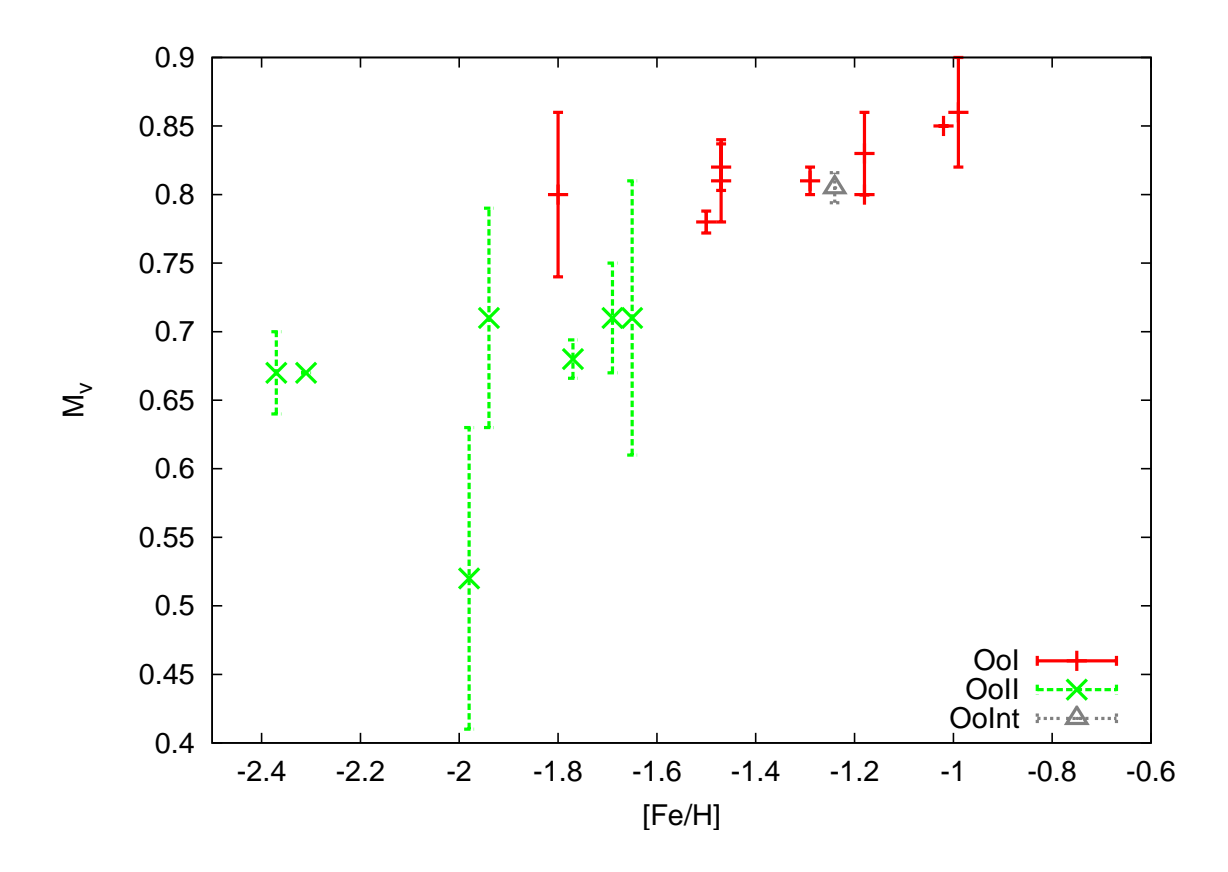


Figure 10.5: The average V-band absolute magnitude,  $\langle M_V \rangle$ , for RRab stars in previously studied globular clusters vs cluster metallicity.

Table 10.3: Mean Physical Properties Obtained for RRab Stars in Globular Clusters in the LMC

Cluster	Oo Type	# Stars	[Fe/H]	$\langle T_{\rm eff} \rangle$	$\langle M_V \rangle$
NGC 1466	Int	13	-1.64	6427	0.78
Reticulum	Ι	12	-1.66	6428	0.77
NGC 1786	II?	7	-1.77	6300	0.71
NGC 2210	Int	3	-1.65	6341	0.71

Table 10.4: Mean Physical Properties Obtained for RRc Stars in Globular Clusters in the LMC

Cluster	Oo Type	# Stars	[Fe/H]	$\langle M/M_{\odot} \rangle$	$\langle log(L/L_{\odot}) \rangle$	$\langle T_{eff} \rangle$	$\langle Y \rangle$
NGC 1466	Int	7	-1.64	0.60	1.71	7244	0.27
Reticulum	I	3	-1.66	0.63	1.73	7265	0.27
NGC 1786	II?	6	-1.77	0.69	1.76	7221	0.25
NGC 2210	$\operatorname{Int}$	4	-1.65	0.71	1.75	7242	0.26

Figures 10.6-10.10 show the relationships between RR Lyrae physical properties and cluster metallicity, this time with the addition of the four LMC clusters discussed in this dissertation. In general the four clusters agree very well with the trends seen in the Milky Way halo clusters. In the plot of RRc luminosity vs cluster metallicity (Fig. 10.7) NGC 1786 and NGC 2210 appear to be slightly brighter than the trend, but are consistent within the error bars. NGC 1786 and NGC 2210 again appear to be outliers when one looks at the relationship between RRc mass and cluster metallicity (Fig. 10.8); NGC 2210 may still be consistent within the error bars but NGC 1786

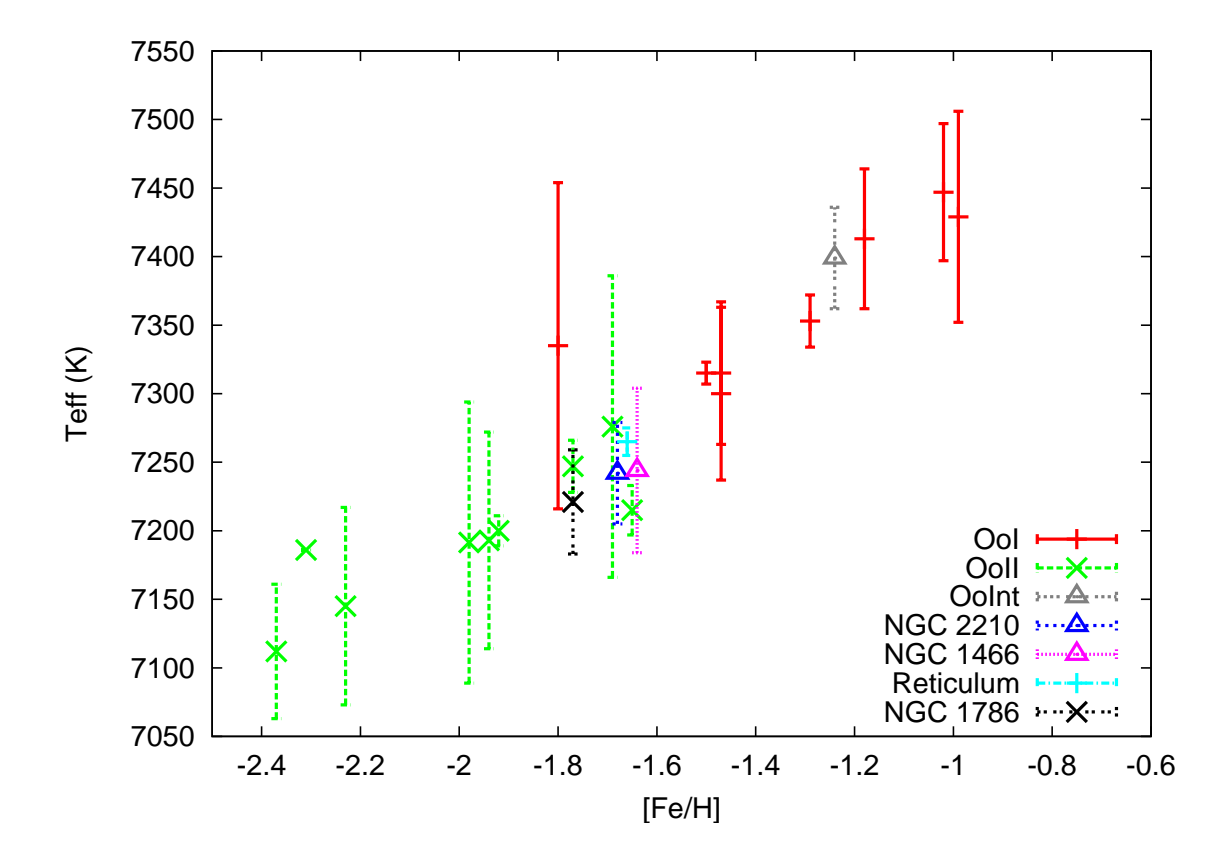


Figure 10.6: The average effective temperature,  $\langle T_{\rm eff} \rangle$ , for RRc stars vs cluster metallicity.

is not. However, the presence of other clusters that do not follow the general trend suggests that the relationship between RRc mass and cluster metallicity may not be as tight as the relationships for the other physical properties.

Perhaps the most interesting of these relationships is the one between the V-band absolute magnitude for RRab stars and cluster metallicity. As stated previously, this relationship shows a break between Oo-I and Oo-II clusters. Oo-I clusters show a slight trend toward brighter magnitudes at lower metallicities. Oo-II clusters may show a similar trend, though with a shallower slope. The Oo-int clusters straddle the break; NGC 1466, like M75, falls along the Oo-I trend while NGC 2210 fits with the Oo-II clusters. As discussed in section 5.5, while NGC 1466 is an Oo-Int object, it has some characteristics that appear similar to Oo-I clusters: clustering of some

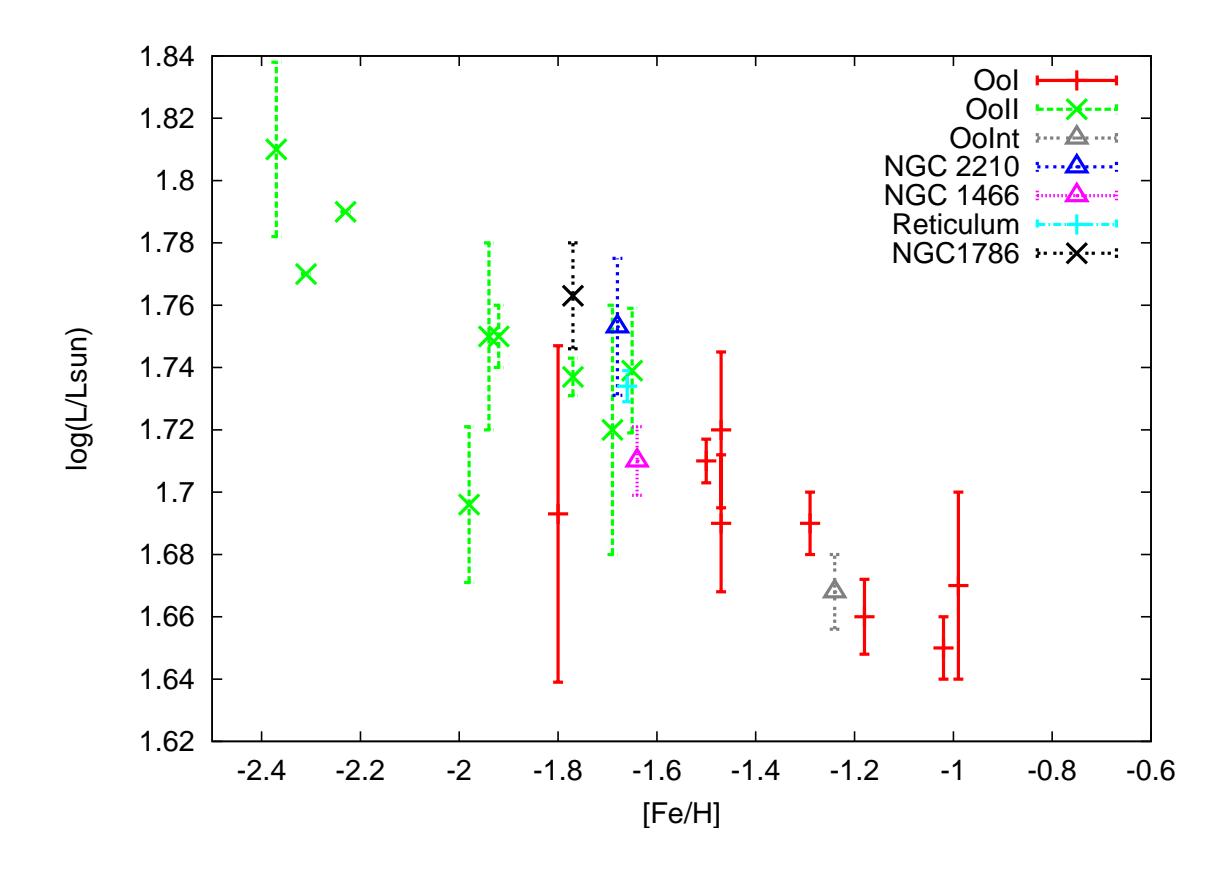


Figure 10.7: Average luminosity (in terms of the luminosity of the Sun),  $\langle L/L_{\odot}\rangle$ , for RRc stars vs cluster metallicity.

RRab stars around the Oo-I locus on the Bailey diagram and RRd stars that fall in the same region on the Petersen diagram as Galactic Oo-I clusters. Thus it is not necessarily a surprise that NGC 1466 behaves like an Oo-I cluster when looking at the RRab absolute magnitude vs cluster metallicity trend. Likewise, NGC 2210 showed clustering along the Oo-II locus in the Bailey diagram by a portion of its RRab stars, which is consistent with its Oo-II like behavior here. This difference in absolute magnitude is also consistent with the difference in Bailey diagram behaviors of NGC 1466 and NGC 2210 as discussed in Section 9.3.2; the observed difference in the positions of the RRab stars in the two clusters is consistent with NGC 2210 RR Lyrae stars being more luminous than their counterparts in NGC 1466.

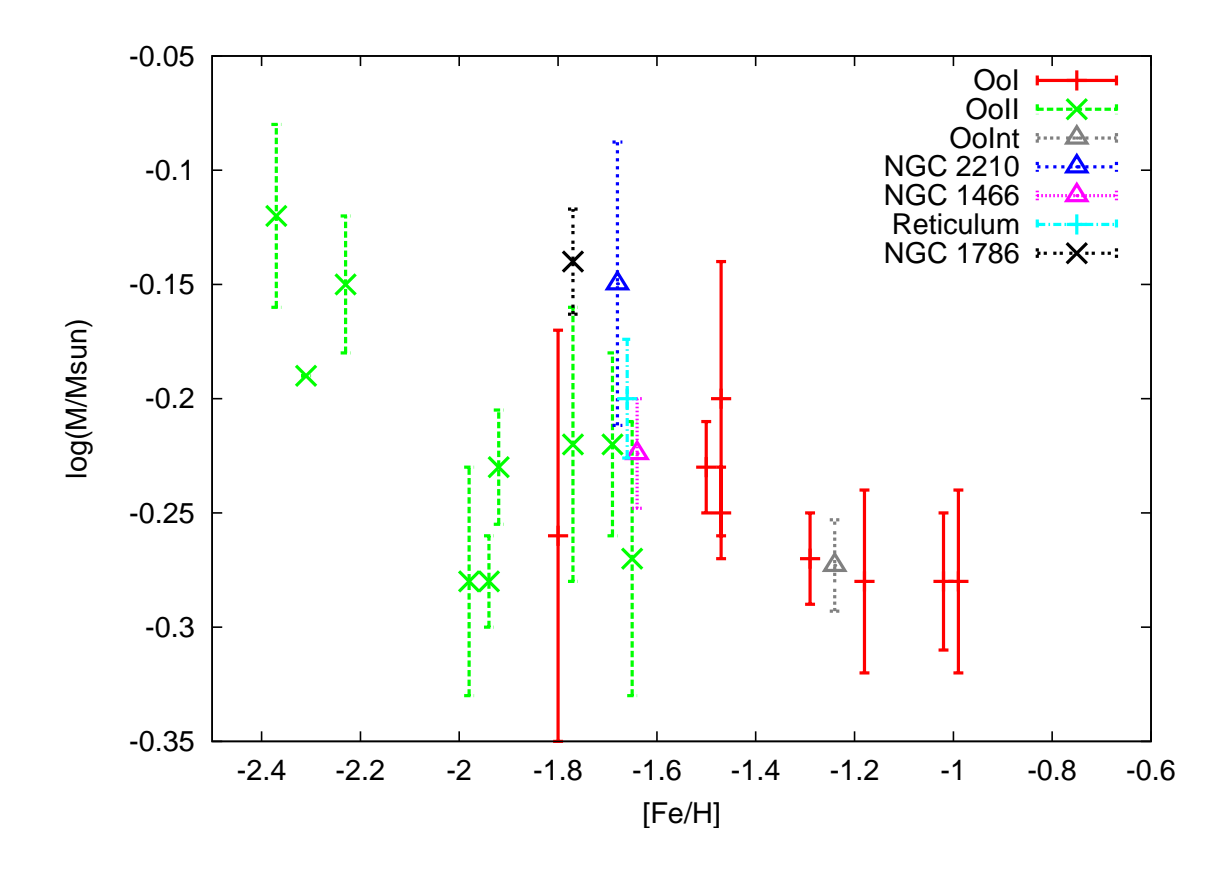


Figure 10.8: Average mass (in terms of the mass of the Sun),  $\langle M/M_{\odot} \rangle$ , for RRc stars vs cluster metallicity.

The fact that the LMC globular clusters follow the same trends of physical property vs cluster metallicity as Galactic globular clusters indicates that the processes involved in the formation of the RR Lyrae stars are the same in both LMC and Galactic globular clusters. Clusters in all three Oosterhoff groups follow the same general trends and there is a smooth transition between Oosterhoff groups, except for the RRab V-band absolute magnitude vs cluster metallicity relationship. The behavior of the Oo-int clusters supports the idea that they represent a transition between Oo-I and Oo-II objects as opposed to a separate, homogenous class.

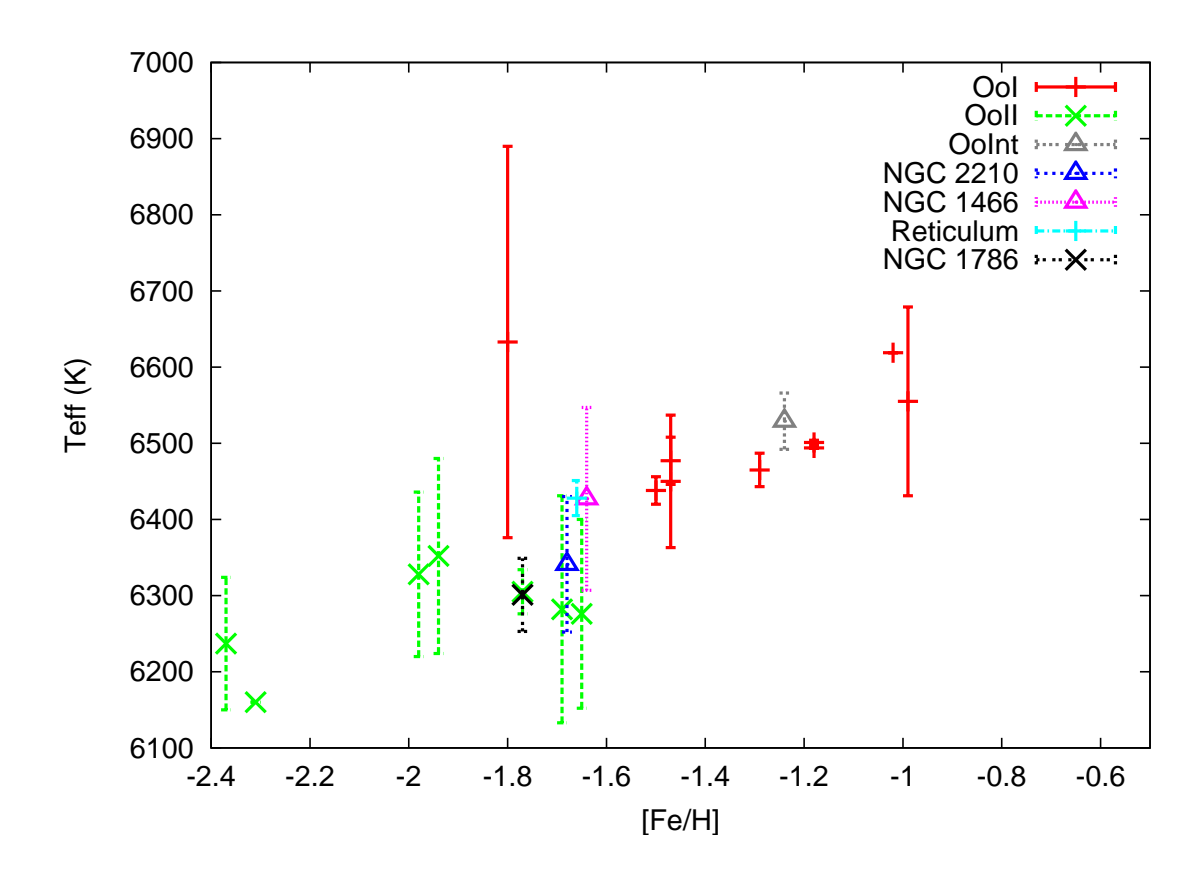


Figure 10.9: The average effective temperature,  $\langle T_{\rm eff} \rangle$ , for RRab stars vs cluster metallicity.

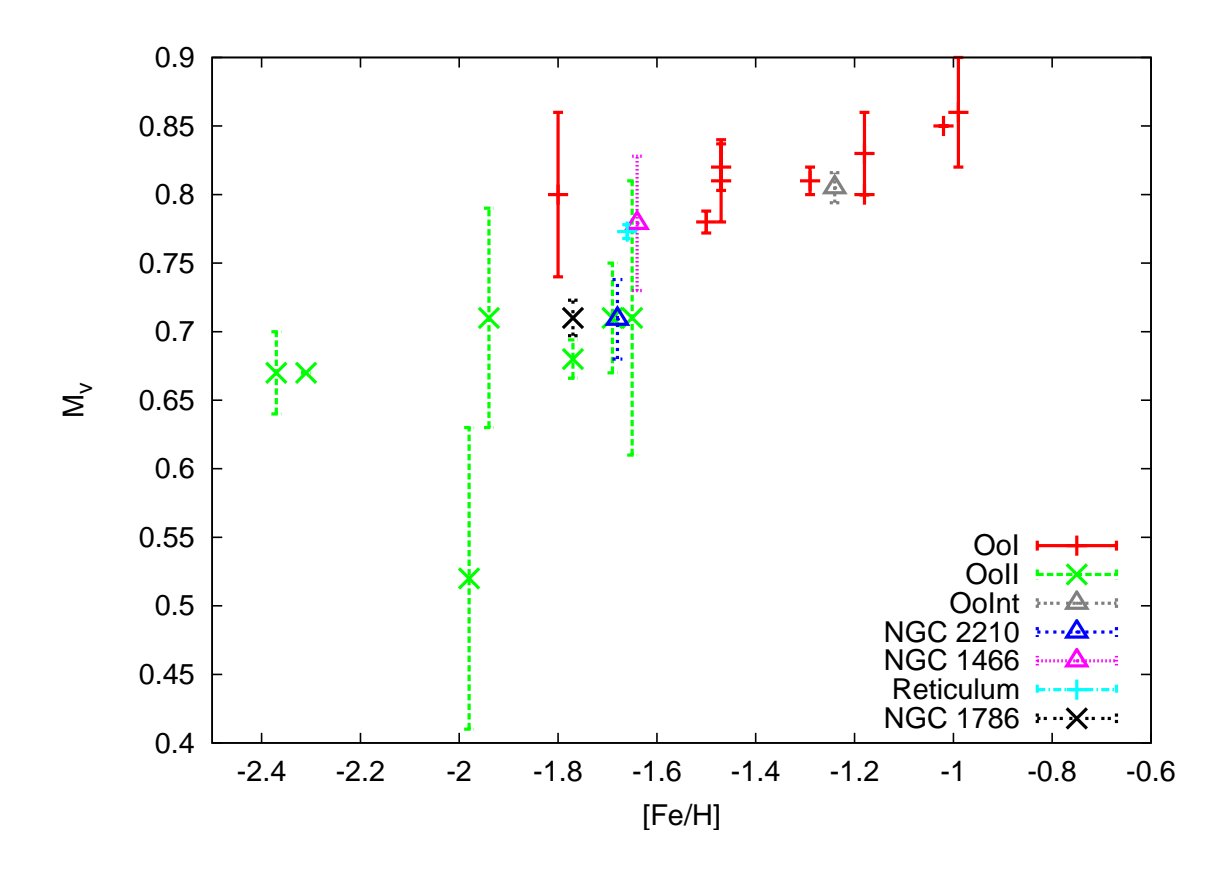


Figure 10.10: The average V-band absolute magnitude,  $\langle M_V \rangle$ , for RRab stars vs cluster metallicity.

## CHAPTER 11: CONCLUSIONS

The data sets obtained for this dissertation are the best BV photometric data sets yet obtained for the target clusters. The size and quality of the data sets allowed for the identification of new variable stars; for previously known variable stars, the data sets yielded better sampled light curves than had been obtained previously. These more complete light curves allowed for the identification of double modes in several RR Lyrae stars that had previously been considered to be single mode pulsators.

Traditionally the number fraction of RRc stars compared to the total number of RR Lyrae stars in a cluster has been used to compare clusters and to serve as an indicator of Oosterhoff status. Since all four of the clusters that were examined turned out to have RRd stars that had been previously misidentified as single mode RR Lyrae stars, mostly RRc stars, it is likely that similarly misidentified RRd stars exist in a large fraction of previously studied globular clusters. Because of this, the number fraction of RRc stars should be changed to the number fraction of first overtone dominant pulsators, RRc and RRd stars. This allows for more accurate comparisons to be made with clusters that have been less well studied, and thus likely have RRd stars included with their RRc stars.

The ability of various properties of the RR Lyrae populations in stellar systems to serve as indicators of Oosterhoff status was examined. The average period of RRab stars provides the definition for the Oosterhoff classes and the correlation between  $\langle P_{ab} \rangle$  and other properties was checked. The minimum period of RRab stars in a

cluster,  $P_{ab,min}$  showed a strong correlation with  $\langle P_{ab} \rangle$  and little overlap in values between Oo-I and Oo-II clusters, making it a good indicator of Oosterhoff status. Ooint clusters fell along the same trend in  $\langle P_{ab} \rangle$  vs  $P_{ab,min}$  as Oo-I and Oo-II clusters, forming a smooth transition between the other two Oosterhoff types. The average RRc period showed a general correlation with the average RRab period but the overlap in values between different Oo-I and Oo-II clusters makes  $\langle P_c \rangle$  not as strong of an indicator of Oosterhoff status. The other two values examined, the number fraction of RRc stars and the maximum period of the RRc stars in a clusters, both showed little correlation with  $\langle P_{ab} \rangle$  and had a significant amount of overlap in values between the Oosterhoff classes, meaning neither quantity is a useful indicator of Oosterhoff type. This is a break from tradition for the number fraction of RRc stars which had previously been used as an indicator of Oosterhoff type.

Physical properties, derived from Fourier decomposition of their light curves, were calculated for the first time for the RR Lyrae stars in the target clusters. This is also the first time that physical properties have been calculated for RR Lyrae stars in extragalactic stellar systems. The physical properties were plotted as a function of cluster metallicity and the results for the clusters in this study were compared against those for previously studied Milky Way globular clusters. Mass, effective temperature, and luminosity of RRc stars and the effective temperature of RRab stars all displayed linear trends when looked at as a function of cluster metallicity. The LMC clusters obeyed the same trends as the Milky Way clusters and all three Oosterhoff types followed the same trends, suggesting that the physical processes involved in the formation of the RR Lyrae stars is the same in Galactic and extragalactic clusters and for all Oosterhoff types.

The absolute V magnitude,  $M_V$ , was the one physical property that did not show a linear trend as a function of cluster metallicity, appearing instead as a step function with Oo-I clusters being fainter than Oo-II clusters. The Oo-int clusters fall on both sides of the step function, with NGC 1466 and the previously studied Milky Way globular cluster lieing with the Oo-I clusters while NGC 2210 fell with the Oo-II clusters.

The behavior of the RRab stars on the Bailey diagram proved to be more complicated for Oo-int clusters than what is seen in Oo-I and Oo-II clusters. The RR Lyrae stars in Oo-I and Oo-II clusters tend to fall around loci on the Bailey diagram. An examination of the Bailey diagrams for NGC 1466 and NGC 2210, as well as the previously studied globular cluster NGC 2257 and dwarf galaxies CVn-I and Draco, reveals that no such locus exists for Oo-int clusters; instead these clusters show a wide range of Bailey diagram behavior. NGC 1466 and Draco have RRab stars that fall near the Oo-I locus while NGC 2210 and NGC 2257 fall near the Oo-II locus. Horizontal branch type seems to be connected to this difference between Oo-int clusters.

The Bailey diagram of NGC 1466 was compared against that of Milky Way globular cluster M3, an Oo-I cluster. The same was done with NGC 2210 and M15, a Milky Way Oo-II globular cluster. The RRab stars in NGC 1466 and NGC 2210 showed similar behavior to the RRab stars in their comparison clusters, though with more scatter in the case of NGC 1466. The difference in  $P_{ab,min}$ , which represents the transition period between RRab and RRc, between NGC 1466/NGC2210 and the clusters they were compared to, seems to be a factor in why these clusters where classified as Oo-int instead of Oo-I/Oo-II.

The RRd stars in the examined clusters showed behavior that was not necessarily related to the behavior of the RRab stars. While the RRd stars in Reticulum and NGC 1466 fell into the region of the Petersen diagram that is occupied by Milky Way Oo-I globular clusters, consistent with the Bailey diagram behavior of their RRab stars, the RRd stars in NGC 2257 and Draco show behavior that is opposite of their RRab stars. There is some indication however that the behavior of the RRd

stars follows the behavior of the RRc stars in the clusters, which is logical as they are all first overtone dominant pulsators.

The results presented in this dissertation concerning the behavior of the RRab and RRd stars and the absolute magnitude of the RRab stars in Oo-int objects show that Oosterhoff intermediate objects do not represent a separate, homogenous class. Instead the Oo-int objects seem to be a sort of transition between Oo-I and Oo-II objects.

This dissertation significantly increased the sample size of Oo-int objects that have been studied to this level of detail; only M75, NGC 2257, and the Draco dwarf galaxy had previously been studied at close to this level of detail. The sample size of well studied Oo-int objects remains small though and additional Oo-int objects need to be looked at in order for this class and the Oosterhoff phenomenon to be fully understood. The RRab stars in CVn-I seem to display a middle-ground between the behavior of the RRab stars in the other Oo-int clusters. This makes CVn-I, and other Oo-int objects that may be similar to it, a target of particular interest for future study.

APPENDICES

## APPENDIX A: NGC 1466 LIGHT CURVES

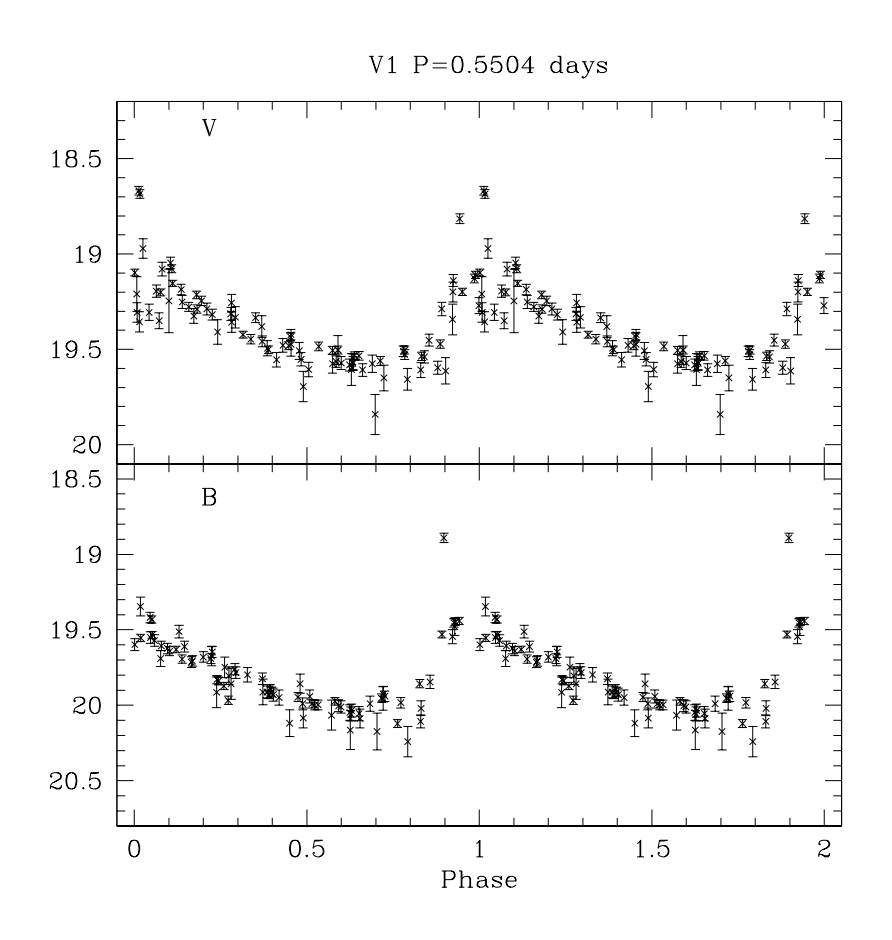


Figure A.1: Light curves for the variable stars in NGC 1466

Figure A.1: Light curves for the variable stars in NGC 1466 (continued) V2  $P_1=0.3534$  days

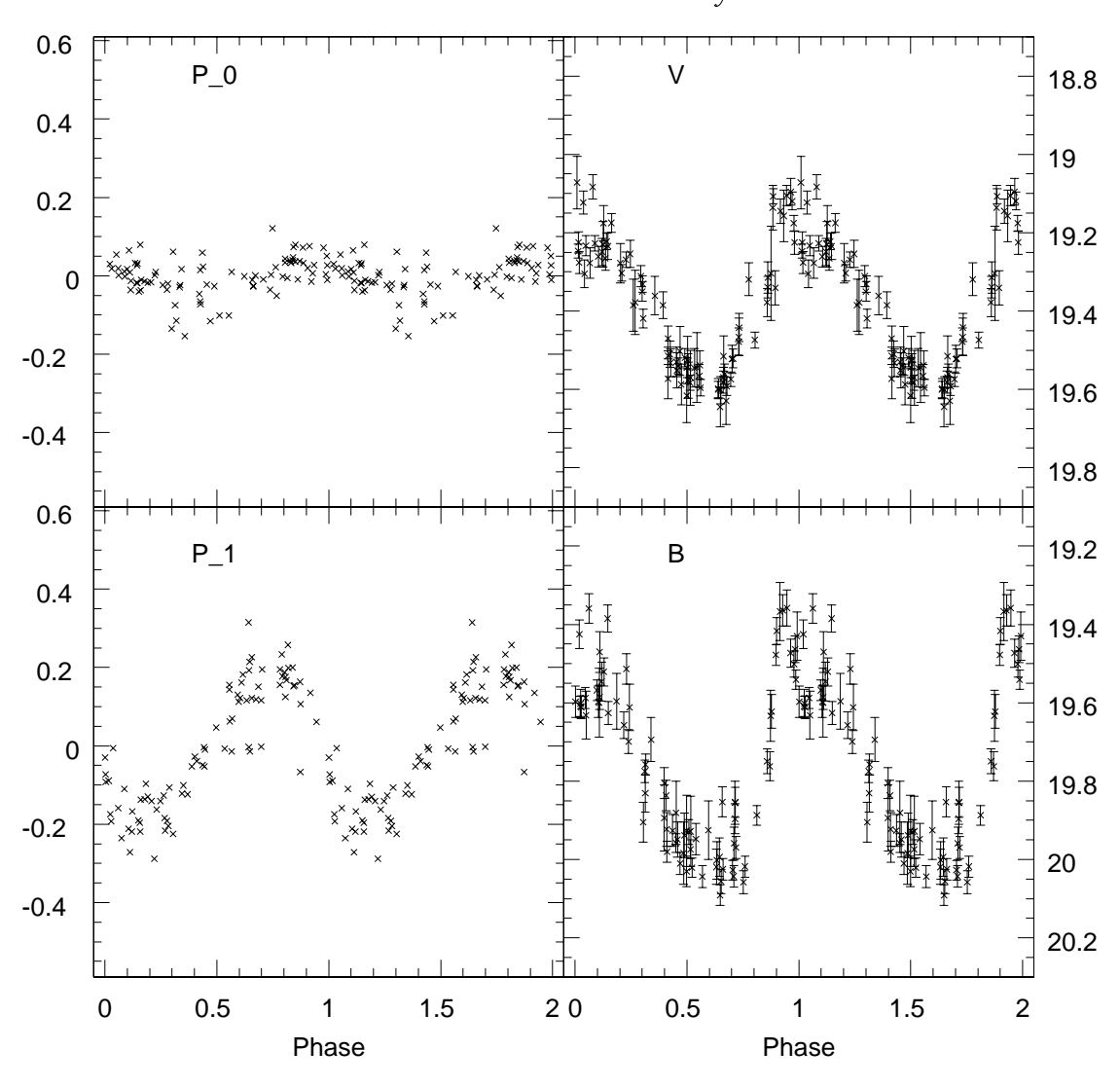


Figure A.1: Light curves for the variable stars in NGC 1466 (continued) V3  $P_1=0.3505$  days

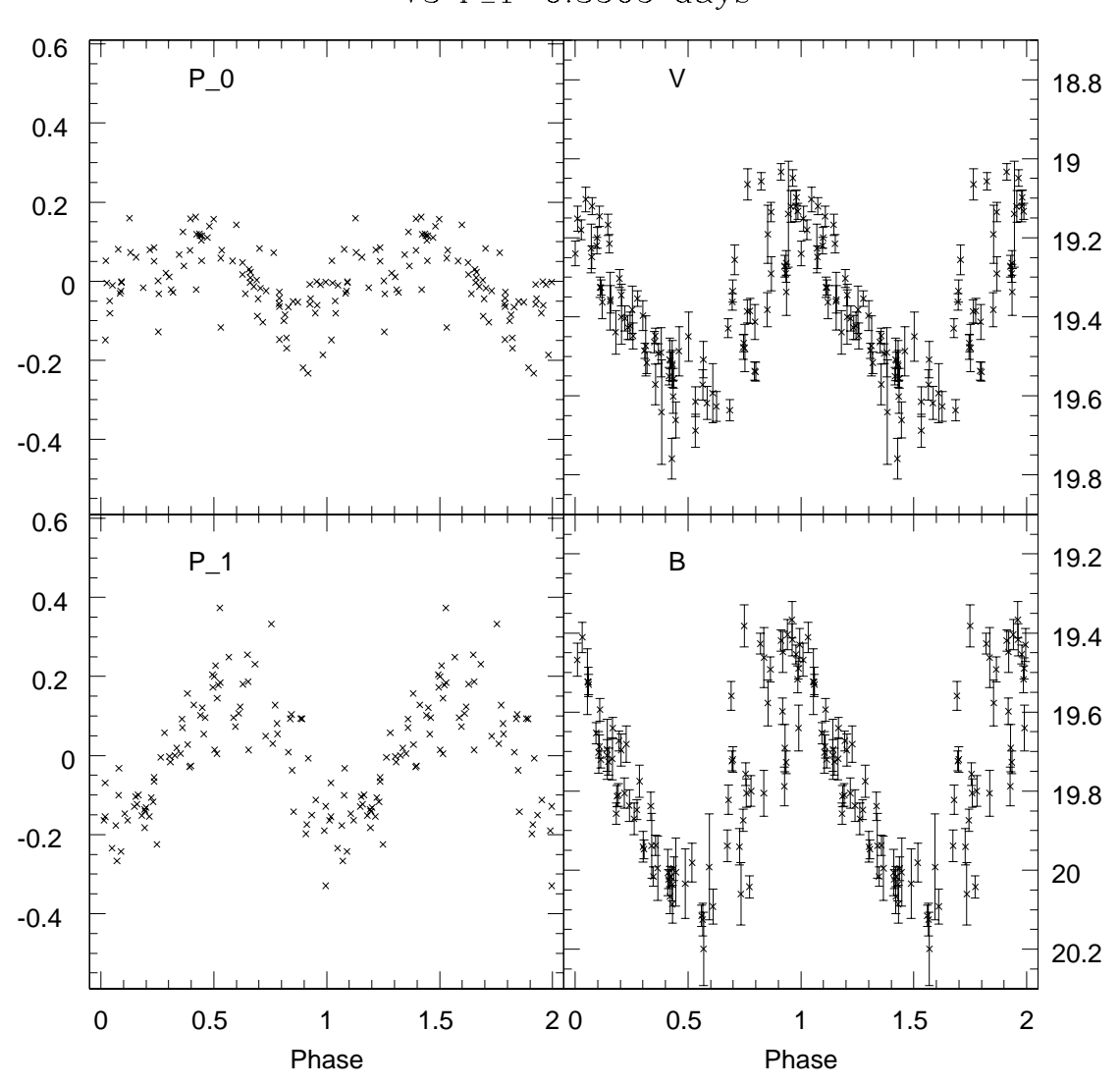


Figure A.1: Light curves for the variable stars in NGC 1466 (continued)  $$\rm V4\ P{=}0.5724\ days$$ 

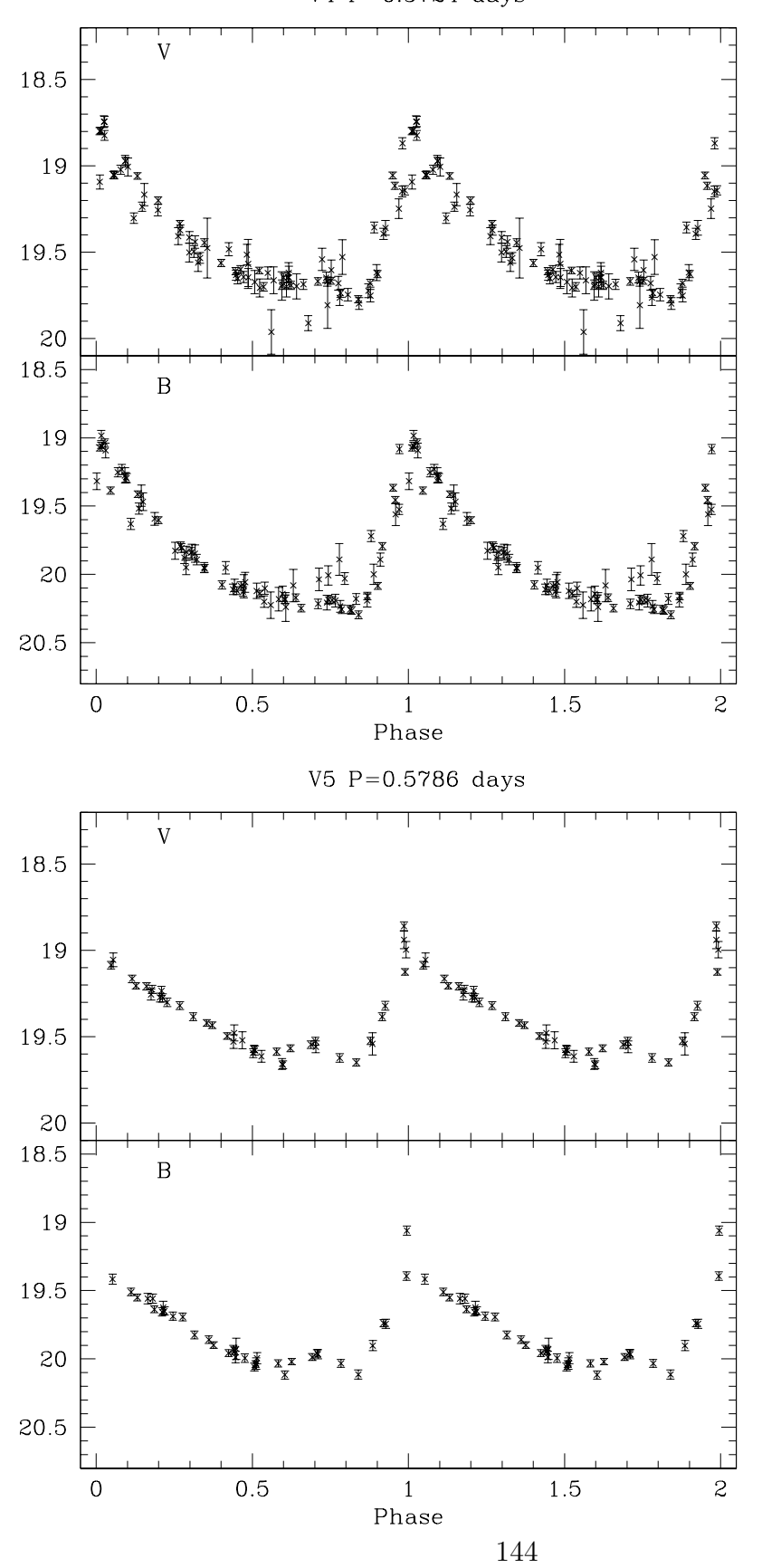


Figure A.1: Light curves for the variable stars in NGC 1466 (continued)  $$\rm V6\ P{=}0.5281\ days$$ 

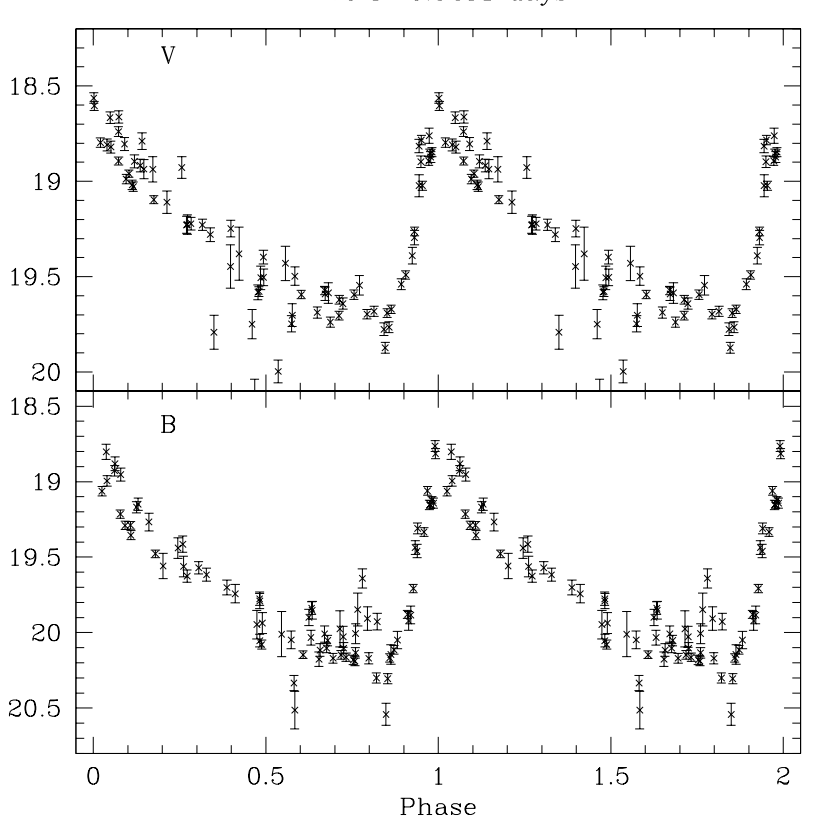


Figure A.1: Light curves for the variable stars in NGC 1466 (continued) V7  $P_1=0.3615$  days

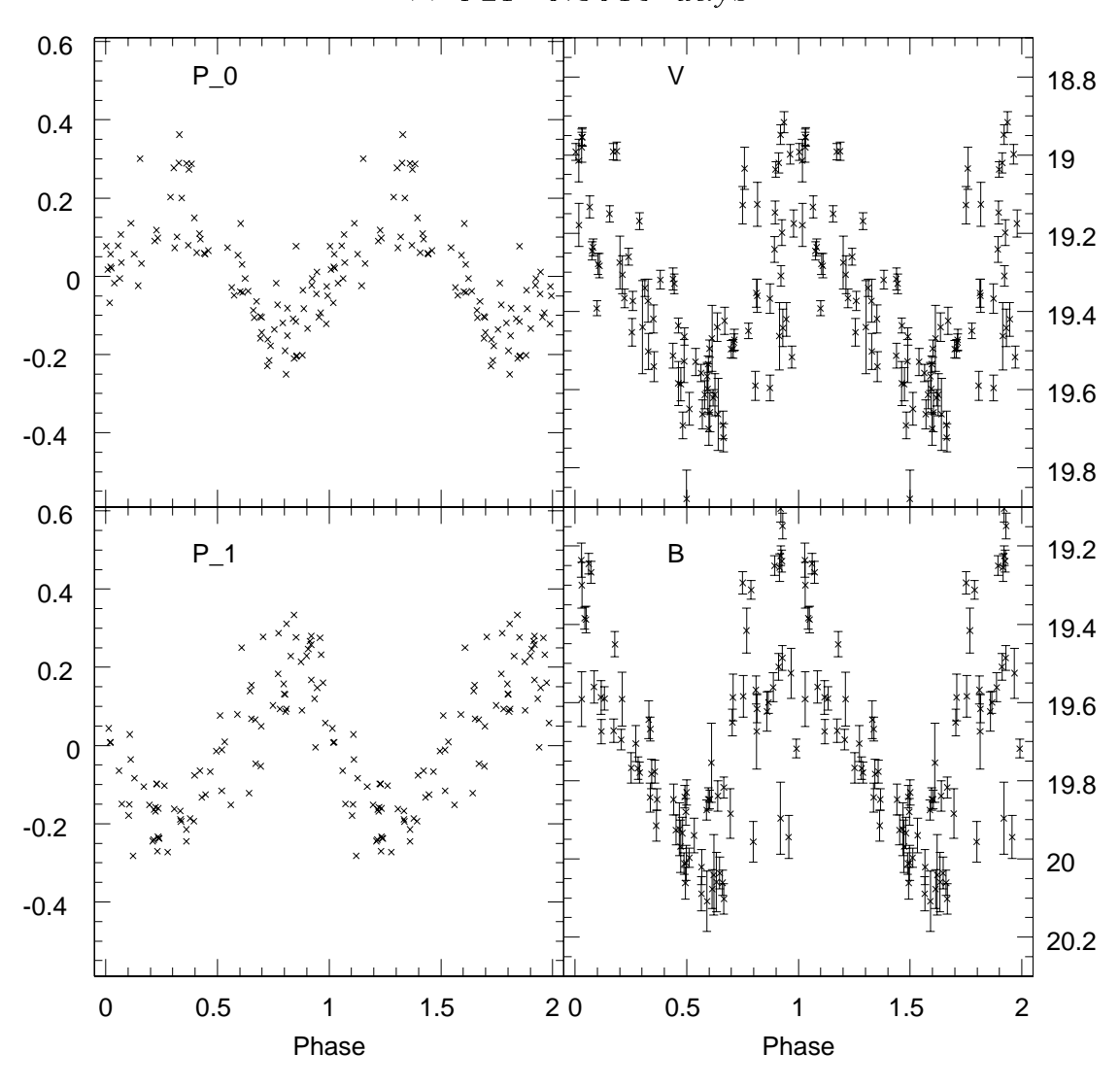


Figure A.1: Light curves for the variable stars in NGC 1466 (continued)  $$\rm V8\ P\!=\!0.5197\ days$$ 

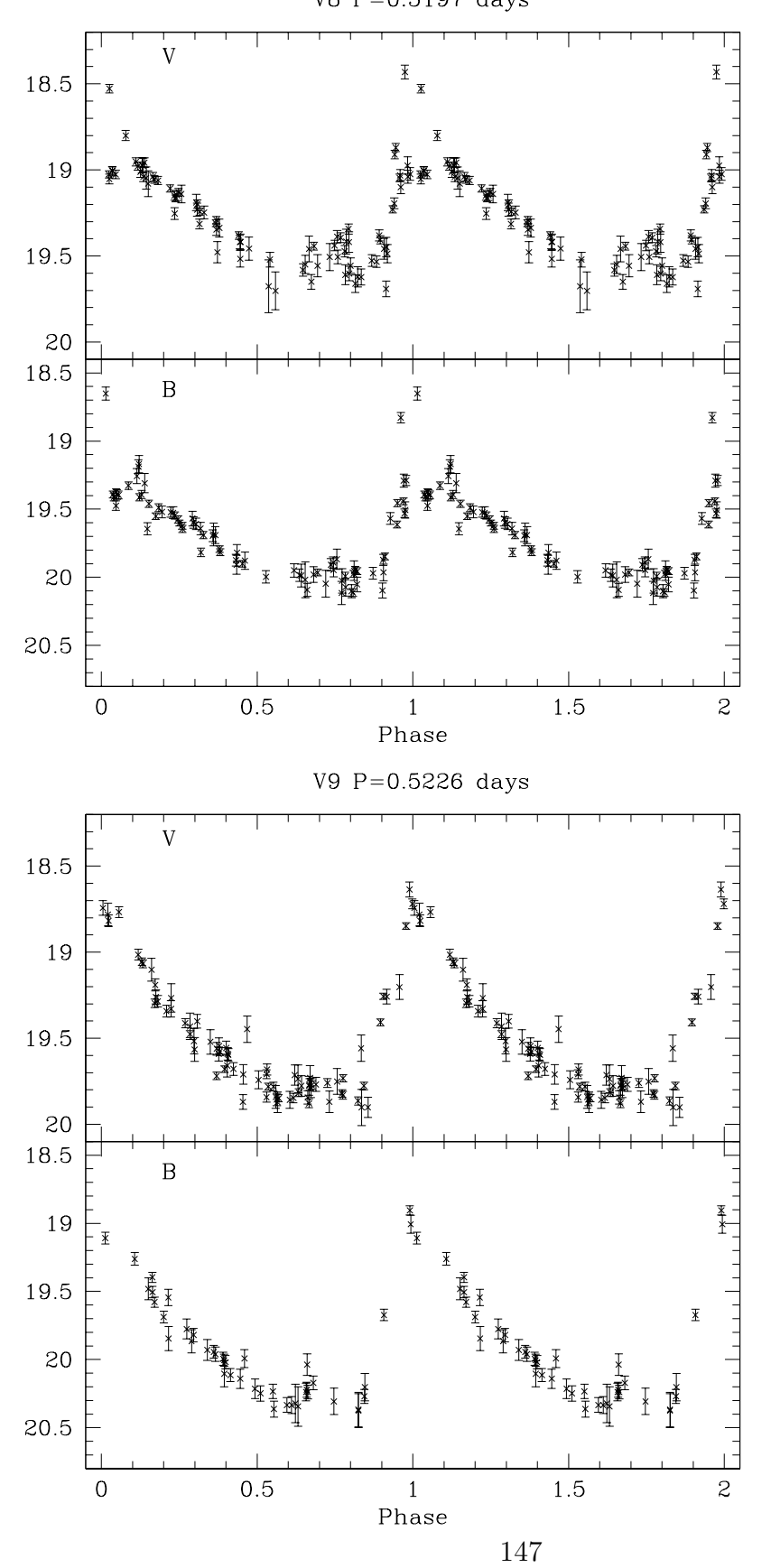


Figure A.1: Light curves for the variable stars in NGC 1466 (continued) V10 P\_1=0.3518 days

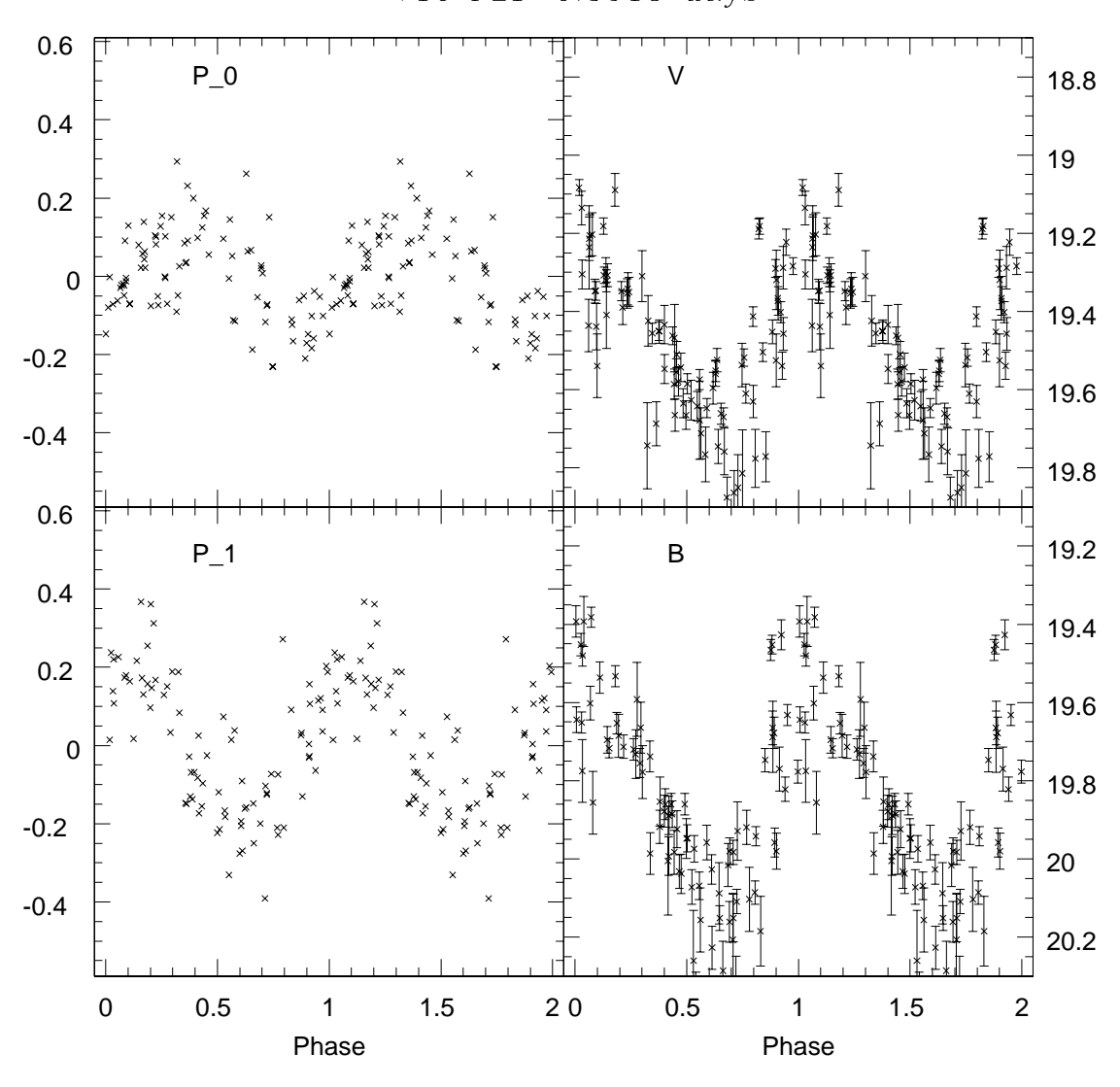
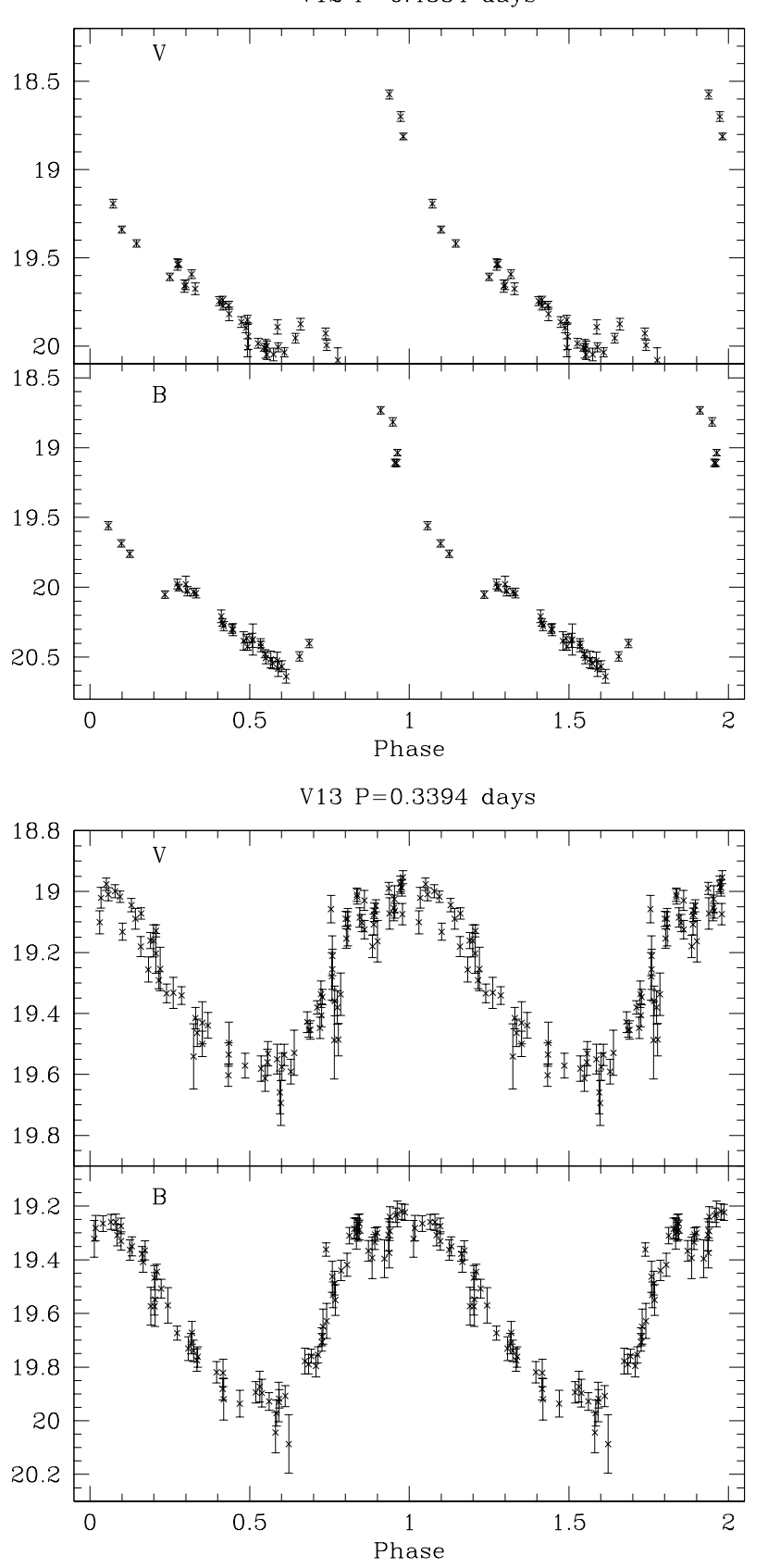


Figure A.1: Light curves for the variable stars in NGC 1466 (continued)  $$\tt V12\ P=0.4884\ days$$ 



149

Figure A.1: Light curves for the variable stars in NGC 1466 (continued)  $$\rm V14\ P\!=\!0.5641\ days$$ 

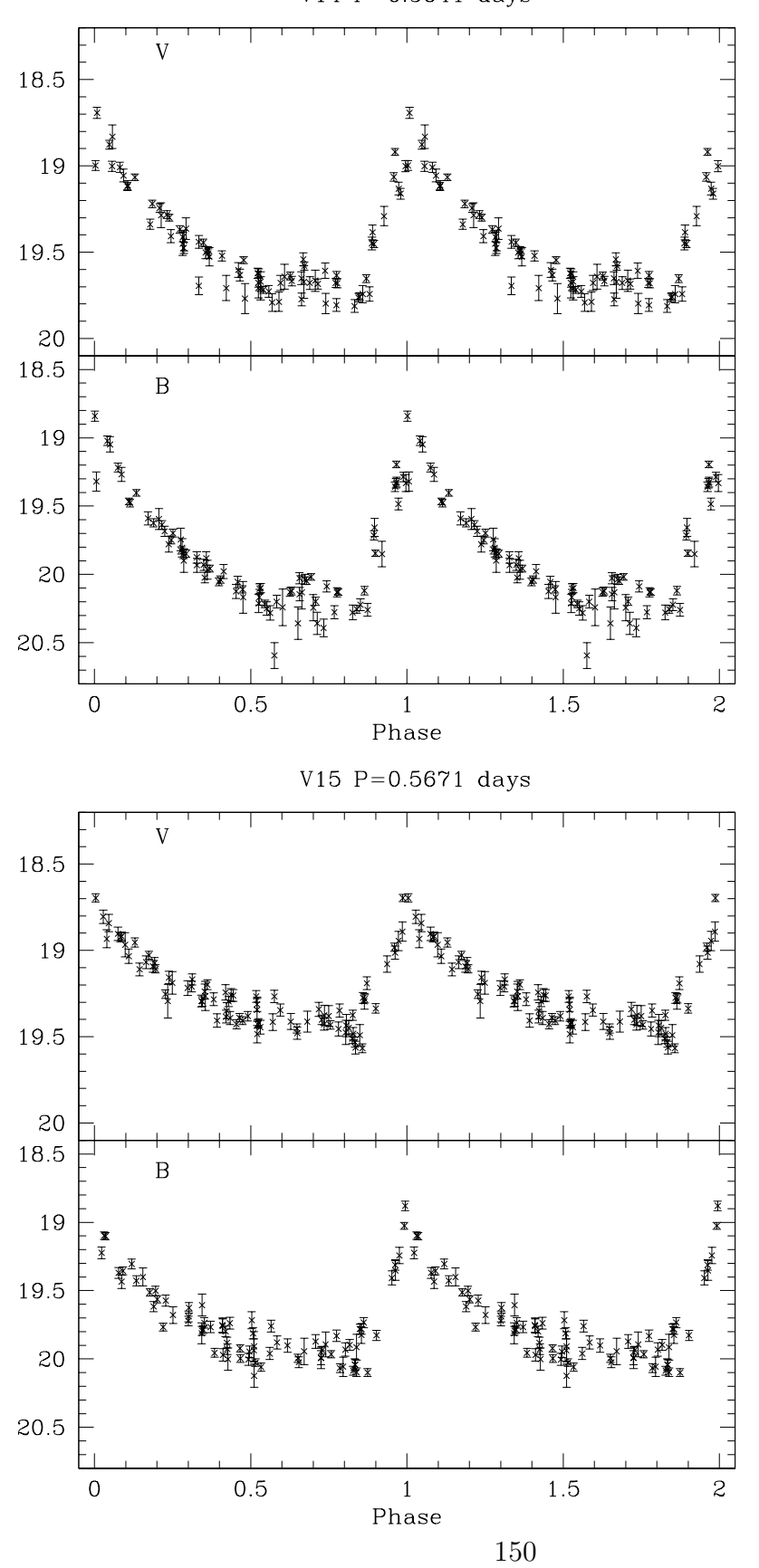
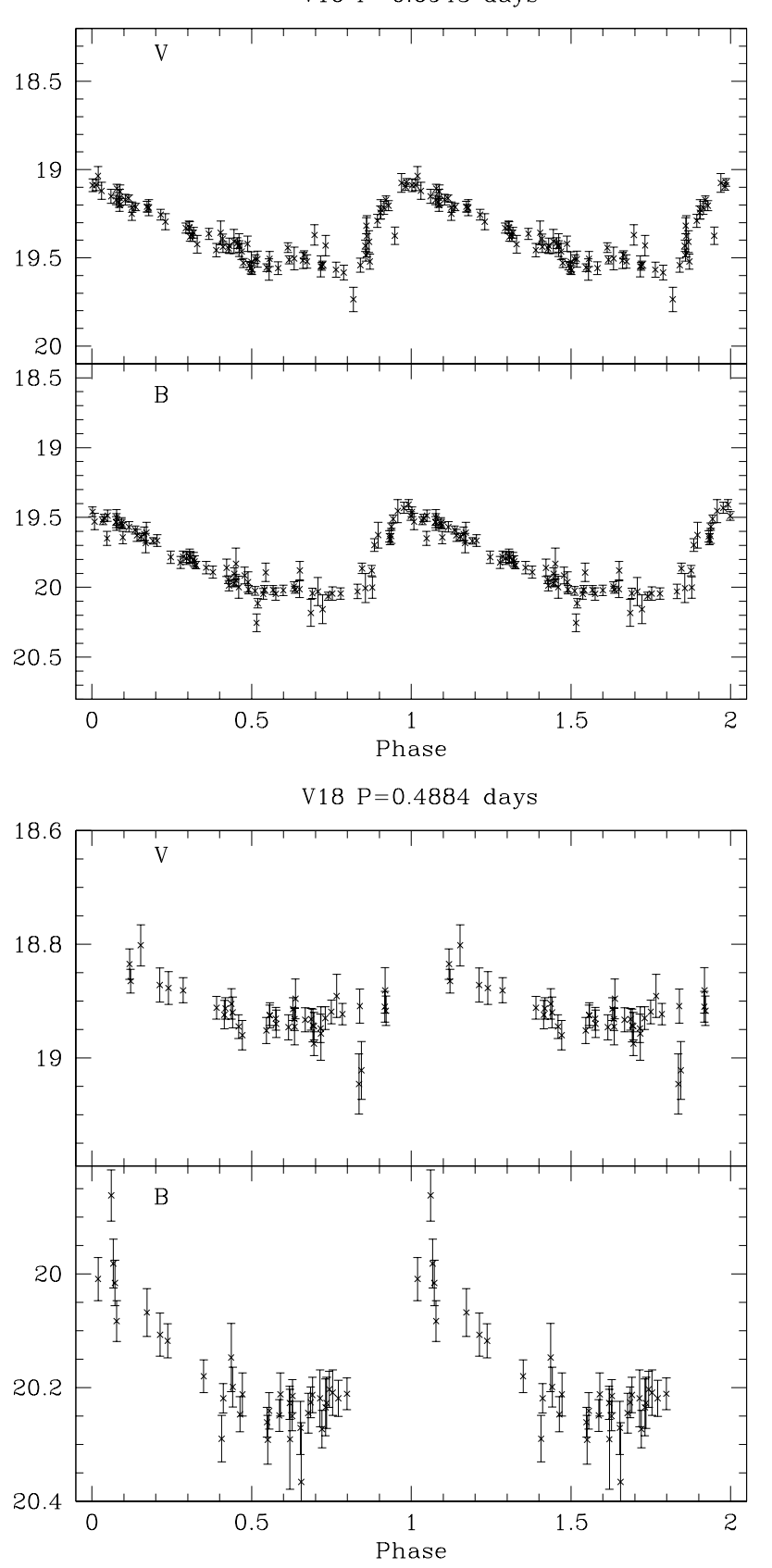


Figure A.1: Light curves for the variable stars in NGC 1466 (continued)  $$\rm V16\ P{=}0.6943\ days$$ 



151

Figure A.1: Light curves for the variable stars in NGC 1466 (continued) V19 P=0.6162 days

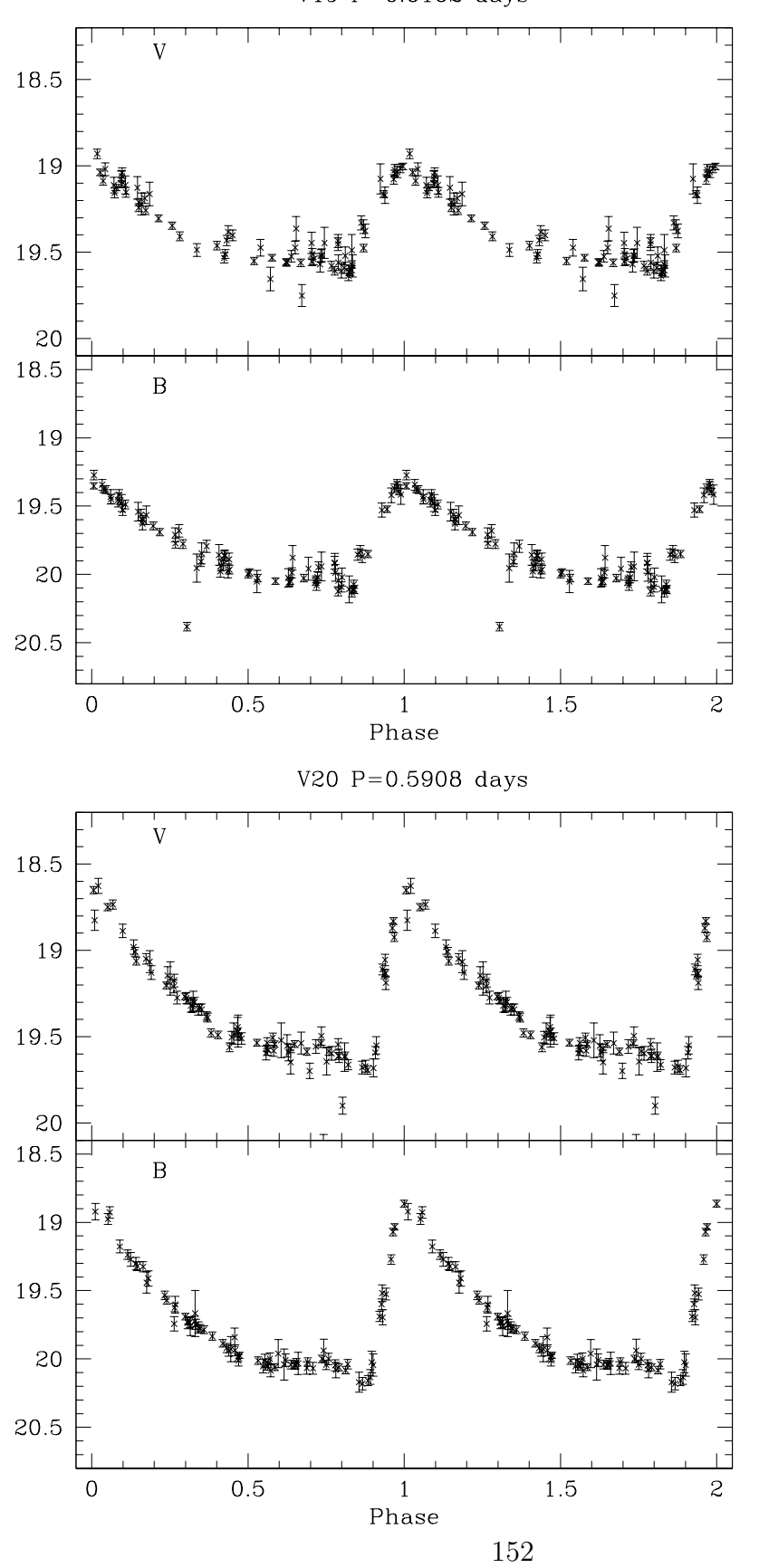


Figure A.1: Light curves for the variable stars in NGC 1466 (continued)  $$\tt V21 \ P=0.5215 \ days$$ 

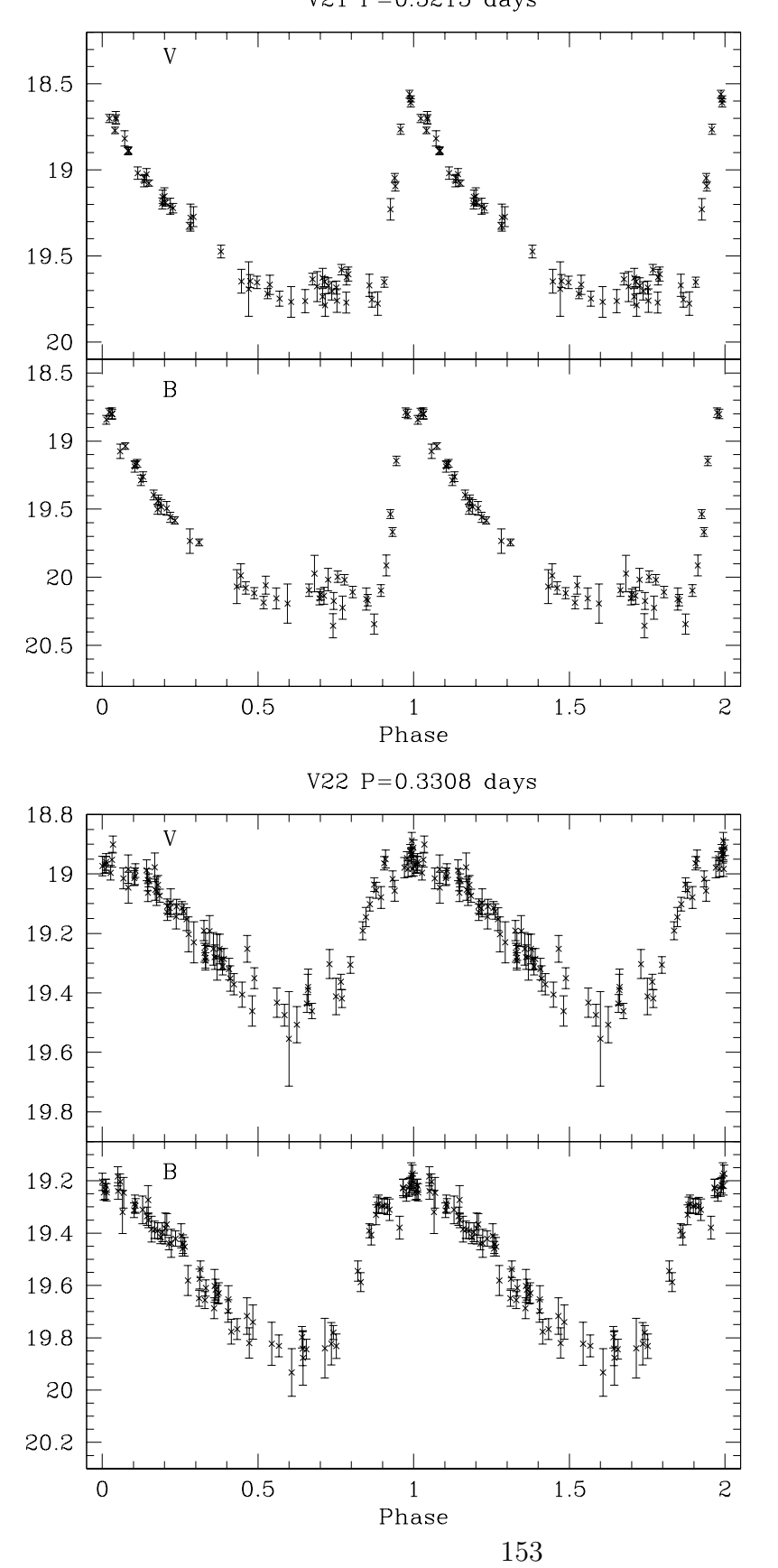


Figure A.1: Light curves for the variable stars in NGC 1466 (continued)  $$\tt V23\ P=0.4934\ days$$ 

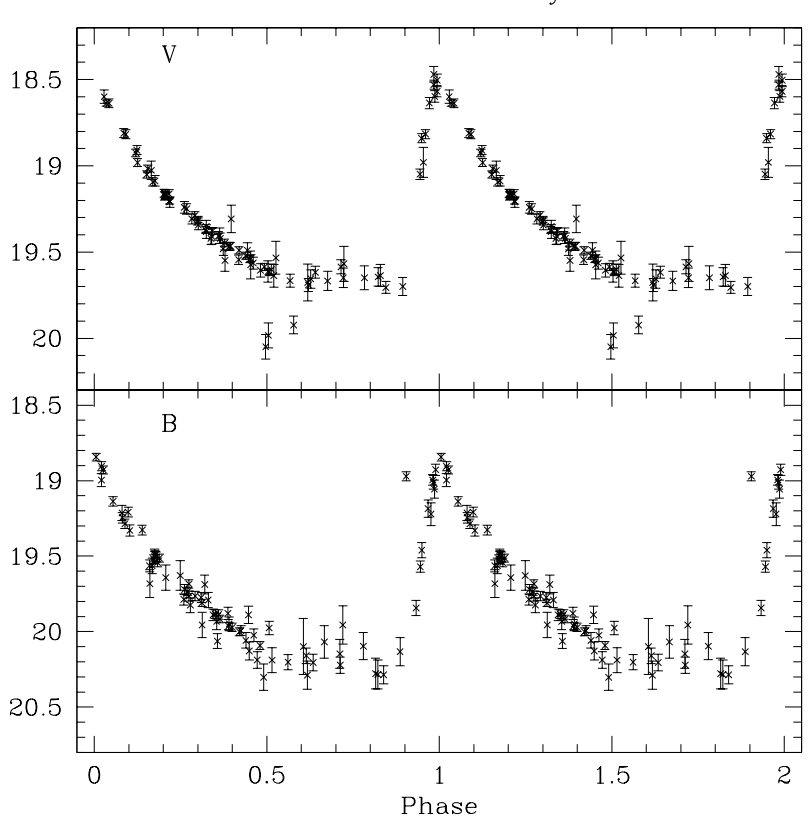


Figure A.1: Light curves for the variable stars in NGC 1466 (continued) V24  $P_1=0.3675$  days

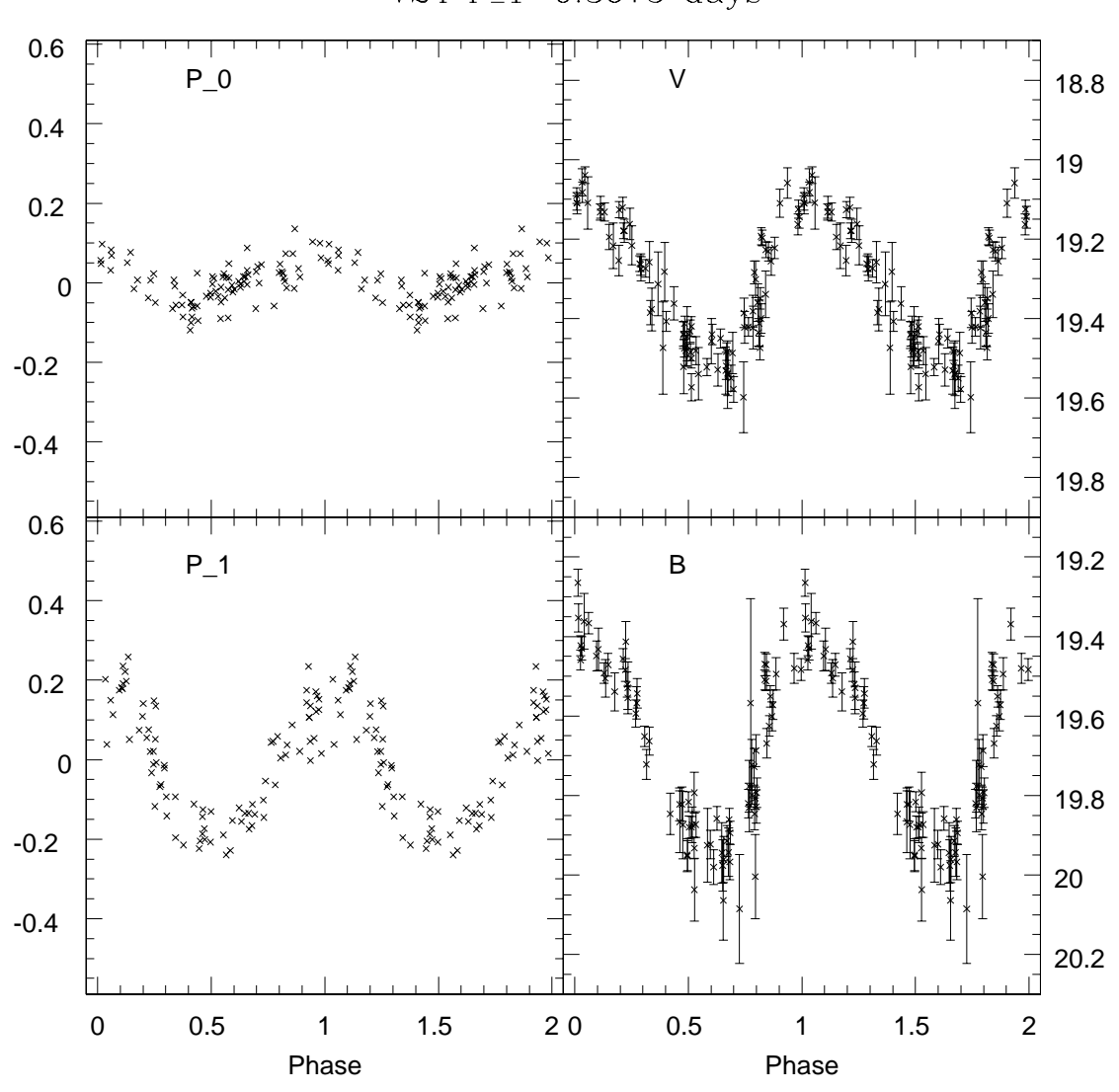


Figure A.1: Light curves for the variable stars in NGC 1466 (continued) V25 P\_1=0.3508 days

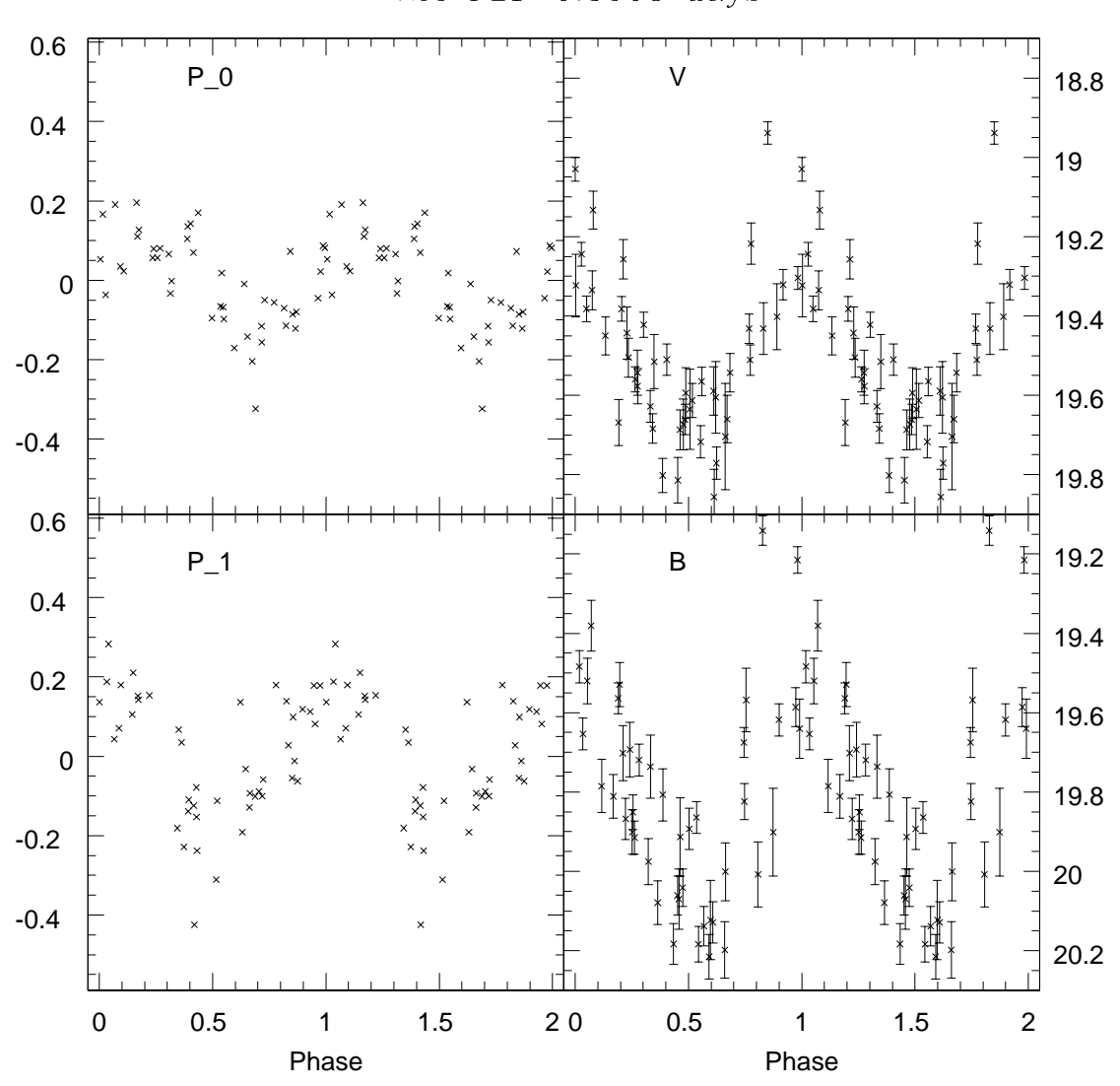


Figure A.1: Light curves for the variable stars in NGC 1466 (continued)  $$\tt V26\ P=0.5136\ days$$ 

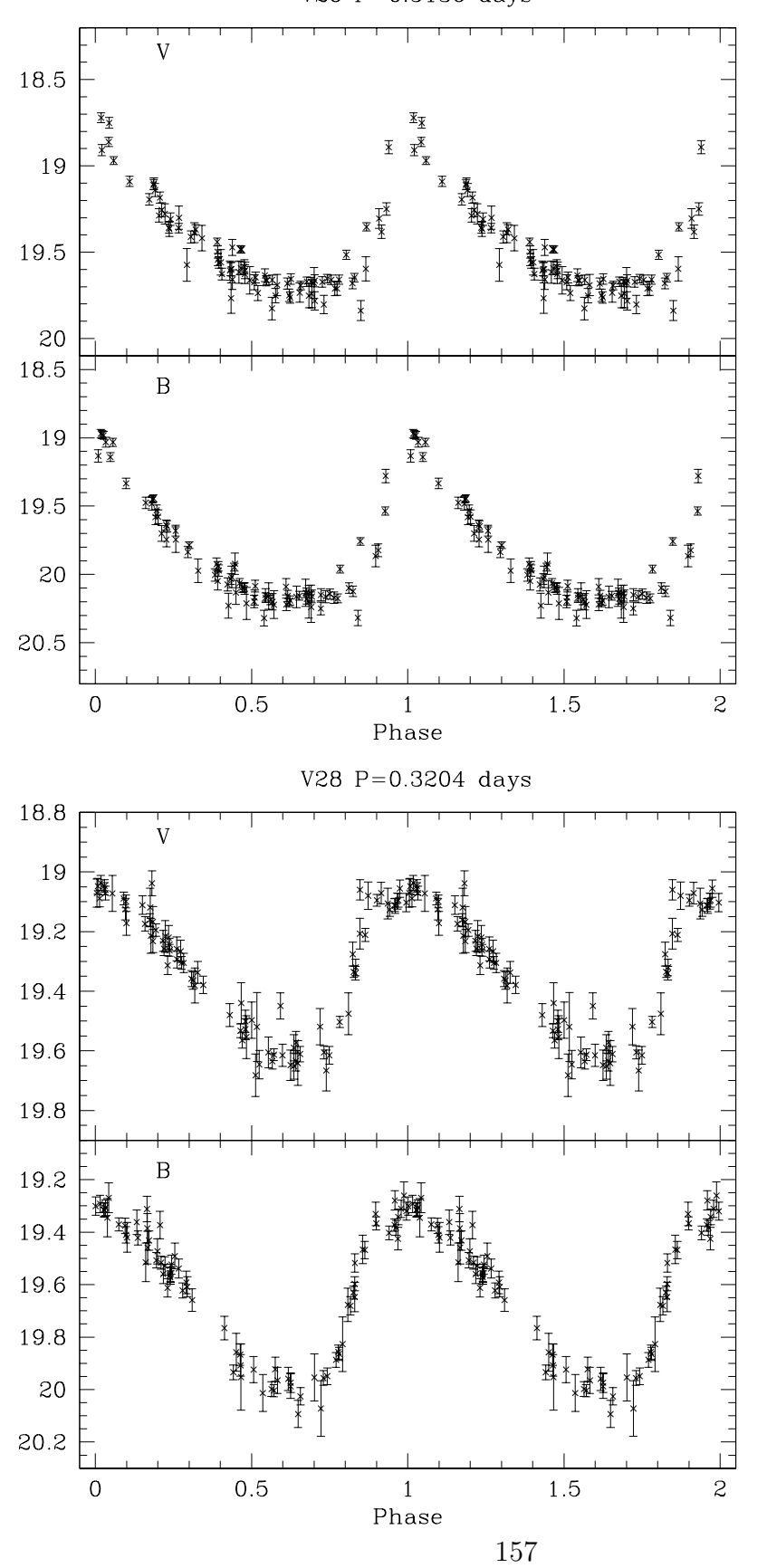


Figure A.1: Light curves for the variable stars in NGC 1466 (continued) V29  $P_1=0.3589$  days

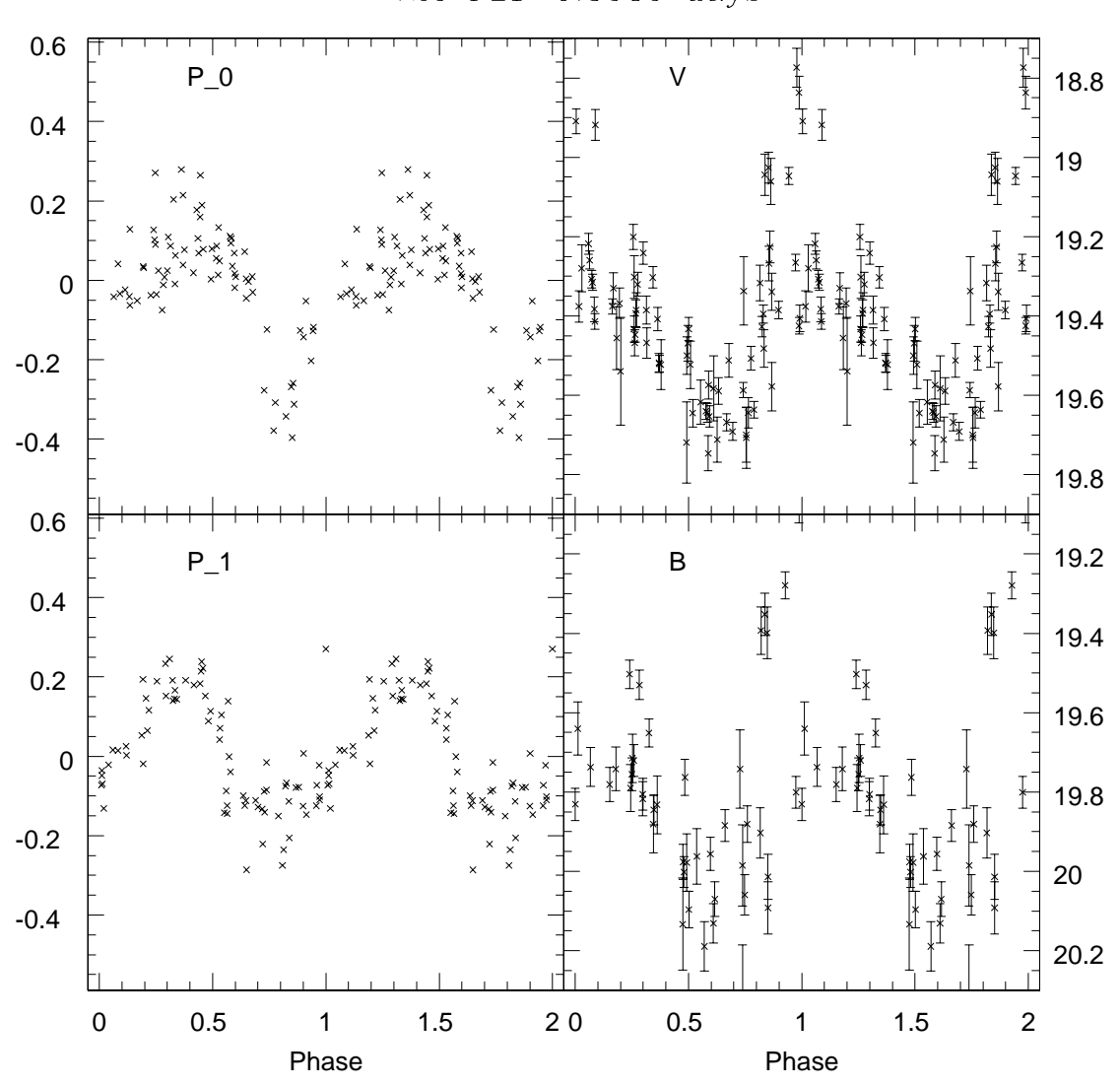


Figure A.1: Light curves for the variable stars in NGC 1466 (continued)  $$\tt V30\ P=0.6945\ days$$ 

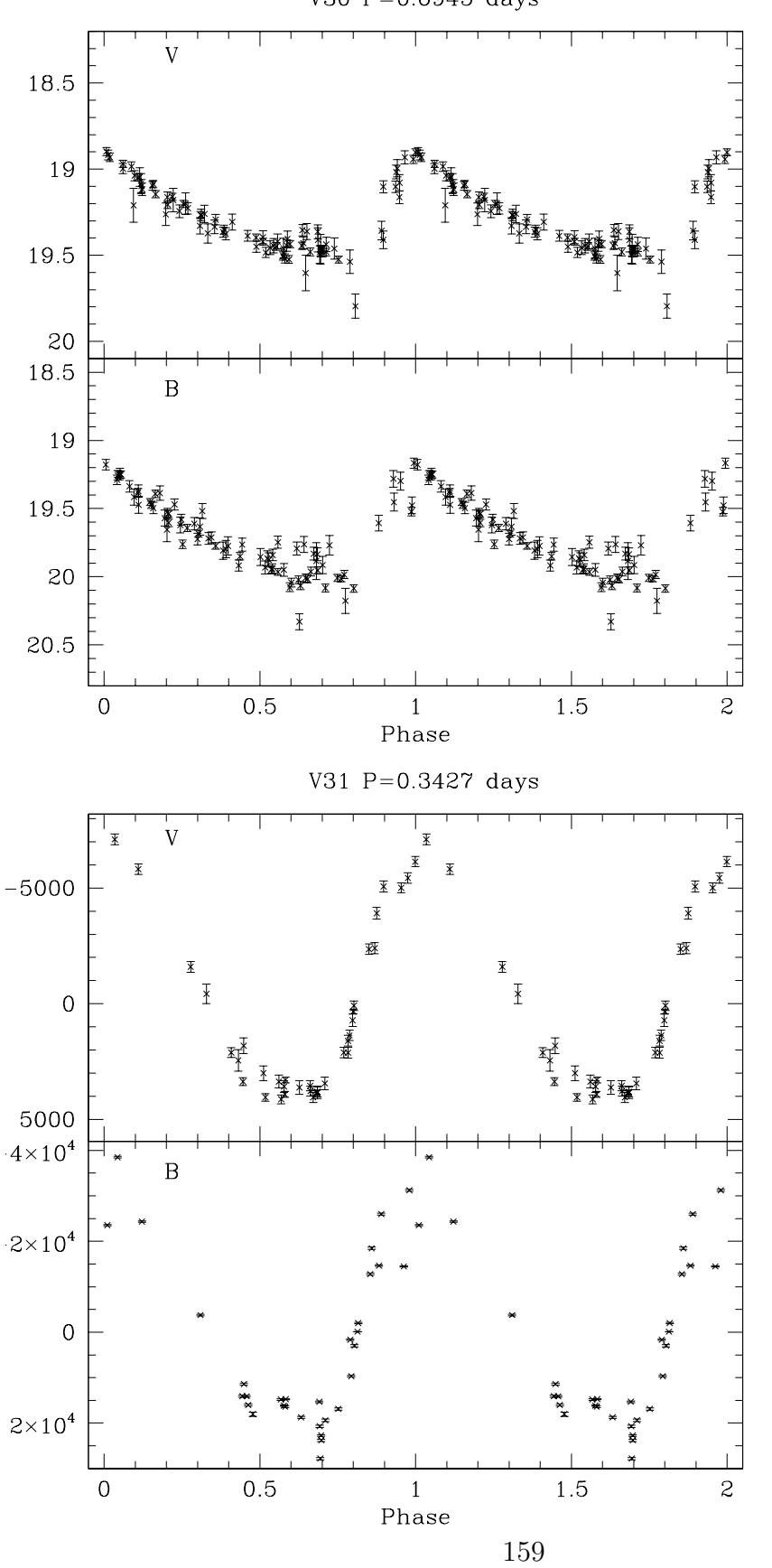


Figure A.1: Light curves for the variable stars in NGC 1466 (continued)  $$\tt V32\ P=0.4966\ days$$ 

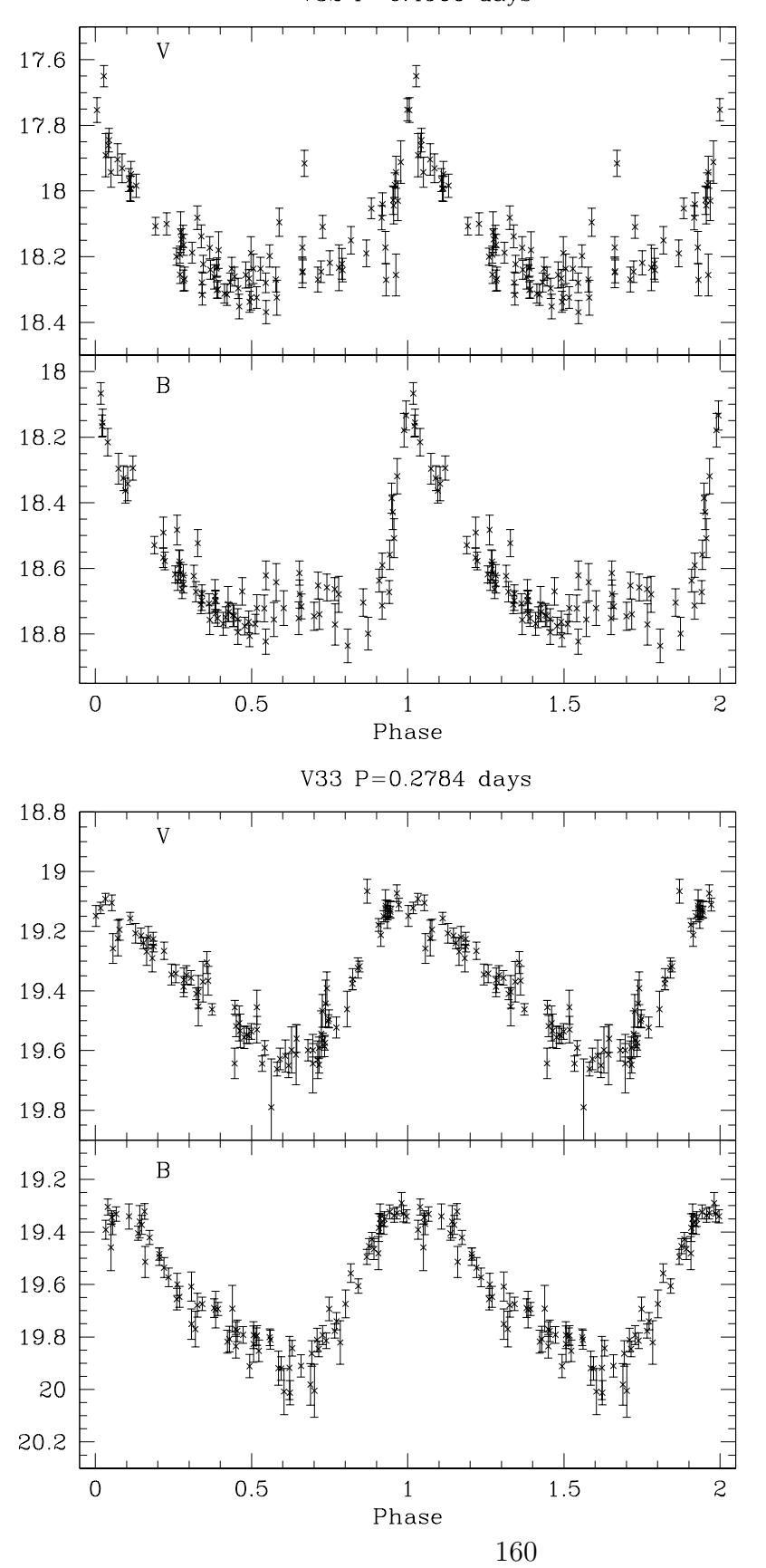


Figure A.1: Light curves for the variable stars in NGC 1466 (continued)  $${\tt V34\ P=0.6186\ days}$$ 

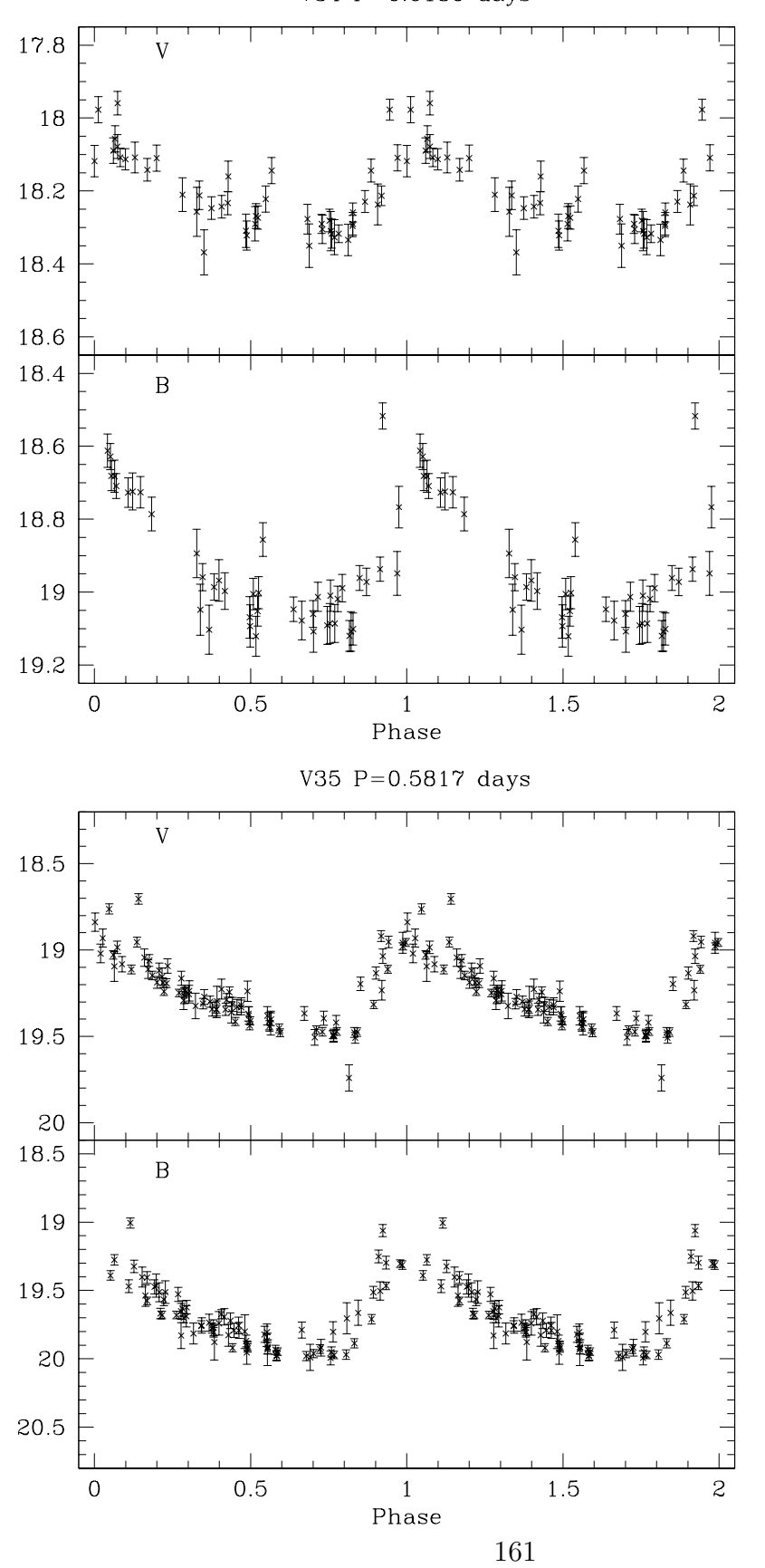


Figure A.1: Light curves for the variable stars in NGC 1466 (continued)  $$\tt V38\ P=0.3486\ days$$ 

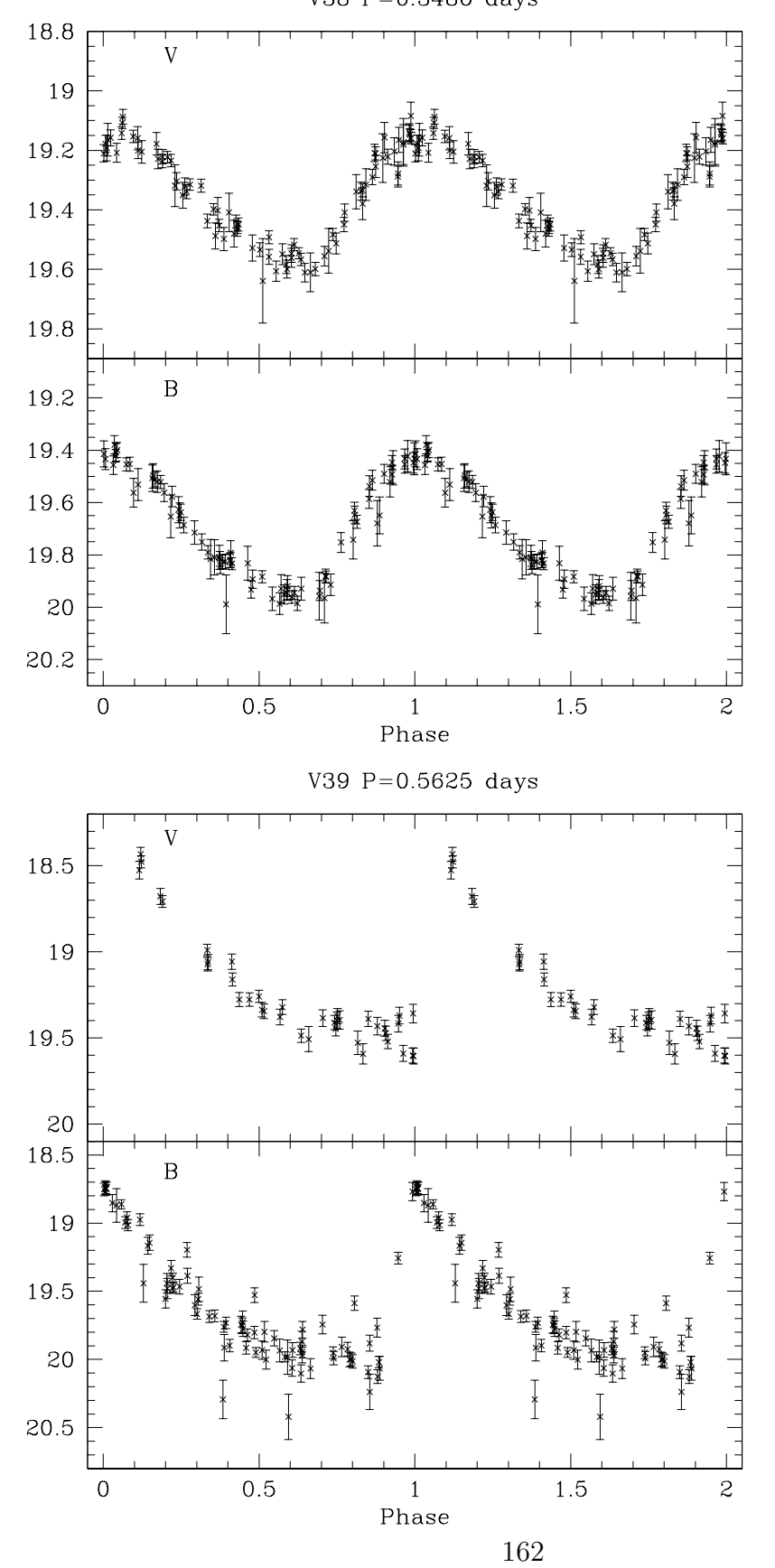


Figure A.1: Light curves for the variable stars in NGC 1466 (continued)  $$\rm V40~P\!=\!0.5361~days$$ 

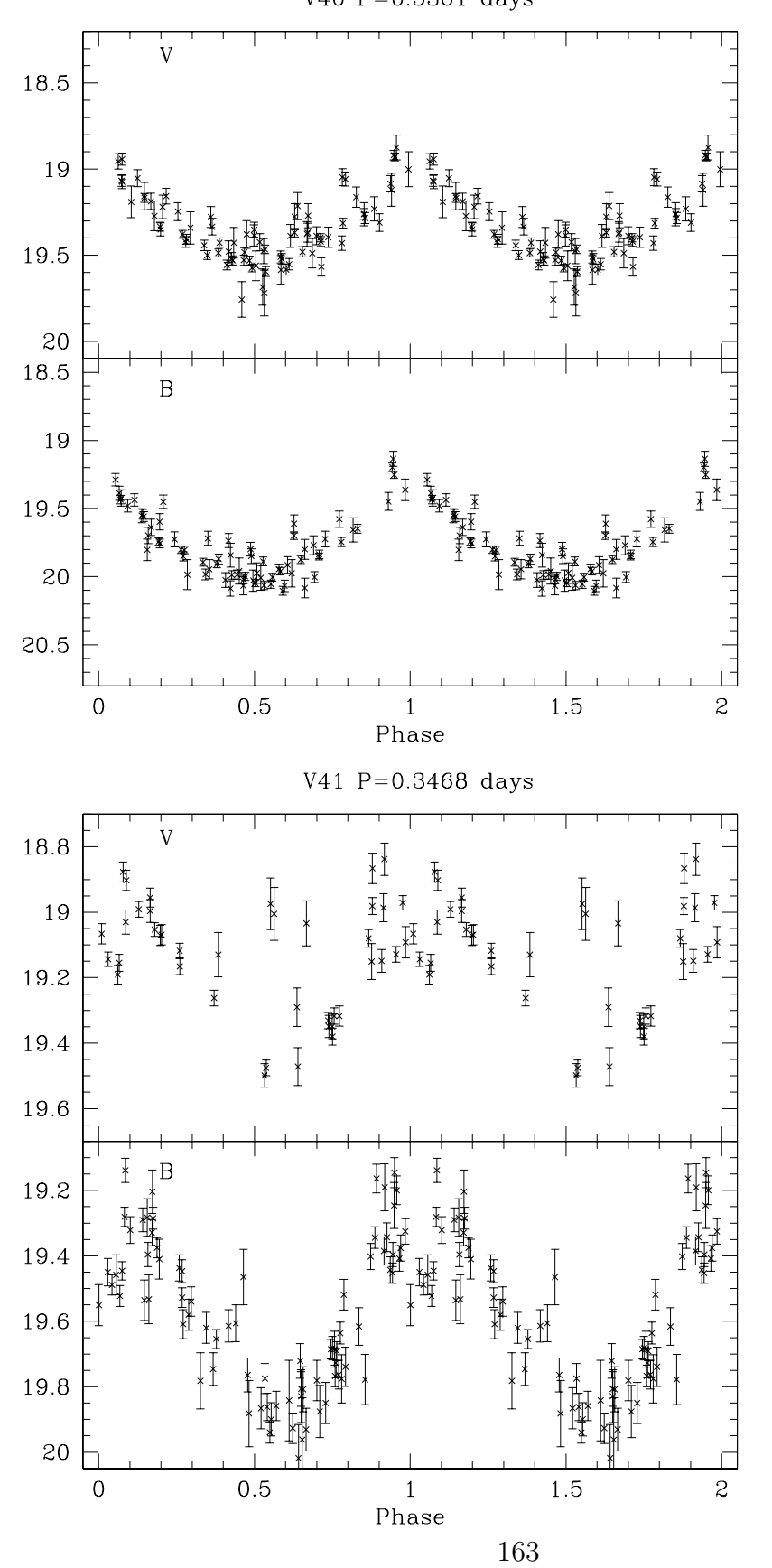


Figure A.1: Light curves for the variable stars in NGC 1466 (continued) V42 P=0.6348 days

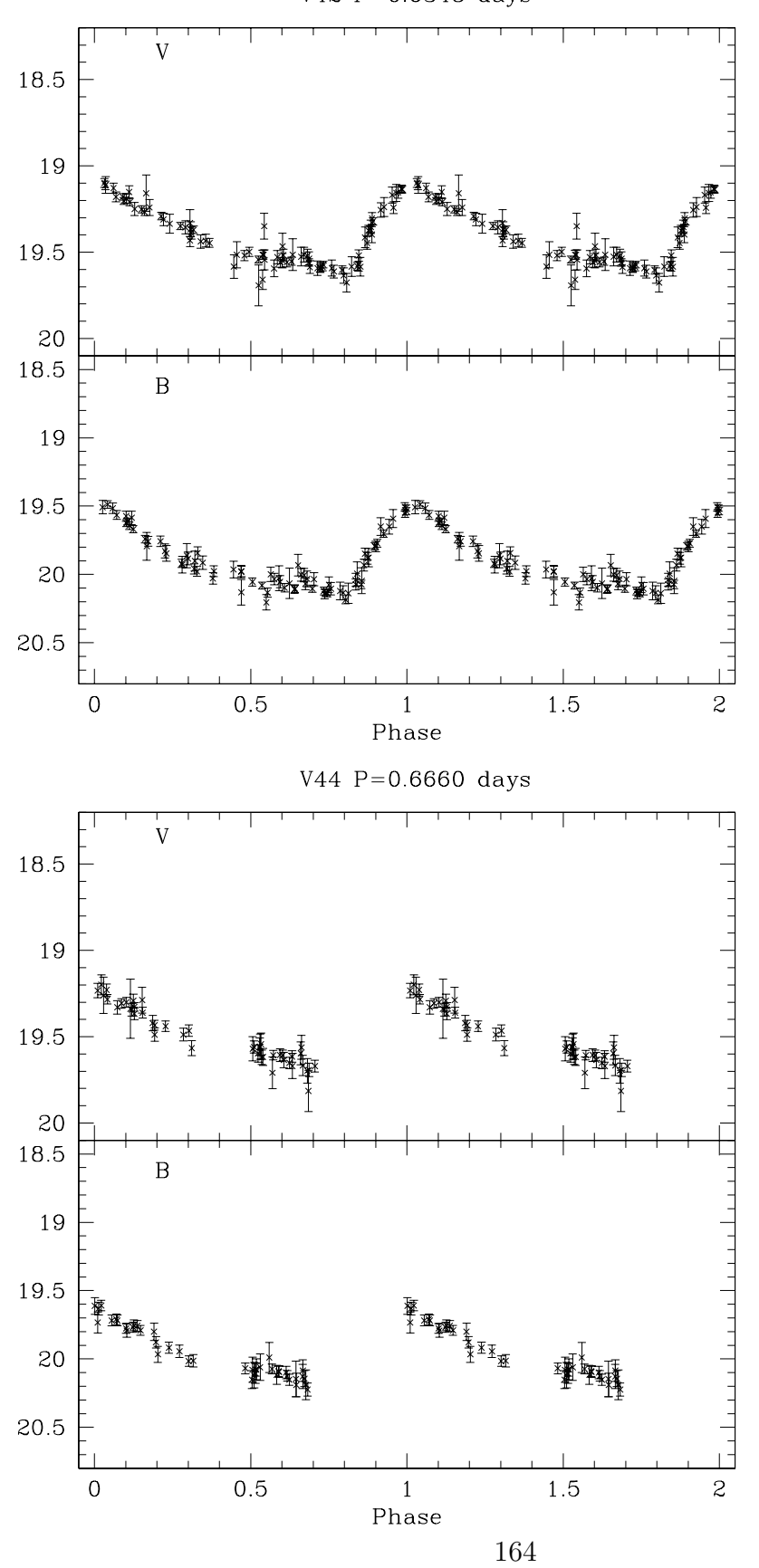


Figure A.1: Light curves for the variable stars in NGC 1466 (continued)  $$\rm V45~P\!=\!0.3104~days$$ 

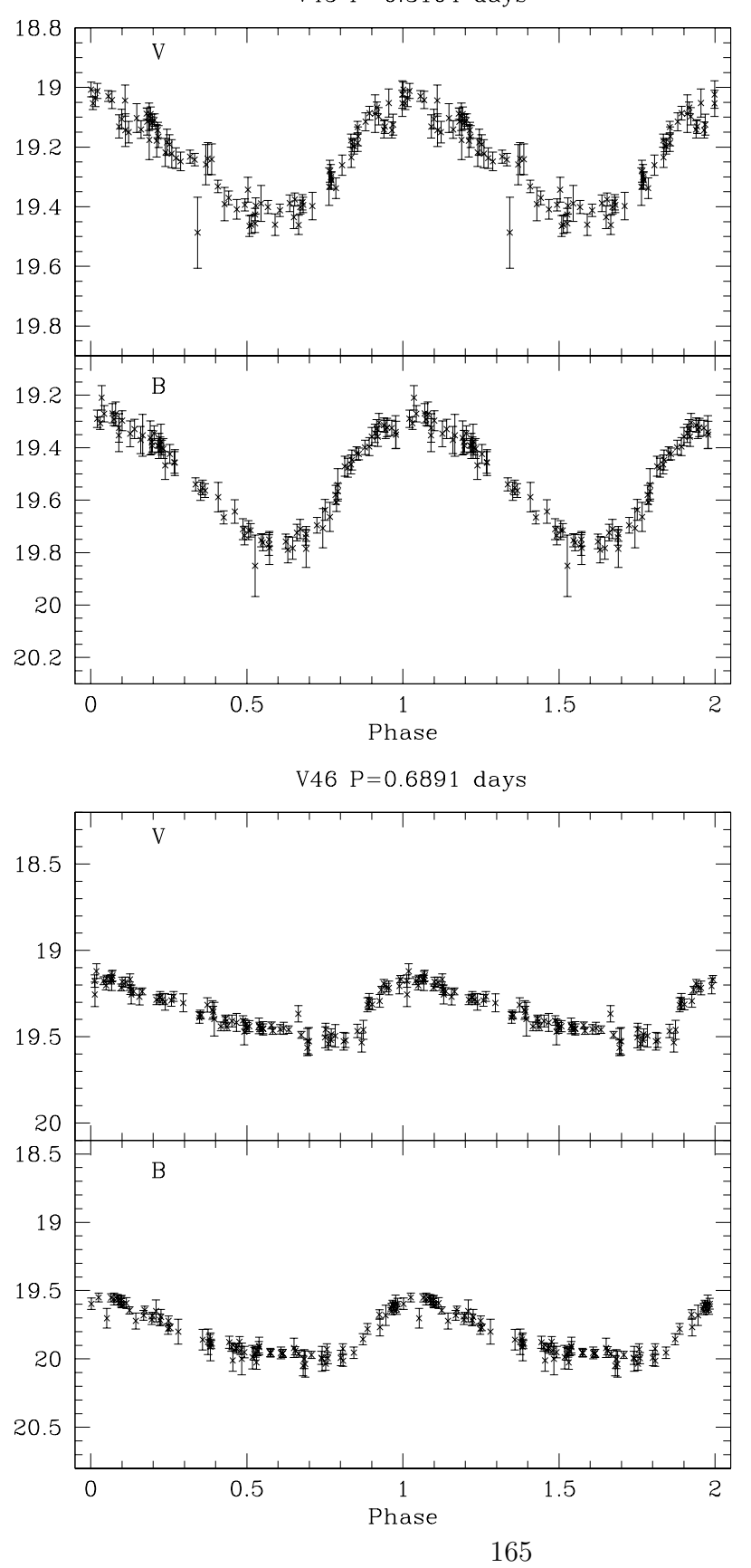


Figure A.1: Light curves for the variable stars in NGC 1466 (continued) V47 P\_1=0.3519 days

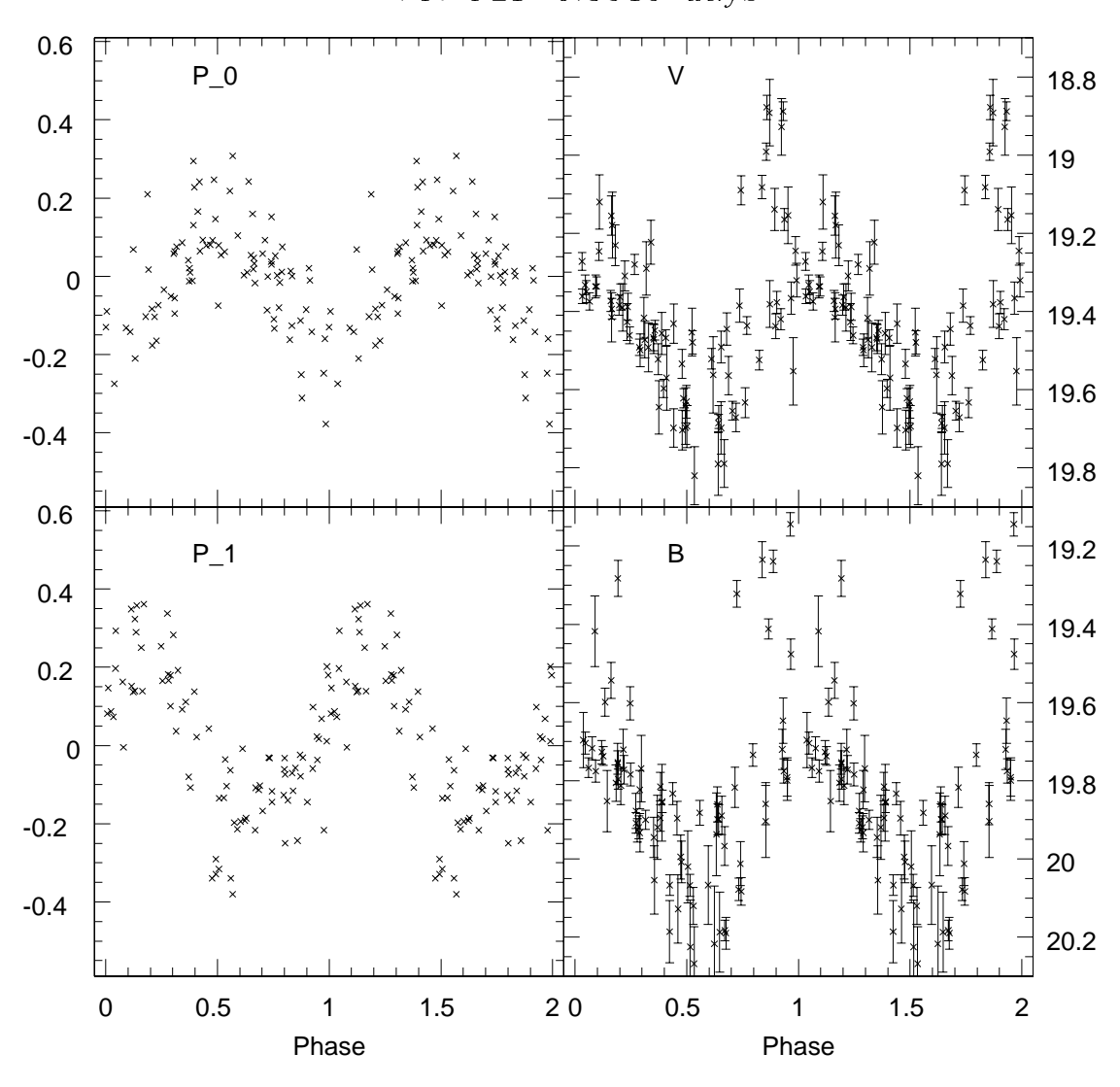


Figure A.1: Light curves for the variable stars in NGC 1466 (continued)  $$\rm V48~P\!=\!0.3770~days$$ 

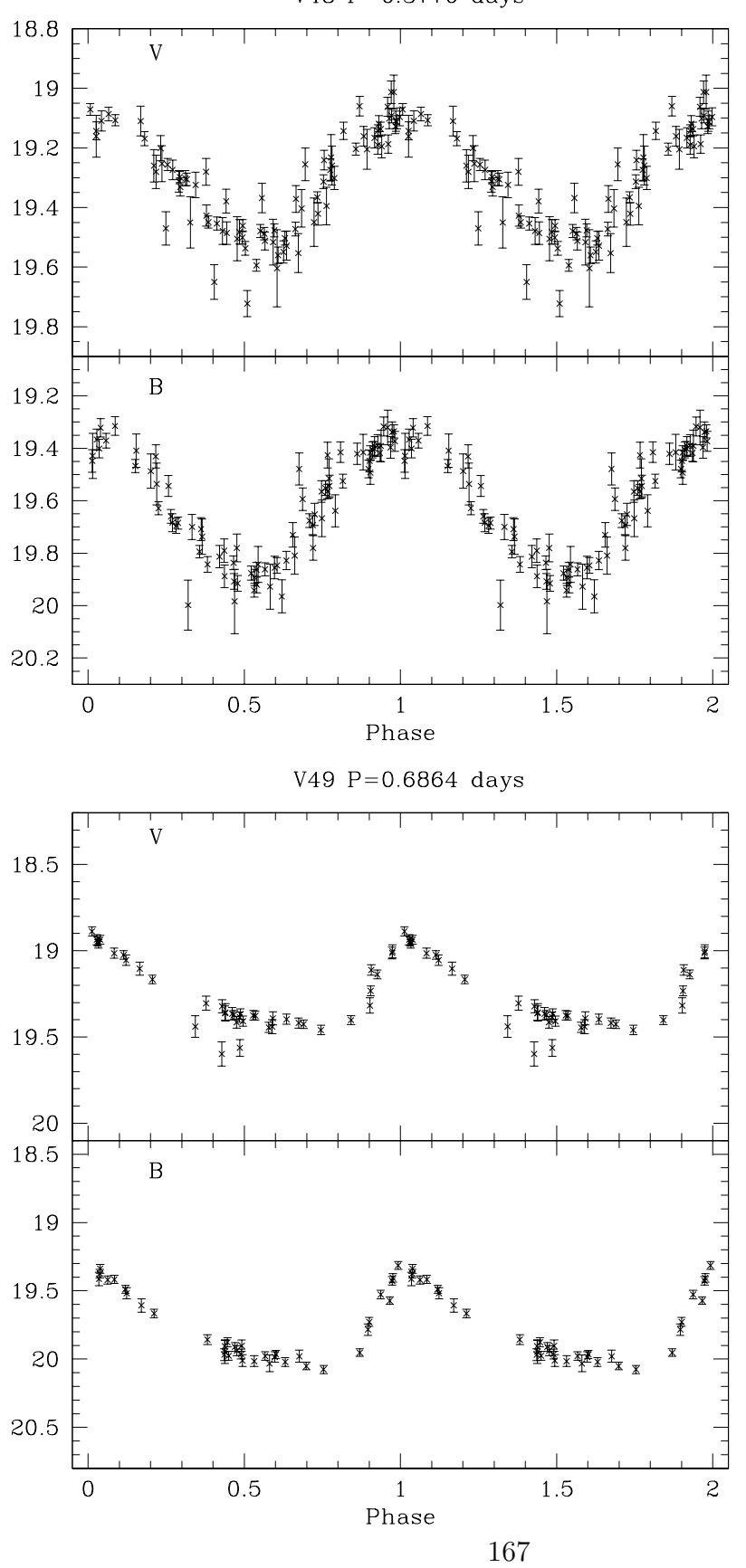


Figure A.1: Light curves for the variable stars in NGC 1466 (continued)  $${\tt V50\ P=0.5819\ days}$$ 

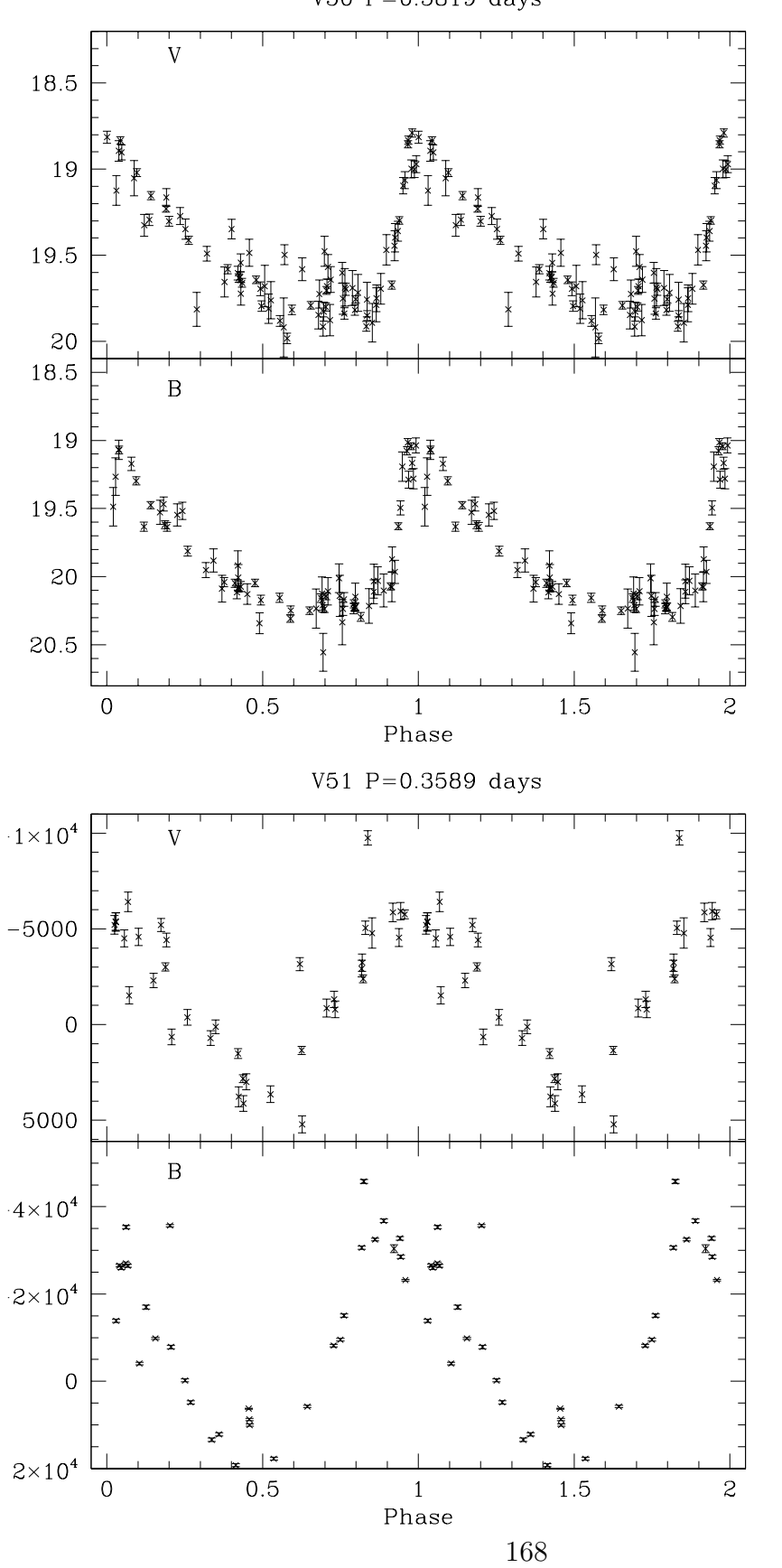


Figure A.1: Light curves for the variable stars in NGC 1466 (continued)  $$\tt V52\ P=0.3499\ days$$ 

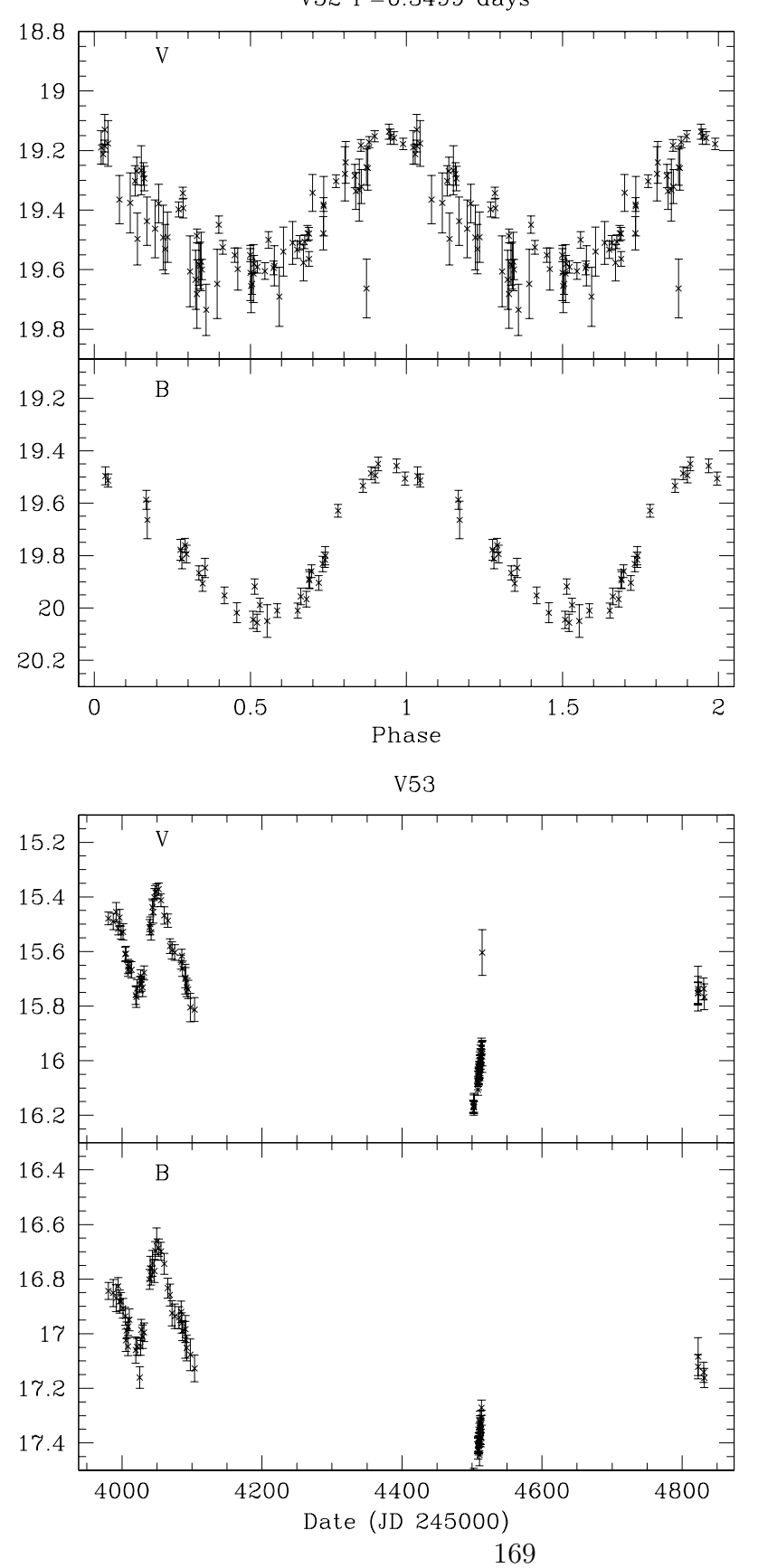


Figure A.1: Light curves for the variable stars in NGC 1466 (continued)  $$\tt V54\ P=0.5561\ days$$ 

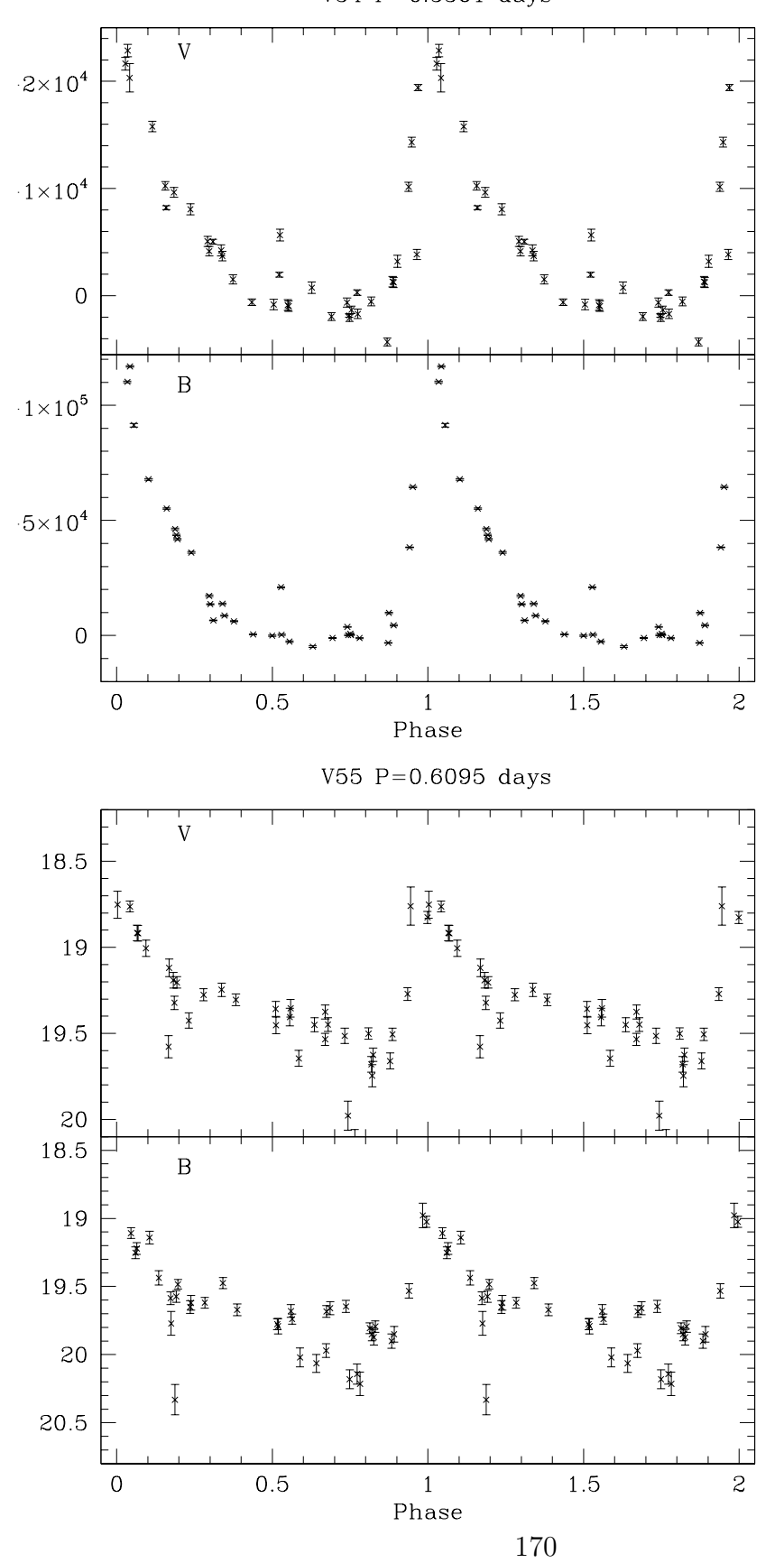


Figure A.1: Light curves for the variable stars in NGC 1466 (continued)  $$\tt V56\ P=0.6224\ days$$ 

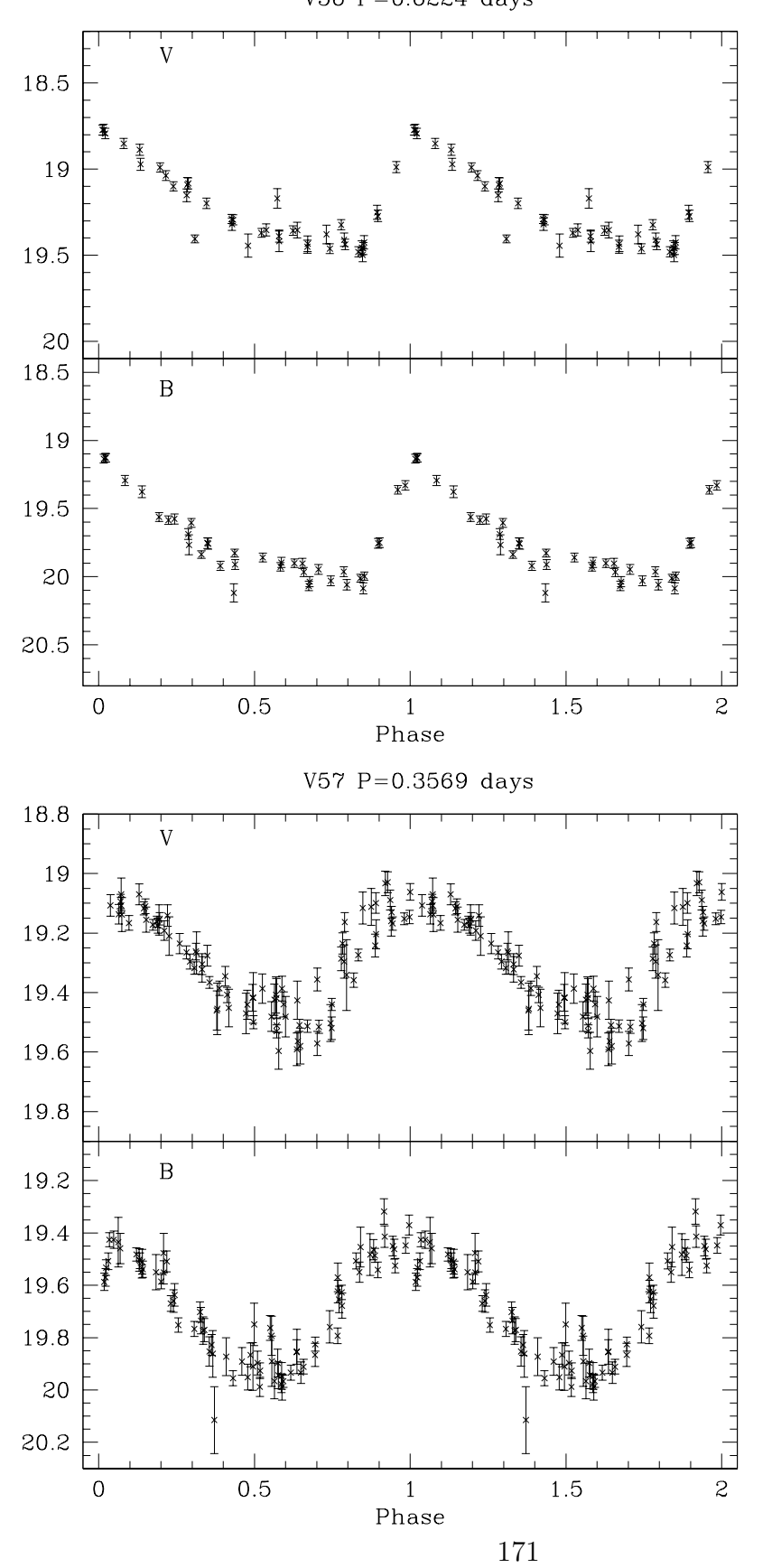


Figure A.1: Light curves for the variable stars in NGC 1466 (continued)  $${\tt V58\ P=0.5675\ days}$$ 

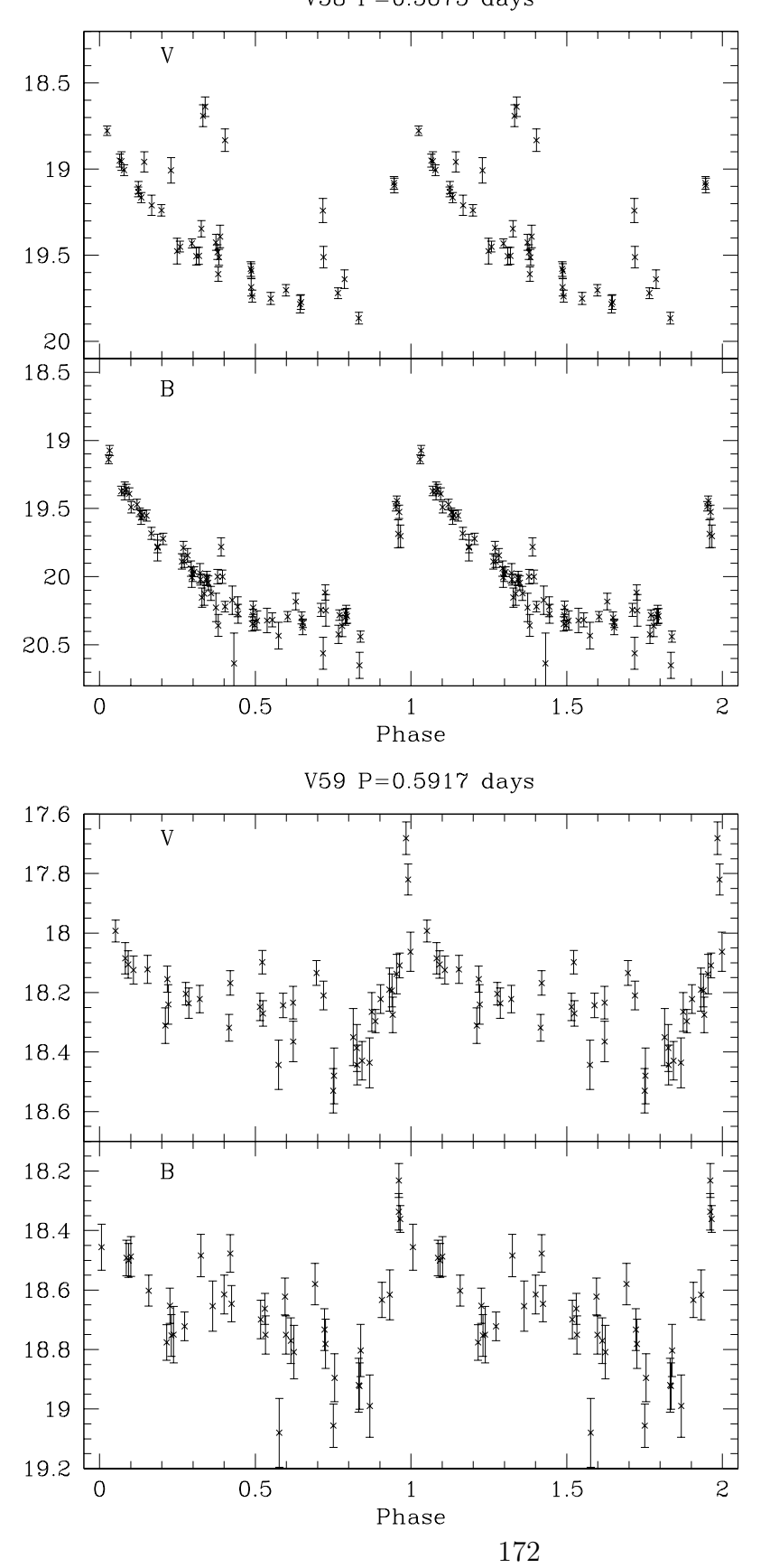


Figure A.1: Light curves for the variable stars in NGC 1466 (continued)  $${\tt V60\ P=0.5221\ days}$$ 

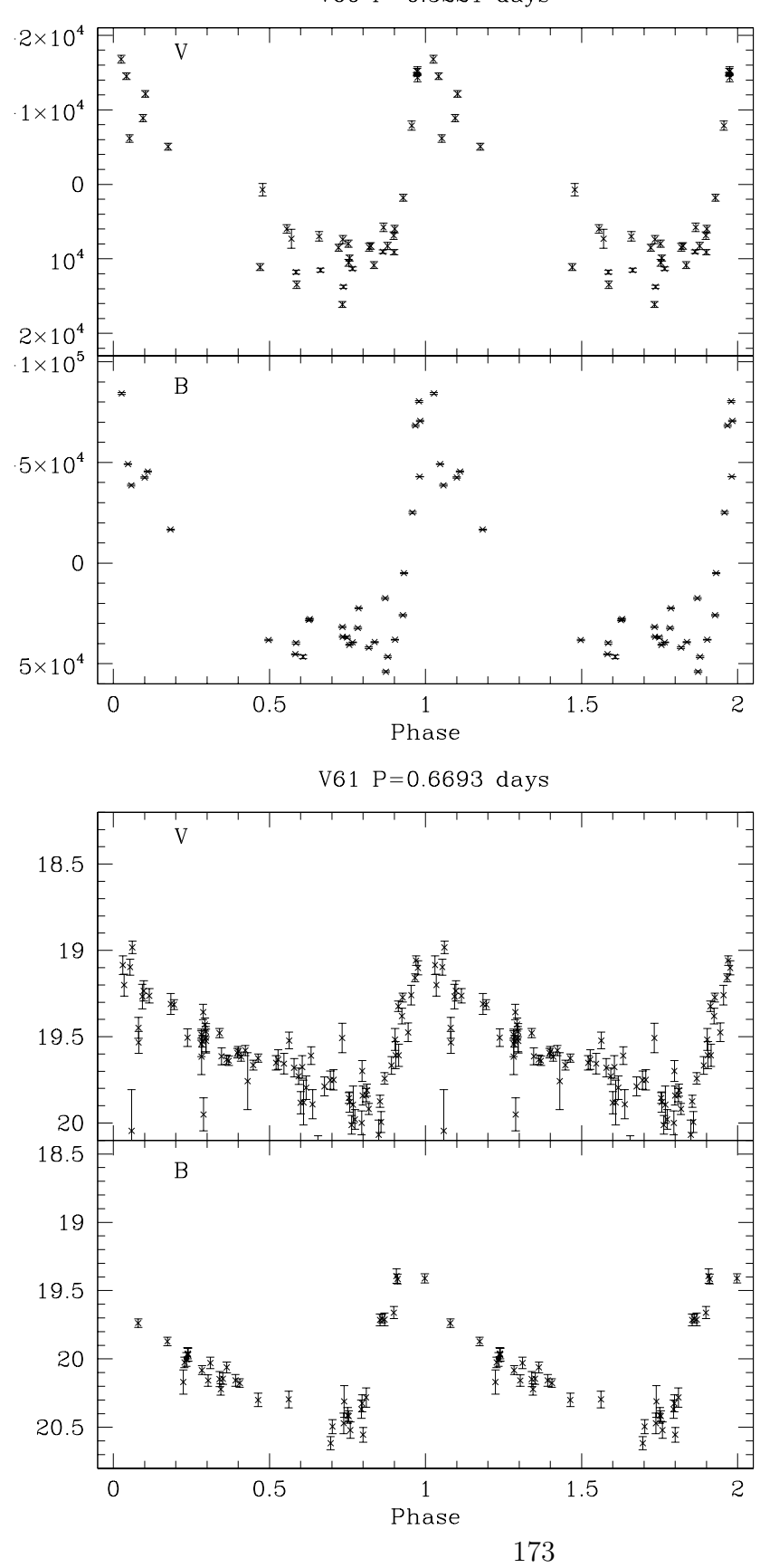


Figure A.1: Light curves for the variable stars in NGC 1466 (continued) V62 P=0.5041 days

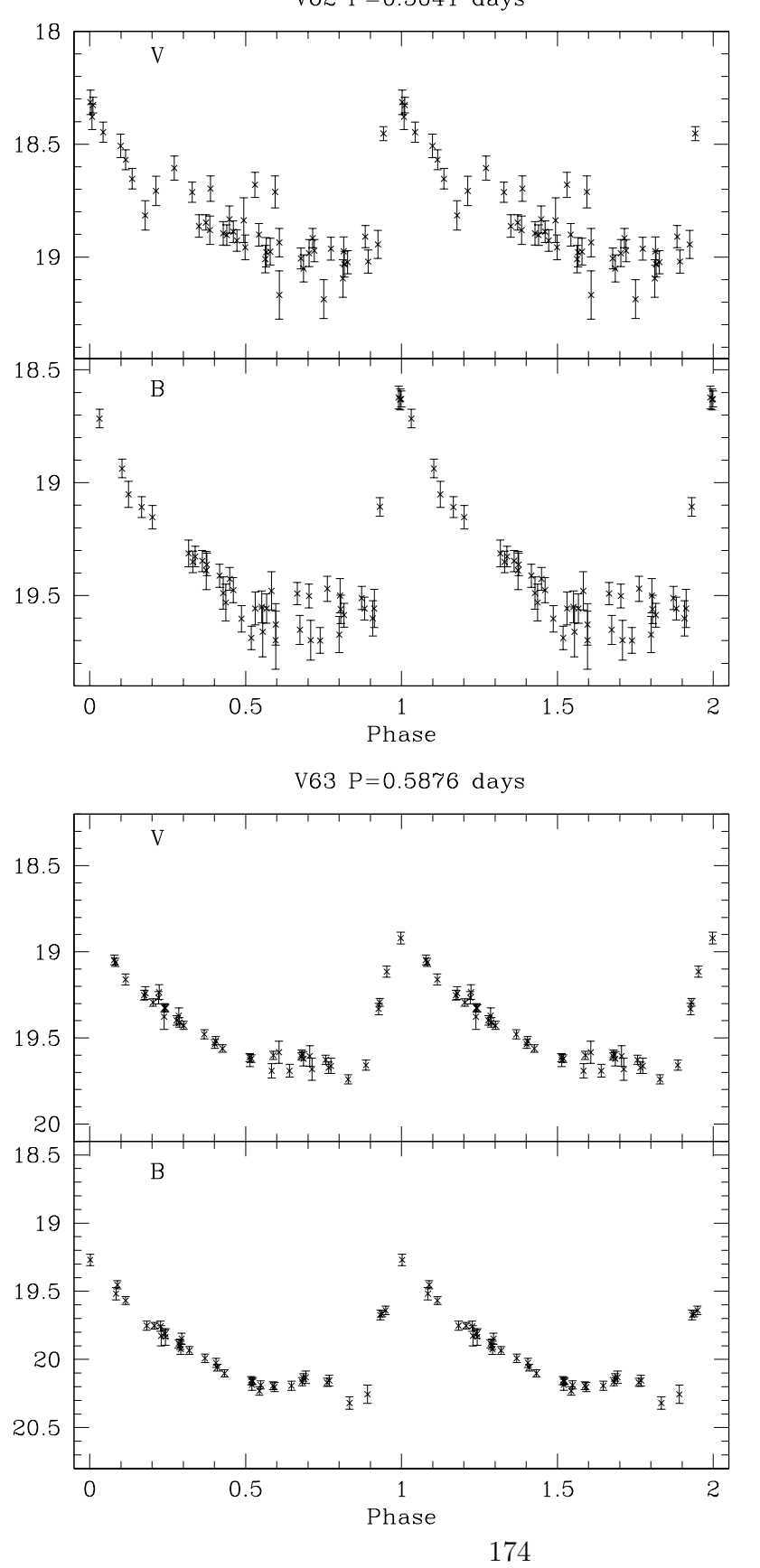


Figure A.1: Light curves for the variable stars in NGC 1466 (continued)  $${\tt V64\ P=0.6877\ days}$$ 

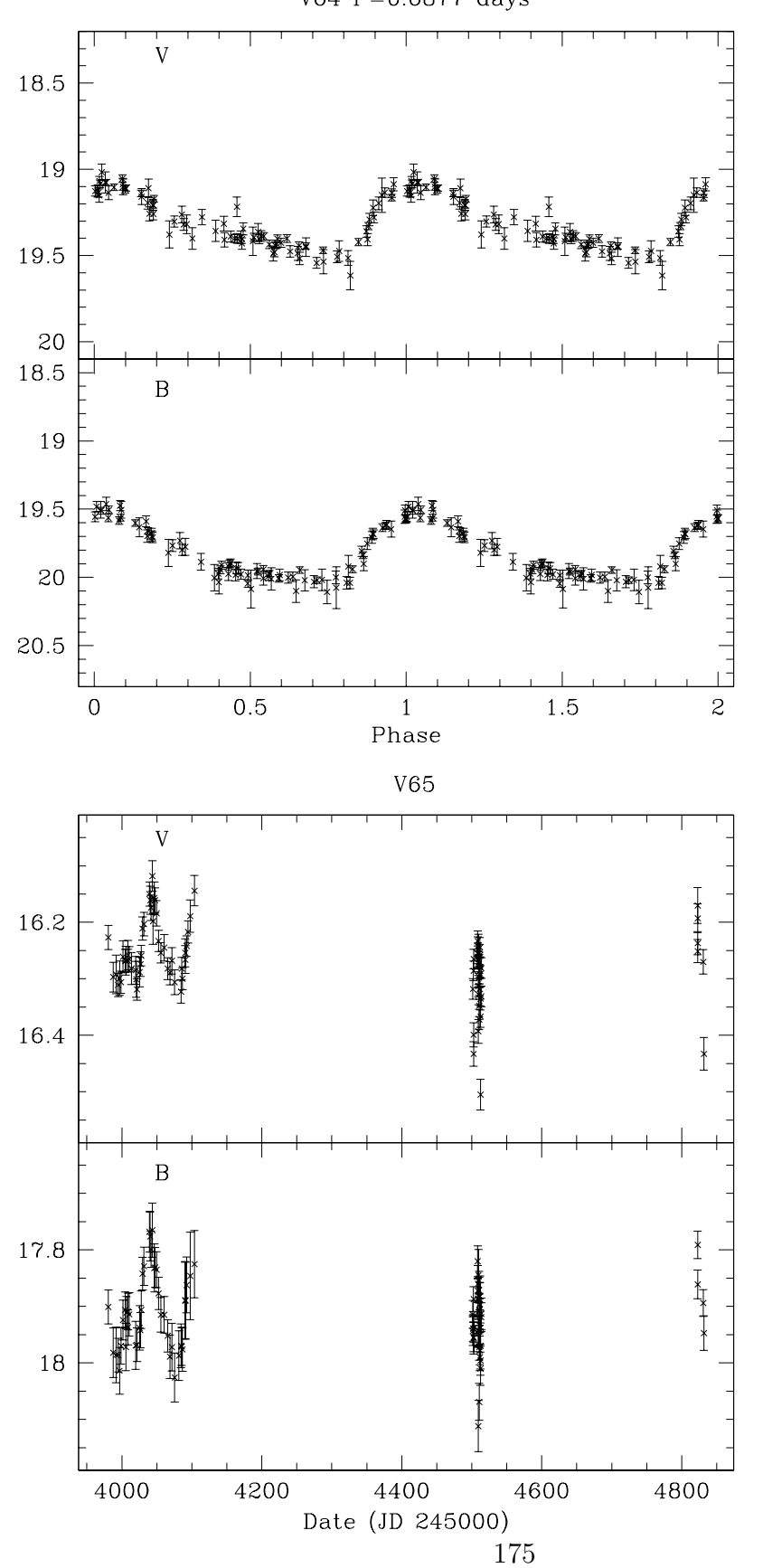
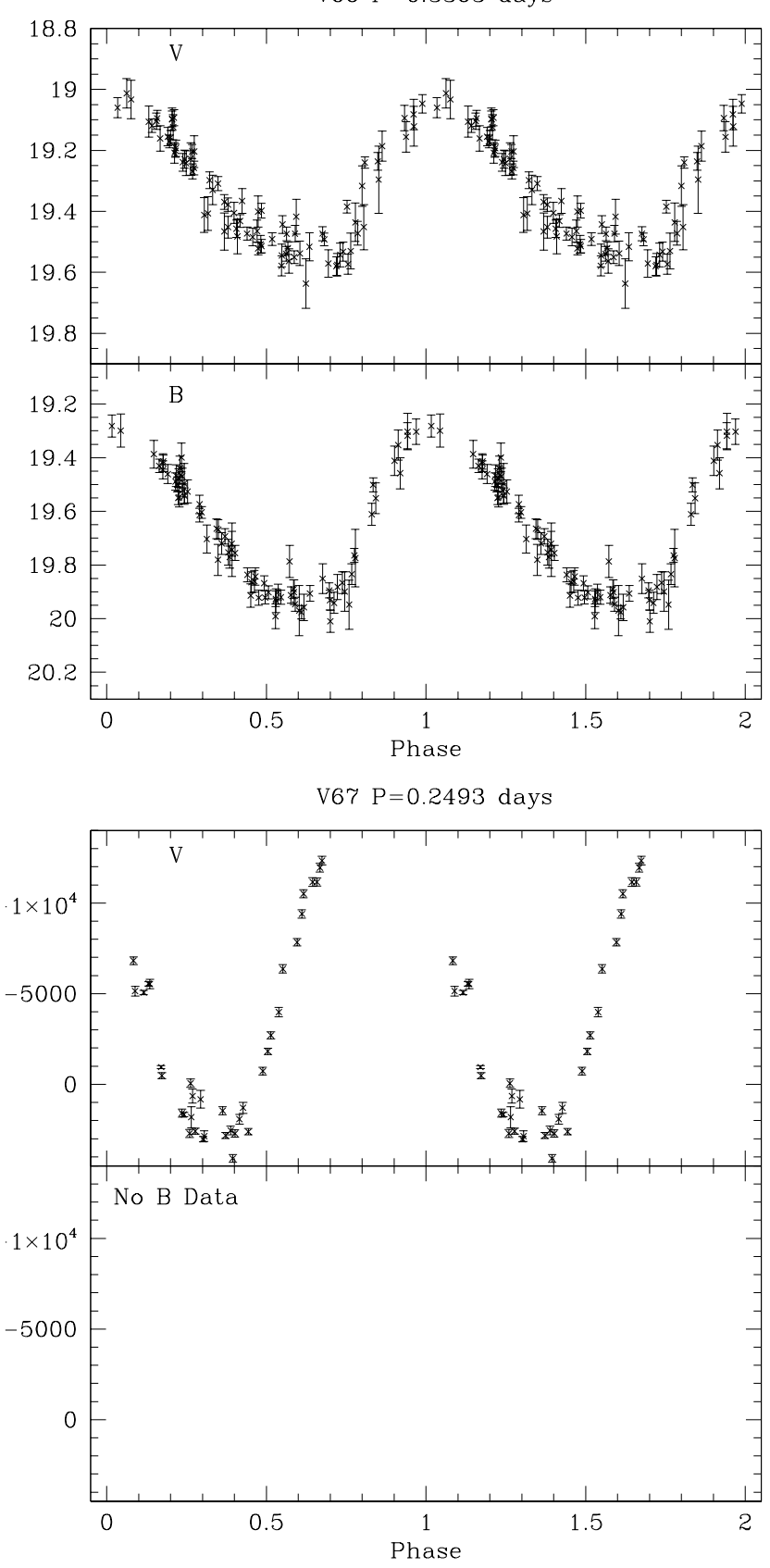
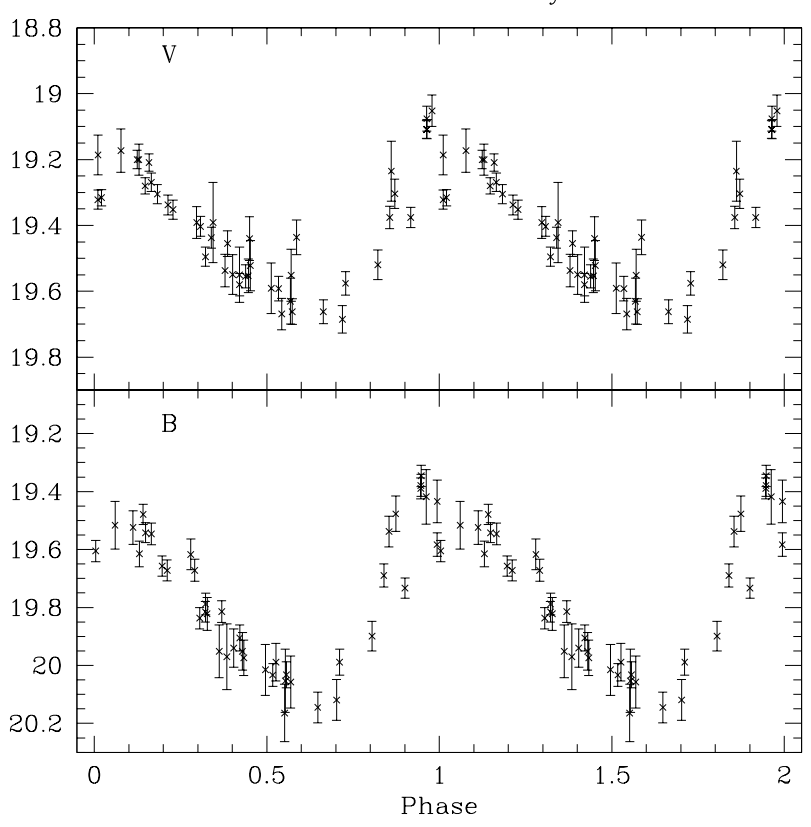


Figure A.1: Light curves for the variable stars in NGC 1466 (continued)  $${\tt V66\ P=0.3363\ days}$$ 



176

Figure A.1: Light curves for the variable stars in NGC 1466 (continued)  $_{\rm V68~P=0.3491~days}$ 



## Appendix B: Reticulum Light Curves

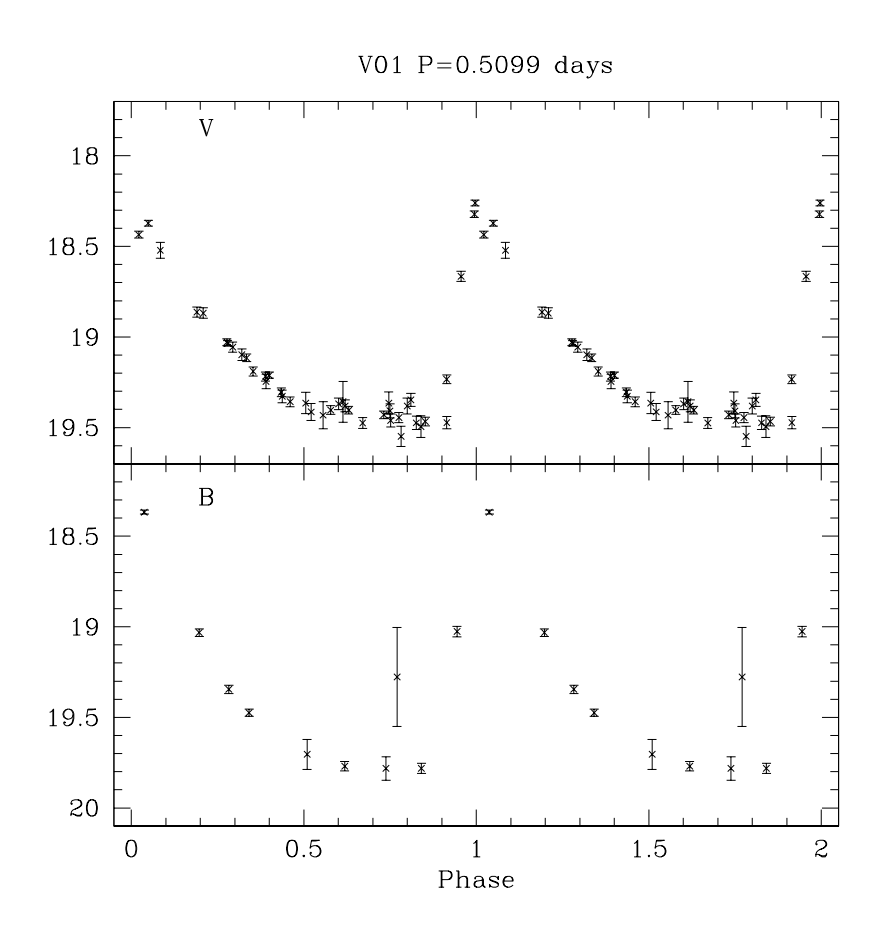


Figure B.1: Light curves for the variable stars in Reticulum

Figure B.1: Light curves for the variable stars in Reticulum (continued)  $$\tt V02\ P=0.6187\ days$$ 

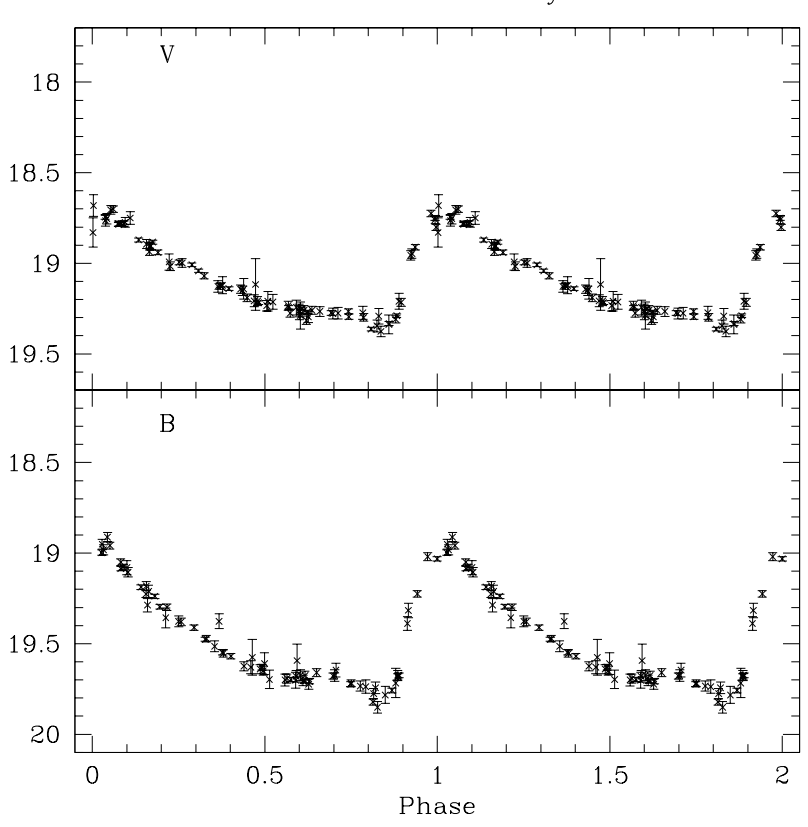


Figure B.1: Light curves for the variable stars in Reticulum (continued) V03  $P_1=0.3538$  days

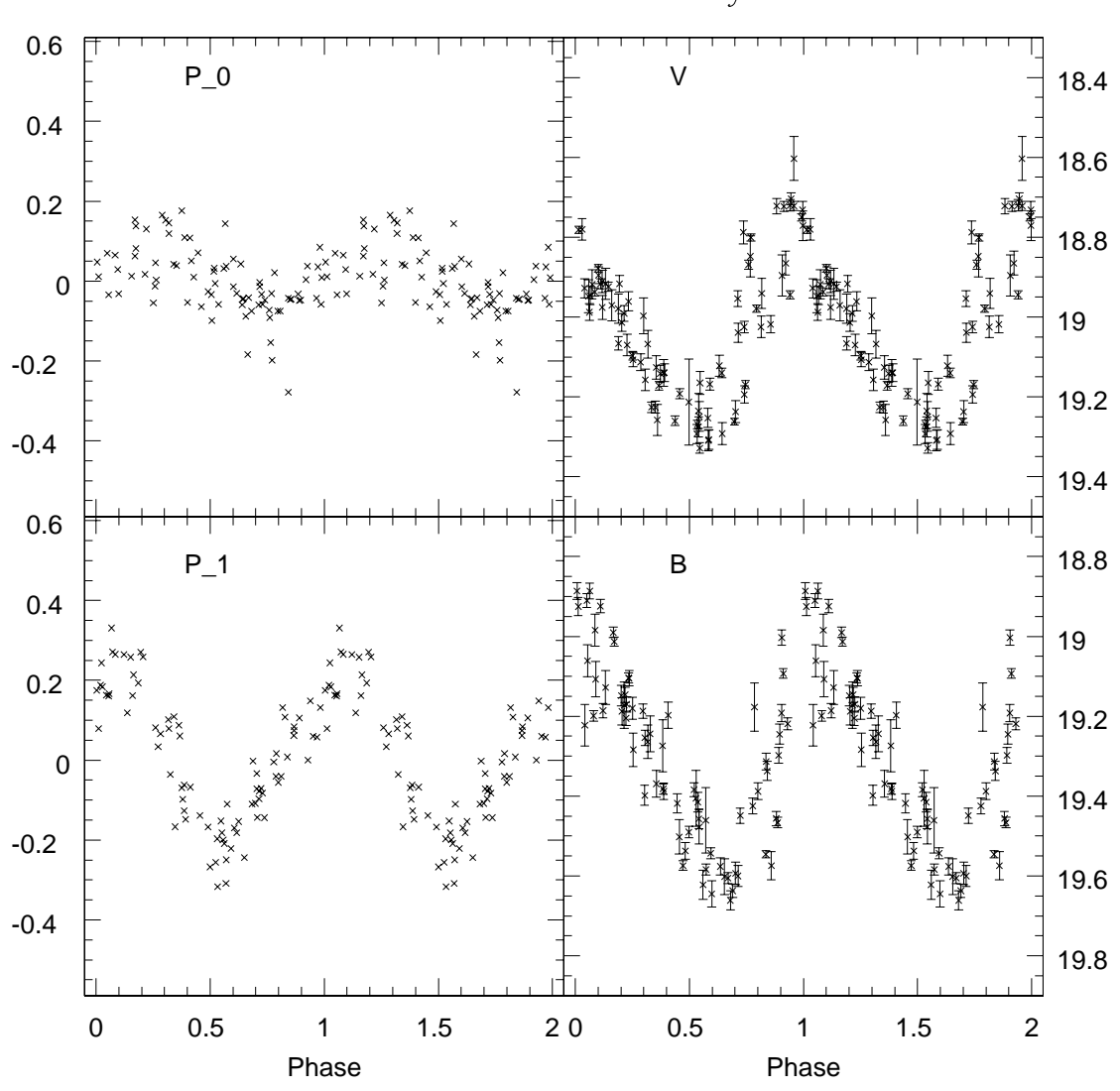


Figure B.1: Light curves for the variable stars in Reticulum (continued) V04 P\_1=0.3532 days

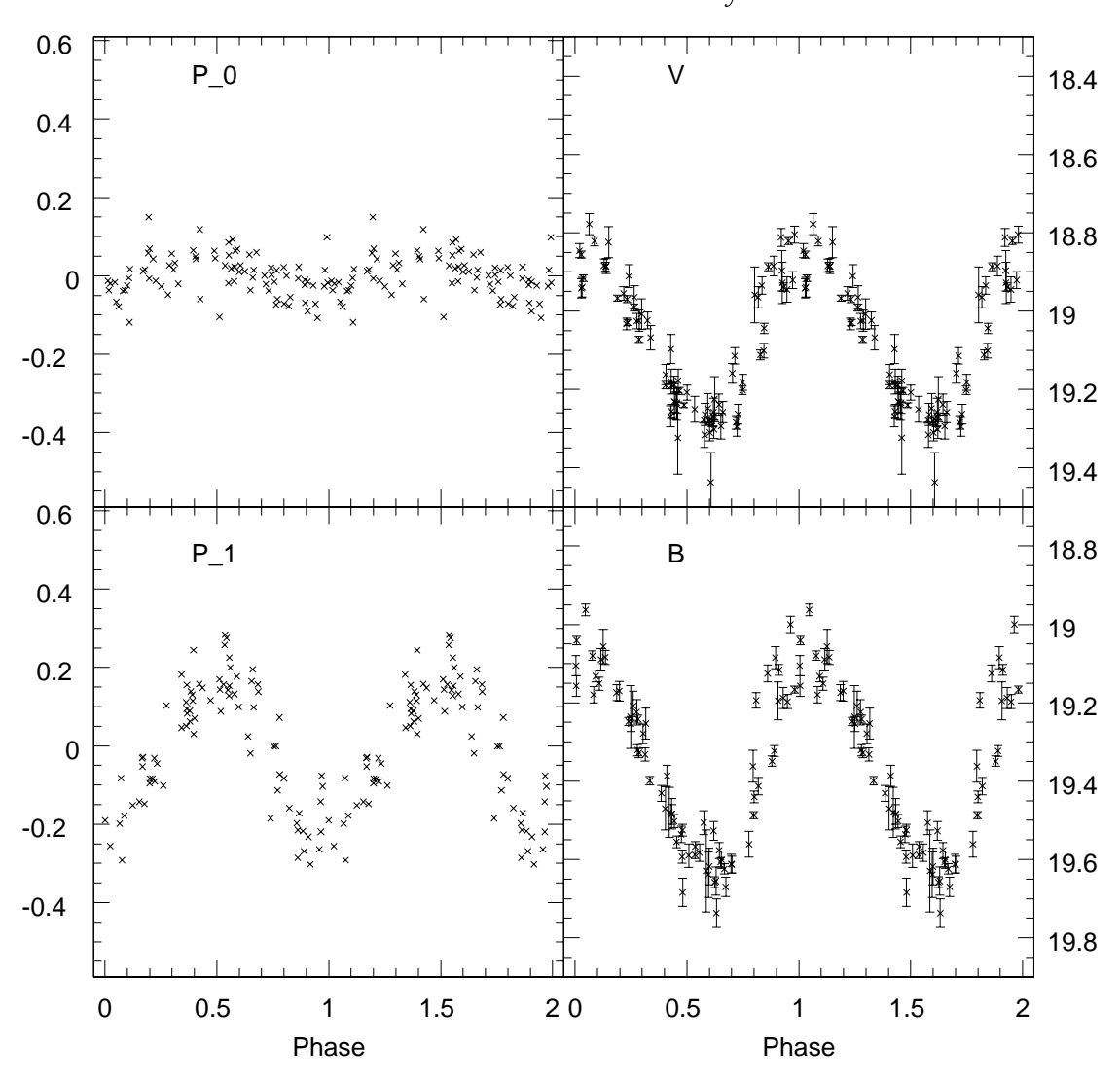


Figure B.1: Light curves for the variable stars in Reticulum (continued)  $$\rm V05~P{=}0.5718~days$$ 

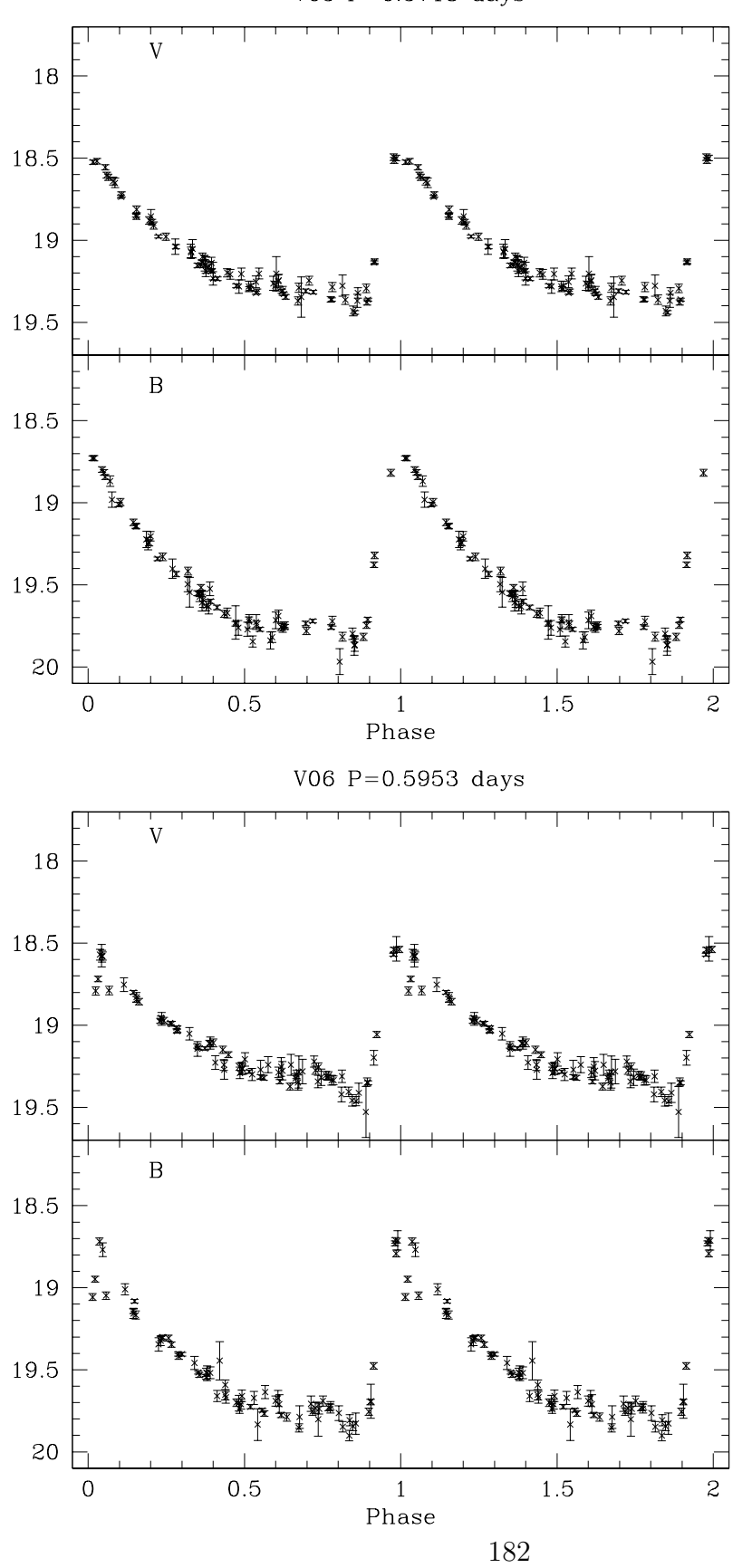


Figure B.1: Light curves for the variable stars in Reticulum (continued)  $$\tt V07\ P=0.5104\ days$$ 

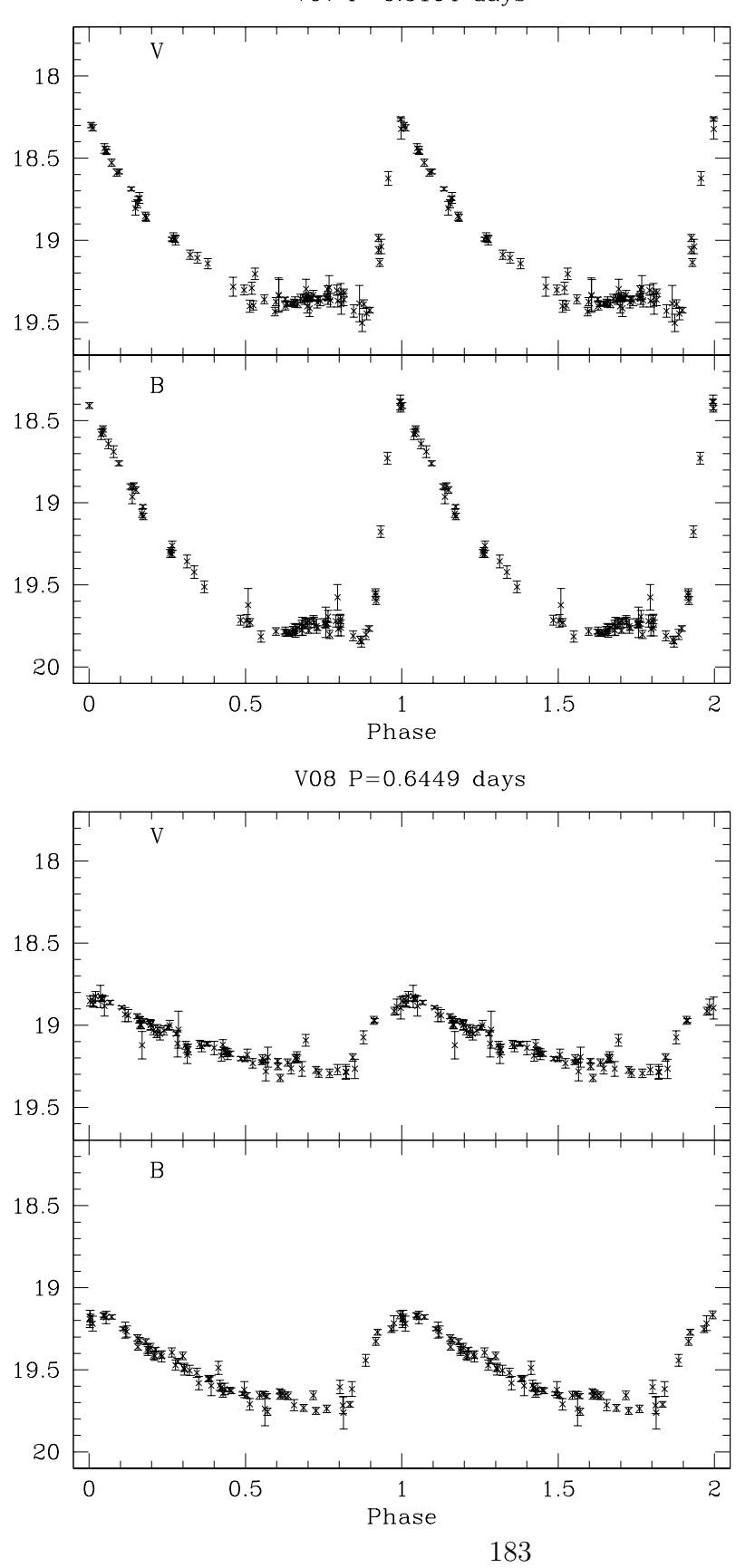


Figure B.1: Light curves for the variable stars in Reticulum (continued)  $$\rm V09~P\!=\!0.5449~days$$ 

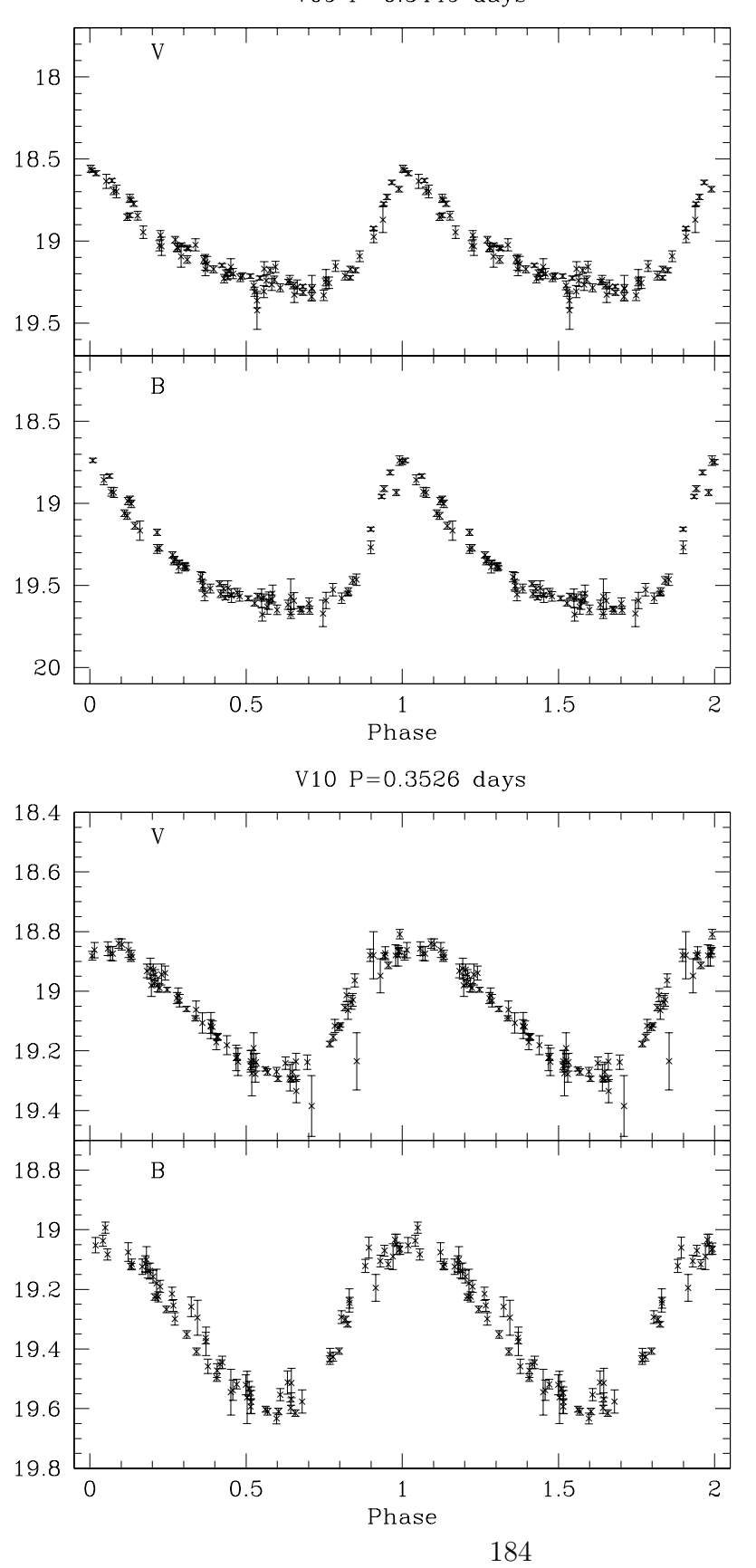


Figure B.1: Light curves for the variable stars in Reticulum (continued)  $$\rm V11\ P{=}0.3572\ days$$ 

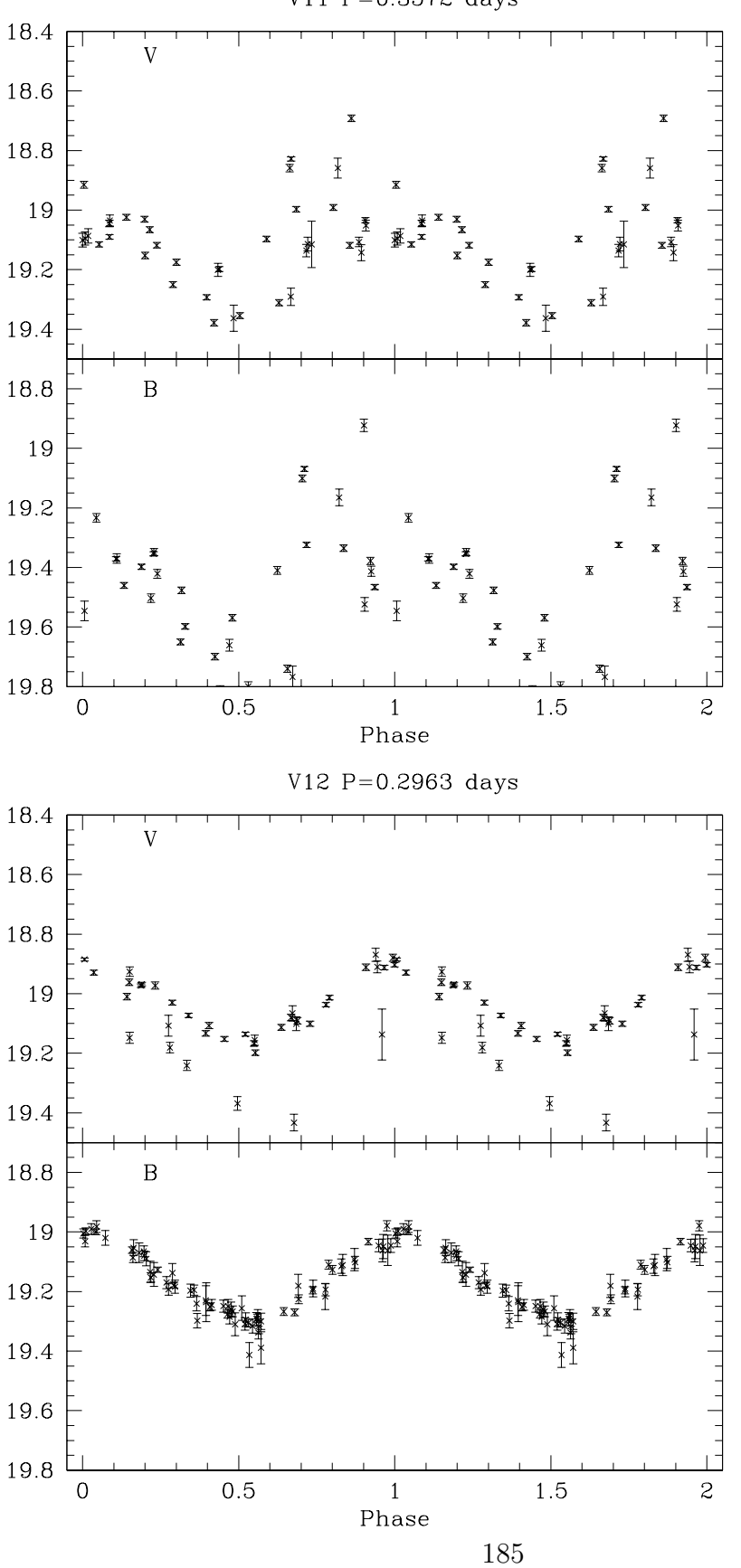


Figure B.1: Light curves for the variable stars in Reticulum (continued)  $$\rm V13~P\!=\!0.6096~days$$ 

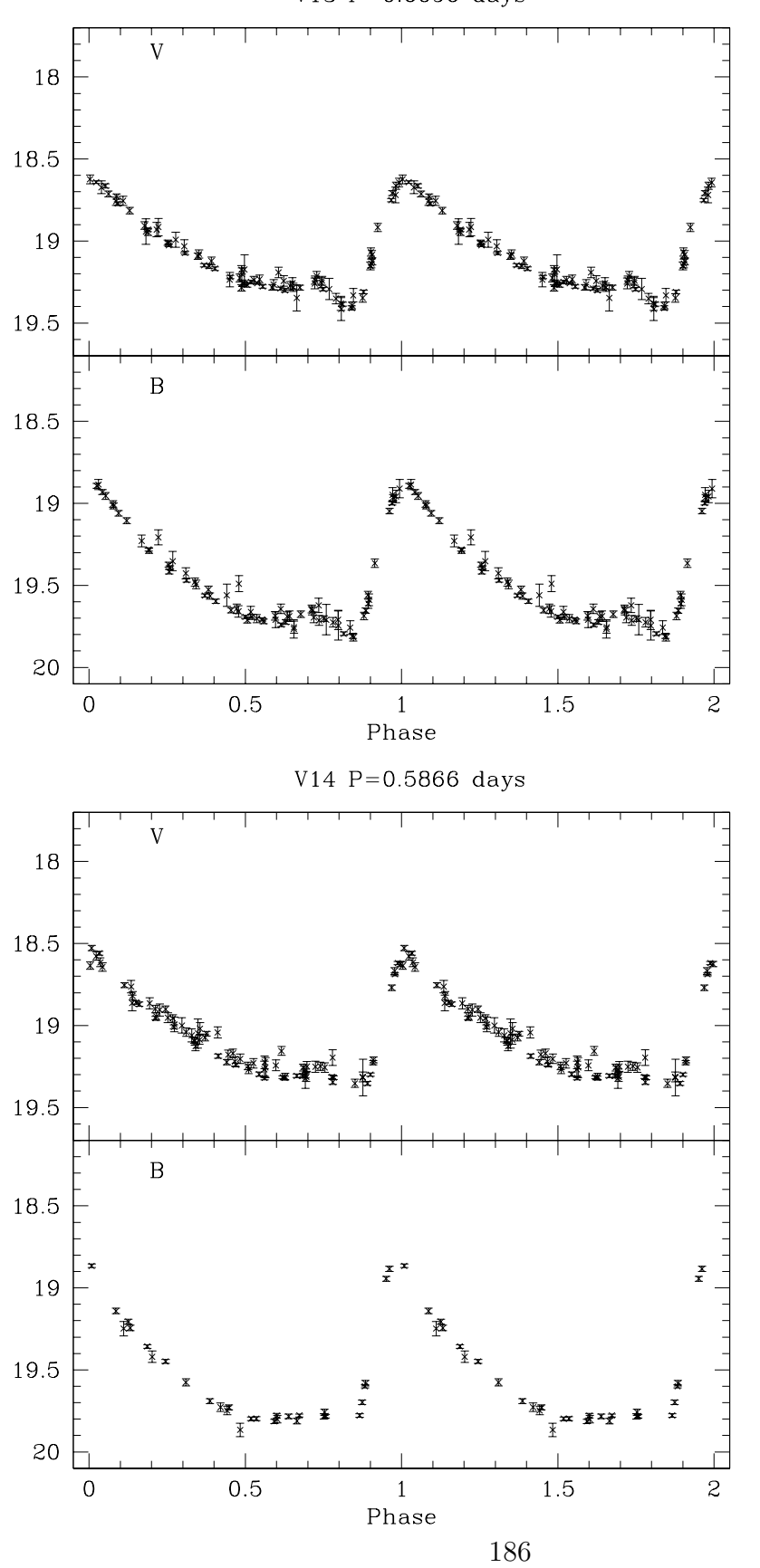


Figure B.1: Light curves for the variable stars in Reticulum (continued) V15 P\_1=0.3548 days

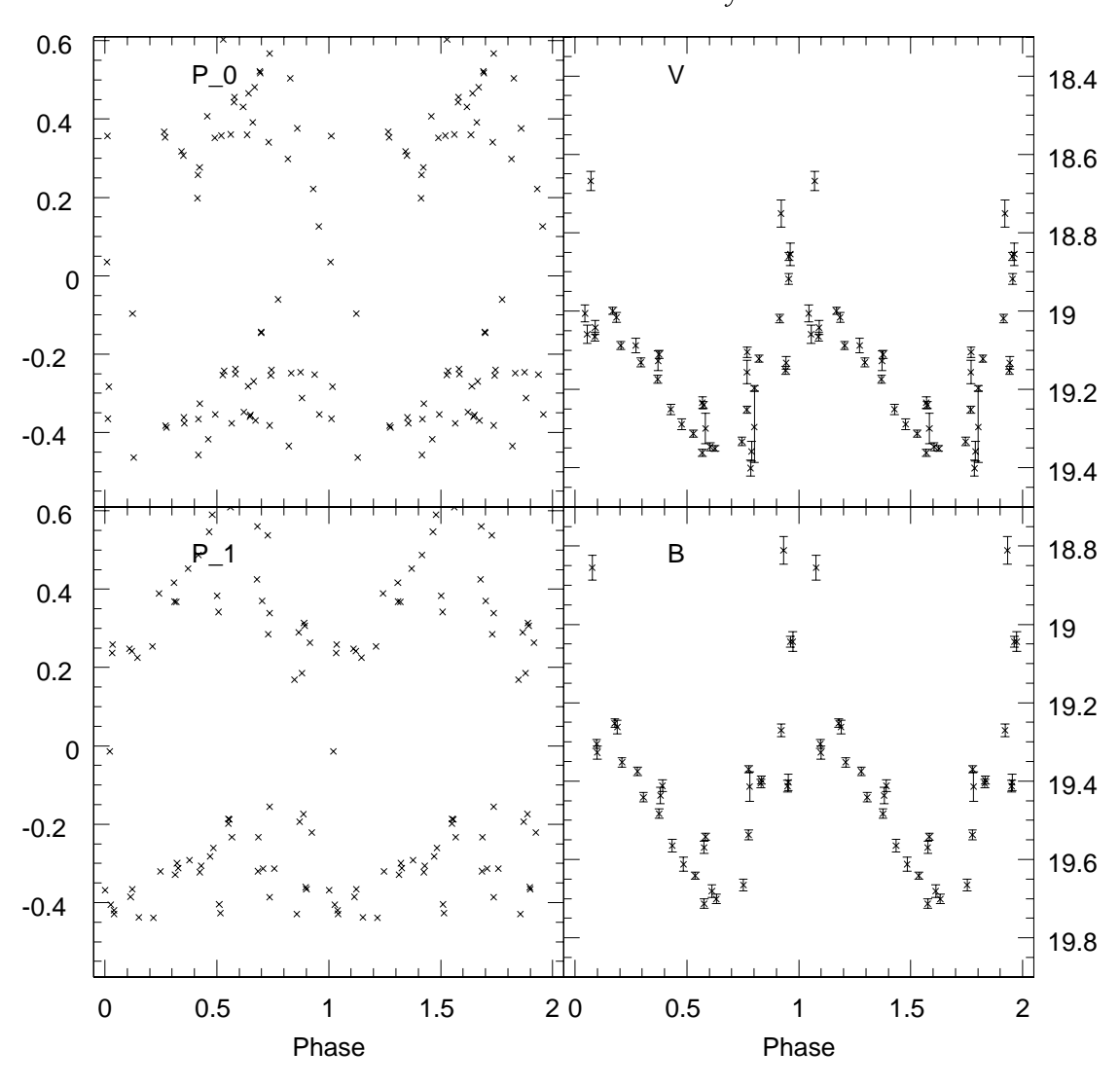


Figure B.1: Light curves for the variable stars in Reticulum (continued)  $$V16\ P{=}0.5229\ days$$ 

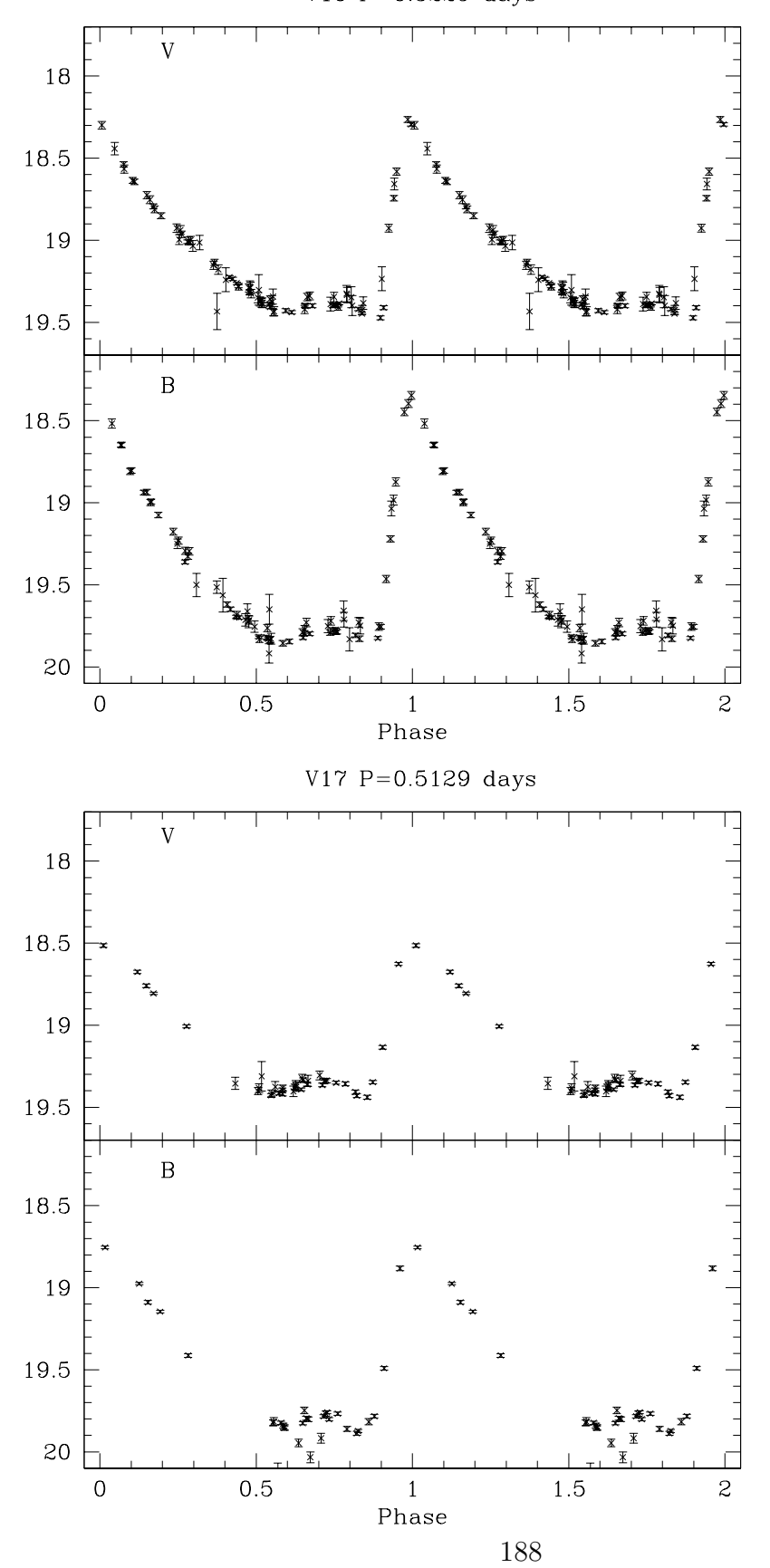


Figure B.1: Light curves for the variable stars in Reticulum (continued)  $$V18\ P{=}0.5601\ days$$ 

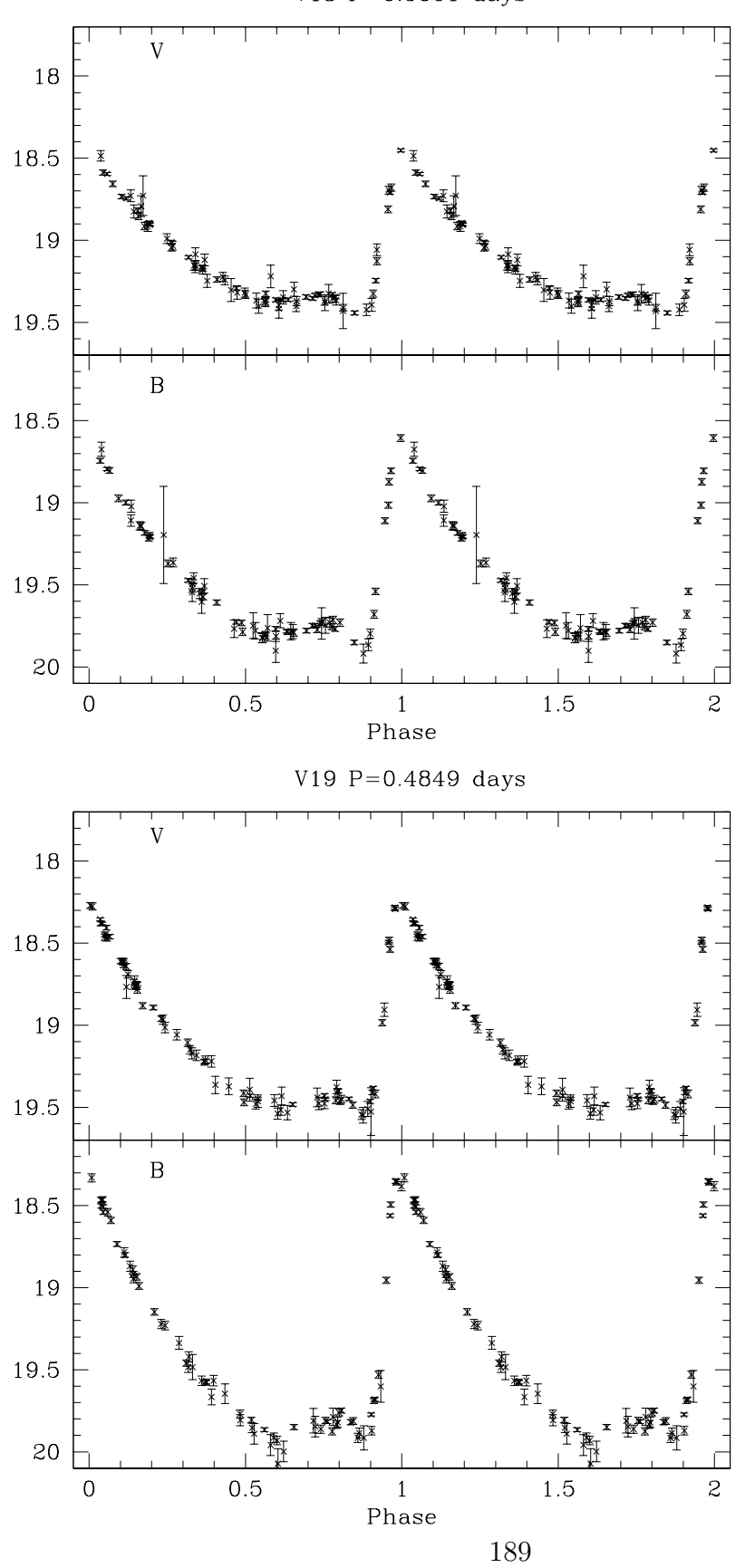


Figure B.1: Light curves for the variable stars in Reticulum (continued)  $$\tt V20\ P=0.5607\ days$$ 

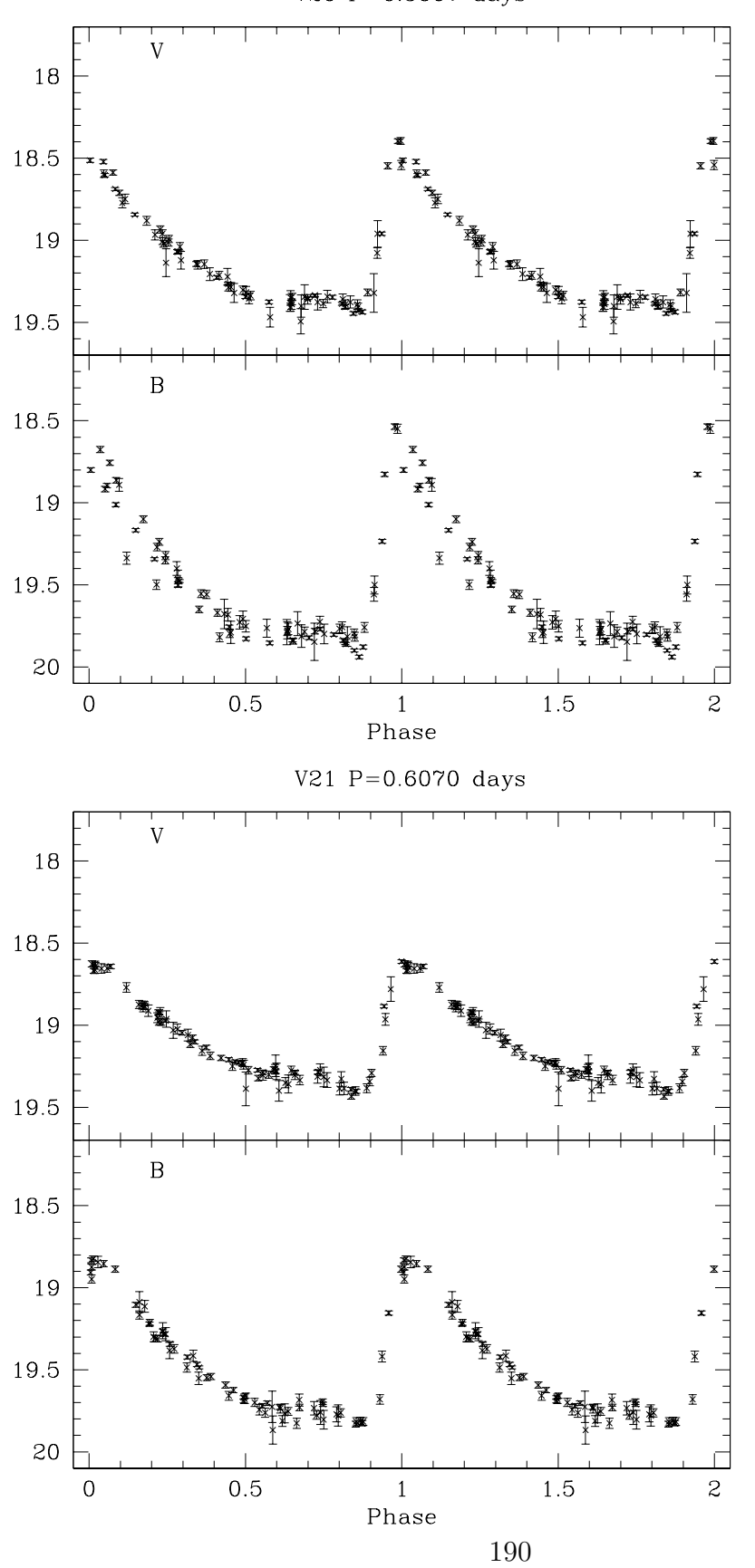


Figure B.1: Light curves for the variable stars in Reticulum (continued)  $$\tt V22\ P=0.5136\ days$$ 

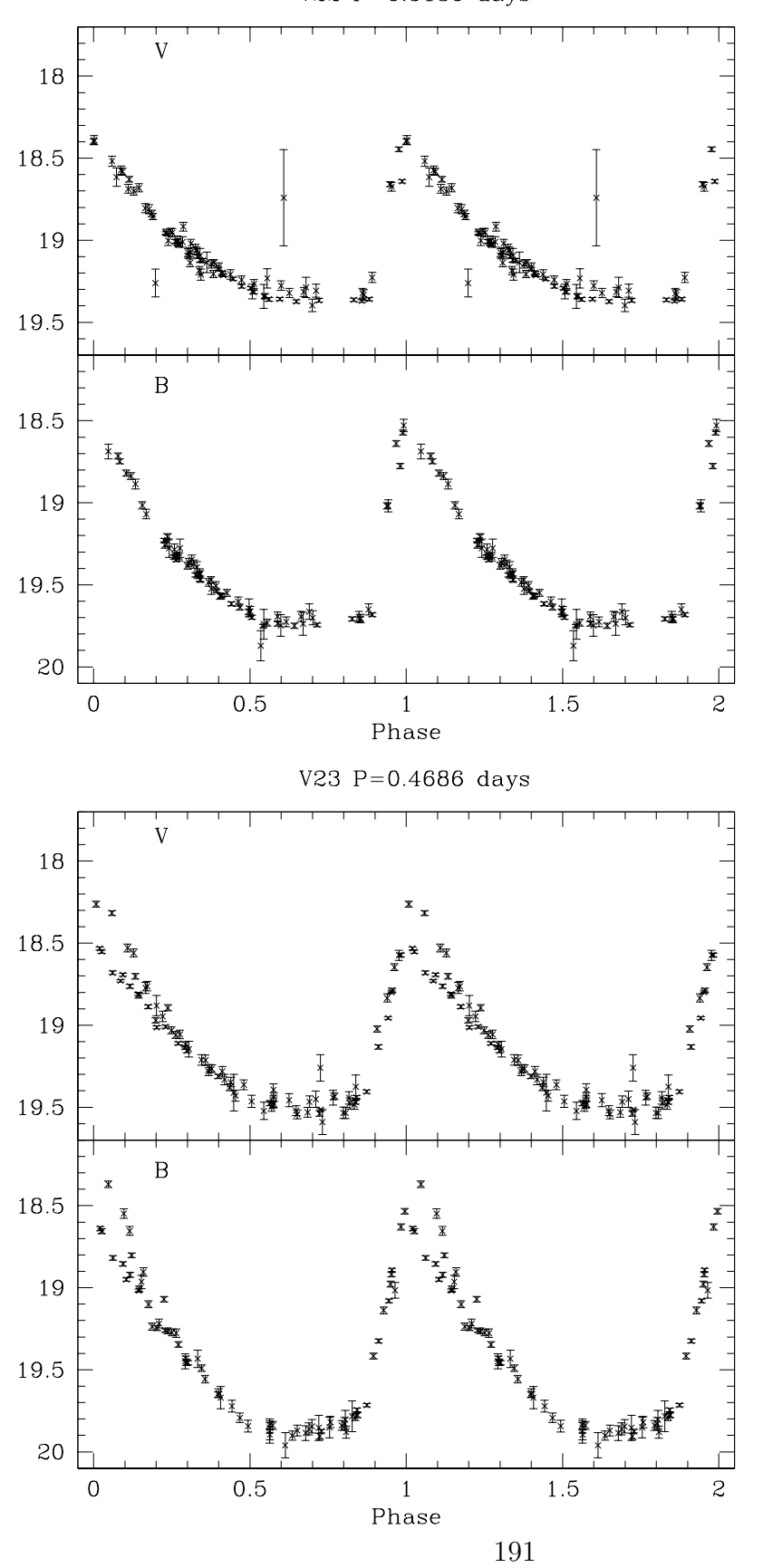


Figure B.1: Light curves for the variable stars in Reticulum (continued) V24  $P_1=0.3476$  days

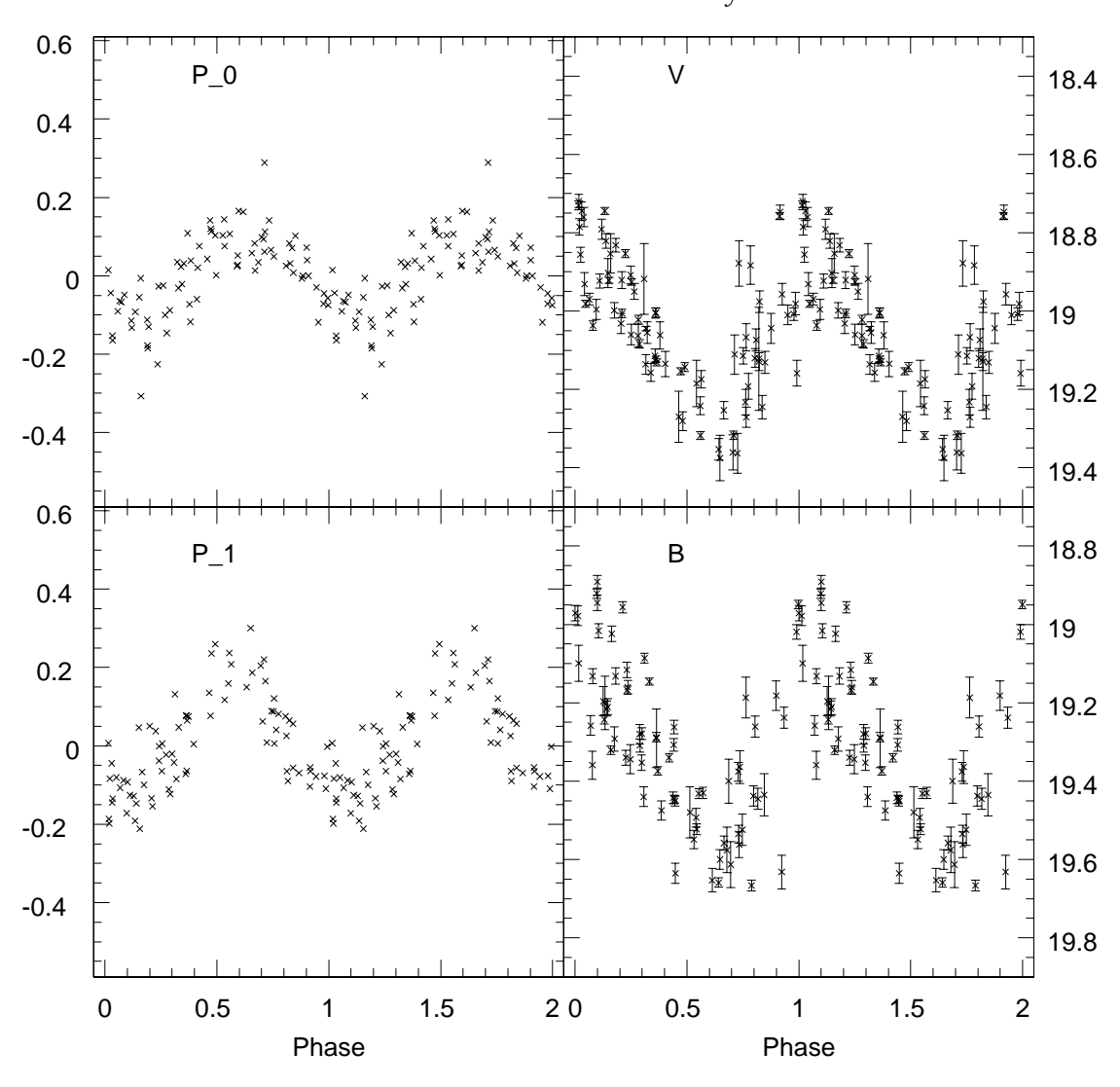


Figure B.1: Light curves for the variable stars in Reticulum (continued) V25 P=0.3299 days

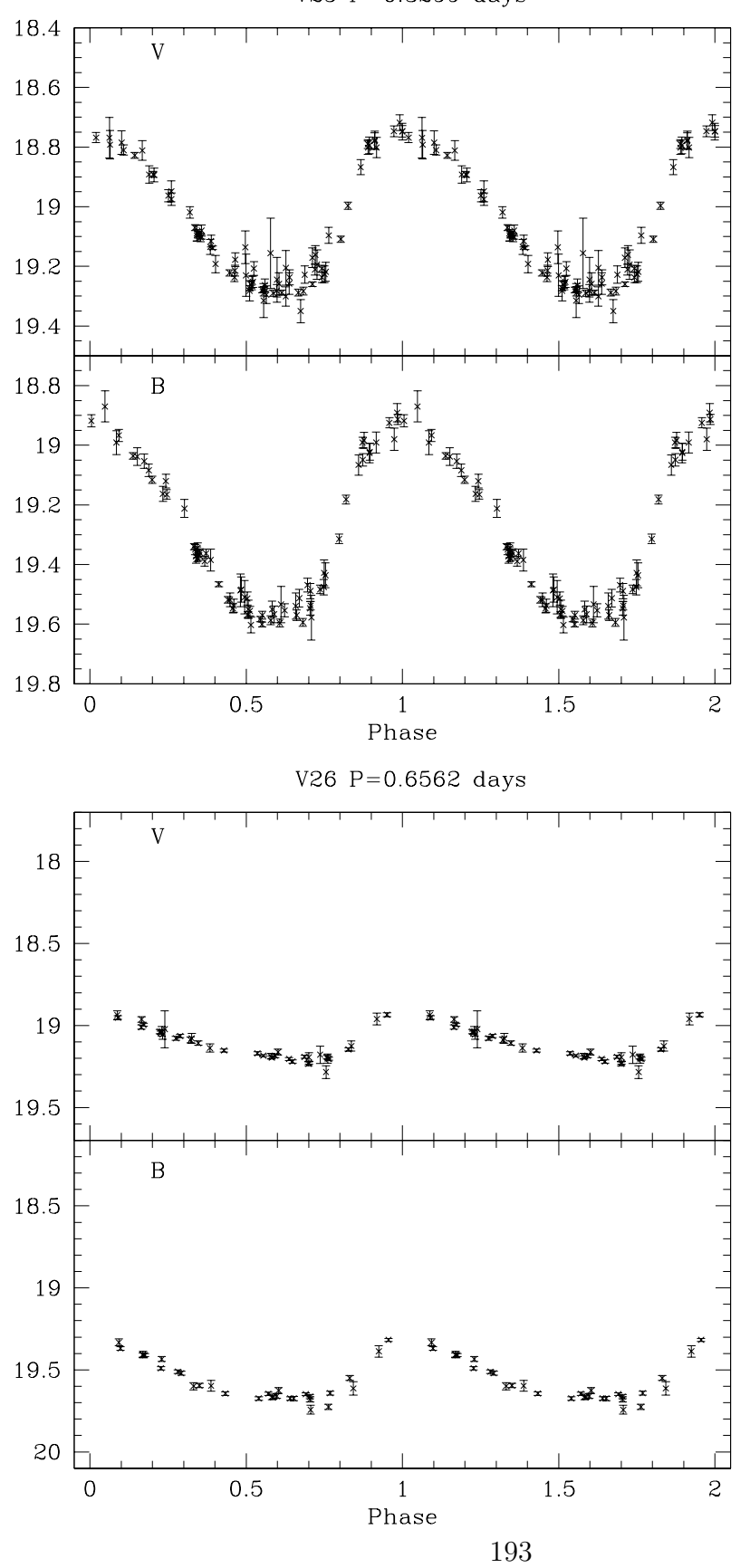


Figure B.1: Light curves for the variable stars in Reticulum (continued)  $$\tt V27\ P=0.5138\ days$$ 

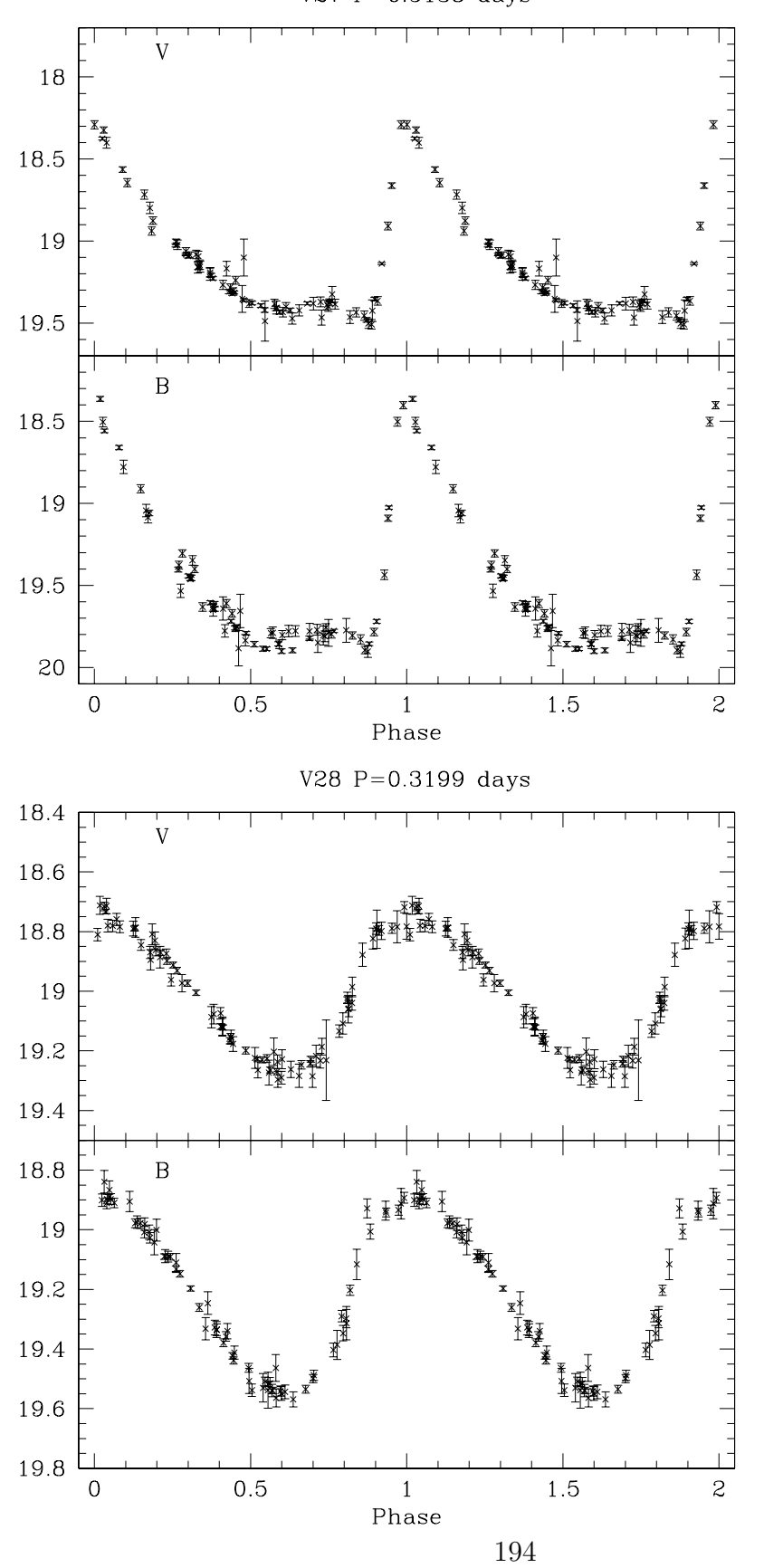


Figure B.1: Light curves for the variable stars in Reticulum (continued)  $$\tt V29\ P=0.5081\ days$$ 

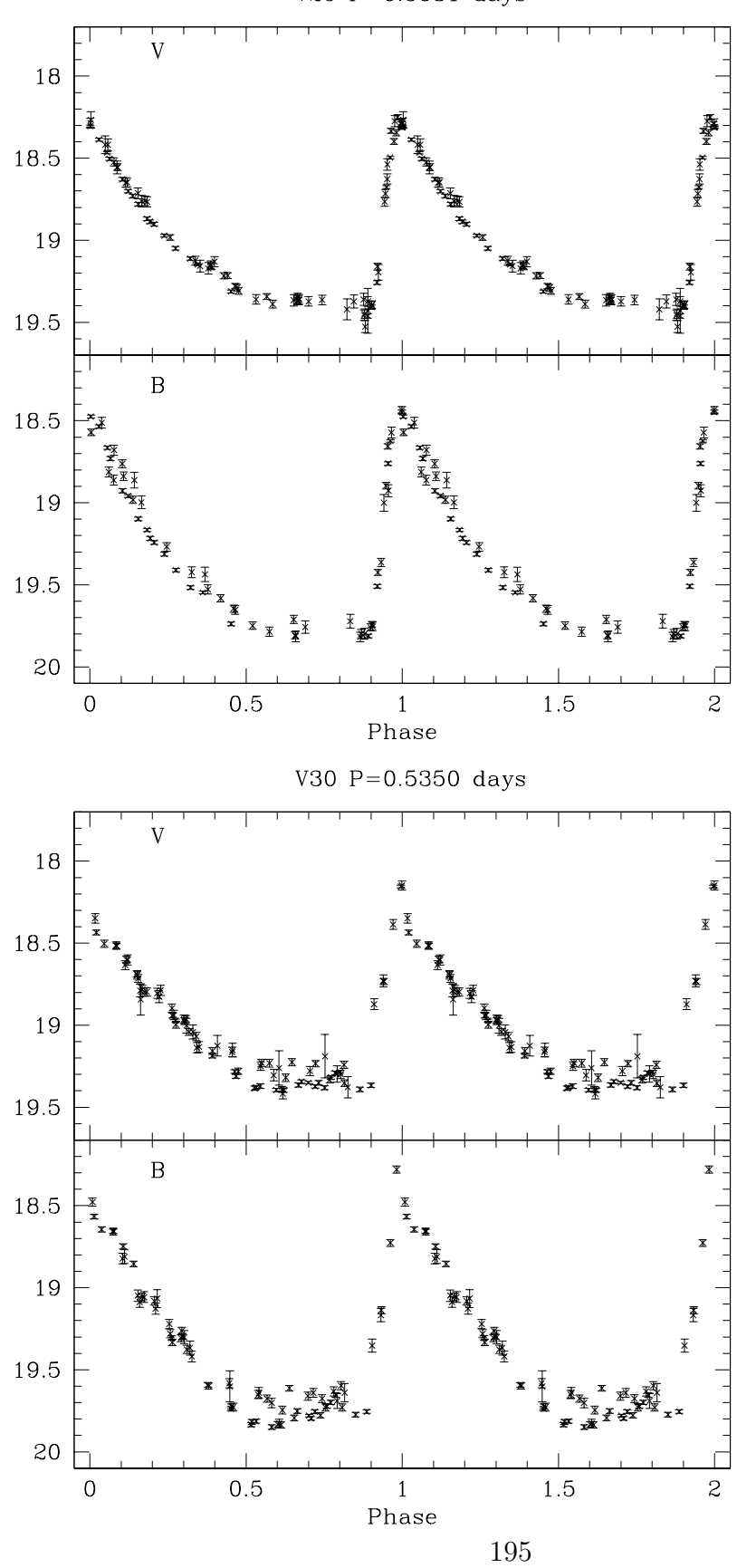


Figure B.1: Light curves for the variable stars in Reticulum (continued)  $$\rm V31\ P{=}0.5052\ days$$ 

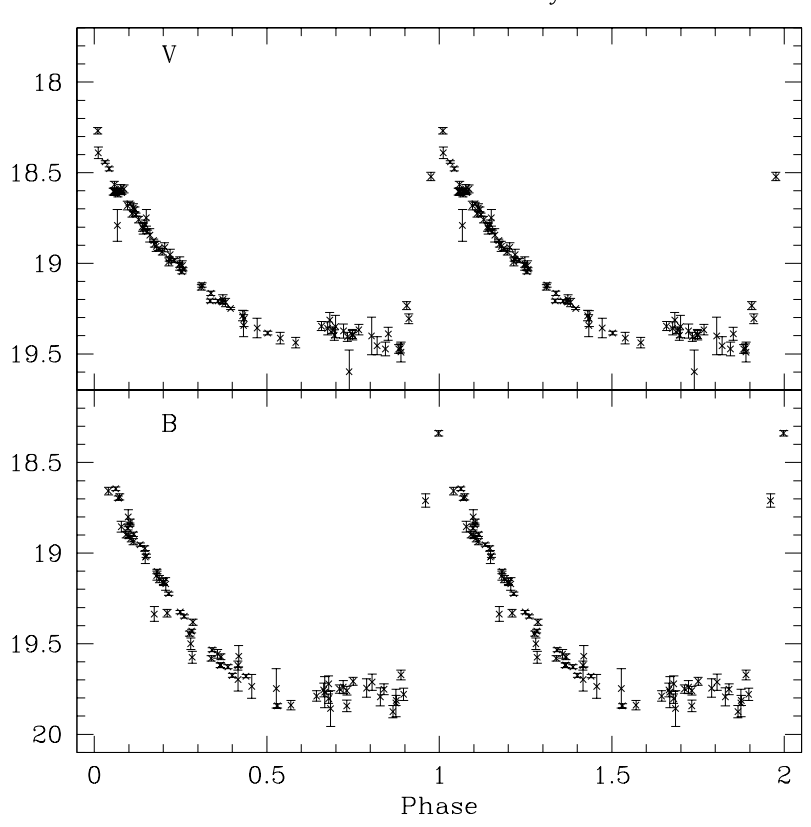
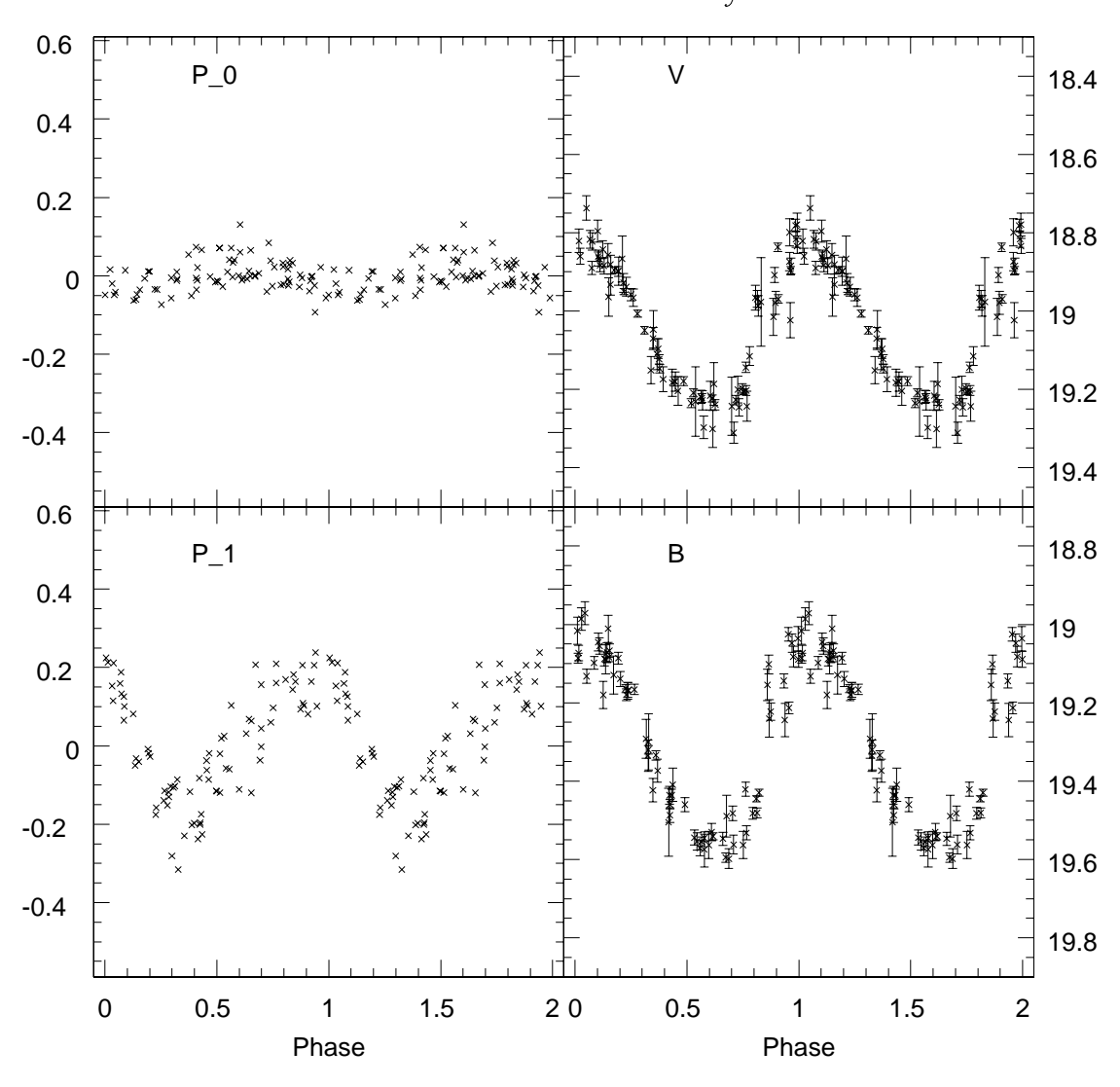


Figure B.1: Light curves for the variable stars in Reticulum (continued) V32  $P_1=0.3523$  days



## APPENDIX C: NGC 1786 LIGHT CURVES

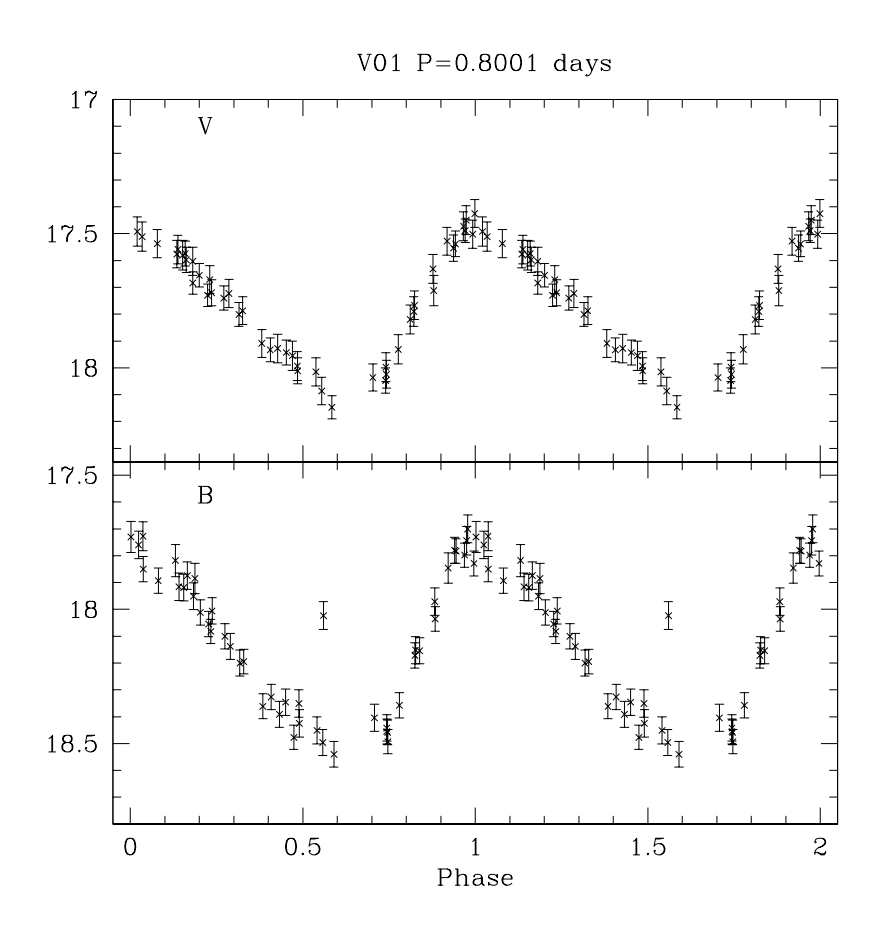


Figure C.1: Light curves for the variable stars in NGC 1786

Figure C.1: Light curves for the variable stars in NGC 1786 (continued) V02  $P_1=0.3647$  days

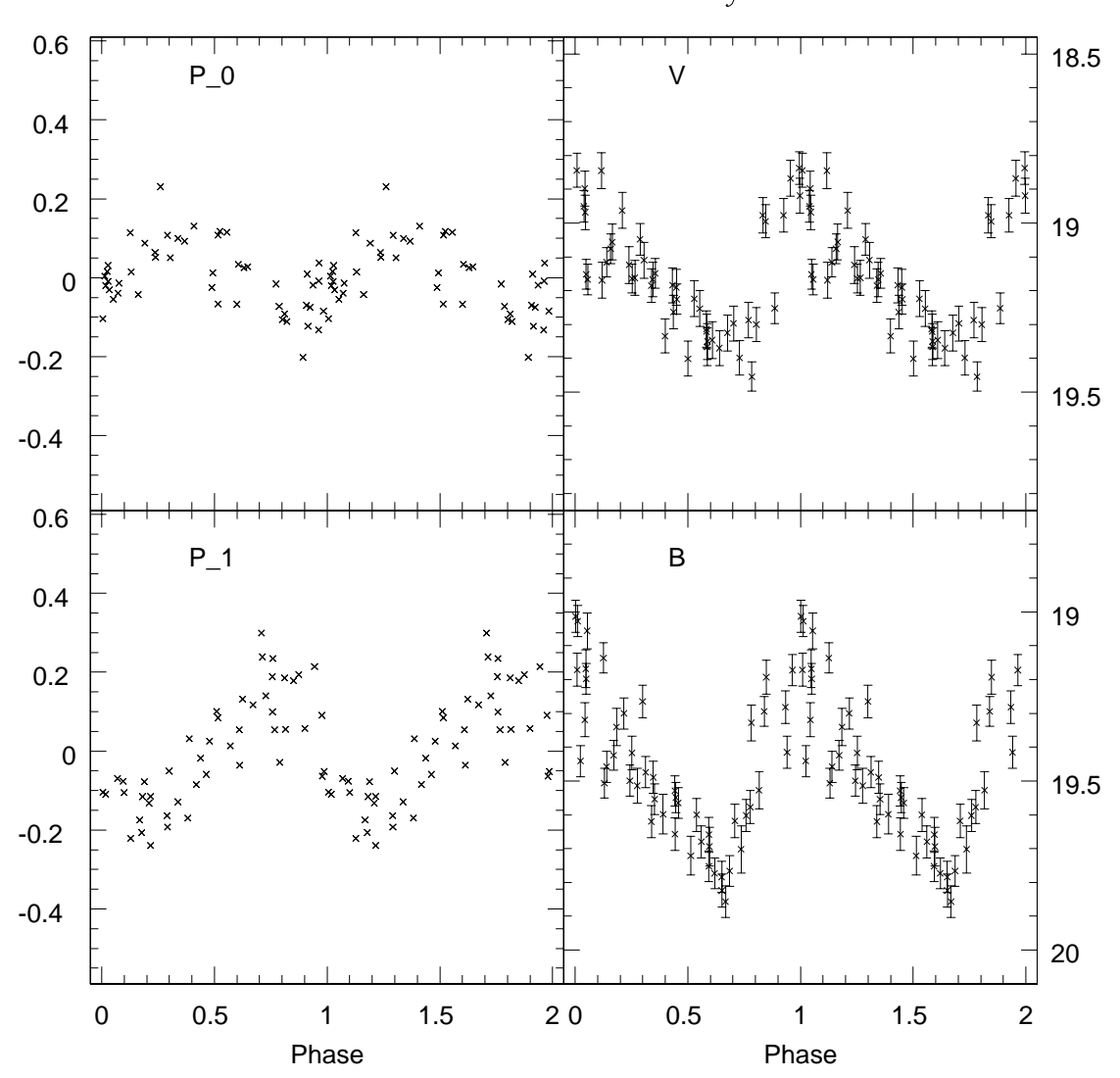


Figure C.1: Light curves for the variable stars in NGC 1786 (continued)  $$\tt V03\ P=0.6220\ days$$ 

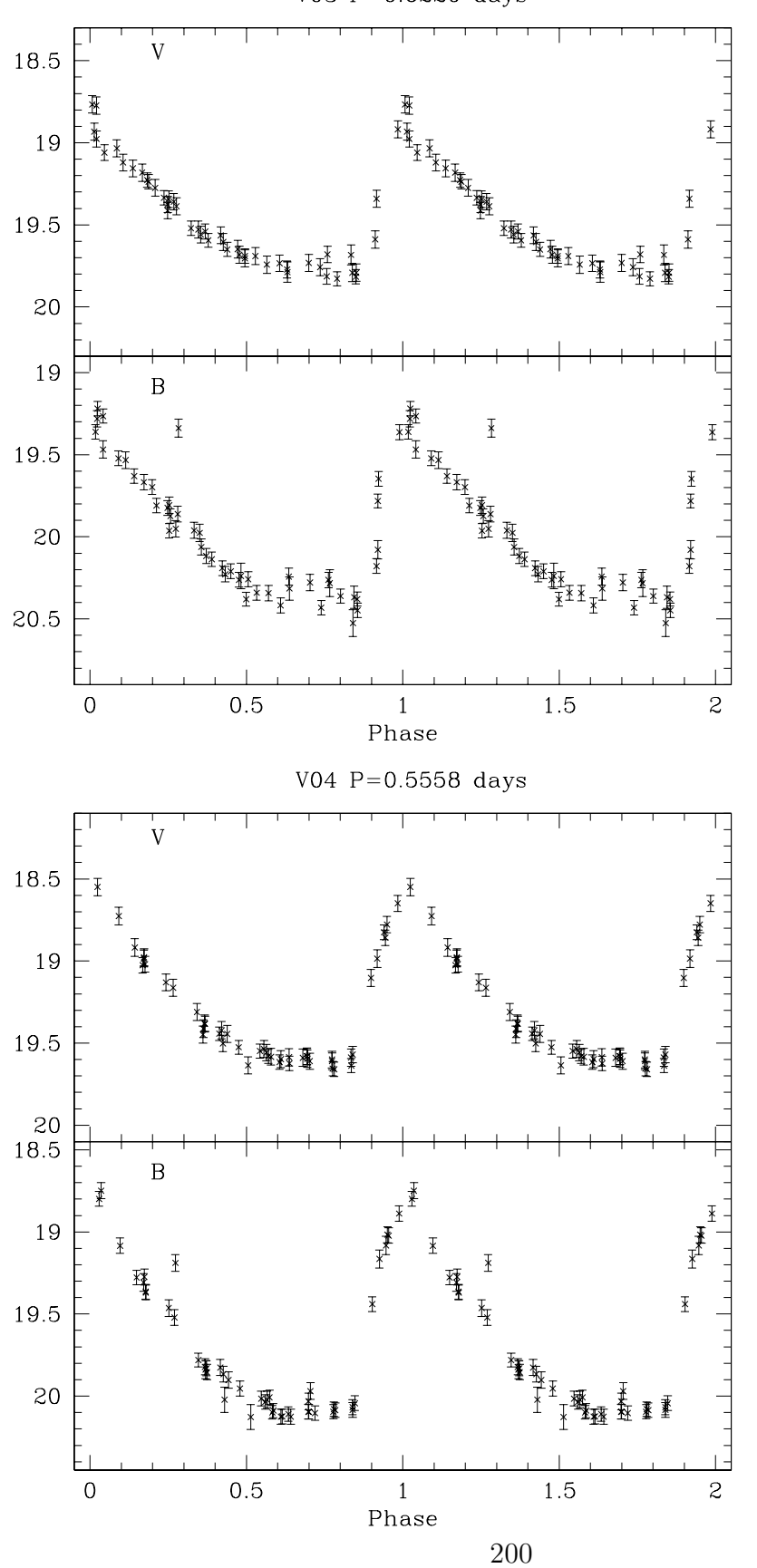


Figure C.1: Light curves for the variable stars in NGC 1786 (continued)  $$\rm V05~P\!=\!0.6971~days$$ 

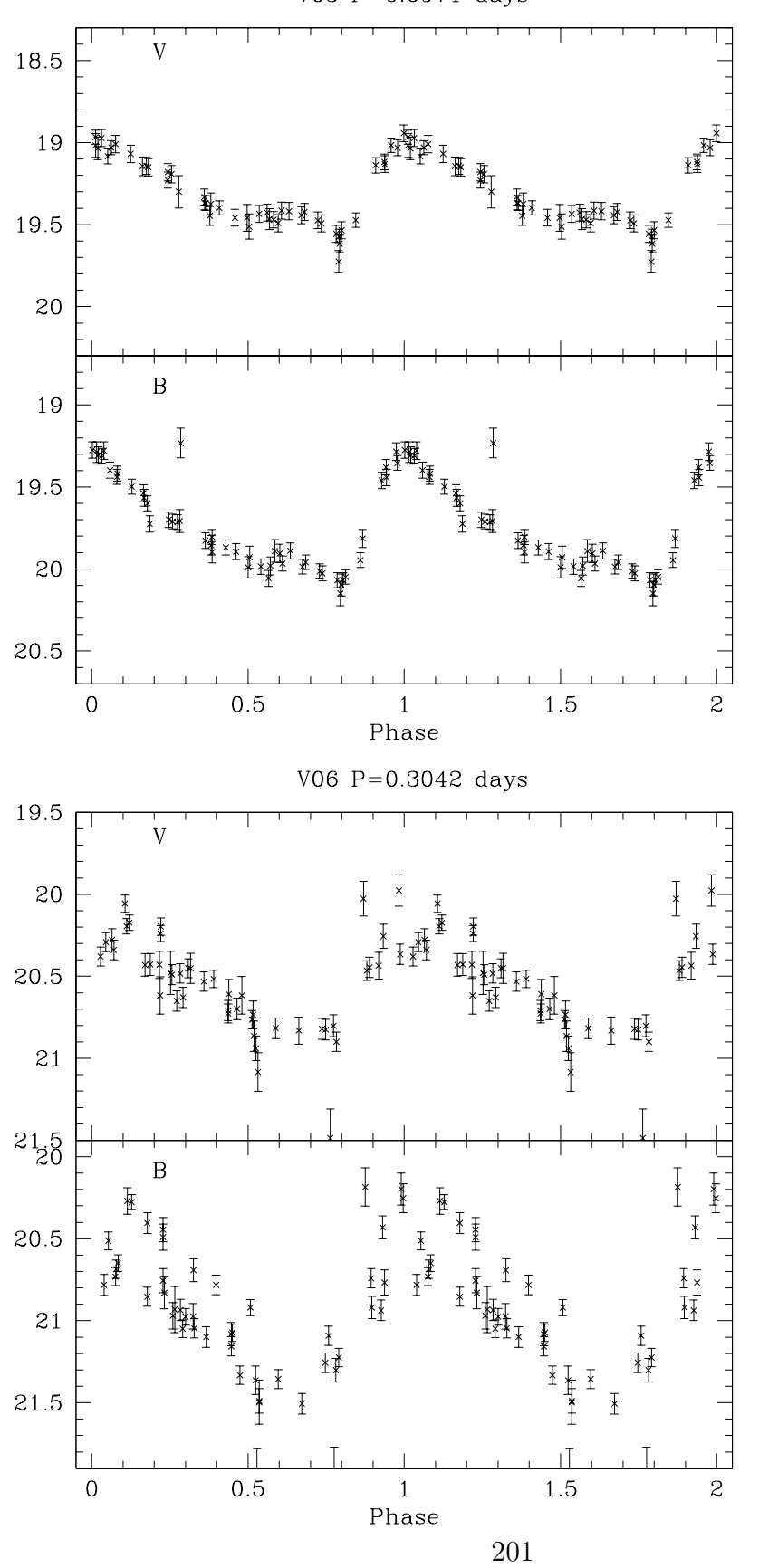


Figure C.1: Light curves for the variable stars in NGC 1786 (continued)  $$\tt V07\ P=0.2954\ days$$ 

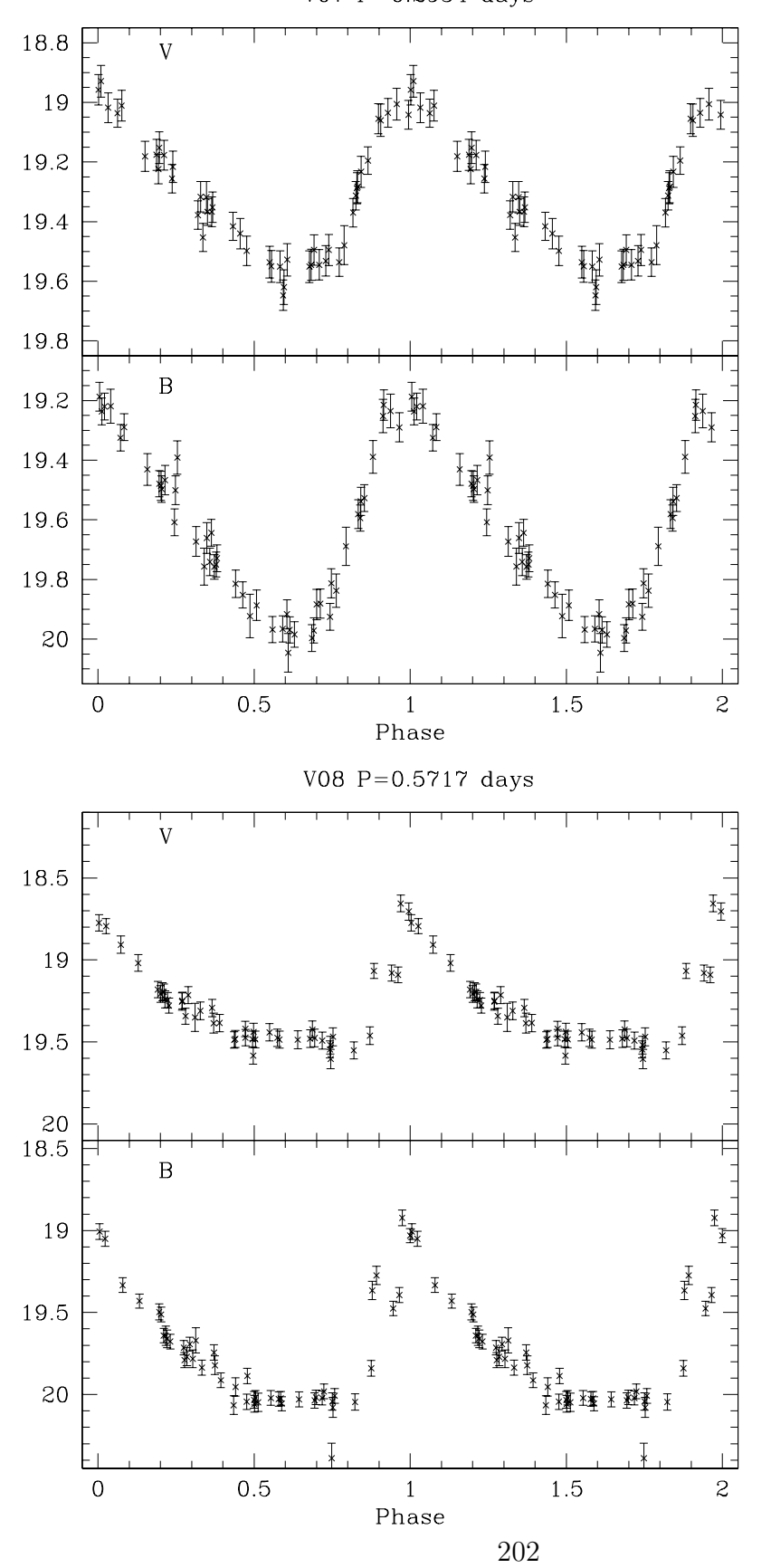


Figure C.1: Light curves for the variable stars in NGC 1786 (continued)  $$\rm V09~P\!=\!0.3635~days$$ 

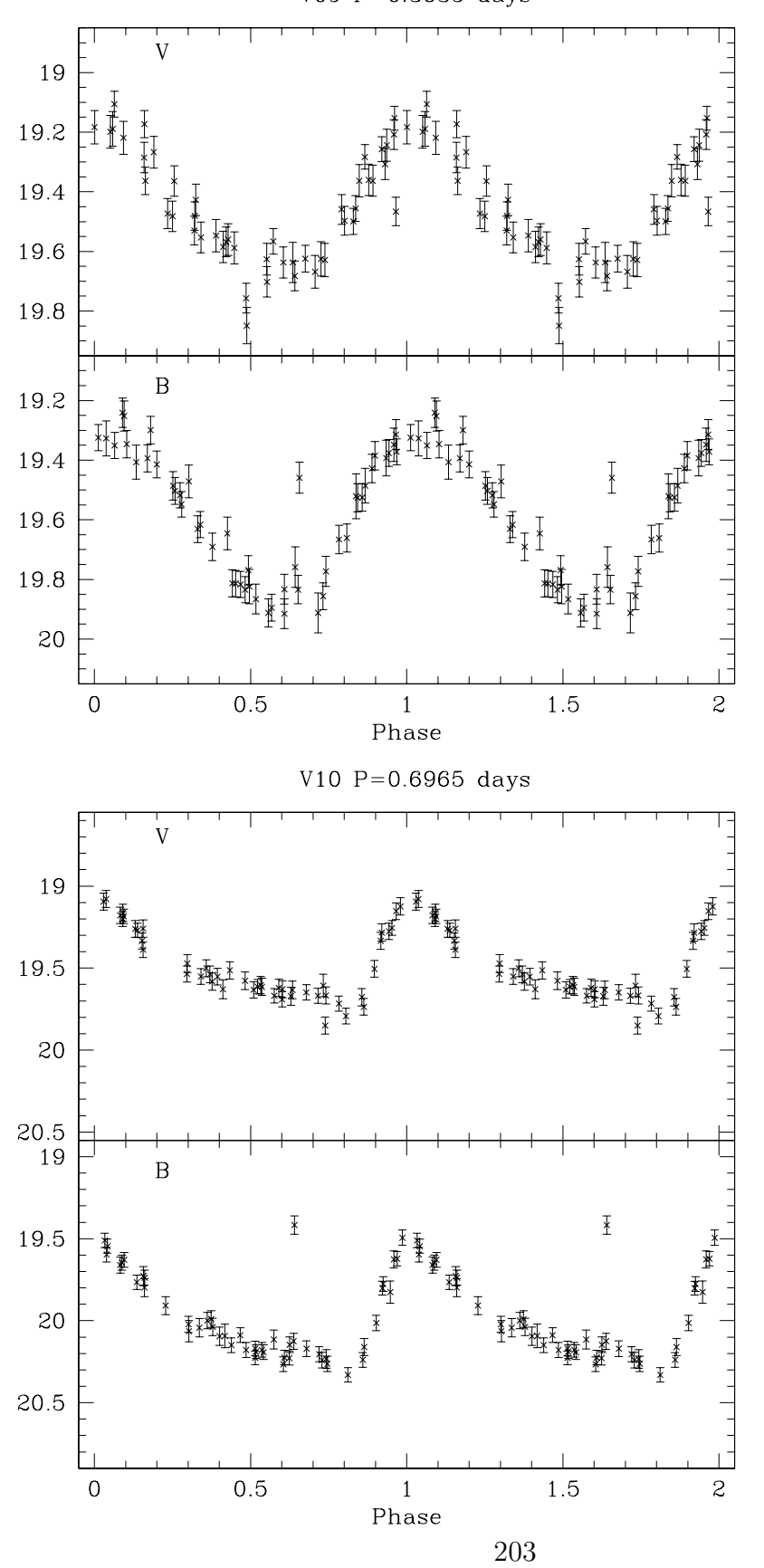


Figure C.1: Light curves for the variable stars in NGC 1786 (continued)  $$\rm V11\ P\!=\!0.3154\ days$$ 

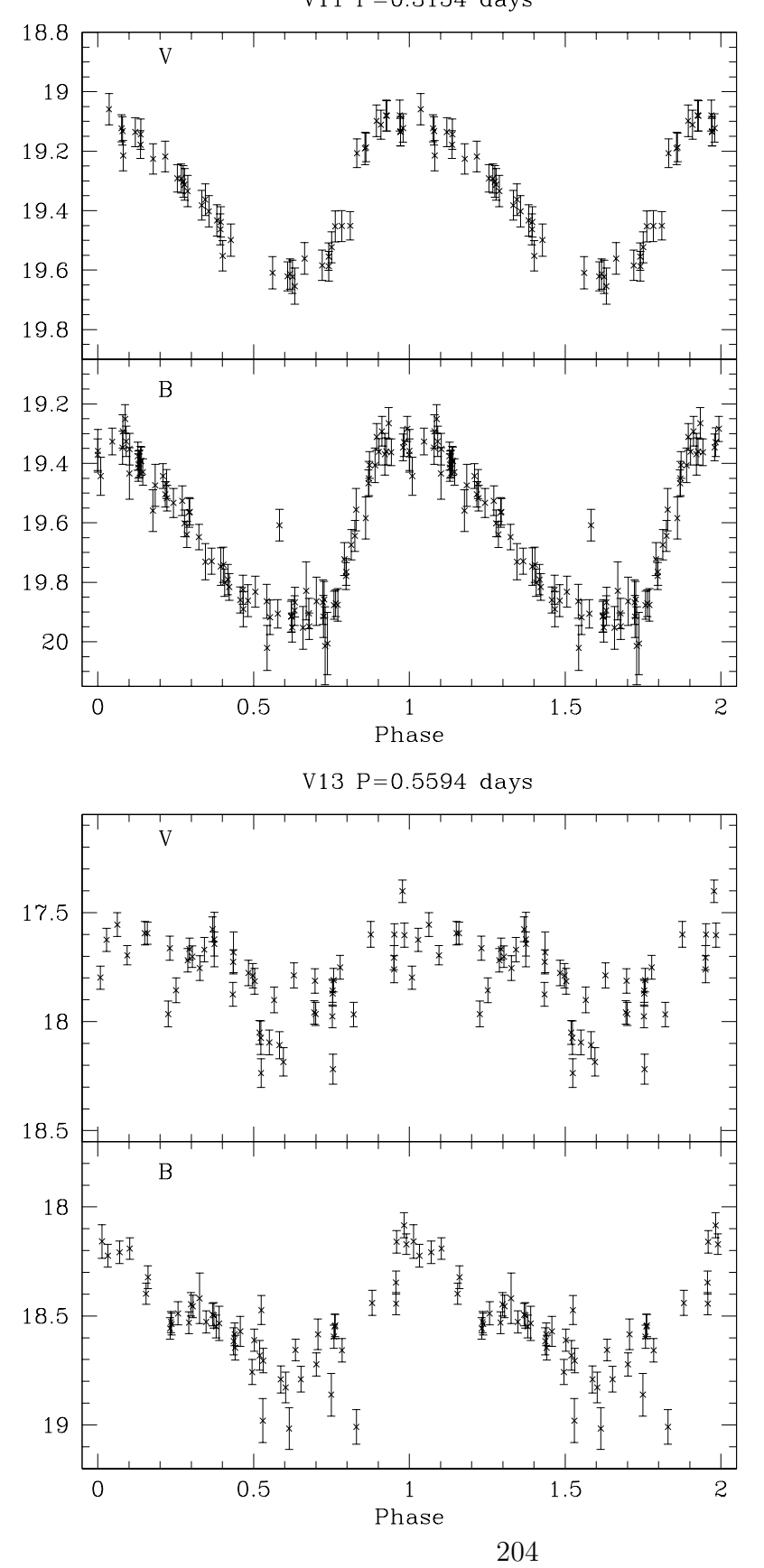


Figure C.1: Light curves for the variable stars in NGC 1786 (continued)  $$\rm V14\ P\!=\!0.3179\ days$$ 

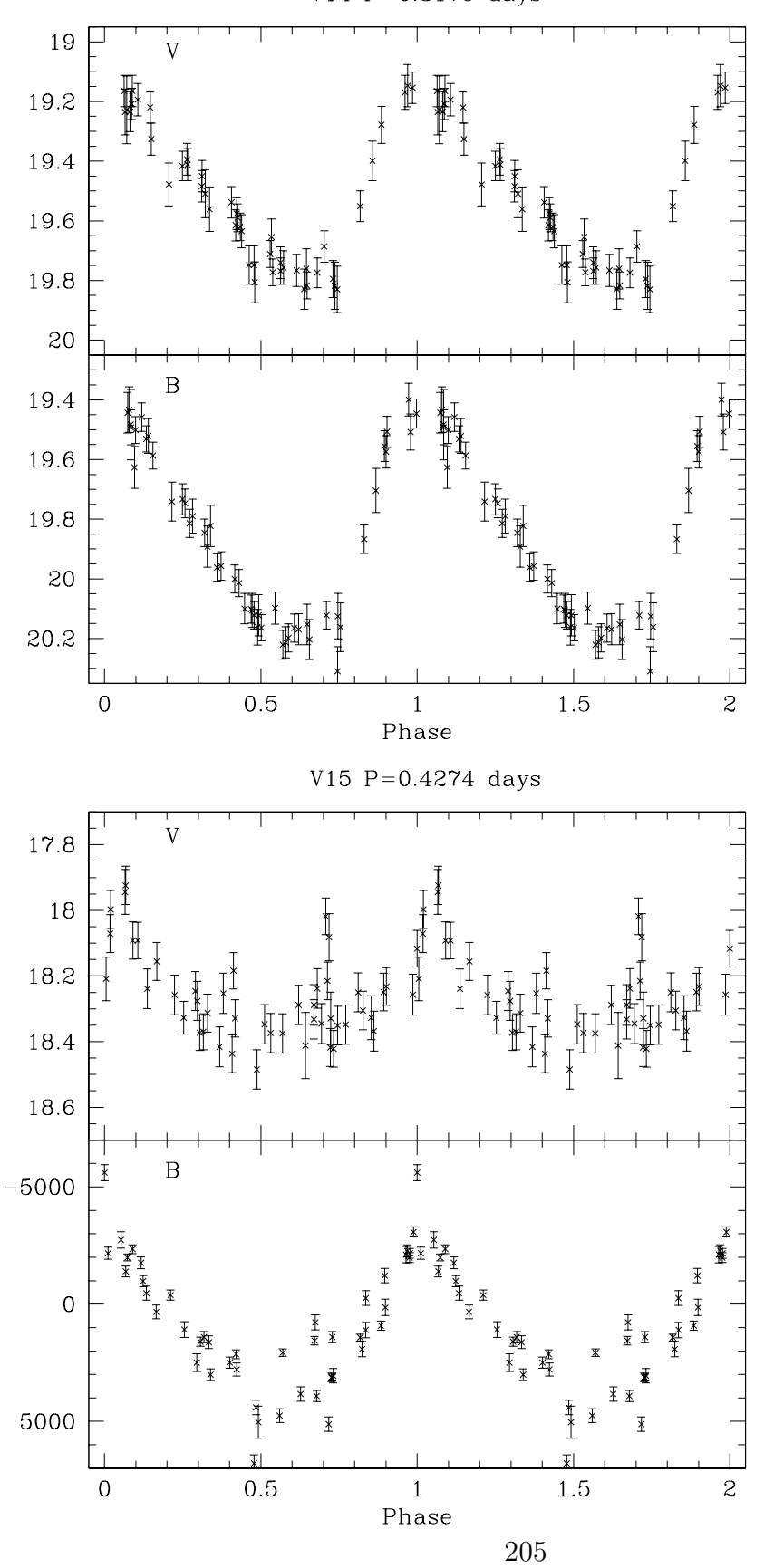


Figure C.1: Light curves for the variable stars in NGC 1786 (continued)  $$\rm V16\ P{=}0.3543\ days$$ 

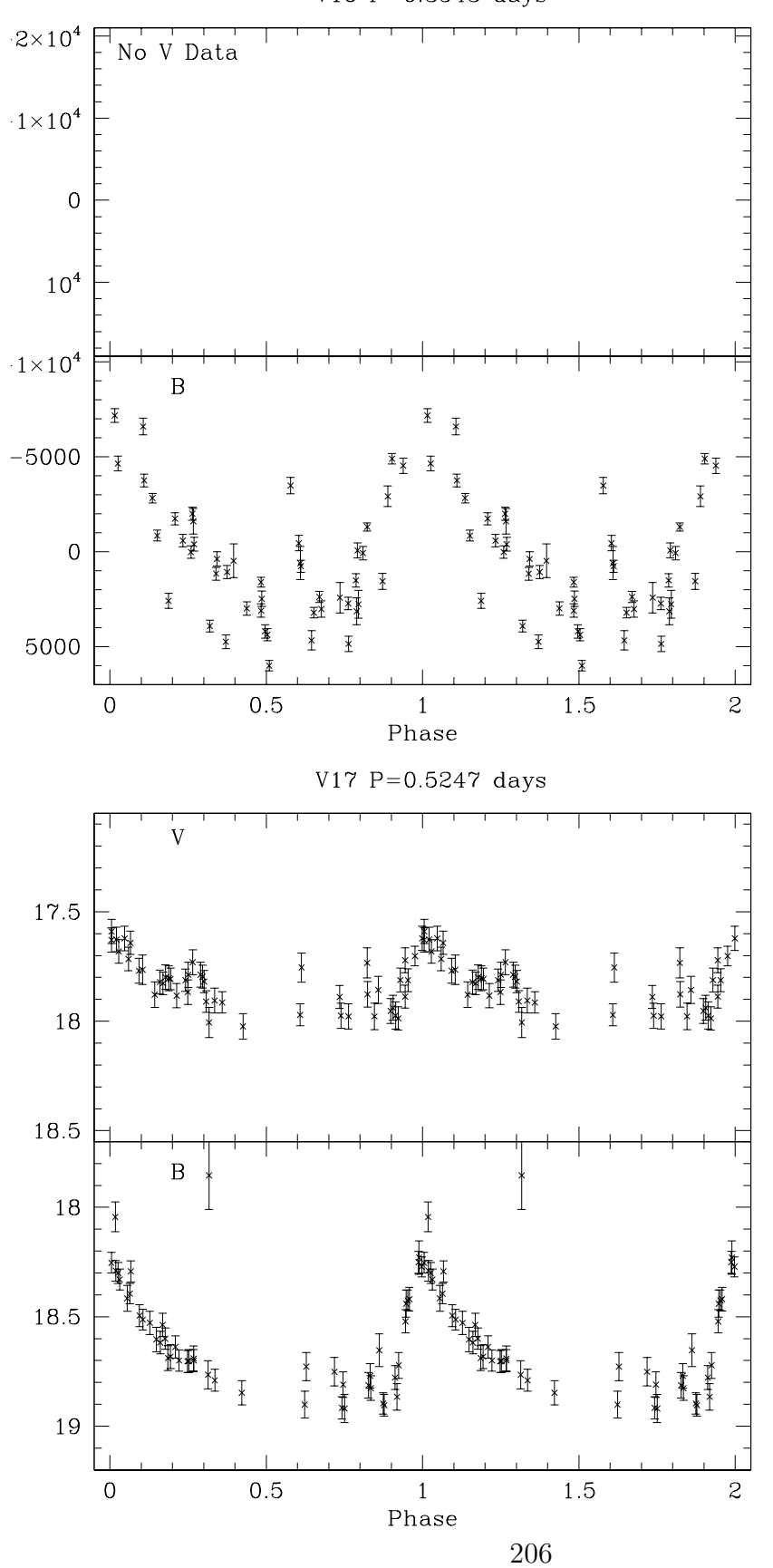


Figure C.1: Light curves for the variable stars in NGC 1786 (continued)  $$\rm V18\ P{=}0.6451\ days$$ 

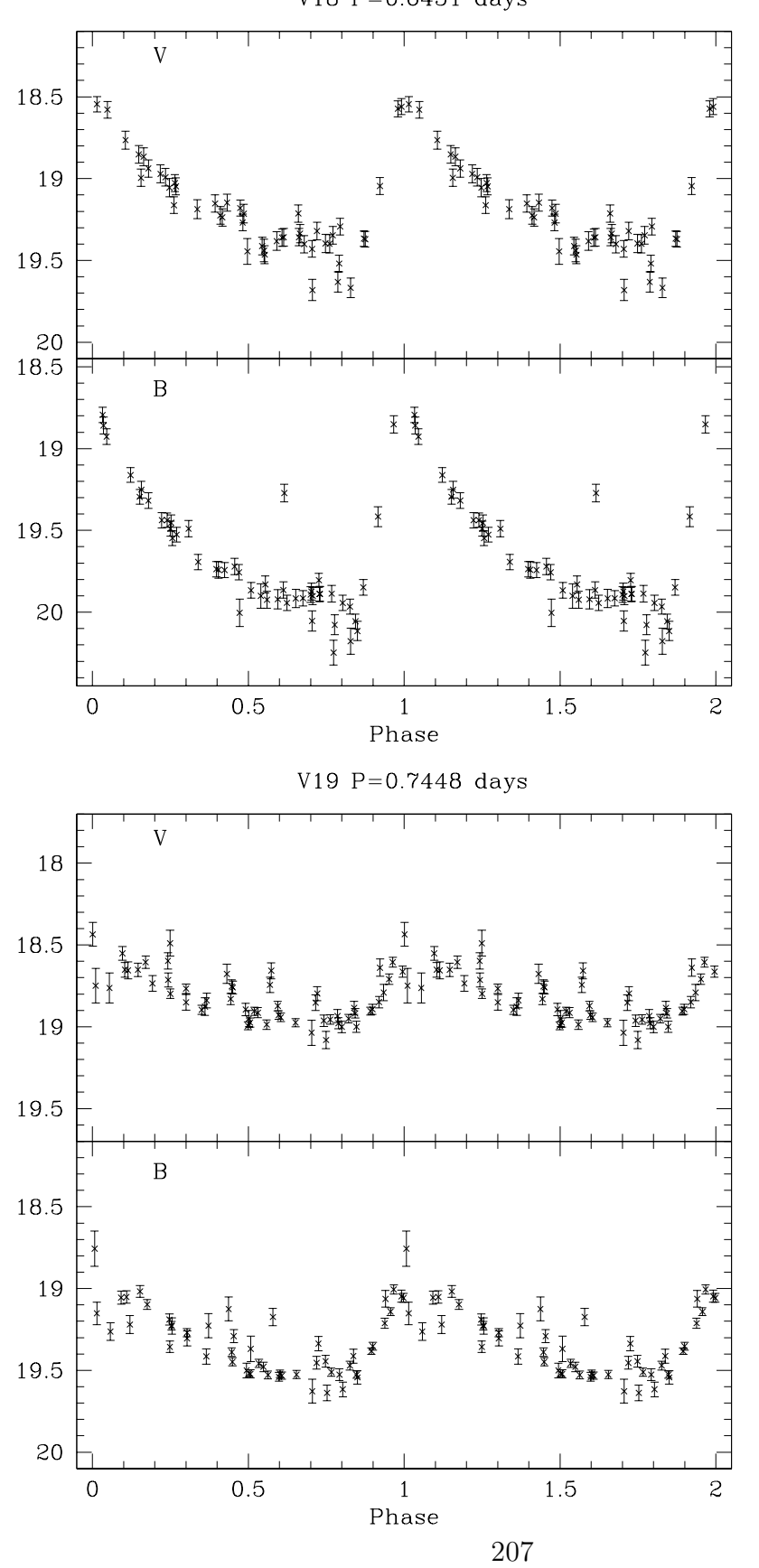


Figure C.1: Light curves for the variable stars in NGC 1786 (continued)  $$\tt V20\ P=0.2919\ days$$ 

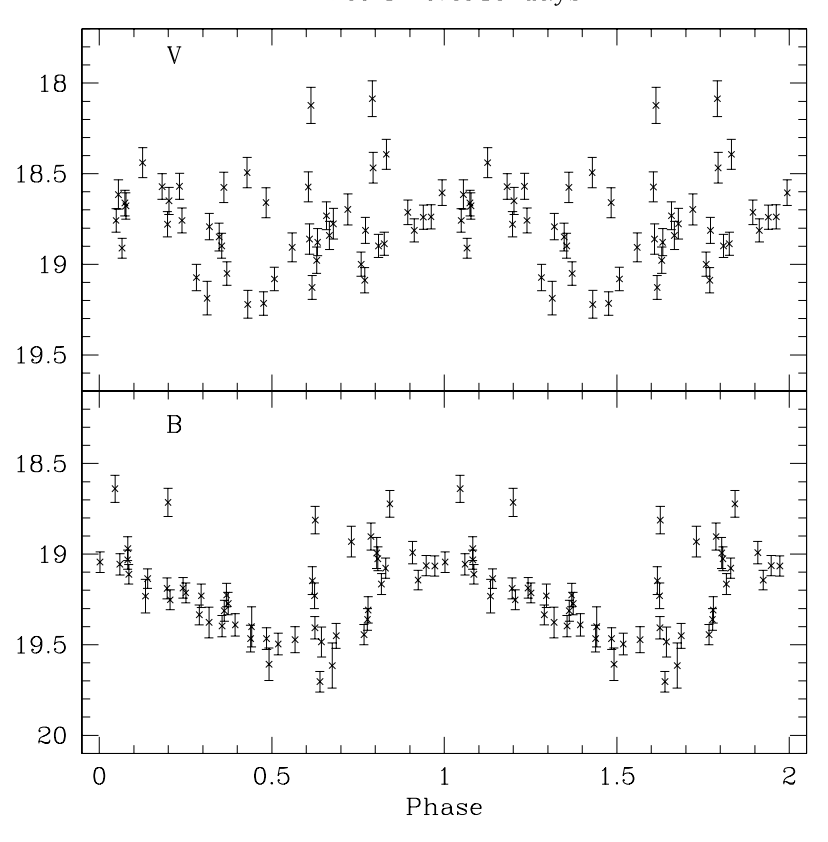


Figure C.1: Light curves for the variable stars in NGC 1786 (continued) V21  $P_1=0.3664$  days

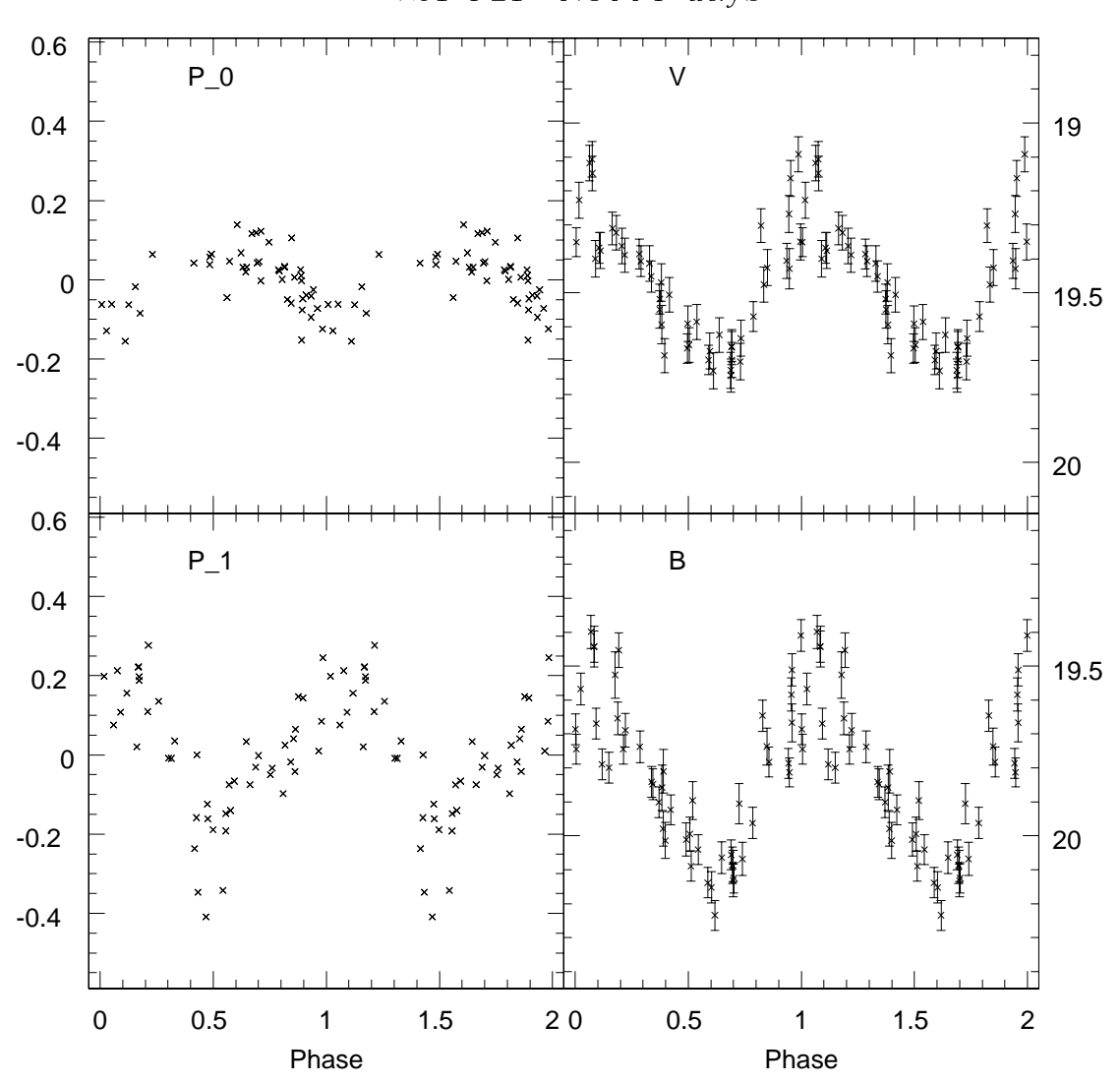


Figure C.1: Light curves for the variable stars in NGC 1786 (continued)  $$\tt V22\ P=0.3292 \ days$$ 

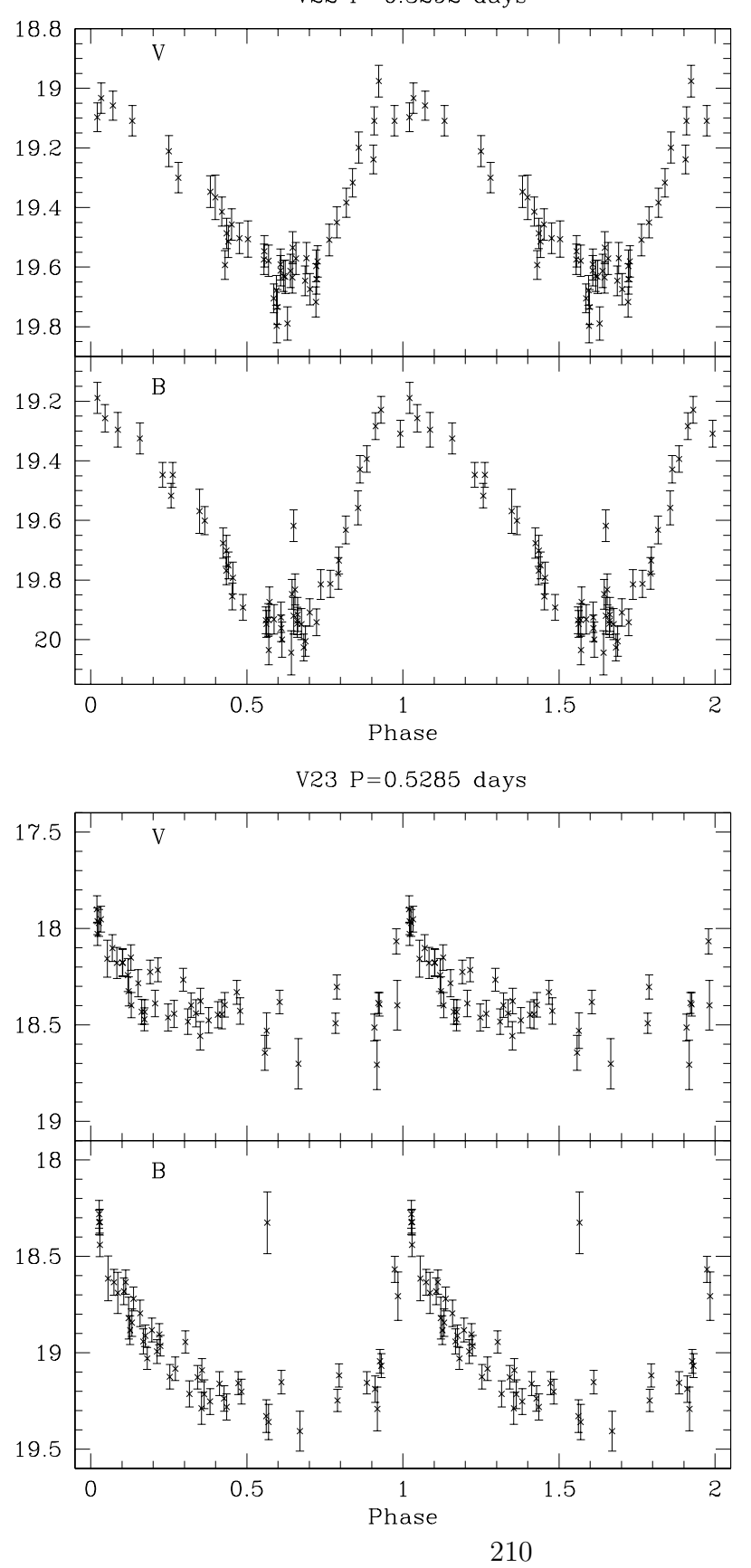


Figure C.1: Light curves for the variable stars in NGC 1786 (continued)  $$\tt V24\ P=0.4111\ days$$ 

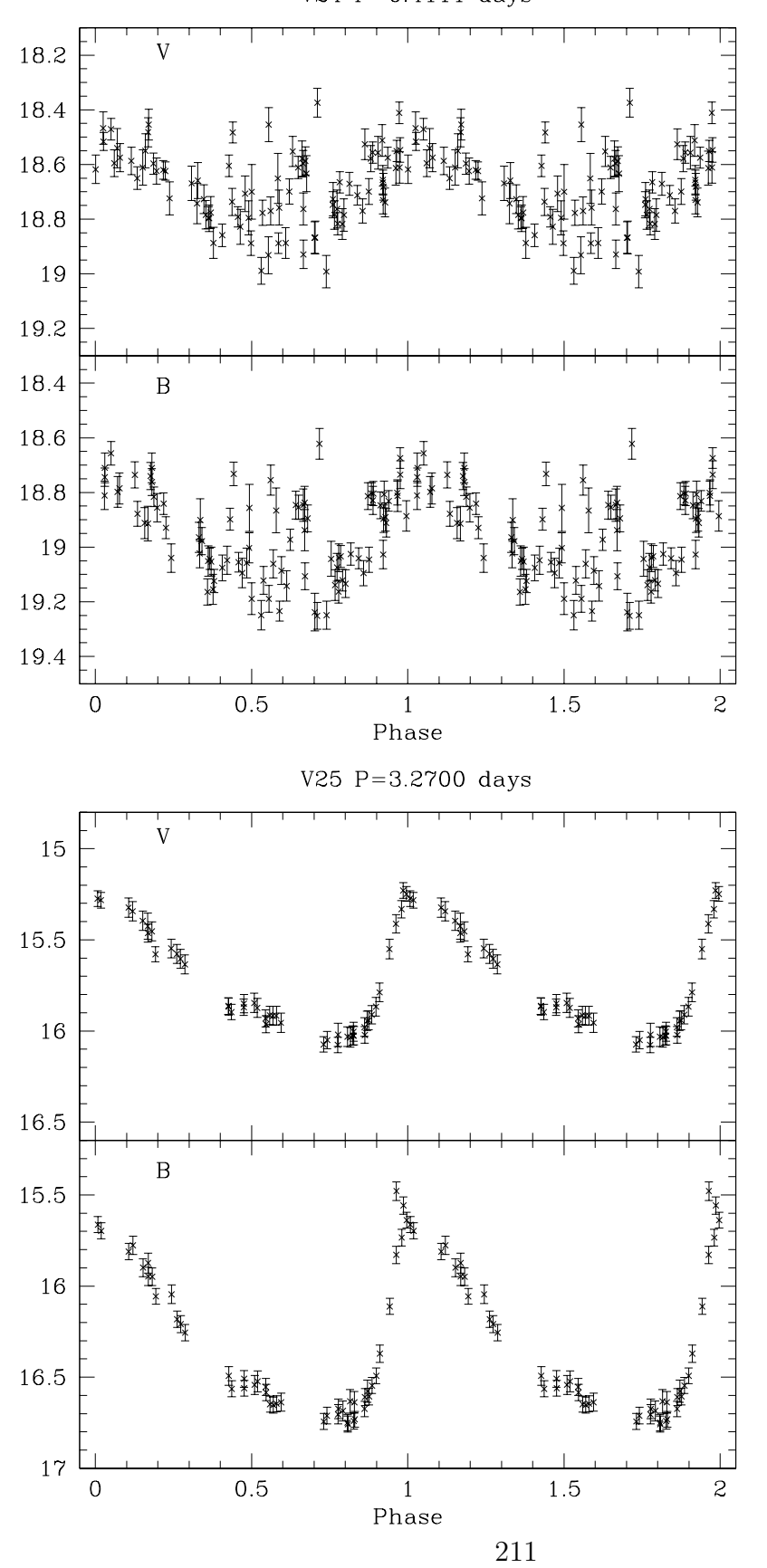


Figure C.1: Light curves for the variable stars in NGC 1786 (continued)  $$\tt V26\ P=0.7389\ days$$ 

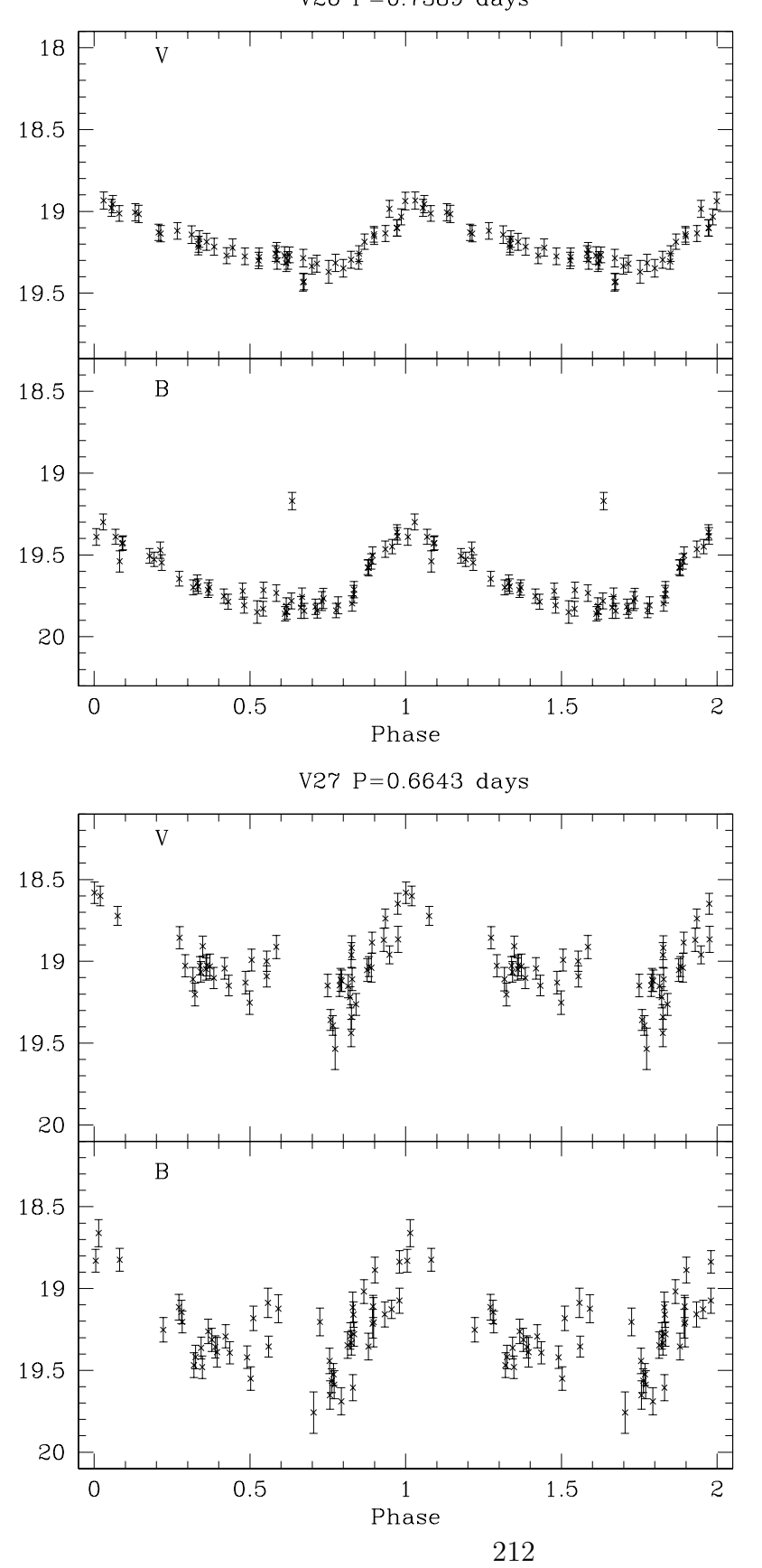


Figure C.1: Light curves for the variable stars in NGC 1786 (continued) V28  $P_1=0.3605$  days

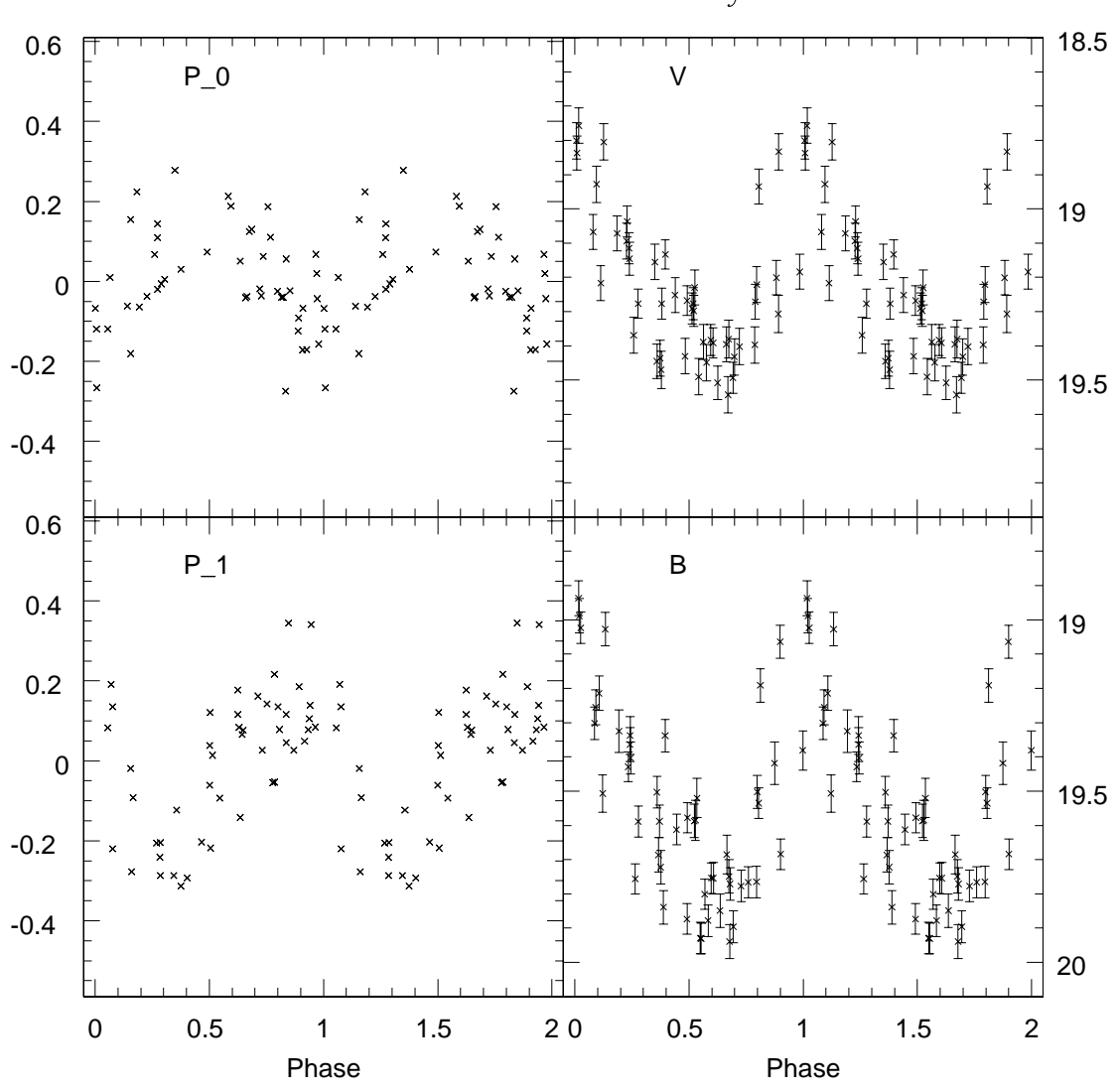


Figure C.1: Light curves for the variable stars in NGC 1786 (continued)  $$\tt V29\ P=0.3694\ days$$ 

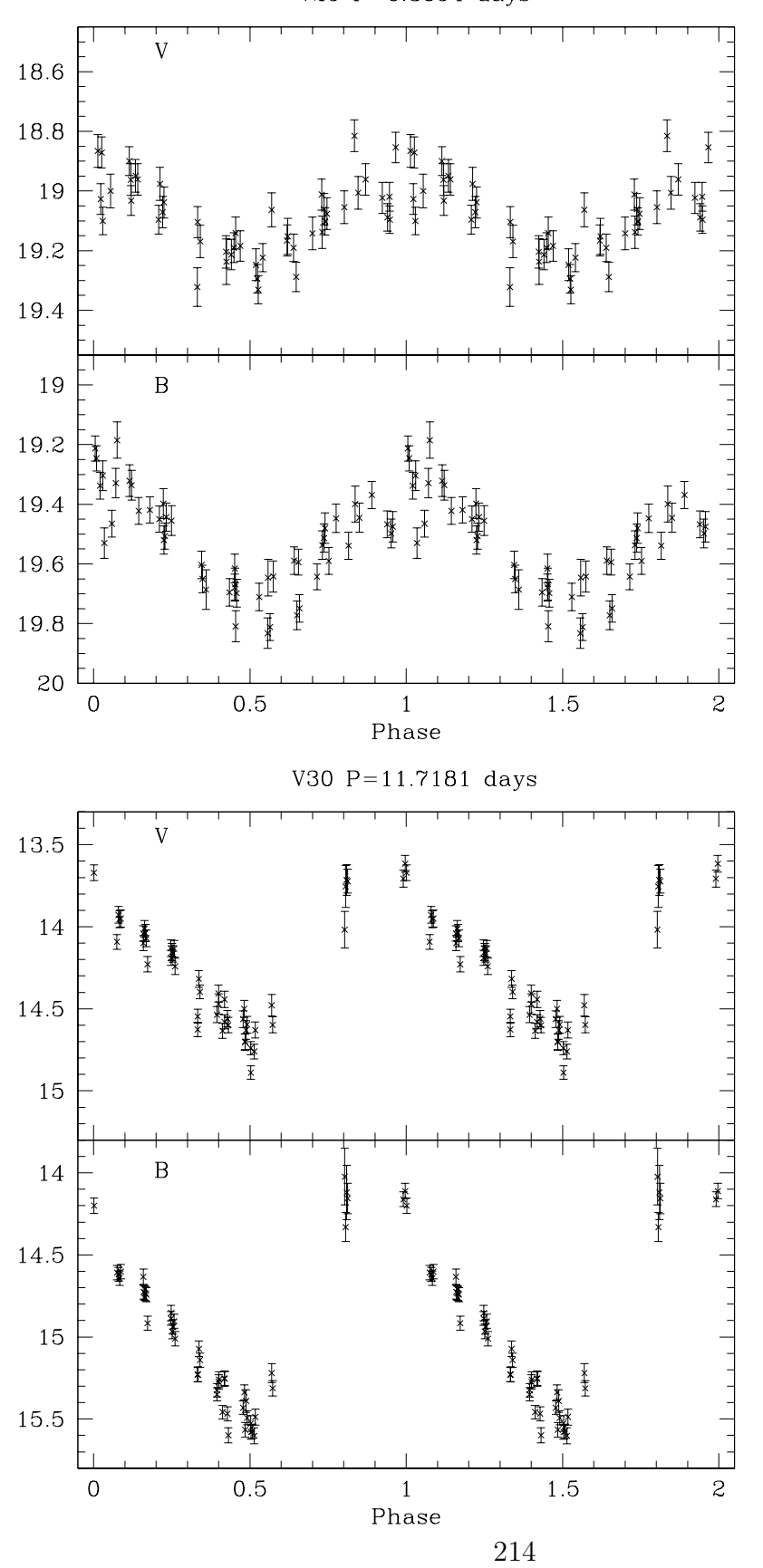


Figure C.1: Light curves for the variable stars in NGC 1786 (continued)  $$\tt V31\ P=0.6160\ days$$ 

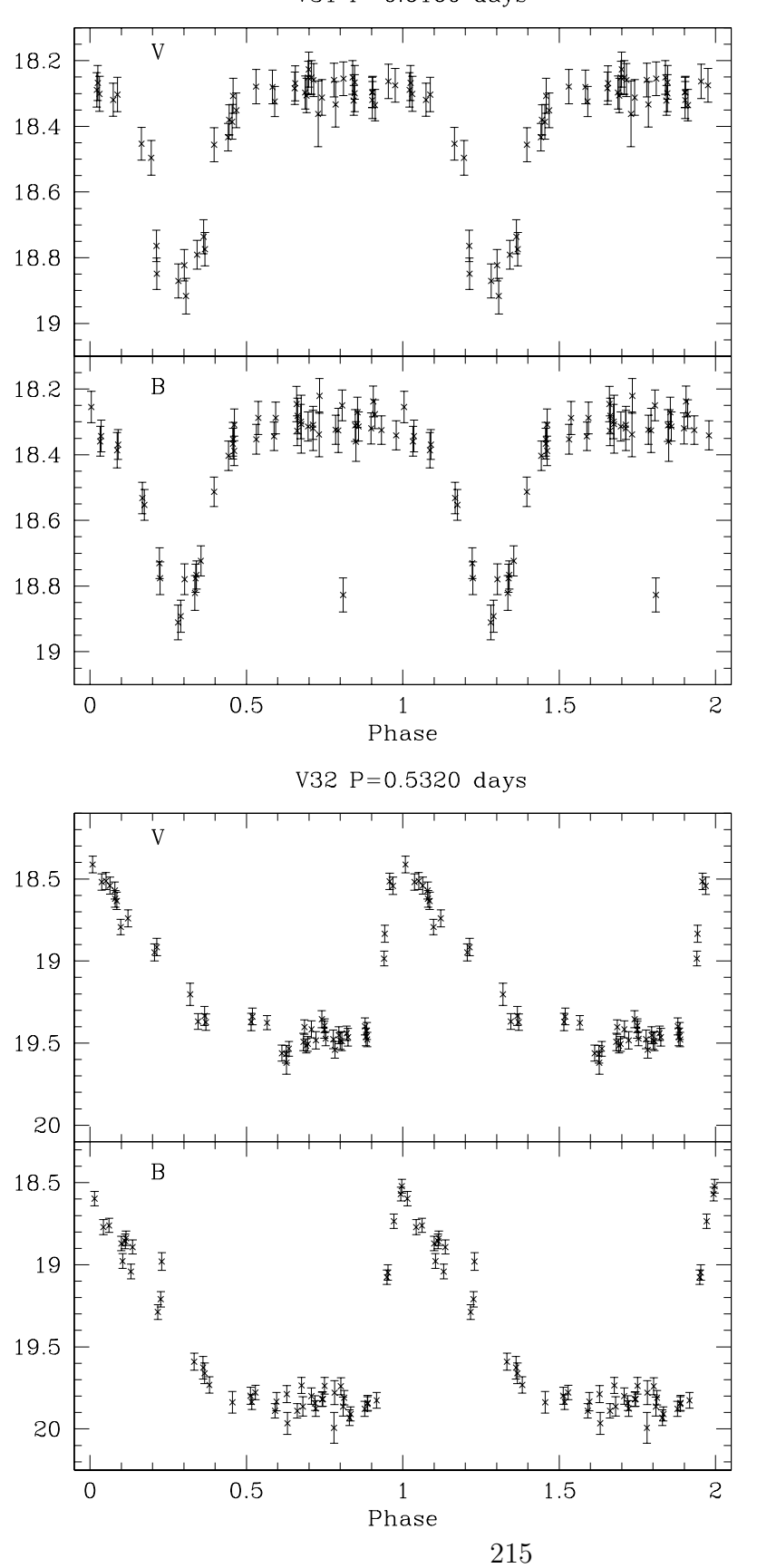


Figure C.1: Light curves for the variable stars in NGC 1786 (continued)  $$\tt V33\ P=0.5328\ days$$ 

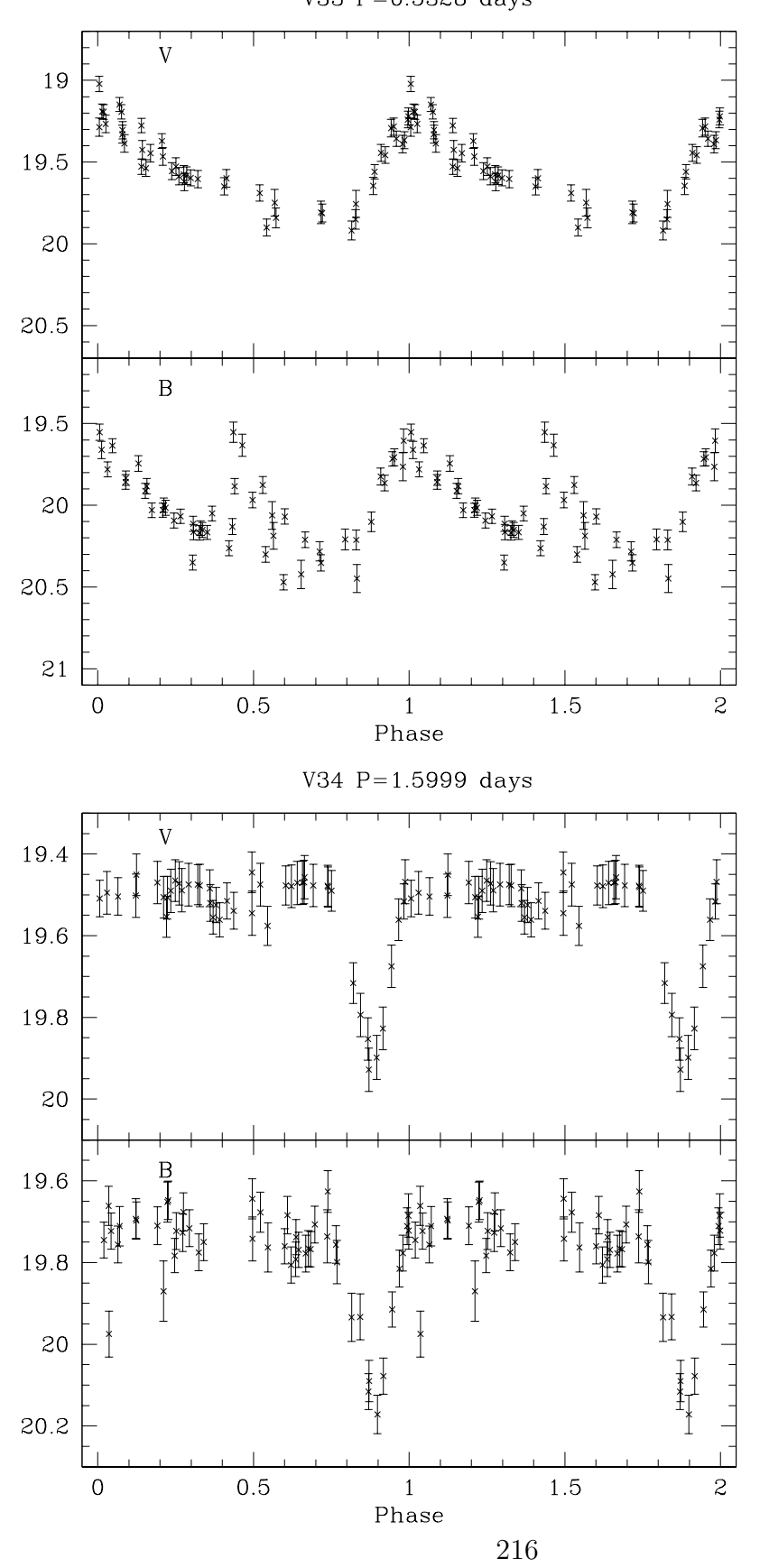


Figure C.1: Light curves for the variable stars in NGC 1786 (continued)  $${\tt V35\ P=0.3306\ days}$$ 

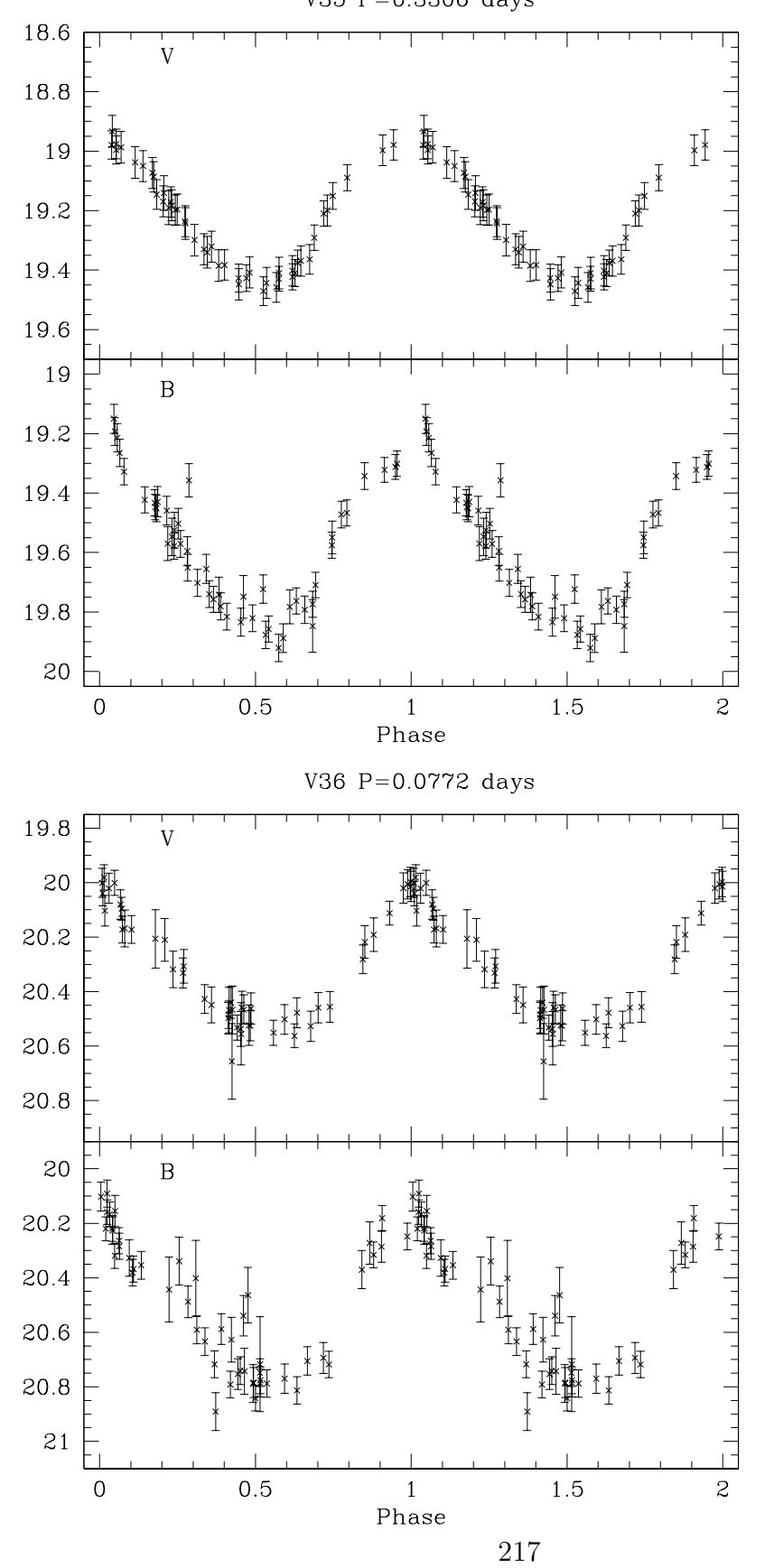


Figure C.1: Light curves for the variable stars in NGC 1786 (continued)  $$\rm V37~P\!=\!0.3553~days$$ 

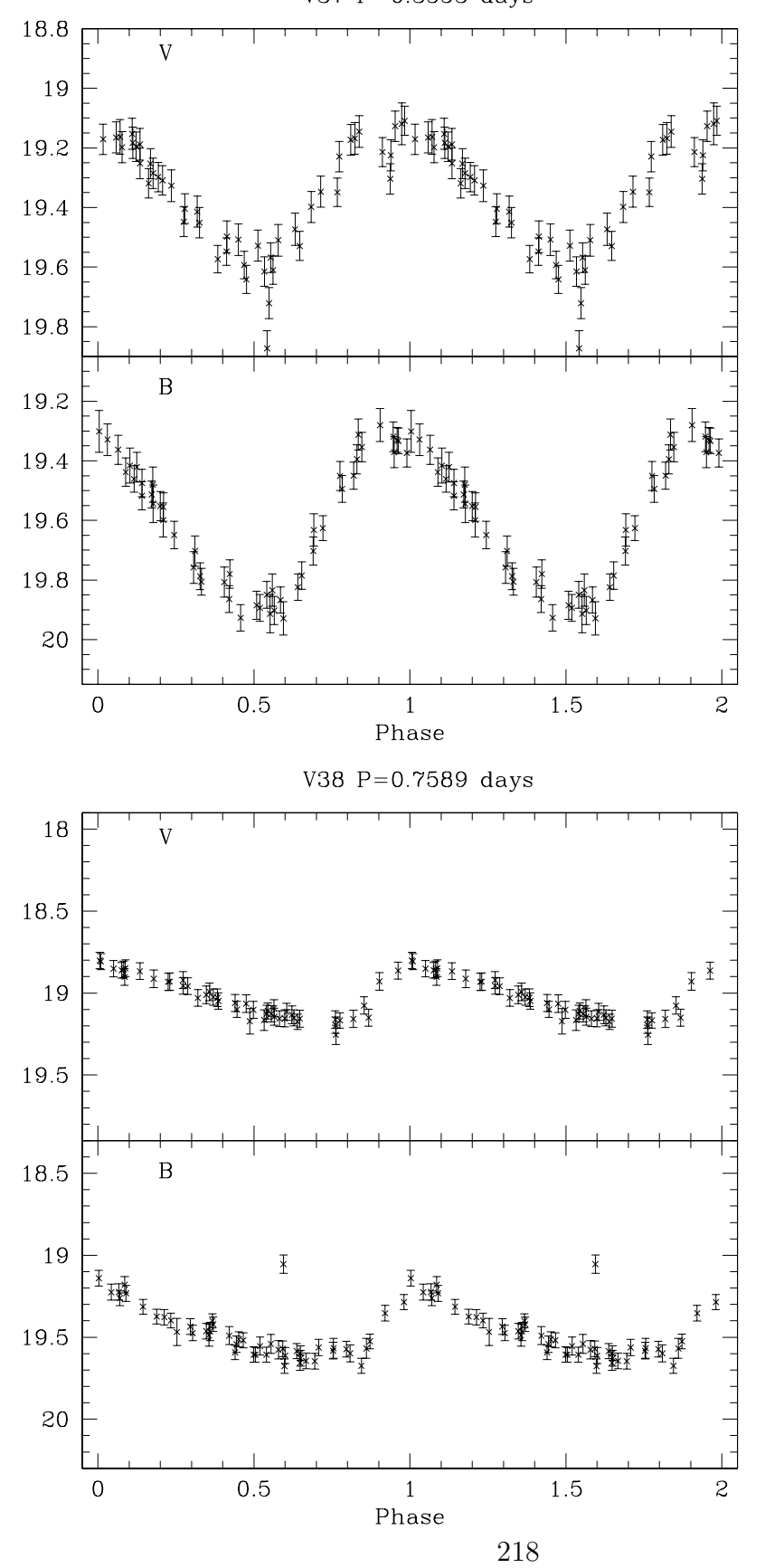


Figure C.1: Light curves for the variable stars in NGC 1786 (continued)  $${\tt V39\ P=0.0804\ days}$$ 

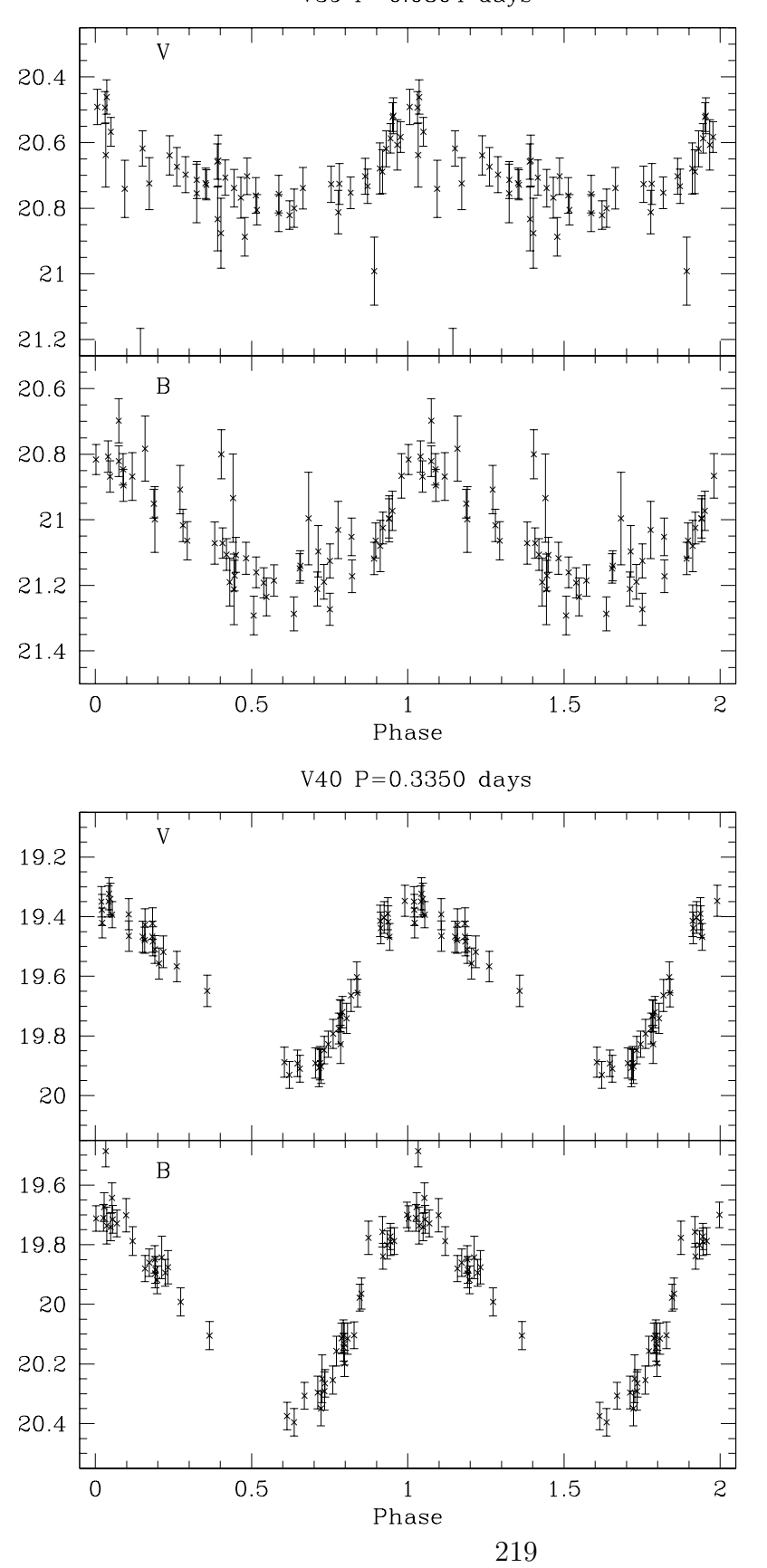


Figure C.1: Light curves for the variable stars in NGC 1786 (continued)  $$\rm V41\ P\!=\!1.1042\ days$$ 

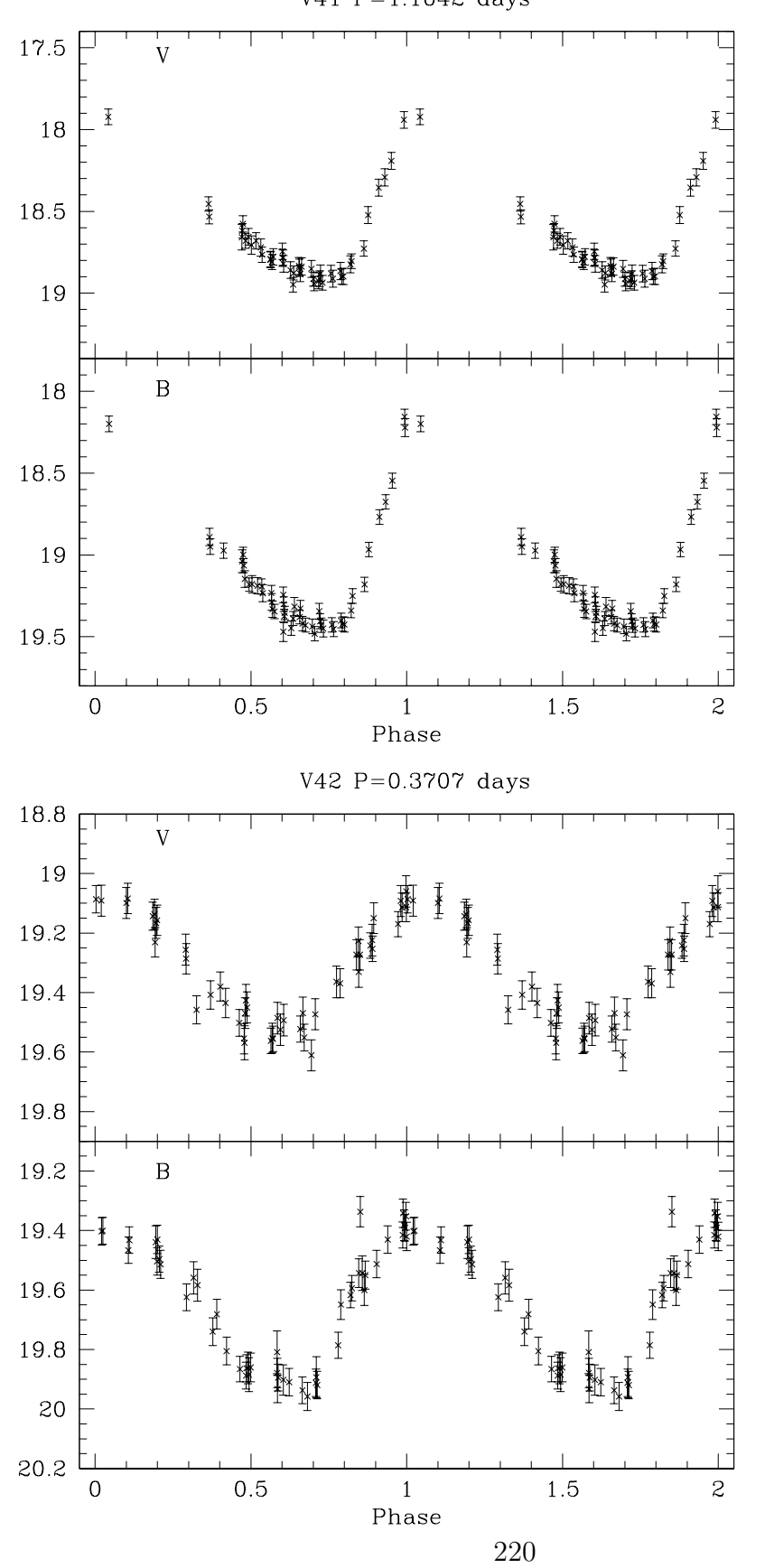


Figure C.1: Light curves for the variable stars in NGC 1786 (continued)  $$\rm V43~P\!=\!0.0610~days$$ 

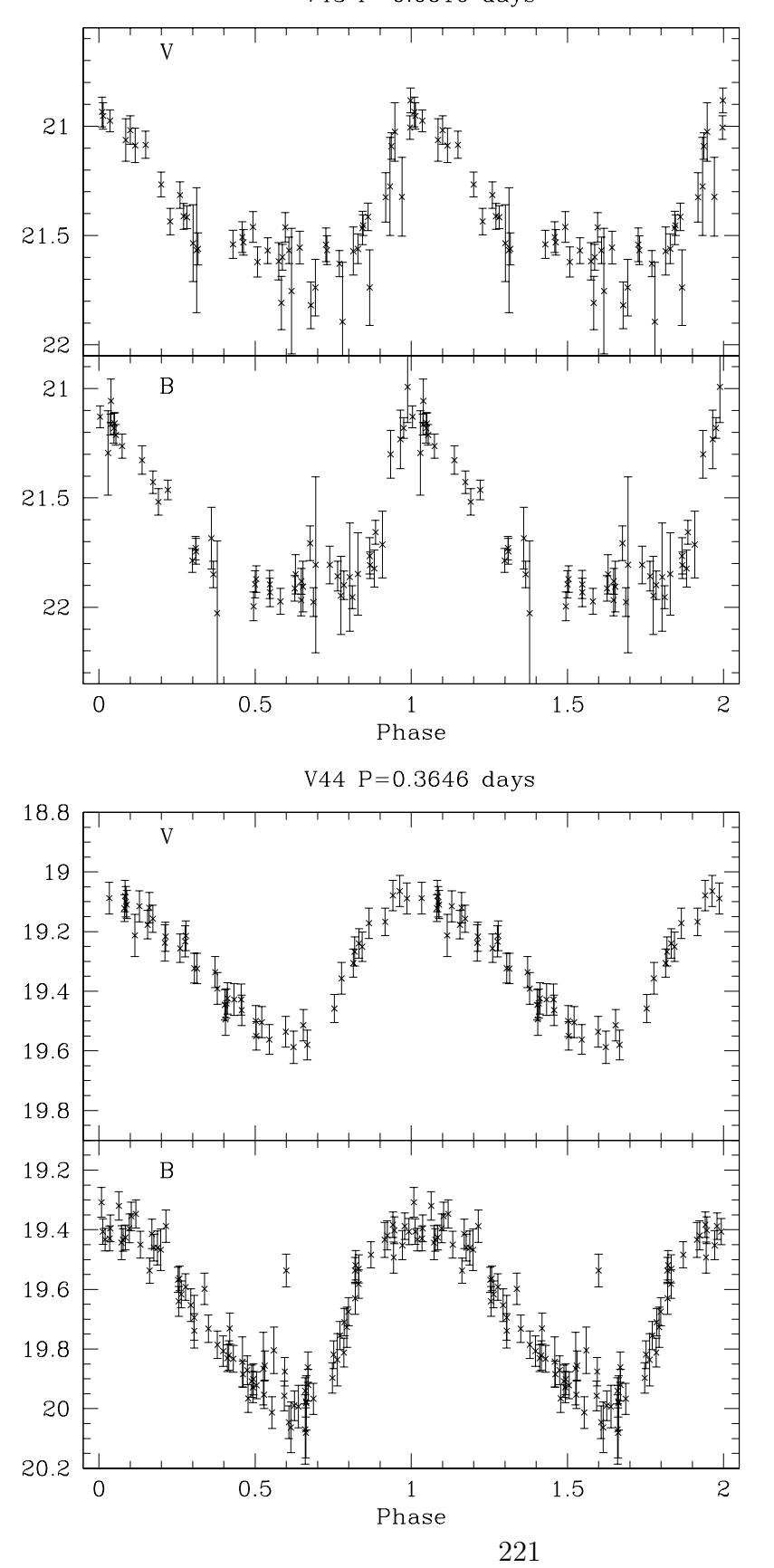


Figure C.1: Light curves for the variable stars in NGC 1786 (continued)  $$\rm V45~P\!=\!0.2991~days$$ 

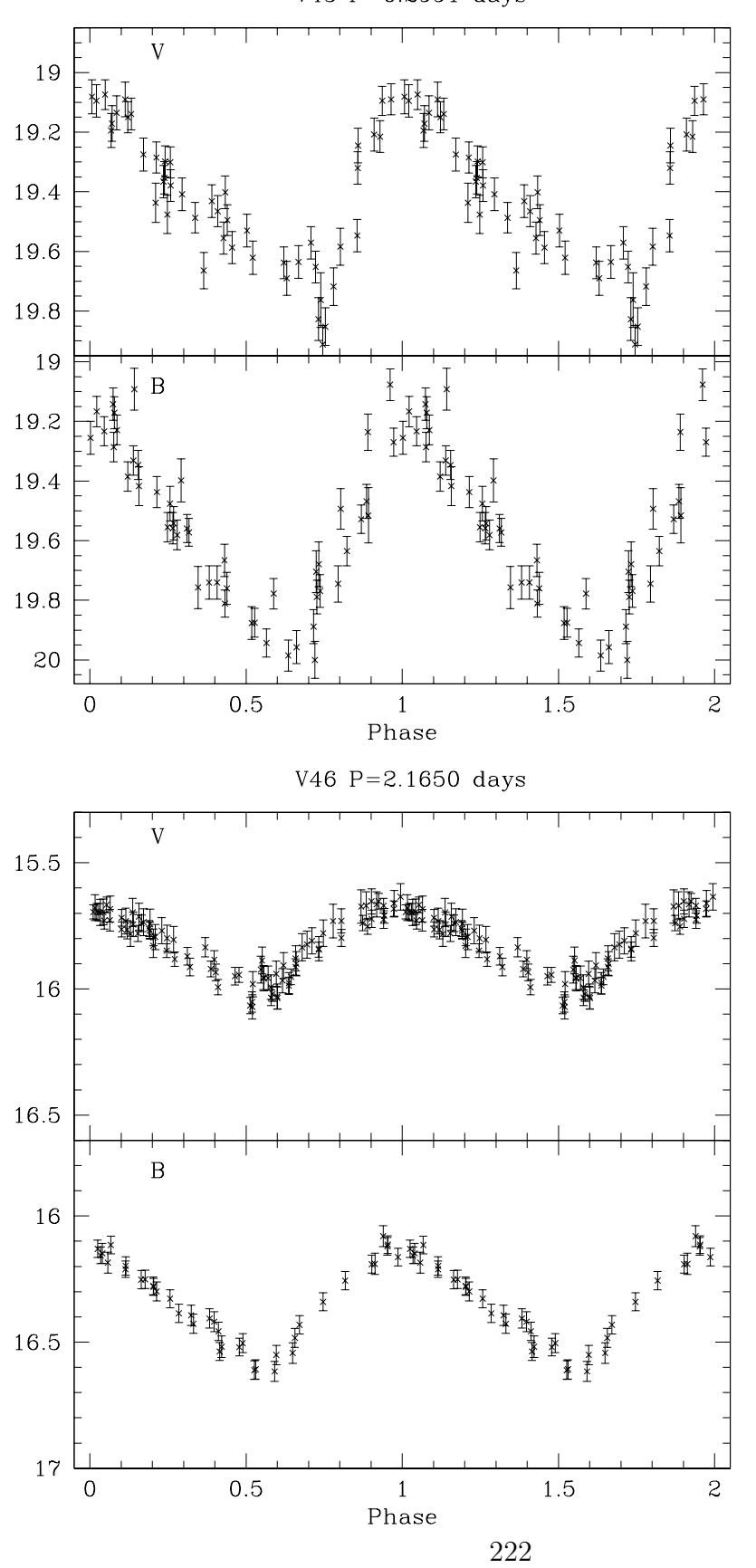


Figure C.1: Light curves for the variable stars in NGC 1786 (continued)  $$\rm V47~P\!=\!0.3708~days$$ 

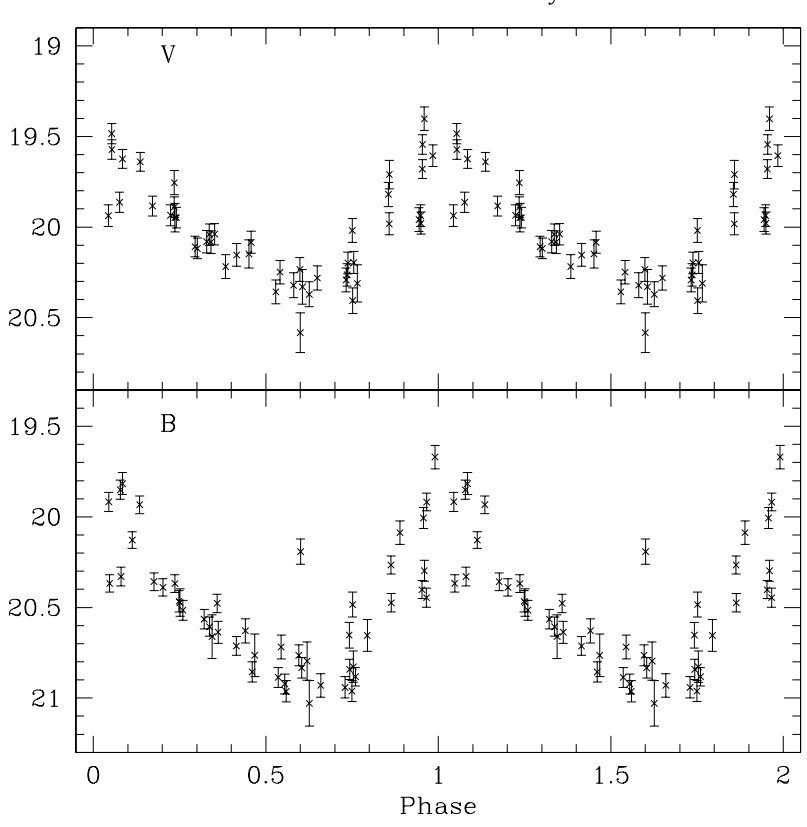


Figure C.1: Light curves for the variable stars in NGC 1786 (continued) V48  $P_1=0.3555$  days

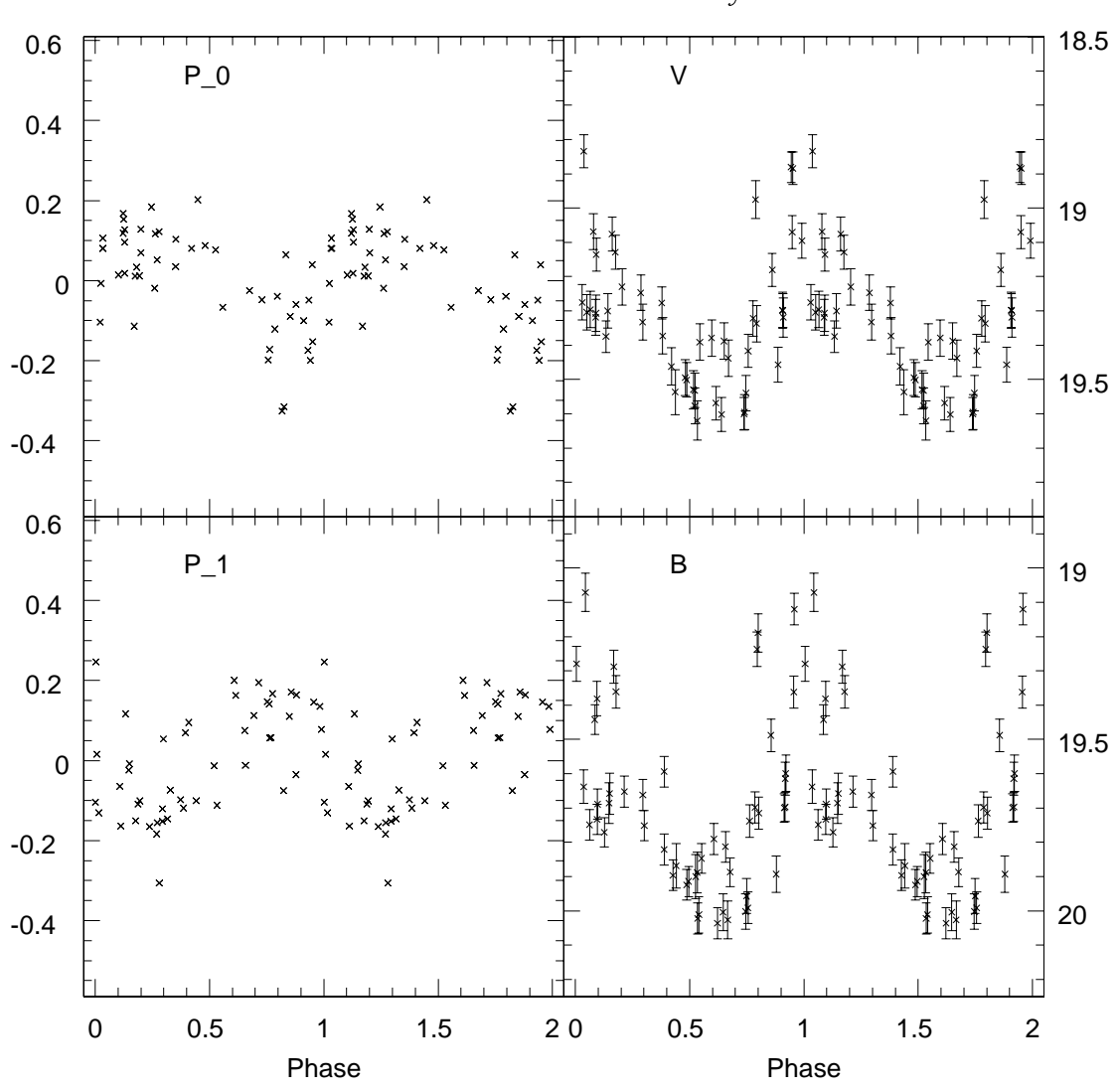


Figure C.1: Light curves for the variable stars in NGC 1786 (continued)  $$\rm V49~P\!=\!0.5540~days$$ 

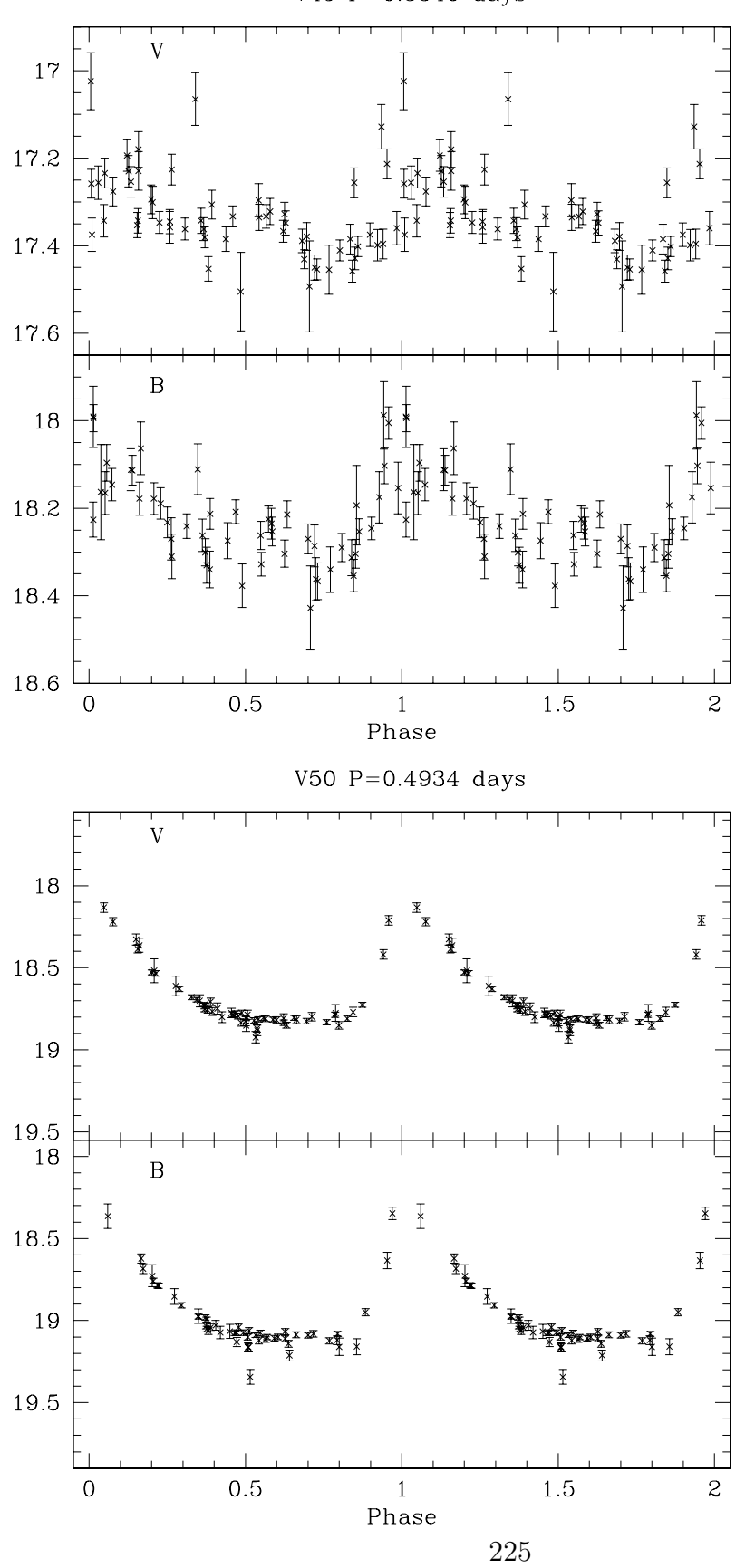


Figure C.1: Light curves for the variable stars in NGC 1786 (continued)  $${\tt V51\ P=0.5636}$$  days

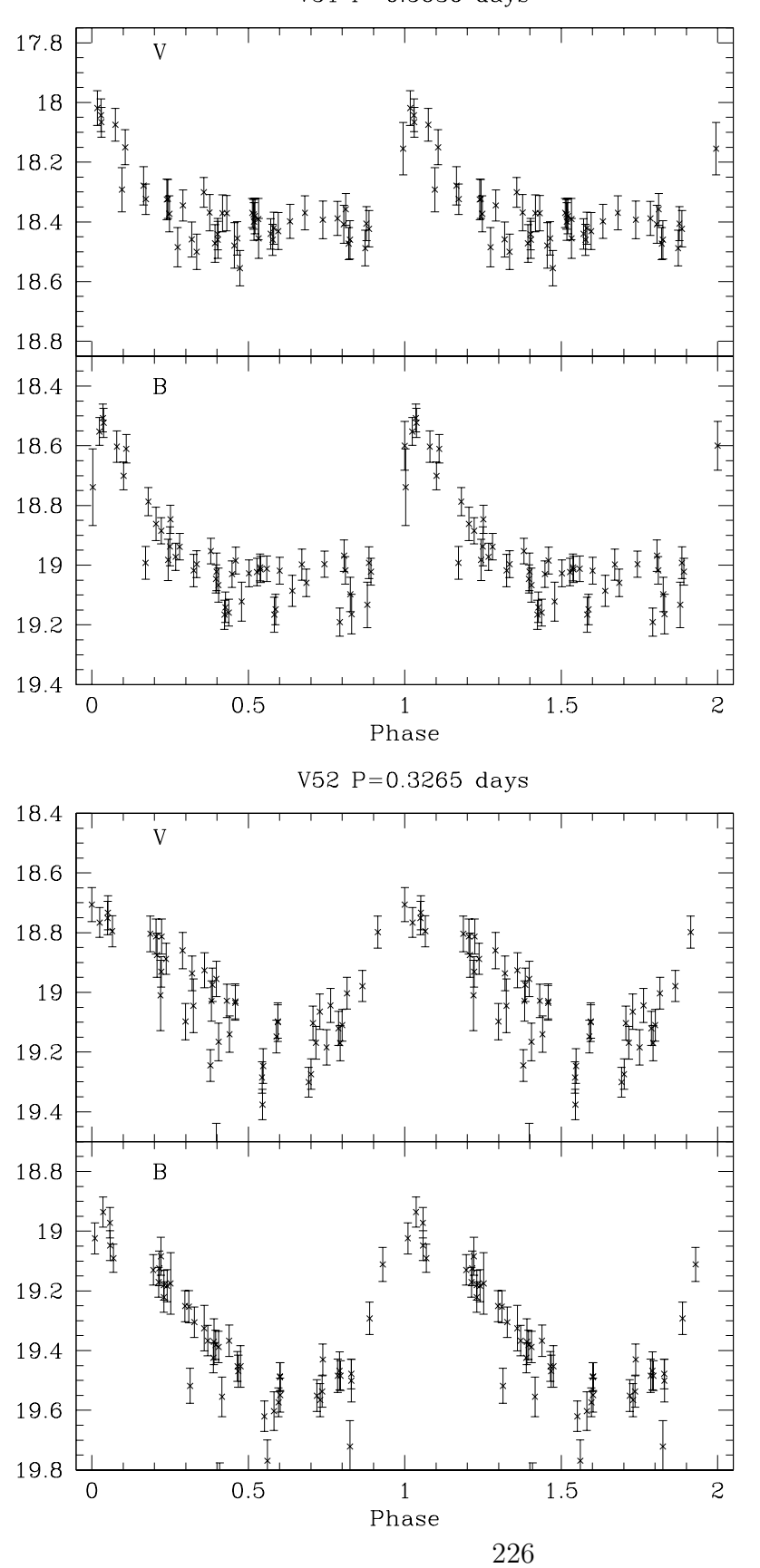


Figure C.1: Light curves for the variable stars in NGC 1786 (continued)  $$\tt V53\ P=0.3682\ days$$ 

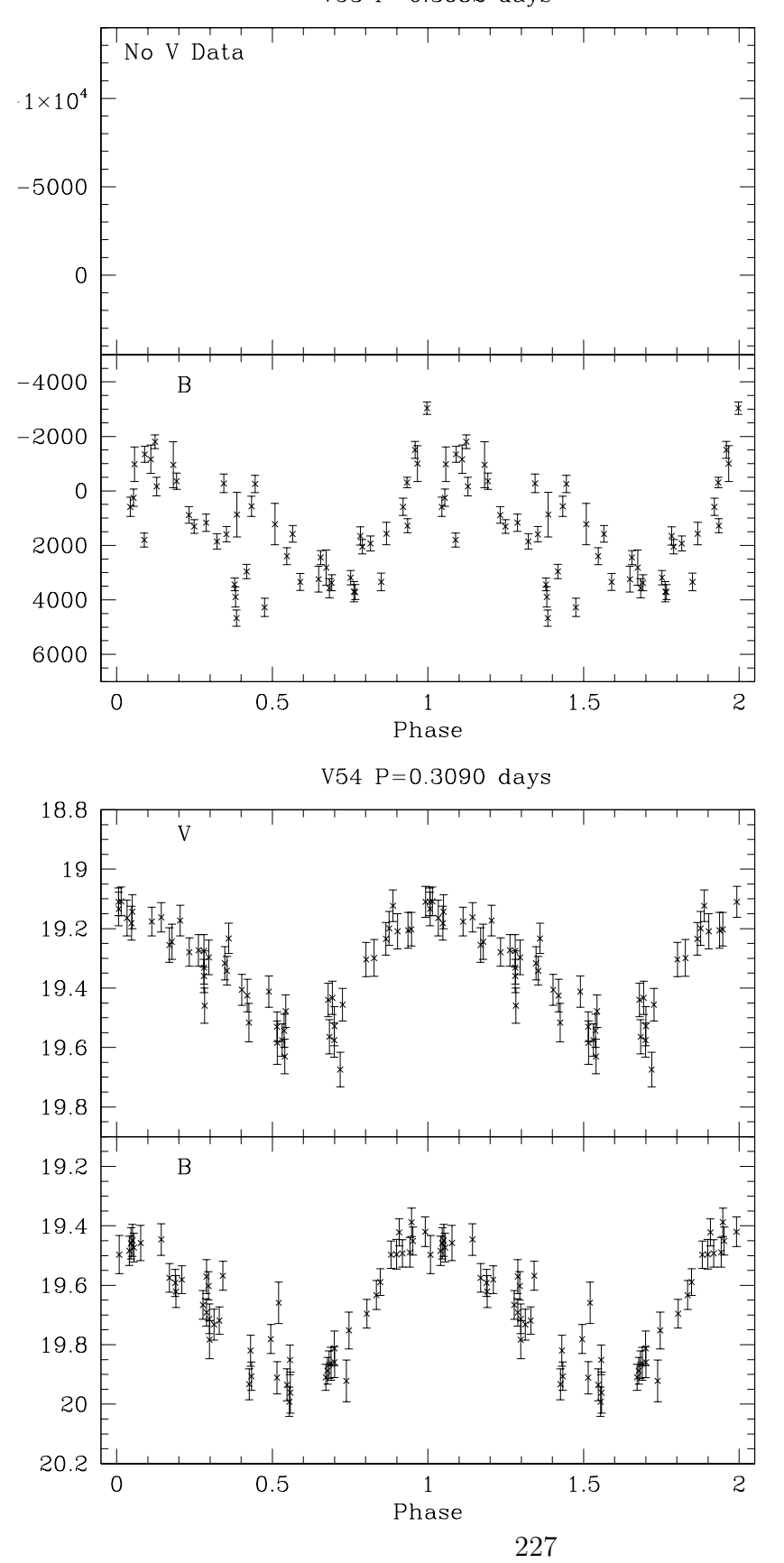


Figure C.1: Light curves for the variable stars in NGC 1786 (continued)  $${\tt V55\ P=0.5190\ days}$$ 

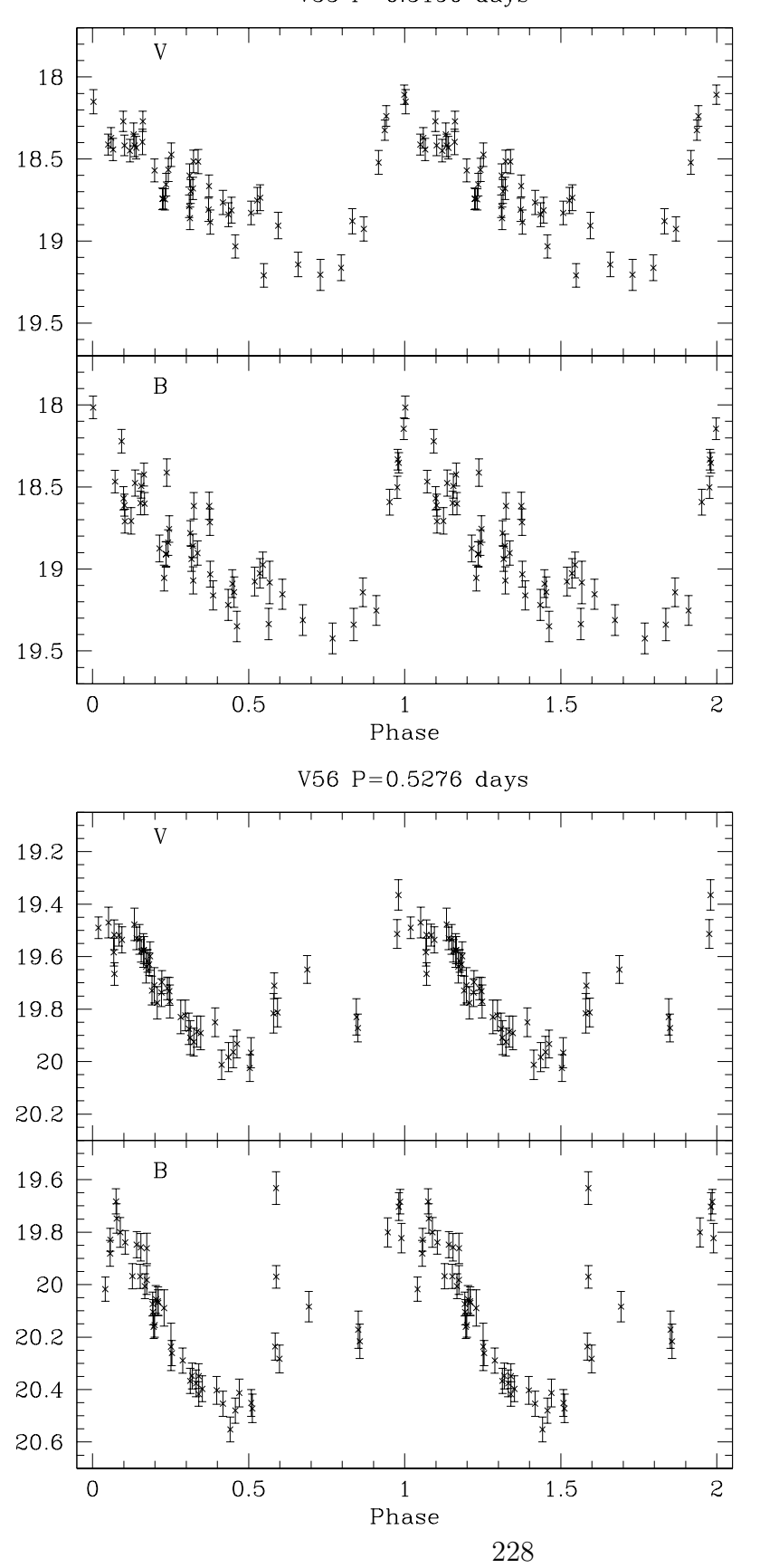


Figure C.1: Light curves for the variable stars in NGC 1786 (continued)  $$\tt V57\ P=0.5208\ days$$ 

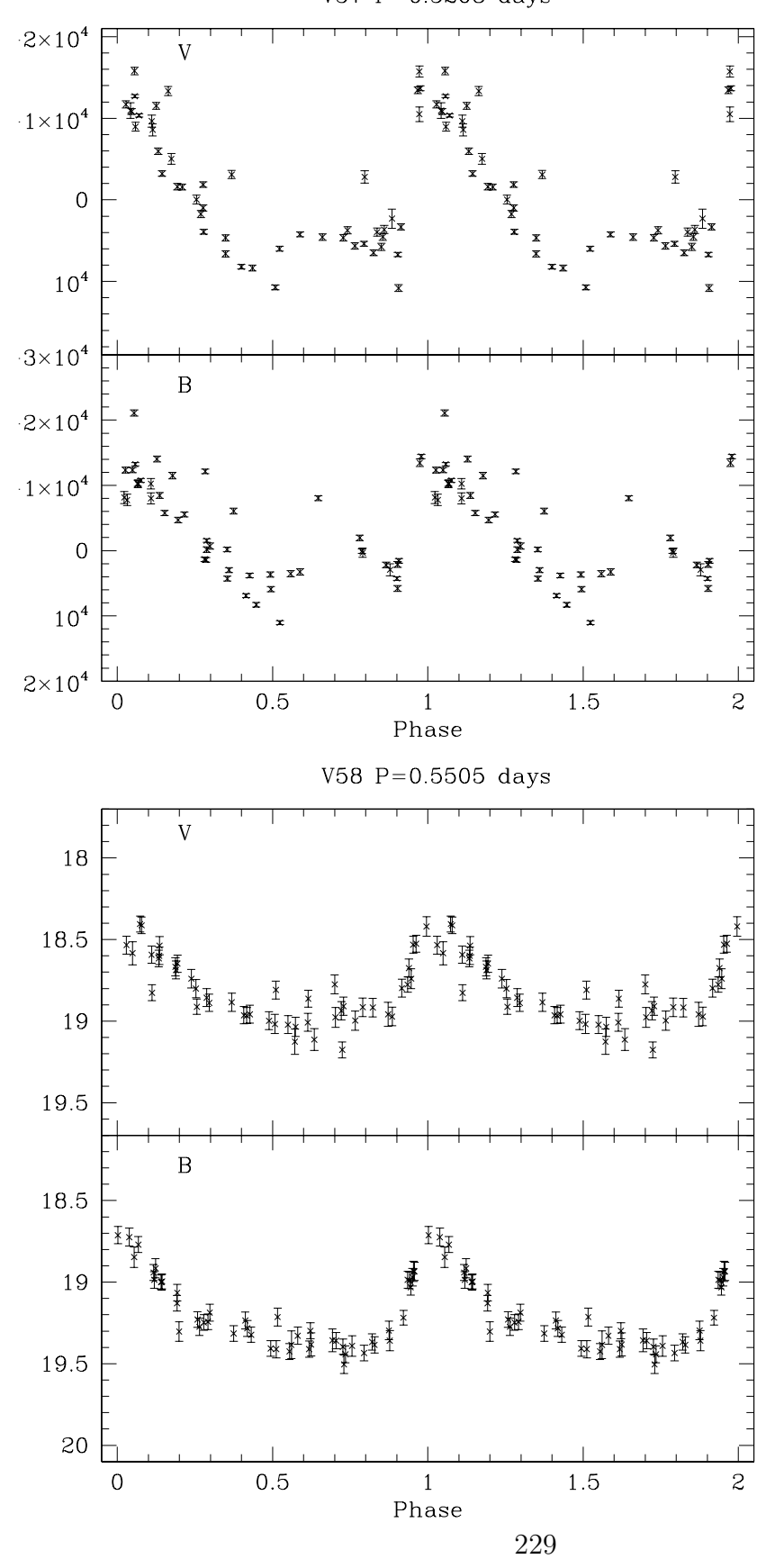


Figure C.1: Light curves for the variable stars in NGC 1786 (continued)  $${\tt V59\ P=0.5651\ days}$$ 

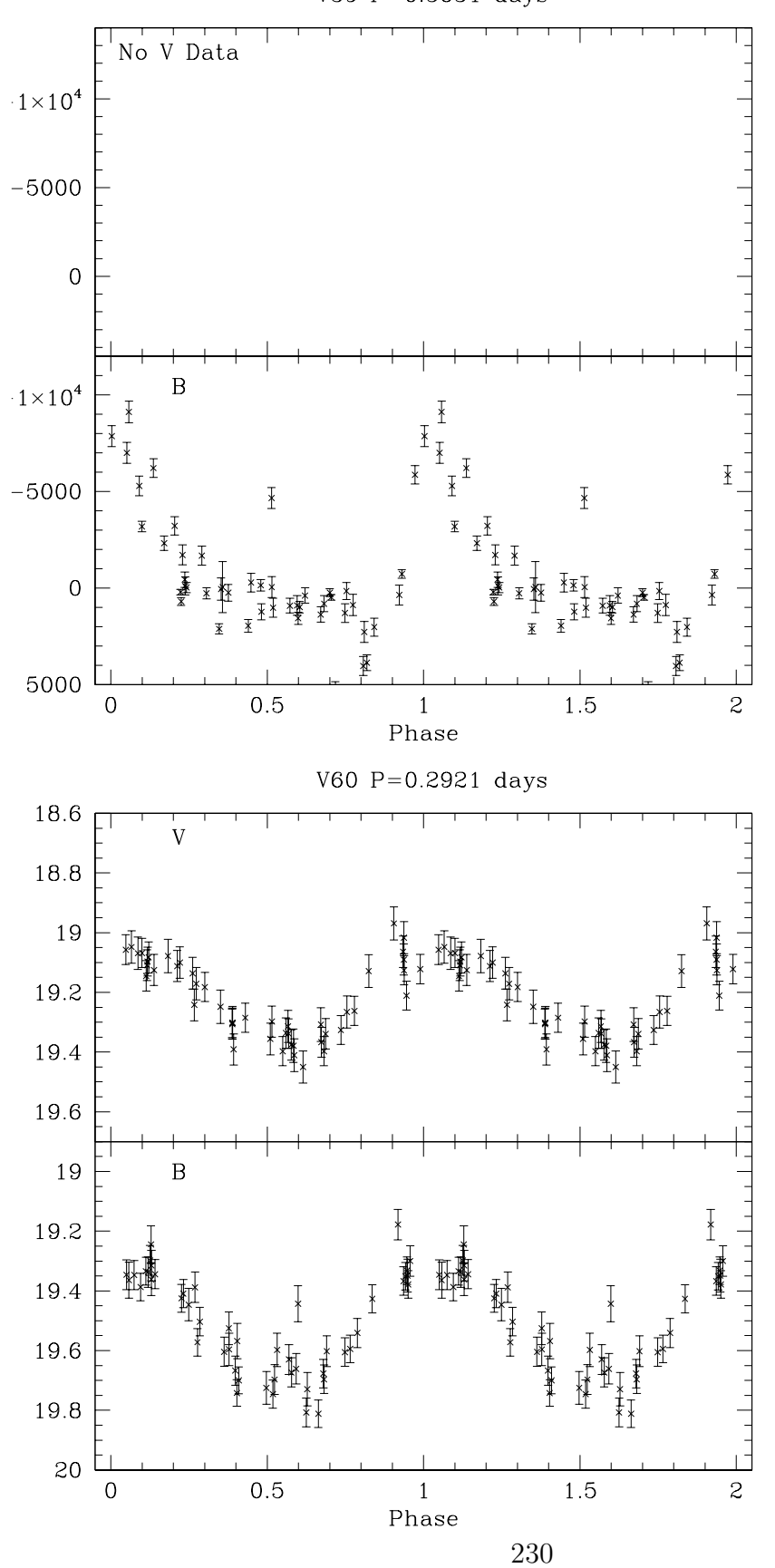


Figure C.1: Light curves for the variable stars in NGC 1786 (continued)  $${\tt V61\ P=0.3606\ days}$$ 

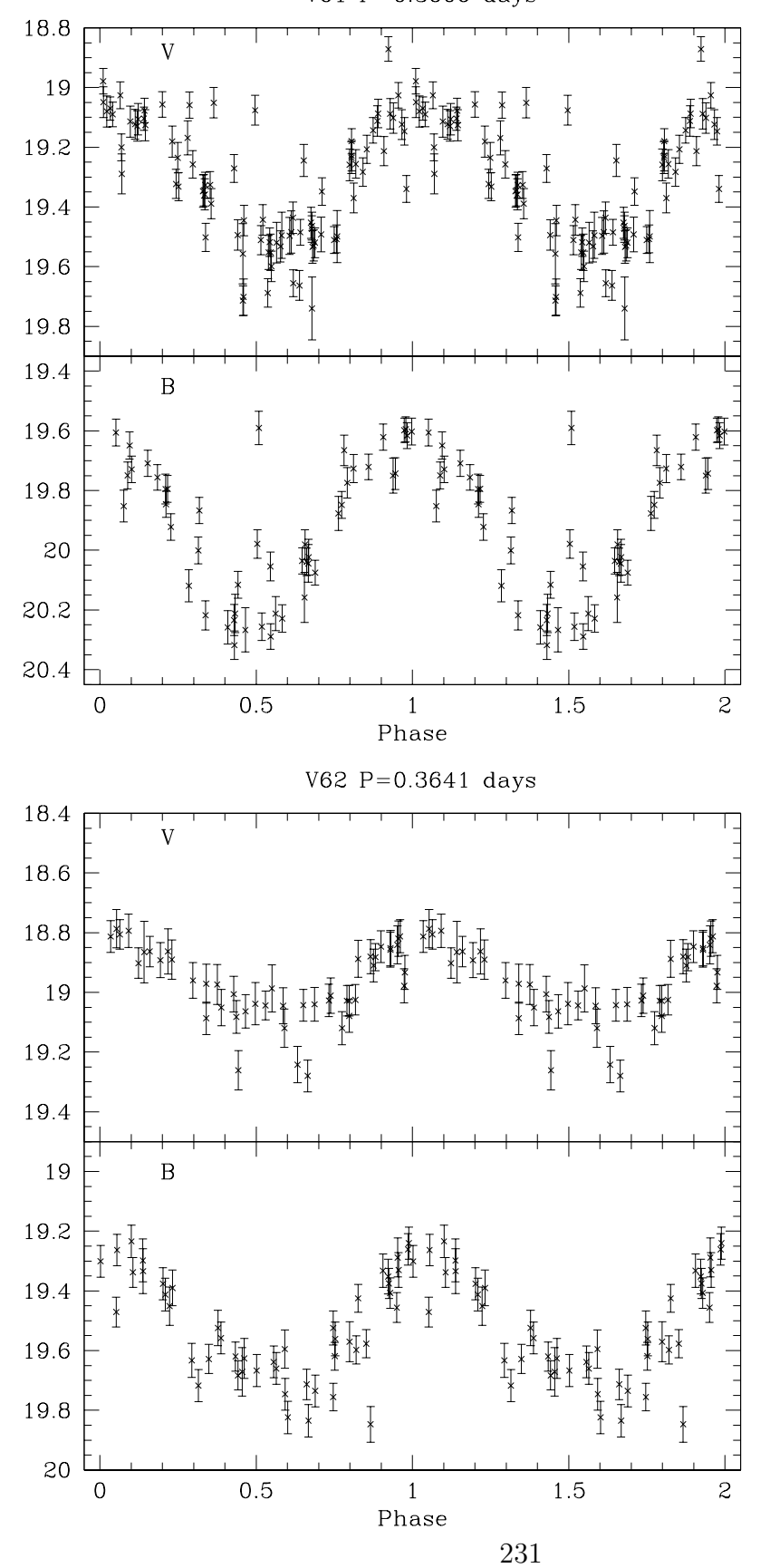


Figure C.1: Light curves for the variable stars in NGC 1786 (continued)  $${\tt V63\ P=0.6231\ days}$$ 

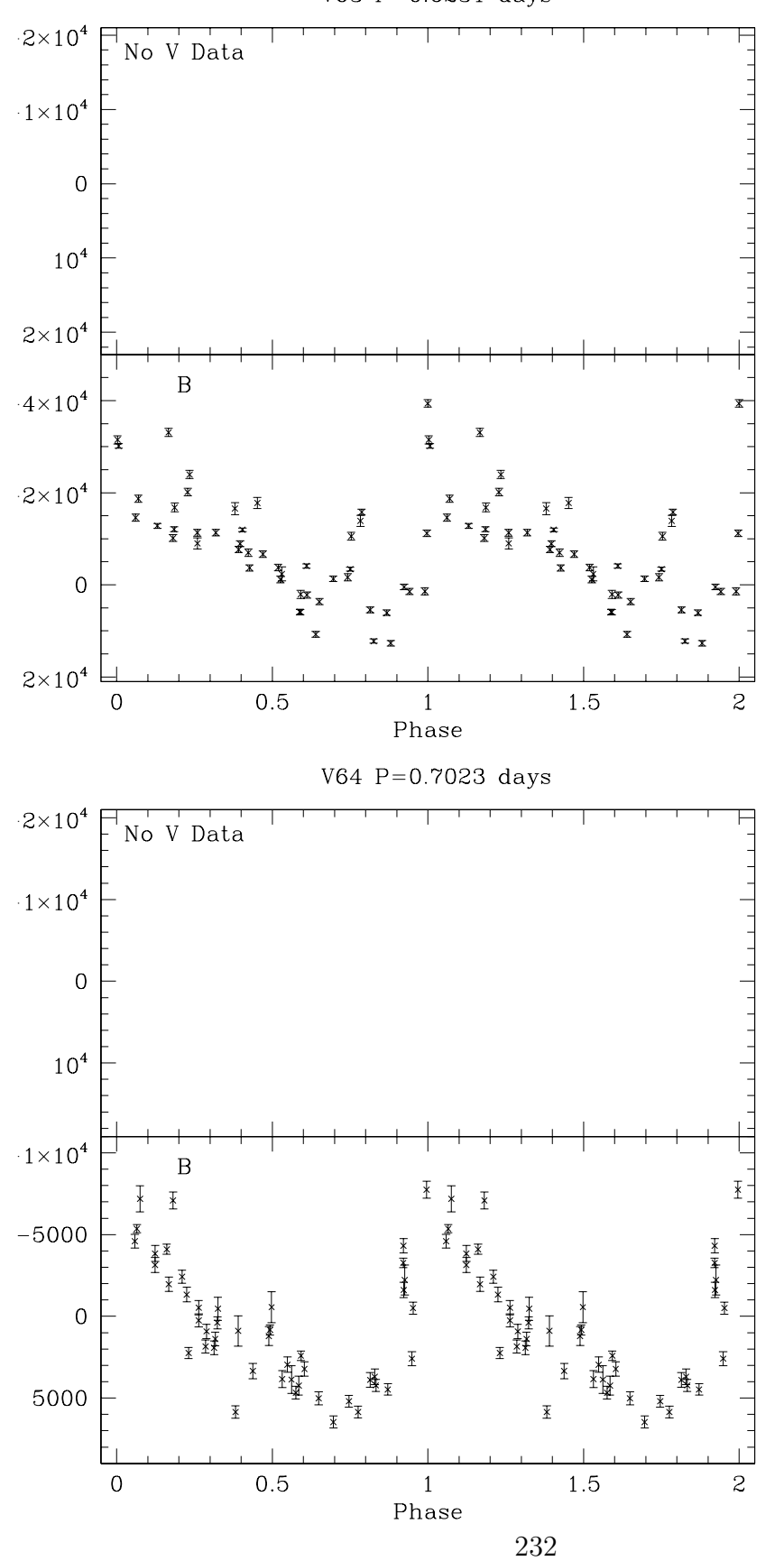
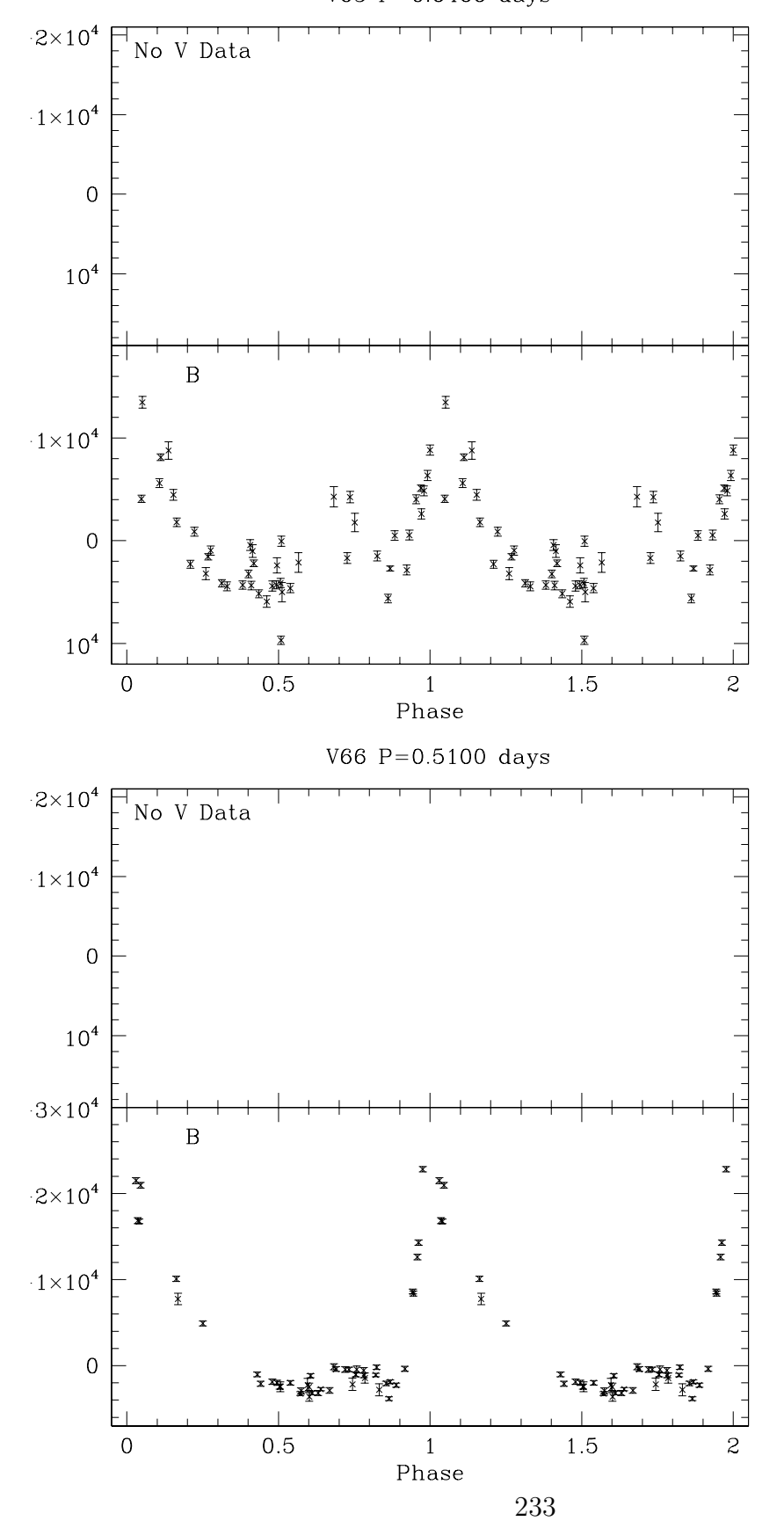


Figure C.1: Light curves for the variable stars in NGC 1786 (continued)  $${\tt V65\ P=0.6466\ days}$$ 



REFERENCES

## REFERENCES

Abadi, M.G., Navarro, J.F., & Steinmetz, M. 2006, MNRAS, 365, 747

Alard, C. 2000, A&AS, 144, 363

Babusiaux, C., et al. 2010, A&A, 519, 77

Bailey, S.I., & Pickering, E.C. 1902, Annals of Harvard College Observatory, 38, 1

Bekki, K., & Chiba, M. 2001, ApJ, 558, 666

Belokurov, V., et al. 2006, ApJ, 642, L137

Belokurov, V., et al. 2007, ApJ, 654, 897

Bica, E., Bonatto, C., Dutra, C.M., & Santos, J.F.C. 2008, MNRAS, 389, 678

Blazhko, S. 1907, Astron. Nachr., 175, 325

Bono, G., Caputo, F., & Stellingwerf, R.F. 1994, ApJ, 423, 294

Bono, G., Caputo, F., & Stellingwerf, R.F. 1995, ApJS, 99, 263

Bullock, J.S., & Johnston, K.V. 2005, ApJ, 474, L15

Cacciari, C., Corwin, T. M., & Carney, B.W. 2005, AJ, 129, 267

Carollo, D. et al. 2011, submitted to ApJ, arXiv1103.3067C

Catelan, M. 2004a, ApJ, 600, 409

Catelan, M. 2004b, in Variable Stars in the Local Group, ASP Conf. Ser., 310, ed. D.W. Kurtz, & K.R. Pollard (San Francisco: ASP), 113

Catelan, M. 2009a, Ap&SS, 320, 261

Catelan, M. 2009b, IAU Symp. 258, 209

Catelan, M., & Cortés, C. 2008, ApJ, 676, L135

Chiba, M., & Beers, T.C. 2000, AJ, 119, 2843

Christy, R.F. 1966, ApJ, 144, 108

Clement, C.M. et al. 2001, AJ, 122, 2587

Clement, C.M., & Rowe, J. 2000, AJ, 120, 2579

Clementini, G., Corwin, T.M., Carney, B.W., & Sumerel, A.N. 2004, AJ, 127, 938

Contreras, R., et al. 2010, AJ, 140, 1766

Corwin, T.M., Catelan, M., Smith, H.A., Borissova, J., Ferraro, F.R., & Raburn, W.S. 2003, AJ, 125, 2543

Corwin, T.M., et al. 2008, AJ, 135, 1459

Deb, S., & Singh, H.P. 2010, MNRAS, 402, 691

De Lee, N. 2008, Ph. D. Thesis, Michigan State University

Demers, S. & Kunkel, W.E. 1976, ApJ, 208, 932

Eggen, O.J., Lynden-Bell, D., & Sandage, A.R. 1962, ApJ, 136, 748

Ferraz-Mello, S. 1981, AJ, 86, 619

Eliche-Moral, M.C., et al. 2010, å, 519, 55

Font, A.S., Johnston, K.V., Bullock, J.S., & Robertson, B.E. 2006, ApJ, 638, 585

Forbes, D.A., & Bridges, T. 2010, MNRAS, 404, 1203

Frebel, A., Kirby, E.N., & Simon, J.D. 2010, Nature, 464, 72

Graham, J.A. 1977, PASP, 89, 465

Graham, J.A. 1985, PASP, 97, 676

Harris, W.E. 2010, arXiv1012.3224H

Hazen, M.L., & Nemec, J.M. 1992, AJ, 104, 111

Ibata, R.A., Gilmore, G., & Irwin, M.J. 1994, Nature, 370, 194

Jerzykiewicz, M., & Wenzel, W. 1977, AcA, 27, 35

Johnson, J.A., Bolte, M., Stetson, P.B., Hesser, J.E., & Somerville, R.S. 1999, ApJ, 527, 1999

Johnson, J.A., Bolte, M., Stetson, P.B., & Hesser, J.E. 2002, IAU Symp. 207, 190

Jurcsik, J. 1995, AcA, 45, 653

Jurcsik, J. 1998, A&A, 333, 571

Jurcsik, J., & Kovács, G. 1996, A&A, 312, 111

Jurcisk, J., & Kovács, G. 1999, NewA Rev., 43, 463

Kinemuchi, K., et. al. 2008, AJ, 136, 1921

King, D.S., & Cox, J.P. 1968, PASP, 80, 365

Kovács, G. 1998, Mem. Soc. Astron. Italiana, 69, 49

Kovács, G., & Walker, A.R. 1999, ApJ, 512, 271

Kovács, G., & Walker, A.R. 2001, A&A, 371, 579

Kuehn, C. et al. 2008, ApJ, 674L, 81

Kuehn, C.A. et al. 2011, submitted to AJ

Landolt, A.U. 1992, AJ, 104, 340

Layden, A.C. 1998, AJ, 115, 193

Lázaro, C. et al. 2006, MNRAS, 372, 69

Lee, Y.S. et al., 2011, submitted to ApJ, arXiv1104.3114

Lenz, P., & Breger, M. 2005, Commun. Asteroseismol., 146, 53

Mackey, A.D., & Gilmore, G.F. 2003, MNRAS, 338, 85

Mackey, A.D., & Gilmore, G.F. 2004, MNRAS, 352, 153

Mackey, A.D., & Gilmore, G.F. 2004, MNRAS, 355, 504

Mackey, A.D. & van den Bergh, S. 2005, MNRAS, 360, 631

Miceli, A., et al. 2008, ApJ, 678, 865

Morgan, S.M., Wahl, J.N., & Wieckhorst, R.M. 2007, MNRAS, 374, 1421

Mucciarelli, A., Origlia, L., Ferraro, F. R., & Pancino, E. 2009, ApJ, 695, 134

Mucciarelli, A., Origlia, L., & Ferraro, F.R. 2010, ApJ, 717, 277

Nemec, J.M. 1981, in Astrophysical Parameters for Gloubular Clusters, IAU Colloquim No. 68, edited by A.G. Davis Philip and D.S. Hayes, p.215

Nemec, J.M., Nemec, A.F.L, & Lutz, T.E. 1994, AJ, 108, 222

Nemec, J.M., Walker, A.R., Jeon, Y.B. 2009, AJ, 138, 1310

Newberg, H.J., et al. 2002, ApJ, 569, 245

Olsen, K.A.G., et al. 1998, MNRAS, 300, 665

Olszewski, E.W., Schommer, R.A., Suntzeff, N.B., & Harris, H.C. 1991, AJ, 101, 515

Oosterhoff, P.T. 1939, The Observatory, 62, 104

Oosterhoff, P.T. 1944, BAN, 10, 55

Ostlie, D.A., & Carroll, B. W. 1996, An Introduction to Modern Stellar Astrophysics, by D.A. Ostlie and B.W. Carroll. Benjamin Cummings. 1996, ISBN 0-201-59880-9

Peñarrubia, J., et al. 2005, ApJ, 626, 128

Petersen, J.O. 1973, A&A, 27, 89

Petersen, J.O. 1986, A&A, 170, 59

Pickering, E.C., & Bailey, S.I. 1985, ApJ, 2, 321

Popielski, B.L., Dziembowski, W.A., & Cassisi, S. 2000, AcA, 50, 491

Pritzl, B.J., Armandroff, T.E., Jacoby, G.H., & Da Costa, G.S. 2002, AJ, 124, 1464

Pritzl, B.J., Armandroff, T.E., Jacoby, G.H., & Da Costa, G.S. 2005, AJ, 129, 2232

Pritzl, B.J., Venn, K.A., & Irwin, M. 2005, AJ, 130, 214

Reid, N. & Freedman, W. 1994, MNRAS, 267, 821

Reimann, J.D. 1994, PhD Thesis (University of California)

Ripepi, V. et al. 2004, CoAst., 145, 24

Ritter, A. 1879, Untersuchungen über die Höhe der Atmosphäre und die Constitution gasförmiger Weltkörper. Annalen der Physik und Chemie, **244** (9), 157-183

Sandage, A., Katem, B., & Sandage, M. 1981, ApJS, 46, 41

Santos Jr., J.F.C., & Piatti, A.E. 2004, A&A, 428, 79

Sawyer, H. 1944, Communications of David Dunlap Obs. Publ. 1, No. 4

Schlegel, D.J, Finkbeiner, D.P., & Davis, M. 1998, ApJ, 500, 525

Searle, L., & Zinn, R. 1978, ApJ225, 357

Sharma, S., Borissova, J., Kurtev, R., Ivanov, V.D., & Geisler, D. 2010, AJ, 139, 878

Sills, A., Karakas, A., & Lattanzio, J. 2009, ApJ, 692, 1411

Simon, N.R., & Clement, C.M. 1993, ApJ, 410, 526

Smith, H.A. 1995, Cambridge Astrophysics Series, Cambridge, New York: Cambridge University Press, —c1995

Smolinski, J.P., et al. 2011, AJ, 141, 89

Soszyński, I., et al. 2003, AcA, 53, 93

Soszyński, I., et al. 2009, AcA, 59, 1

Stellingwerf, R.F. 1975, ApJ, 195, 441

Stellingwerf, R.F., & Bono, G. 1993, in IAU Coll. No. 139, New Perspectives on Stellar Pulsation and Pulsating Variable Stars, ed. J.M. Nemec, & J.M. Matthews (Cambridge: Cambridge University Press), 252

Stetson, P.B. 1987, PASP, 99, 191

Stetson, P.B. 1992, in ASP Conf. Ser. 25, Astronomical Data Analysis Software and Systems I, ed. D.M. Worrall, C. Biemesderfer, & J. Barnes (San Francisco: ASP), 297

Stetson, P.B. 1994, PASP, 106, 250

Stetson, P.B. 2000, PASP, 112, 925

Stetson, P.B., & Harris, W.E. 1988, AJ,96, 909

Szczygiel, D.M., Pojmański, G., & Pilecki, B. 2009, AcA, 59, 137

Thackeray, A.D., & Wesselink, A.J. 1953, Nature, 171, 693

Udalski, A., Szymanski, M.K., Soszynski, I., & Poleski, R. 2008, AcA, 58, 69

van Albada, T.S., & Baker, N. 1973, ApJ, 185, 477

Walker, A.R. 1985, MNRAS, 212, 343

Walker, A.R. 1992, AJ, 103, 1166

Walker, A.R. 1992, AJ, 104, 1395

Walker, A.R. & Mack, P. 1988, AJ, 96, 1362

Wesselink, A.J. 1971, MNRAS, 152, 159

Wolf, M.J., Drory, N., Gebhardt, K., & Hill, G.J. 2007, ApJ, 655, 179

Zinn R. 1993, in Smith G. H., Brodie J. P., eds, ASP Conf. Ser. 48, The Globular Cluster-Galaxy Connection. Astron. Soc. Pac., San Francisco, p. 302

Zinn, R., & West, M.J. 1984, ApJS, 55, 45

Zoccali, M. 2010, in IAU Symp. 265, Connecting First Stars to Planets, ed. K. Cunha, M. Spite, & B. Barbuy (Cambridge: Cambridge Univ. Press), 271

Zorotovic, M., et al. 2010, AJ, 140, 912